UNIVERSIDAD NACIONAL AUTÓNOMA DE MÉXICO

FACULTAD DE CIENCIAS POLÍTICAS Y SOCIALES

UN MODELO DE CARACTERIZACIÓN DE CIENCIA COMO HERRAMIENTA PARA ENTENDER Y UTILIZAR ARTÍCULOS CIENTÍFICOS EN HISTORIAS PERIODÍSTICAS

TESIS

Que para obtener el título de

LICENCIADA EN CIENCIAS DE LA COMUNICACIÓN (PERIODISMO)

P r e s e n t a

MICHELLE MONTSERRAT MORELOS CABRERA

Director de tesis

Fís. FRANCISCO JAVIER CRUZ MENA

Ciudad Universitaria, Cd. Mx., 2018

Índice

Agradecimientos

A mamá por enseñarme en la práctica el concepto de resiliencia

Tía Blanca, la resonancia de tu cariño me da la fuerza para enfrentarme a cualquier reto

Para Uziel, eres el único para mí entre $6{,}5x10^9$. Mi gratitud hacia ti no tiene límite.

Javier y Aleida, lograron echar abajo muchas construcciones intuitivas que tenía de la vida y la investigación, gracias por creer en este proyecto y en mi

Itzel, Denisse y Yanine, esta tesis no existiría si no fuera por su apoyo, gracias por ayudarme a forjar esta investigación a martillazos.

Samedi, gracias por ayudarme a descomponer los problemas en otros pequeños problemas más fáciles de procesar, te quiero mucho.

Jaime y Silvia, la claridad de su mente y sus consejos también hicieron esto posible.

Ñeros y ñoños, ustedes son la mejor simbiosis de trabajo que pude encontrar

Karina, Martz y Diana, gracias por hacerme sentir menos pérdida y ser capaz de enfrentar mis problemas de forma más racional

A todas las integrantes de la A.C.S por crear investigaciones académicas y periodísticas inspiradoras, creativas y dinámicas

A la Biblioteca Vasconcelos, por ofrecerme ese espacio tranquilo para concentrarme y encontrar mi punto de equilibrio

A la Dirección General de Divulgación de la Ciencia por su apoyo para la realización de este proyecto.

Venatu bambi ets...

Introducción

El periodismo especializado enfocado en ciencia es difícil de practicar, en parte por la complejidad de extraer información de sus fuentes primarias como son: ponencias en congresos, entrevistas con investigadores y artículos científicos, sobre todo si se pretende que la reportera busque la ciencia en este tipo de referencias y supere el atractivo de las declaraciones, el encanto de la anécdota o la facilidad de obtener información a través de un boletín de prensa.

Escribir una historia ~~–b~~asándose en uno o más artículos publicados en revistas científicas", admite en su tesis Aleida Rueda, no parece ser una tarea sencilla, pues quien ~~–r~~ecurre a este tipo de fuentes […], debe ser capaz de identificar los elementos informativos indispensables de cada texto y llevarlos al reportaje de modo que conserve íntegra la naturaleza científica de la explicación" [1].

Por tanto, es necesario encontrar soluciones respecto de cómo una reportera puede reconocer la ciencia en artículos arbitrados. En la presente investigación la hipótesis es que es posible caracterizar la ciencia en artículos arbitrados a través de una serie de rasgos identificables con relativa facilidad por periodistas sin preparación científica más allá de la educación preparatoria.

Rueda formuló una primera aproximación a este problema. Con la premisa de que enfrentarse a un artículo científico puede ser comparable con leer una obra desafiante de literatura clásica desarrolló el método de síntesis sucesivas[2], técnica de lectura comprensiva de textos especializados en tiempos periodísticos.

---

[1] Rueda Rodríguez, Aleida. *La síntesis como herramienta en el periodismo de ciencia. un análisis comparativo con su uso en la literatura infantil*. México, FCPyS-UNAM, Tesis de licenciatura, 2007. Consúltese: http://ru.ameyalli.dgdc.unam.mx/123456789/490. P. 64.

[2] Rueda, Aleida *Op cit*. P.84.

En esta tesis se busca brindar una respuesta más profunda a la pregunta de cómo reconocer la ciencia, a partir de un marco conceptual más amplio [detalles en el *Capítulo 2: Perfil de Ciencia: sus rasgos y cómo entenderlos*] que derivó en una herramienta novedosa: el Perfil de Ciencia[3], herramienta original de identificación de contenido científico que puede utilizarse tanto en dimensiones académicas como periodísticas.

Ahora bien, para que el Perfil sirva es indispensable que "represente" a la ciencia en sus fuentes primarias; por tanto, la pregunta disparadora de la investigación fue: ¿este modelo es representativo de la ciencia en artículos arbitrados? Además, del contexto inicial se desprende una segunda pregunta: ¿es apto para ser usado por reporteras sin formación científica?

La presente investigación está dividida en cinco capítulos. En el primero se argumenta que existen pocos estudios prácticos que ayuden a optimizar el ejercicio de la profesión periodística; asimismo se destacan los resultados de investigaciones que analizaron el contenido, la calidad y el nivel de la argumentación científica en coberturas periodísticas coyunturales. El diagnóstico general es que existió poca inclusión de información científica pese a tratarse de temas que lo ameritaban; otros estudios demuestran que al periodista le es difícil extraer la ciencia incluida en los artículos especializados. Estos resultados sirvieron para justificar la necesidad de crear estudios como este que evalúen y/o faciliten el trayecto de artículos científicos a historias periodísticas.

En el segundo capítulo se hace referencia a una serie de autores que plantean algunas soluciones. Ahí se presenta en detalle un nuevo modelo: el Perfil de Ciencia, los rasgos que lo componen y cómo identificar cada rasgo.

El tercer capítulo explica cómo se puso a prueba la hipótesis y la aplicación de la metodología. El corpus de análisis fue compuesto por 19 artículos publicados en 7 revistas

[3] Cruz Mena, *et al. Perfil de ciencia para análisis de contenidos en periodismo*. II Simposio sobre Comunicación de la Ciencia y la Tecnología en Latinoamérica. P.12.

arbitradas; 4 de ellas fueron preseleccionadas por su relevancia como fuentes periodísticas en la cobertura de ciencia a nivel global y las otras 3 fueron elegidas aleatoriamente mediante algoritmos desarrollados específicamente para ese propósito.

En el cuarto capítulo se presentan los resultados de los análisis cuantitativo y cualitativo. El del primer tipo consistió en dar a conocer la frecuencia de apariciones por artículo y por disciplina científica; por otro lado, en la revisión cualitativa de los resultados se examinó si el Perfil es apto para ser utilizado por periodistas sin una formación científica más allá de la obtenida en el nivel Medio Superior.

Finalmente el capítulo 5 conjunta las interpretaciones de los hallazgos y las limitaciones de este estudio, el cual puede tomarse como un análisis exploratorio e interpretativo.

En conclusión, a lo largo de este trabajo de tesis se presentó la suficiente evidencia empírica a favor de la representatividad de la ciencia a través de los rasgos de este modelo.

Capítulo 1

El uso actual del artículo científico en historias periodísticas

El ejercicio del periodismo especializado en ciencia es importante porque se fomenta el pensamiento crítico de los ciudadanos, contribuye a la construcción de una realidad pública capaz de visibilizar y examinar sus problemas, así como ayuda a elevar la calidad de la discusión, y en el mejor de los casos, sensibilizar para que las personas tomen decisiones individuales y como sociedad a favor de los temas de índole científico.

Sin embargo, para llegar a tener el periodismo que la sociedad mexicana requiere aún falta mucho por hacer: ~~l~~a sensación es que México ha hablado mucho y hecho poco en periodismo científico"[4] aseguró Pere Estupinyà, ex miembro del *Knight Science Journalism Program* en el *Massachusetts Institute of Technology*, luego de que durante 5 años escribió semanalmente en su blog *el rastreador científico en español* sobre la cobertura de ciencia realizada por distintos medios iberoamericanos

Por lo que es pertinente revisar y analizar algunas percepciones e ideas sobre la problemática del periodismo de ciencia, las cuales justifican el desarrollo de más y mejores propuestas de solución que ayuden a realizar contenidos de calidad con información científica entendible para un público no especializado.

Algunos de los retos a los que se enfrenta la práctica de esta profesión han sido documentados desde 2007 en la Unidad de Periodismo de la Dirección General de Divulgación de la Ciencia de la UNAM (DGDC). Un caso de análisis de una de las investigaciones fue la Décimo Sexta Conferencia de las Partes sobre Cambio Climático (COP16) realizada en México en 2010, ya que no sólo era un evento sobre un tema de gran

[4] Estupinyà, Pere. *El periodismo científico en América Latina ha mejorado en los últimos 5 años* en *El rastreador científico en español*. 28 de agosto de 2014. Consúltese en: https://undark.org/2014/08/18/el-periodismo-cientifico-en-america-latina-ha-mejorado-bastante-en-los-ultimos-5-anos/.

interés noticioso, sino uno en que la información científica habría sido fundamental para comprender el impacto del cambio climático en nuestro día a día. Isela Alvarado Cruz, en su tesis de licenciatura[5], realizó un análisis de 59 piezas transmitidas en tres noticiarios televisivos nacionales *prime time* (Noticieros Televisa, Hechos y Noticias 22) durante cuatro semanas (la previa, las dos semanas de realización y la posterior al evento).

Entre sus resultados destaca la falta de un discurso científico articulado en los tres noticiarios; los ciudadanos, después de ver alguno de esos programas (en caso hipotético) tendrían bases débiles para tomar decisiones informadas en materia de mitigación para reducir los gases de efecto invernadero o para adaptarse al fenómeno climático[6]. Confirmando que la atención de los medios tiende a enfocarse a difundir ~~–a~~vances" o ~~–h~~allazgos" y deja de lado los efectos y alcances que la ciencia puede tener.

Esta situación no se limita a coberturas especiales de eventos, también se presenta en momentos en los que estar informados sobre un tema era fundamental para tomar una decisión que podría repercutir en la integridad física inmediata del ciudadano. Ese fue el caso de la cobertura del brote de influenza A (H1N1) en televisión y revistas analizada por Denisse Flores en su tesis de licenciatura[7].

Otros de sus apuntes hicieron evidente que por momentos se percibe o cree que existe una amplia variedad mediática gracias a un vasto número de periódicos o canales que pueden transmitir su señal a las casas de las personas. Sin embargo, esa *gran* oferta no significa que se fomente una cobertura distinta de los temas de interés. Flores analizó un total de 179 piezas del noticiario *prime time* de Proyecto 40, y 36 textos publicados en las revistas *Emeequis, Newsweek en Español, Día Siete* y *Milenio Semanal*. Su investigación demostró

[5] Alvarado Cruz, Rosa Isela. *Diagnóstico de contenidos de ciencia en noticiarios televisivos nacionales a través del protocolo sobre cambio climático y del modelo de funcionalidad del periodismo: conferencia de las partes (cop 16)* México, FCPyS-UNAM, Tesis de licenciatura. Consúltese en: http://ru.ameyalli.dgdc.unam.mx/handle/123456789/510.
[6] Alvarado Cruz, Rosa Isela. *Op cit*. P.112
[7] Flores González, Denisse Joana. *Análisis de la cobertura de la pandemia de influenza A (H1N1) en revistas y televisión mexicana desde el punto de vista de la función social del periodismo de ciencia*. México, FCPyS-UNAM, Tesis de licenciatura, 2015. P. 168. Consúltese en: http://132.248.9.195/ptd2014/mayo/302149519/Index.html.

que las revistas analizadas se inclinaron por los testimonios de los ciudadanos afectados, mientras que la televisión por los personajes de la política. En conclusión: ~~–~~existen indicios de que los enfoques o encuadres científicos quedaron subordinados, pese a tratarse de un tema que necesitaba información científica para comprender su origen, trascendencia y consecuencias"[8].

1.1 | Análisis de la función y la actividad del periodista de ciencia

John Oliver, comediante, analista y conductor de *Last week tonight*, en la emisión titulada: *Scientific Studies*[9], mencionó cómo múltiples programas de TV en EU replican estudios sin ningún tipo de rigor, así como una serie de problemáticas relativas a la producción científica, como lo son: la presión hacia los investigadores por publicar y producir conclusiones llamativas para justificar o aumentar los recursos de sus laboratorios; la poca valoración a la replicación de investigaciones; la extrapolación incorrecta de trabajos realizados con animales a seres humanos; estudios financiados por grandes marcas, etc.

Durante la emisión se expusieron algunos de errores ~~–~~obvios", los cuales tuvieron repercusiones en los medios originales en los que fueron publicados. Por ejemplo, el texto de la revista TIME, *"Scientists say smelling farts prevents cancer"*, luego de ser puesto en evidencia durante el programa gracias a su título sensacionalista, tuvo que ser corregido por ~~–~~*A stinky compound may protect against cell damage, study finds"*, el cual resultaba mucho más preciso a lo escrito en el artículo científico realizado por los investigadores de la Universidad de Exeter, ~~–~~*The synthesis and functional evaluation of a mitochondria-targeted hydrogen sulfide donor, (10-oxo-10-(4-(3-thioxo-3H-1,2-dithiol-5-yl)phenoxy)decyl)triphenylphosphonium bromide (AP39)".*

Evidencia anecdótica como la anterior revela que algunos medios internacionales, en mayor o menor medida, utilizan o han utilizado como fuentes investigaciones en las que las

[8] Flores González, Denisse Joana. *Op cit.* P. 169.
[9] Stanton, Liz. *Last Week Tonight with John Oliver*. HBO https://www.youtube.com/watch?v=0Rnq1NpHdmw.

correlaciones se entienden como causas. Este posicionamiento no es muy distinto a la experiencia del periodismo de ciencia en México, en el cuál se le otorga más importancia al acontecer político minimizando la sección de ciencia a "datos curiosos", las buenas noticias, y el ―¿sabías que?"

Un ejemplo que lo documenta fue el análisis realizado por Keninseb García Rojo en su tesis de licenciatura sobre la cobertura de la prensa del brote de influenza A (H1N1) en abril y mayo de 2009. Entre sus resultados preliminares destaca que ―los *intereses ciudadanos* que aluden directamente al por qué científico del hecho noticioso ―como la gravedad de la epidemia o las medidas de protección― ocuparon sólo 1% del espacio total de la cobertura"[10].

Este tipo de situaciones se presentan con mayor notoriedad en las coberturas realizadas en nuestro país frente a las realizadas por medios extranjeros. Con base en los resultados de la investigación de Cecilia Rosen[11], sobre la cobertura periodística del Tercer Informe de Evaluación (TAR) del Panel Intergubernamental sobre Cambio Climático (IPCC) en 2001, demostraron que la prensa nacional (*La Jornada, El Universal y Reforma*) publicó un total de 4 notas sobre el TAR, mientras que *Le Monde, The New York Times y El País* informaron en 25 ocasiones sobre la publicación del TAR. Además, Rosen detectó la inexistencia de seguimiento informativo de la noticia en los diarios mexicanos.

Optar por salidas fáciles como *copiar* y *pegar* lo que afirman en el boletín de prensa y publicar esa información como noticia demerita la profesión, y lejos de ser periodista se convierte en vocero del medio o instituto que envía el boletín. Al respecto, Kovach y Rosenstiel, describen a cierto tipo de periodistas como meros registradores de la actualidad,

[10] García Rojo, María Keninseb. *Evaluación de la calidad del periodismo de ciencia en la prensa escrita mexicana desde un modelo de funcionalidad. La cobertura del brote de influenza A (H1N1) en abril y mayo de 2009 como caso de estudio* [Tesis en progreso]

[11] Rosen ferlini, Cecilia. *Análisis de la cobertura periodística del cambio climático en 2001 desde un modelo de funcionalidad.* México, FCPyS-UNAM, Tesis de licenciatura, 2008 P. 140. Consúltese en: http://ru.ameyalli.dgdc.unam.mx/handle/123456789/523.

en un contexto en el que los argumentos baratos y polarizados dominan de manera abrumadora sobre la información[12].

En la sesión –*Boosting science journalism in Latin America: global or local?"* realizada en la Conferencia Mundial de Periodistas de Ciencia 2015 (WSCJ por sus siglas en inglés), Rosen presentó los resultados preliminares de su tesis de doctorado, generados a partir de la realización de entrevistas a 21 periodistas y comunicadores, además de realizar un análisis de notas publicadas por una parte de ellos (100 textos en total). Lo dicho al respecto fue retomado por Aleida Rueda para el sitio de la Red Mexicana de Periodistas de Ciencia[13]:

> –Algunos se asumen como periodistas y no como divulgadores o promotores de la ciencia. Y, sin embargo, cuando se abunda un poco más en su percepción de la ciencia y de su labor, resultan mucho más cercanos a la divulgación, con una visión poco crítica hacia la ciencia".

Las periodistas deberían evitar convertirse en –porristas" de la ciencia y trabajar para "transmitir una imagen de la realidad en la que los ciudadanos sean capaces de actuar"[14]. El problema se manifiesta cuando la reportera, a pesar de sus posibles intenciones de hacer su trabajo lo mejor posible, posee una baja cultura científica, recursos alternativos limitados, preparación periodística deficiente y condiciones de trabajo desfavorables.

En el reporte final de la "Encuesta para identificar a los periodistas de ciencia en la Ciudad de México"[15], realizada por Somedicyt, 56% del total de periodistas encuestados no había tomado ningún curso o capacitación enfocados al periodismo de ciencia en los 3 años previos a la encuesta.

---

[12]Kovach, Bill, Rosenstiel, Tom**.** *Op. cit*. P. 57.
[13] Rueda, Aleida. *Latinoamérica… ¿el patito feo del periodismo de ciencia?* https://redmpc.wordpress.com/2015/06/21/latinoamerica-el-patito-feo-del-periodismo-de-ciencia-parte-ii/
[14] Kovach, Bill, Rosenstiel, Tom**.** *Op. cit*. P. 62.
[15] Somedicyt. *Encuesta para identificar a los periodistas de ciencia en la Ciudad de México Reporte de Resultados.* 2016.

El ejercicio periodístico preciso y riguroso debiera ir ligado a buenas condiciones laborales, a una remuneración económica justa, es decir, vivir dignamente a partir del buen ejercicio de tu trabajo. El mismo estudio reveló que sólo 21% de las periodistas de ciencia o divulgadores con más de 10 años de experiencia cubrían arriba del 80% de sus necesidades con el ingreso que reciben por comunicar ciencia en los medios. Es decir, ~~l~~os años de experiencia posiblemente no aseguran un mejor salario"[16].

Si a lo anterior se suma un bajo apoyo o soporte de los directores del medio y/o editores de la sección de ciencia a las periodistas, el superar ciertos vicios de la práctica periodística se vuelve aún más complicado. ~~M~~Muchos de los reporteros creen que sus directores se han pasado al otro lado", mencionó Deborah Howell, Directora del grupo *Newhouse Newspapers*[17], respecto a los intereses políticos y comerciales que algunos directores privilegian versus la total libertad de sus periodistas.

Los grandes conglomerados de medios tienden a no vigilar el bien común sino velar por intereses privados ~~l~~os corporativos [mediáticos] tienen *de facto* la capacidad de decidir qué aparece o no publicado en un mercado que funciona con base en intereses comerciales y no en contribuir al debate público"[18].

Ante esa situación es fundamental que las empresas y medios públicos de comunicación entiendan la importancia que tienen las periodistas en la construcción de una relación de compromiso con el auditorio. Si se aspira a tener un periodismo de calidad, será necesario crear y fortalecer las redes de apoyo que tienen las reporteras para mejorar su ejercicio profesional y defenderse ante alguna injusticia o cualquier indicio de censura por parte de sus medios. Por ejemplo, la Red Mexicana de Periodistas de Ciencia desde 2016 trabaja para ~~i~~impulsar el periodismo de ciencia, tecnología e innovación y su ejercicio libre en México, poniendo énfasis en la calidad, la veracidad y el rigor periodístico…"[19], hasta

[16] Somedicyt. *Ibidem.* P. 7.
[17] Cita retomada de Kovach, Bill, Rosenstiel, Tom**.** *Op. cit*. 200. P. 54.
[18] Guerrero Martínez, Manuel Alejandro. *Op. Cit.* P. 17.
[19] Red Mexicana de Periodistas de Ciencia. *Crean formalmente la red mexicana de periodistas de ciencia (redmpc).* https://redmpc.wordpress.com/2016/01/13/crean-formalmente-la-red-mexicana-de-periodistas-de-ciencias-redmpc/. Consultado el 17 de julio del 2016.

finales de 2017, la Red contaba con más de 85 miembros en toda la República, 56 mujeres y 29 hombres, y un 80% residen en la Ciudad de México, el porcentaje restante se encuentran en Michoacán, Monterrey, Jalisco entre otros.

Cuando las reporteras[20] a partir de su trabajo logren satisfacer sus necesidades económicas básicas, reciban capacitación constante y tengan la suficiente cultura científica, será más factible que puedan llegar a enfocarse mejor en el desarrollo de sus historias periodísticas.

Mientras en los medios se le exija al periodista tener la capacidad de ~~–e~~ubrir de todo", tal como lo documenta Denisse Flores en las entrevistas semiestructuradas exploratorias que realizó a nueve periodistas para su tesis de Maestría[21], y tener que entregar hasta nueve notas durante el día, enfrentarse al favoritismo de algunos editores, a la falta de transparencia y escenarios laborales discrecionales, difícilmente podremos pensar en que el periodismo de ciencia riguroso e interpretativo se podría encontrar en los grandes conglomerados de comunicación en México.

1.2 | ¿Cómo pueden verificar las fuentes las periodistas de ciencia?

Se propone que una de las obligaciones morales y éticas de quienes ejercen la profesión periodística es tener en cuenta que ante todo trabajan para los ciudadanos; la función social del periodista[22] hacia el público debería estar presente desde antes de comenzar cualquier proceso de investigación y escritura.

Lo siguiente es reconocer que una de las características de la información periodística es la veracidad; más allá de incluir contexto, datos y hechos para lograr una interpretación más

[20] Se observa en las estadísticas de la RedMPC que claramente hay un mayor número de personas del género femenino trabajando en esta área.
[21] Flores Gonzáles, Denisse Joana. *La cobertura de la contingencia ambiental (2016) en portales digitales de la ciudad de México. un estudio desde la sociología de producción de noticias.* Universidad Iberoamericana. México, Tesis de maestría, 2018, P.102.
[22] Se entiende como función social del periodismo a la elaboración de coberturas periodísticas que logren satisfacer las necesidades de información del público con el objetivo de que los ciudadanos tomen decisiones potenciales.

fidedigna de la realidad, las reporteras necesitan generar espacios que fomenten el debate público, y enfocarse en la síntesis y la verificación para el desarrollo de sus contenidos.

La Real Academia de la Lengua en su versión en línea define verificar como: "comprobar o examinar la verdad de algo"[23], coincide el Diccionario de Lógica y Filosofía de la Ciencia al mencionar que para ―verificar un aserto es establecer su verdad"[24]. Se podría entender, tal como aseguran Kovach y Rosenstiel que la esencia del periodismo es la verificación de las fuentes como disciplina de trabajo. La búsqueda de la verdad por principio.

―El periodismo debe destilar un problema y luego transmitirlo de una forma atrayente como sea posible, pero sin exagerar. El periodista está capacitado para hacerlo de la misma manera que un científico riguroso está capacitado para crear un experimento", compara Richard Flaste, editor del libro *Book of Science Literacy*[25].

Una de las propuestas para que las periodistas puedan conseguir que una afirmación coincida con los hechos es a partir del desarrollo y la implementación de un método de investigación formal más definido. Phill Meyer, catedrático de Periodismo de la Universidad de Carolina del Norte, hace alusión a la cercanía del periodismo y la ciencia, ambas, asegura, tienen las mismas raíces intelectuales. El investigador señala que ambos se originaron durante el periodo de la ilustración y en esencia, buscan a partir de una multiplicidad de voces y puntos de vista, identificar una verdad.

Sin embargo, para concatenar los posibles rasgos que caracterizan a la ciencia[26] en una historia, es aconsejable que además de seguir el ―instinto" periodístico, la reportera también pueda auxiliarse de modelos y métodos que le ayuden a incluir la ciencia en sus textos:

> ―…Creo que deberíamos hacer hincapié en la objetividad del método. Así es el método científico, nuestra humanidad, nuestros impulsos subjetivos orientados a la

[23] Diccionario de la Real Academia de la Lengua [En línea] Consúltese en: http://dle.rae.es/?id=beGg9NJ
[24] Mosterín, Jesús. *Et al. Diccionario de Lógica y Filosofía de la Ciencia. 2002.* P. 609.
[25] Flaste Richard (et.al), *The New York Times Book of Science Literacy*, The New York Times, 1992, USA, P.3.
[26] Revisar propuesta de rasgos Perfil de Ciencia Cap. 2.

> decisión de qué hay que investigar por medios objetivos. Bajo esta perspectiva, la imparcialidad y la equidad adquieren nuevo significado. Más que elevados principios son en realidad técnicas, mecanismos, que guían a los periodistas en el desarrollo y verificación de su trabajo"[27].

Emplear un método entendido como ~~–u~~n camino, un orden, conectado directamente a la objetividad de lo que se desea estudiar"[28], es muy útil para la escritura de textos sobre todo los especializados en ciencia debido a que las temáticas o las fuentes de donde proviene la información tienden a ser complicadas. Tom Siegfried, jefe de redacción de *Science News*, comenta que así como los periodistas enfocados a deportes cubren juegos u eventos especializados, los artículos científicos definidos como ~~–i~~nformes escritos que describen los resultados originales de una investigación ya realizada"[29] son la materia prima para las reporteras de ciencia.

Una de las características de este tipo de literatura especializada es su lenguaje monosémico, que no permite que una palabra tenga varios significados. La información expresada en este tipo de literatura es precisa, tal como el rigor de la ciencia lo demanda. Esa exactitud en los términos hace que su lectura sea por lo general densa, con una jerga compleja y difícil de ser entendida por alguien no especializado dentro del área de estudio.

Por ejemplo, la situación descrita por Aleida Rueda, coordinadora de la Unidad de Comunicación del Instituto de Física de la UNAM, y también conductora y guionista del programa *La ciencia en todos lados*[30] y *Refracción*[31], al enfrentarse a la lectura de artículos publicados en la literatura especializada: ~~–e~~l tema, el lenguaje, los conceptos y los procesos que describía me eran desconocidos, y el texto no sólo no los explicaba sino que daba por

[27] Kovach, Bill, Rosenstiel, Tom**.** *Op. cit.* 200. P. 64.
[28] Iglesias, Severo. *Principios del método de la investigación científica*. 1981. P. 12.
[29] Blanco Altozano, Pilar. *El artículo científico: puntualizaciones acerca de su estructura y redacción.* Consúltese en: http://www.ub.edu/doctorat_eapa/wp-content/uploads/2012/12/El-art%C3%ADculo-cient%C3%ADfico_aspectos-a-tener-en-cuenta.pdf.
[30] Una voz con todos (OPMA). *La ciencia en todos lados* Consúltese en: http://www.unavozcontodos.mx/
[31] TV UNAM, *Refracción*, Consúltese en: https://www.youtube.com/playlist?list=PLLYD2qbK_hDvM1FrpwRoqBeHsDISUk35Y.

hecho que yo (o cualquier lector) los conocería lo suficiente como para brincarse a niveles de complejidad mayores" [32].

Es por eso que el tema de facilitar la intrusión de los artículos científicos en los medios se vuelve una tarea compleja pero necesaria a la hora querer profundizar y dar a entender un tema de ciencia desde su origen.

1.2.1 | Trascendencia del uso de fuentes primarias

Para cumplir con el objetivo de aspirar a un periodismo que responda a las necesidades informativas de los ciudadanos, ~~el~~ tema de elección de fuentes debe ser atendido con mayor sofisticación pero también con agilidad"[33]. Se necesita incluir referencias capaces de ser verificadas, con las cuales se logre construir una mejor explicación a la hora de elaborar un trabajo periodístico.

Una de las propuestas para que las reporteras superen la tentación de sólo quedarse con la opinión no argumentada de unos cuantos científicos célebres y acudan a otro tipo de fuentes especializadas, menciona Gema Revueltas, subdirectora del Observatorio de la Comunicación Científica de la Universidad Pompeu Fabra, es procurar ~~el~~ contacto directo con los investigadores, asistir a congresos o reuniones profesionales y consultar revistas científicas"[34]

Las fuentes tienen la autoridad suficiente, cuando la investigación realizada por cada una de ellas ha sido exhaustiva y el método que utilizan es claro y digno de soportar cualquier escrutinio. Si las periodistas de ciencia quieren entrar en contacto con la comunidad

[32] Rueda, Aleida. *La síntesis como herramienta en el periodismo de ciencia. un análisis comparativo con su uso en la literatura infantil*. México, FCPyS-UNAM, Tesis de licenciatura, 2007. Consúltese: http://ru.ameyalli.dgdc.unam.mx/123456789/490.

[33] Cruz Mena, Javier. *Cómo elegir (y comprender) las fuentes en el periodismo de ciencia* en Jornalismo e ci ncia: uma perspectiva ibero-americana. Coordena o: Luisa Massarani. Rio de Janeiro: Fiocruz COC Museu da Vida, 2010, P. 50.

[34] Revueltas, Gema. *Fuentes de información en periodismo científico: congresos, revistas y press releases* en Jornalismo e ci ncia: uma perspectiva ibero-americana. Coordena o: Luisa Massarani. Rio de Janeiro: Fiocruz / COC / Museu da Vida, 2010, P. 54.

científica y encontrar la mejor información, una de las formas que pueden resultar más certeras es la lectura de artículos científicos.

Un artículo científico –también conocido popularmente en su término anglosajón como *paper*– se publica en revistas científicas especializadas. Un estándar de las secciones en las que se divide un texto especializado son: título, a*bstract*, introducción, materiales y métodos, resultados y conclusiones; el orden de aparición de estos apartados puede variar entre una revista a otra, e incluso tener más secciones si la investigación así lo amerita. Un ejemplo es *Proceedings of the National Academy of Sciences (PNAS)* revista que incluye la sección ~~–i~~mportancia" (*significance*), la cual puede ofrecer un resumen más profundo a las periodistas que quisieran escribir al respecto del artículo.

El también conocido como artículo de investigación (*research paper)* representa el conocimiento científico, su ~~–c~~redibilidad y prestigio se deben al sistema de revisión de pares o *peer review*"[35], el cual es el proceso de evaluación de los manuscritos enviados por los autores de una investigación en el que dos o más revisores externos, tan expertos en el tema o más que los propios autores, verifican la relevancia, autenticidad, originalidad, metodología, etc. de la investigación.

Existen parámetros que al ser aplicados ofrecen una cierta correlación respecto a la calidad o prestigio de una revista científica que publica un artículo y que la reportera puede utilizar como guía a la hora de elegir una publicación (*journal)*. Por ejemplo, el *factor de impacto* entendido como *"*el número de veces que se cita por término medio un artículo"[36]. Este sistema a pesar de ser el indicador bibliométrico ~~–m~~ás conocido y el más valorado por los organismos de evaluación de la actividad investigadora"[37], es objeto de críticas como que su base de datos de más de 12 mil revistas evaluadas no cubre ni el 50% del catálogo total que existe a nivel mundial, o de tener un fuerte sesgo a las publicaciones escritas en inglés.

[35] Guevara, Cervera *et al. Revisión por pares: ¿Qué es y para qué sirve?* P. 259
[36] Universidad de Salamanca. *Factor de impacto.* Consúltese en: https://bibliotecas.usal.es/factor-de-impacto
[37] Biblioteca Universidad de Sevilla. *Factor de Impacto: Journal Citation Reports (JCR).* Consúltese en: http://guiasbus.us.es/factordeimpacto

A lo largo de este trabajo de investigación se propone que al emplear fuentes originales de manera correcta y eficiente es una forma de mejorar la inclusión de la ciencia en trabajos periodísticos.

En estos momentos una de las fallas que se pueden encontrar en los medios es ~~–la~~ incapacidad de los reporteros de entender la ciencia a fondo"[38], dijo Antonio Lazcano, científico especializado en el origen y la evolución temprana de la vida, por lo que desarrollar modelos sugestivos para que las periodistas puedan entender mejor la esencia de la investigación podría ser una de las posibles respuestas para combatir dicha problemática.

Se pretende que las historias en las que se citan fuentes primarias sobresalgan de las que sólo se limitan a incluir anécdotas, personalizaciones o información enfocada a apoyar o perjudicar a ciertos grupos, para luego dejar que la sociedad reaccione y el proceso de discernimiento crezca.

El trabajo que aquí se desarrolla aborda uno de los grandes problemas dentro de esta área del periodismo especializado y es cómo las periodistas pueden informar la ciencia de forma más precisa. Esta tesis resulta importante porque como fin último pretende que gracias a la aplicación del modelo que será descrito ampliamente en el capítulo 2, el periodista pueda ser realmente crítico, tanto con los funcionarios encargados de manejar el gasto público – exigir rendición de cuentas – y sobretodo, con una de sus principales fuentes de información: los científicos. Más allá de mostrar lo ~~–d~~ivertida" e ~~–in~~teresante" que puede ser la ciencia, abrirla al escrutinio y a la crítica.

1.2.2 | Retos y alternativas para abordar la ciencia contenida dentro de un artículo científico

A partir de finales del siglo XX han aumentado las vías de acceso para consultar artículos científicos en línea, lo que ha impulsado su uso como fuente de las periodistas que escriben

[38] Antonio Lazcano. *Periodistas V.S científicos ¿se llevan o no se aguantan?* en el Primer Foro de Periodismo de la Ciencia, 28 de octubre del 2013, FCPyS.

sobre ciencia, así lo demuestra *Source diversity among journals cited in Science Times*[39], análisis de contenido de la sección de ciencia del diario *The New York Times* entre 1998 y 2012.

Esta situación también se observa en un sector de periodistas que laboran en la capital del país, al ser los artículos científicos una de las fuentes a las que más se apoyan quienes ejercen la profesión, según dice una encuesta de la Sociedad Mexicana para la Divulgación de la Ciencia y la Técnica, A.C.,[40]. Sin embargo, algunos estudios identifican graves dificultades al tratar de explicar artículos científicos a textos periodísticos[41] .

Las reporteras de ciencia usualmente cuentan con poco tiempo para la elaboración de sus textos, lo que hace que incluir información de artículos científicos sin investigación previa pueda convertirse en un reto proclive al fracaso. Cruz Mena asegura que ~~h~~ay que ofrecer al reportero herramientas para meterse en las revistas especializadas sin temor a perder el control sobre el proceso si es que hemos de sugerirle que las utilice como fuentes de información"[42].

En un intento por avanzar en el desarrollo de herramientas para incluir artículos científicos como fuente periodística, investigadores y periodistas han producido trabajos formales al respecto.

Una de ellas fue Aleida Rueda, quien en su tesis de licenciatura propuso una forma de leer artículos científicos a partir del concepto de síntesis, entendida como una ~~e~~xposición breve que incluye únicamente las ideas principales, los elementos informativos esenciales, que se necesitan para entender un texto original"[43].

[39] Kiernan, Vincent. *Source diversity among journals cited in Science Times*. P. 199.
[40] Somedicyt. *Encuesta para identificar a los periodistas de ciencia en la Ciudad de México*, Reporte de Resultados. 2016.
[41] F. Veneu, L.H. Amorim, L. Massarani. *Science journalism in Latin America: how the scientific information from a scientific source is accommodated when it is transformed into a journalistic story.* 2008. P.5.
[42] Cruz Mena, Javier. *Op Cit*. P. 50.
[43] Rueda, Aleida, *Op Cit*

El reto de enfrentarse a un artículo arbitrado, menciona Rueda, puede ser semejante al de leer una obra de literatura clásica, por lo que propone ~~–e~~l método de síntesis sucesiva", herramienta que auxilia a las reporteras a ser capaces de extraer la ciencia del artículo, a partir de la lectura del resumen del artículo. Un primer acercamiento para alcanzar lo que ella llama ~~–s~~íntesis científica digerida" es ~~–d~~esmenuzar", definir los conceptos elementales que explican la ciencia de la historia, los cuales pueden resultar desconocidos para el periodista. La reportera deberá recurrir a diferentes medios de investigación (Internet, libros, entrevistas, etc.) para descifrar su significado.

La clave para encontrar la ciencia de la historia, menciona Rueda, es entender la manera en que los autores argumentan sus conclusiones resumidas en el resumen (*abstract*). En el trabajo de Rueda, la argumentación se utiliza de dos formas: para distinguir entre una verdad o falsedad dentro de un artículo arbitrado y para explicar de forma lógica el contenido científico en un reportaje periodístico. Sin embargo, ~~–e~~l *abstract* en ocasiones no hace ninguna referencia a argumentos de tipo lógico, lo que obliga a la reportera a leer el artículo completo con el fin de descubrirlos"[44].

Al respecto, Jennifer Raff, escritora en la sección de ciencia en *The Huffington* Post y *The Social Evolution Forum*, en *How to read and understand a scientific paper: a guide for non- scientists* sugiere investigar el vocabulario científico del artículo científico que no se entienda pero advierte que no es aconsejable revisar el resumen hasta después de haber leído completo el artículo porque es posible que ~~–i~~nadvertidamente, se vuelvan sesgados los resultados por la interpretación de los autores"[45].

Raff aconseja revisar las publicaciones citadas en el *paper* con el objeto de encontrar trabajos relevantes en ese campo de estudio y encontrar más fuentes para contar la historia. Ella sugiere que el lector realice preguntas específicas acerca del texto en un inicio: ¿Qué

[44] *Ibíd*, P.93.
[45] Jeff, Jeniffer. *How to read and understand a scientific paper: a guide for non-scientists.* Disponible en Internet ¨. https://violentmetaphors.com/2013/08/25/how-to-read-and-understand-a-scientific-paper-2/ Disponible en Internet: [Consultado el 19 de diciembre del 2016]

es lo que quieren responder con su investigación? y ¿cómo planean responderlo? mientras en los resultados ¿se contestan las preguntas específicas? ¿Qué es lo que piensan los investigadores que los resultados significan? ¿Identificaron debilidades en su estudio? ¿Qué es lo que proponen para un siguiente paso?

Otros autores que se han sumado a este esfuerzo por facilitar el uso de textos de investigación como referencia fueron Bernard Appiah, sub editor regional para la edición de África Subsahariana y Juan Casasbuenas, coordinador de capacitaciones de SciDev.Net, quienes en –Cómo reportar a partir de un artículo científico" corroboran la propuesta de Jennifer Raff de leer un *paper* enfocándose en diversos aspectos específicos incluidos en cada sección, por ejemplo: en *metodología* revisar el tamaño de la muestra; y coincide con los resultados del trabajo de Rueda al hacer explicita la idea de que en la última parte del *resumen* se encuentran descubrimientos claves de la investigación.

El trabajo de todos ellos trata de ser una respuesta proactiva ante el escenario en que en ocasiones las periodistas hacen un uso errado de los artículos científicos, sin embargo hacen falta incrementar esfuerzos para realizar más trabajos de investigación a gran escala en la materia desde ambos sentidos: la academia y en la práctica periodística.

En la Unidad de Periodismo (UdP) de la DGDC desde 2004, se proponen y desarrollan herramientas para realizar análisis de contenido más robustas comparadas con las tradicionales y se elaboran instrumentos que buscan ayudar a las periodistas a generar historias para satisfacer las necesidades informativas que requieren los ciudadanos: "en la evaluación de la calidad del periodismo de ciencia debe verse más allá del mero espectro temático en busca de lo que es la esencia del discurso científico: la lógica de la argumentación"[46], explica Javier Cruz Mena, editor en jefe de la UdP.

[46] Cruz Mena, Javier. *Las universidades como fuentes de información científica en crisis sociales: La epidemia del SARS como caso de estudio* Primer Congreso Iberoamericano de Comunicación Universitaria, México, 2003, p11

El trabajo de la UdP está orientado a que periodistas sin más formación científica que la adquirida durante la educación pre universitaria – preparatoria o bachillerato– puedan verificar la ciencia en cada historia periodística por redactar.

En una primera aproximación se podría entender que un texto es de *ciencia* si se requiere incluir razonamientos lógicos rigurosos de, por ejemplo, relaciones causa y efecto, además debe estar fundamentado en afirmaciones racionales, explicaciones y evidencia empírica que ayude a entender el argumento básico de un acto de ciencia; el problema es cuando las reporteras se preguntan ¿cómo es posible incluir todos estos elementos en mis labores cotidianas?

En los últimos cuatro años, como parte de los proyectos teóricos impulsados en comunicación pública de la ciencia en México, la UdP ha construido una herramienta de investigación periodística que tiene como uno de sus objetivos finales el facilitar a periodistas el acceso a la información científica, a pesar de las limitaciones de tiempo y espacio que el medio de comunicación por lo regular impone. Su ventaja reside en:

—[En la UdP] trabajamos con la hipótesis de que es posible acercarse al dominio de estas habilidades mediante tres hebras de actividad: el ejercicio, la docencia y la investigación académica del periodismo de ciencia"[47]. Dentro de esta última parte, se busca desarrollar vías que ayuden a la identificación de la ciencia contenida en artículos arbitrados para que sea incorporada en la narrativa periodística, sin importar el área de estudio.

Con el auxilio de este tipo de herramientas se pretende que el profesionista mantenga el rigor fundamental para elevar la calidad del debate y logre adquirir la experiencia necesaria para proporcionar la información relevante para fomentar los procesos de decisión ciudadana.

Se busca que luego de la aplicación del modelo, el cual será descrito a detalle a continuación, sea posible identificar contenido de ciencia. El Perfil de Ciencia fue diseñado

[47] [47] Ibíd, P,43.

para operar en dimensiones académicas y periodísticas. En la presente investigación se revisará el grado en que los rasgos del Perfil representan la ciencia en donde es comunicada por primera vez, en los artículos científicos.

Capítulo 2

Perfil de Ciencia: sus rasgos y cómo entenderlos

Centrar las historias de comunicación de la ciencia en ―avances" o ―hallazgos" y dejar de lado los efectos y el alcance de las investigaciones científicas es una situación que se presenta en los medios masivos[48]. La tendencia a la homogeneización de la información como resultado de la influencia de boletines de prensa generados por agencias noticiosas y universidades, unidades de comunicación, organismos gubernamentales y de la sociedad civil organizada[49] puede afectar la práctica del periodismo de ciencia.

Ambas situaciones han sido documentadas previamente [*Revisar 1.2 Análisis de la función y la actividad del periodista de ciencia*]. En el caso de la cobertura de fuentes primarias, Veneu, Amorim y Massarani[50] rastrearon la forma como fue retomada la información científica publicada en cuatro artículos de las revistas *Science* y *Nature* por siete diarios latinoamericanos, incluido el periódico mexicano *Reforma*. En el estudio, con una muestra de 482 historias analizadas, se observó que las reporteras al momento de trasladar la ciencia introducen cambios importantes de las ideas originales del artículo científico, e incluyen información que aparece o desaparece deliberadamente, así como se presentan errores por traducciones deficientes[51].

De igual forma en *From journal to headline: the accuracy of climate science news in Danish high quality newspapers* se realizó un estudio para examinar la precisión de los

[48] Flores González, Denisse Joana. *Op cit.* P. 169.
[49] Arboleda,Tania, *Et al; Ciencia y Tecnología en los telediarios colombianos: sobre lo que se cubre y no se cubre.* P. 220
[50] Veneu, Fernanda, *OP Cit* P. 6
[51] Luego de comparar el artículo original con la nota ―Hallan antiguo fósil de gato domesticado" se encontraron las siguientes diferencias: "El esqueleto del gato estaba ubicado en la misma unidad estratigráfica a tan solo 40 cm de un entierro humano", en cambio lo reportado por *Reforma* fue: El esqueleto de un gato de 40 cm fue encontrado por Jean-Denis Vigne y sus colegas de Museo Nacional de Historia Natural en Francia.

diarios daneses al momento de citar revistas científicas. De 88 artículos publicados entre 1997 a 2009, 46 contenían inexactitudes, aunque la mayoría los autores consideraron como intrascendentes[52].

Algunos de sus resultados fueron: errores de dedo en el 16% de los artículos analizados; transcripción deficiente de términos científicos básicos; confusión entre las afirmaciones revisadas por pares en las publicaciones científicas con las declaraciones orales realizadas por el investigador; parafraseo extraído del boletín de prensa que se hace pasar por información incluida en el artículo científico e hipótesis que se entendieron como hechos.

A pesar de que ambas investigaciones verifican las equivocaciones ocurridas durante este proceso, en el caso del periodismo realizado en Dinamarca se presentaron avances: –En el primer año de análisis (1997), 63% de los artículos citados como fuente periodística contenían inexactitudes, en cambio para 2009, sólo 38% presentaron errores" [53] Lystbæk considera que esto corresponde al foco de atención que los medios de comunicación concedieron al tema, es decir, entre mayor cobertura hubo al respecto se obtuvieron mejores bases para entender el tema y, por lo tanto, favorece a la especialización periodística en la ciencia del cambio climático.

Lo anterior confirma la necesidad de contar con mayor preparación para abordar asuntos que requieren explicar su ciencia. El objetivo es mejorar la práctica periodística, y por ende, lograr que más editores puedan justificar y hacer presión para conseguir espacios en sus medios: –según Lewenstein (1987), los primeros éxitos de la sección fueron utilizados por una cadena de editores de periódicos. . . para justificar sus propias nuevas secciones científicas"[54].

[52] Lystbæk, Gunver. *From journal to headline: the accuracy of climate science news in Danish high quality newspapers.* P. 3
[53] Lystbæk, Gunver. *Op cit* . P. 4
[54] Clark, Fiona, et al. *A Longitudinal Study of the New York Times Science Times Section.* P. 31

En general, pocos se han encargado de realizar análisis que revisen el recorrido de la información científica de los reportes originales a los medios masivos. Tando Veneu como Lystbæ en sus artículos de investigación hacen explicita esta preocupación, por lo que abonar en trabajos que ahonden al respecto se vuelve un imperativo para contribuir en la formalización de análisis en temas de cobertura científica.

Dentro de estos esfuerzos es importante considerar el trabajo de investigación realizado por Aleida Rueda, texto analizado a detalle en el capítulo 1 de esta tesis, con el cual se establecieron las bases para que las periodistas entendieran la ciencia gracias a la detección de ciertos detalles de la demostración lógica: la causa y efecto de un fenómeno, así como la evidencia empírica y/o inferencias estadísticas que dan pie a las conclusiones.

Este análisis representa la extensión de dicho proyecto. La construcción del Perfil de Ciencia fue desarrollada entre Javier Cruz, Michelle Morelos, Itzel Gómez y Yanine Quiroz, la cuales es un componente más reciente de la primera propuesta que Rueda estableció; ahora esta versión cuenta con más rasgos y es más robusta para cumplir el objetivo de facilitar el proceso de entender e incluir la ciencia en un trabajo periodístico.

En esta tesis se propone que el Perfil puede servir para el análisis de contenido en productos periodísticos ya publicados o servir como instrumento para la planeación de un trabajo de periodismo de investigación para reporteras.

Esta herramienta se integra dentro de un modelo de verificación periodística de ciencia, desarrollado gracias a las aportaciones teóricas de las tesis de licenciatura realizadas en la Unidad de Periodismo de la Dirección General de Divulgación de la Ciencia de la UNAM. Estas herramientas son: una Tabla de Intereses Ciudadanos para identificar los puntos de información esenciales; y un método de lectura comprensiva de artículos científicos en tiempos periodísticos.

2. 1| Categorías de análisis

Con el fin de establecer y optimizar trabajos teóricos capaces de optimizar la utilización de artículos en historias periodísticas, hemos desarrollado este modelo original de identificación de contenido de ciencia para operar en dimensiones académicas y periodísticas.

–El Perfil de Ciencia lleva implícita la hipótesis de que puede hacerse un "retrato hablado" de la argumentación científica a partir de un conjunto relativamente pequeño de "rasgos" de la ciencia, cada uno de los cuales responde, además, a una pregunta periodística"[55].

Esta herramienta se compone de las siguientes categorías:

1. Definiciones	¿Qué significa este término? Proviene del latín *definitio*, que significa delimitar. Conjunto de palabras que expresan con claridad y precisión la significación de un concepto, palabra o frase. Ayuda a generar la comprensión del término y delimita lo que es para distinguirlo con respecto a lo que no es. En ciencia, las definiciones tienden a ser monosémicas (i.e., con un solo significado).
2. Magnitud	¿Cuáles son las dimensiones de este fenómeno? Da idea de la grandeza y la importancia, absoluta o relativa, de forma cuantitativa o cualitativa. Cuando el fenómeno es percibido como "problema", importan las magnitudes de: i) el

[55] Cruz, Mena. *Un modelo de formación universitaria en Periodismo de Ciencia* presentado en Simposio PCST Costa Rica –Comunicación científica como profesión: Formación, responsabilidades y roles". 2016. P. 5.

	problema; ii) la intervención; y iii) los efectos de la intervención.
3. Evidencia empírica	¿Cómo saben lo que afirman? De la raíz indoeuropea *per-* (poner a prueba, arriesgar), es conocimiento producido mediante actos de ciencia que buscan "ver" en un sentido amplio: mediciones, experimentos, observaciones, simulaciones por computadora, pruebas clínicas, encuestas, etc.; y suele presentarse en forma de tablas, gráficas, esquemas, fotografías, animaciones, material audiovisual, etc.
4. Incertidumbre	¿Qué seguridad tienen de los valores numéricos encontrados y las aseveraciones propuestas? Toda medición lleva asociado un rango en cuyo interior se encuentra, con la mayor probabilidad, el valor de la variable medida. (Cuanto más ancho es ese intervalo, menor es la precisión de la medida.) Los reportes científicos suelen señalar las limitaciones de la investigación; éstas sirven para estimar la incertidumbre no cuantitativa de sus conclusiones.
5. Hipótesis	¿Qué sospechan que sucede y por qué? Del griego τεσιζ (proposición), es la base de un argumento aún por sustanciar. Relación de causa-efecto (A=>B) respecto de la cual hay razones para creer que es cierta, pero que aún no ha sido plenamente demostrada.
6. Explicación	¿Por qué y cómo suceden las cosas de cierta forma? Del latín *explanare* (hacer plano, claro), expone las razones de

	los fenómenos mediante la secuencia en que las causas siguen a los efectos.
7. Desarrollo Matemático	Formulación y solución de ecuaciones; cálculos algebraicos; inferencia estadística; aproximaciones y simplificaciones.
8. Predicción	¿Qué afirman que sucederá? Relación de causa-efecto para la cual se tiene un alto nivel de convicción con base en un buen número de verificaciones previas. Suele formularse como una relación causal en que, si la casa ocurre en el presente, el efecto se manifestará, consecuentemente, en el futuro.

Tabla 2.1. Perfil de Ciencia

Esta versión del Perfil se ha utilizado desde hace un año, tanto en este trabajo de tesis como en otros[56]proyectos, los cuales han tenido resultados definitivos y preliminares robustos.

La herramienta forma parte de una investigación realizada en la Unidad de Periodismo de la DGDC de la UNAM busca revisar si los rasgos del Perfil son susceptibles a ser identificados en artículos publicados en la literatura especializada. Durante los siguientes apartados se explicará cada uno de los rasgos junto con tres ejemplos que ayuden a la comprensión de los mismos.

[56] Los otros tres proyectos de investigación que aplican el Perfil de Ciencia tienen como título: "Periodismo ambiental: un examen de la ciencia contenida en la cobertura de la Cumbre del Clima de París (COP21) en TV pública"; –Infografías de ciencia: un análisis en el periodismo visual" y –Análisis de noticias de ciencia en cinco medios televisivos públicos: nacionales e internacionales con base en un modelo de verificación periodística de la ciencia".

Capítulo 3

Metodología de análisis: Diseño de algoritmos y proceso selectivo de lectura

Con el objetivo de analizar en qué medida los ocho rasgos del modelo presentado caracterizan la ciencia dentro de los artículos arbitrados, se elaboró una prueba que consistió en dos etapas. Primero, la conformación de un *corpus* de 19[57] artículos publicados en 7 revistas arbitradas: 4 de ellas preseleccionadas por su relevancia como fuentes periodísticas en la cobertura de ciencia a nivel global (*Nature, Science, Proceedings of the National Academy of Science y Public Library of Science PLOS ONE*), y 3 elegidas de manera aleatoria mediante algoritmos específicos[58]descritos cada uno a continuación.

Para encontrar los artículos individuales en las publicaciones se establecieron una serie de pasos a realizar para cada caso. El desafío general consistió en encontrar: una página, un número y volumen de una publicación, y en el caso de las revistas no predeterminadas, incorporado en una publicación igualmente desconocida.

Para la obtención de dicha información se decidió que fuese a partir de la generación de números aleatorios obtenidos por medio de una plataforma disponible en línea; la pregunta de trabajo fue: ¿cuántos dígitos eran necesarios? Esta búsqueda se muestra gráficamente de la siguiente manera:

[57] En este trabajo de investigación se aplicó la metodología a 20 artículos científicos, sin embargo, se detectaron irregularidades en su proceso de selección lo que provocó fuera desechado para la contabilización de resultados.

[58] La creación e idea de los algoritmos descritos en este capítulo fueron desarrollados en conjunto con el director de esta tesis, Javier Cruz Mena.

Página	->	Número / *Issue*	->	Volumen	->	Título*
Objetivo final						*Sólo en el caso de revistas no predeterminadas

Fig. 3.1 **Representación del flujo de búsqueda**

Después de establecer los dígitos con base en una serie de lineamientos que serán explicados a lo largo de este capítulo se ejecutaron los algoritmos de general a particular, es decir, encontrar primero el título de la revista, el volumen, número y, al final, hasta determinar la página:

Número aleatorio	Título	->	Volumen	->	Número /Issue	-> Página

Fig. 3.2 **Lógica de ejecución de algoritmo**

Una vez encontrado el nombre del artículo, se ejecutó la segunda parte del trabajo: realizar un proceso de lectura a cabalidad de los diecinueve *papers*, identificando los rasgos del Perfil que aparecían en cada uno para ser registrados después en un formato específico.

3. 1 | Selección aleatoria de publicaciones y artículos científicos

3.1.1 Publicaciones no predeterminadas

La pre-condición indispensable fue eliminar toda posiblidad de sesgo en la recopilación de la muestra. La manera de hacerlo fue gracias al desarrollo de un proceso de selección aleatoria capaz de determinar títulos de revistas.

El reto fue ubicar nombres al azar de publicaciones arbitradas dentro del universo de revistas científicas alojadas en un repositorio que tuviera un gran número de títulos en su base de datos. Para lo cual se tuvieron que realizar dos tandas de números aleatorios de seis

cifras: la primera para encontrar el título de la revista, la segunda para determinar el título del artículo. Los detalles de la propuesta se describen a continuación.

3.1.1. Proceso aleatorio para determinar títulos de revistas

Para seleccionar el título de un artículo científico de forma aleatoria se siguió un proceso de búsqueda similar al que se sigue para encontrar un libro en una biblioteca cuando se desconoce el título del documento. Al inicio se camina ~~"a~~ ciegas" por el recinto, dirigiéndose intuitivamente a un pasillo sin saber qué ruta elegir.

Con esta metáfora se eligió a la ~~"b~~iblioteca virtual" SERIUNAM, el catálogo de revistas de la UNAM, el cual tiene una base de datos de más de 53 mil títulos de revistas y 9 millones de fascículos de publicaciones que cubren prácticamente todas las áreas del conocimiento científico y cultural.

El orden de los pasillos fue con base en la Clasificación de la Biblioteca del Congreso de los EEUU (LCC, por sus siglas en inglés), elegido para encontrar los documentos por analizar debido a su importancia y organización estructurada de las distintas áreas de la ciencia. Un gran número de bibliotecas o centros de investigación académica, incluidas las de la UNAM, utilizan el LCC para su organización. Éste emplea las letras de uso estándar del abecedario para catalogar y ordenar libros de ciencia e interés general. El sistema se compone por tres letras y números: la primera letra representa una categoría, y las dos siguientes, de izquierda a derecha, definen una sub categoría; los números que lo conforman pueden ser de tres a cuatro dígitos. Las temáticas de esta clasificación son:

A	Obras generales
B	Filosofía. Psicología. Religión
C	Ciencias Auxiliares de la Historia
D	Historia, General y Antigua
E	Historia: Estados Unidos
F	Historia Local de los Estados Unidos y de América Inglesa, Holandesa, Francesa y Latina
G	Geografía. Antropología. Recreo
H	Ciencias Sociales
J	Ciencia Política
K	Derecho
L	Educación
M	Música y Libros sobre Música
N	Bellas Artes
P	Lengua y Literatura
Q	Ciencia
R	Medicina
S	Agricultura
T	Tecnología
U	Ciencia Militar
V	Ciencia Naval
Z	Bibliografía. Biblioteconomía. Recursos Informativos (General)

***Figura 3.3*. Clasificación de categorías generales del LCC**

El LCC incluye áreas como: ~~–~~Religión y Ética" o ~~–~~Bellas artes. Música", las cuales no son una ciencia, por lo tanto, son eliminadas para esta investigación. Es decir, esos ~~–~~estantes" de la biblioteca no serán consultados, las letras se descartan y sólo se toman en cuenta áreas relacionadas con la variedad temática de los artículos a analizar con el Perfil de Ciencia: G, H, Q, R, S y T [Véase: *Figura 3.3. Clasificación de categorías generales del LCC*].

3.1.1.1 Categoría general del LCC

Para asegurar la aleatoriedad de los resultados y lo que va a dictar el rumbo desconocido durante el camino por el recinto, se empleó el Generador de Números en línea *Nosetup* (http://nosetup.org/php_on_line/numero_aleatorio_2). La pregunta inicial fue: ¿cuántos dígitos aleatorios se necesitan para elegir ~~–a~~ ciegas" un título de revista? Para ello, se convirtieron las primeras dos letras del LCC a números.

El primer paso es sustituir la letra por un dígito para encontrar la categoría a utilizar. Se enumera en orden progresivo cada una:

1-> G Geografía, antropología

2-> H Ciencias sociales

3-> Q Ciencias

4-> R Medicina

5-> S Agricultura

6-> T tecnología

El número por seleccionar es de un solo digito y debe encontrarse dentro de 1 a 6. El problema con esta alternativa es que *Nosetup* arroja resultados del 1 a 9, es decir, en ocasiones el dígito máximo establecido puede ser superado. La solución fue restarle el límite superior del rango (6) al dígito obtenido, que puede ser 7, 8 y 9 de esta forma el número resultante siempre está incluido entre algunas de las categorías[59].

En resumen, para encontrar la categoría del LCC se elaboró el criterio de intercambiar letras por dígitos, y cuando fue necesario, se establecieron reglas para que el número conservara su carácter de número aleatorio. Si seguimos la analogía, lo anterior permite que el generador de números al azar dicte el rumbo por avanzar en la biblioteca, y en caso de extravío en un área de estudio distinta a la de interés, se conozca la ruta de regreso.

3.1.1.2 Sub categoría general del LCC

El segundo paso fue encontrar la subcategoría, compuesta por la unión de un área general [Véase: *3.1.1.1 Categoría general del LCC*] y una nueva letra que determina una temática de estudio más específica. Tal como en el paso anterior, se tomó la decisión de continuar

[59] Este algoritmo no cumple con el criterio de asegurar aleatoriedad luego de su aplicación por lo que se recomienda no sea utilizado en otra investigación. En este trabajo de tesis no se reflejó ningún tipo de sesgo en los resultados finales luego de utilizar este algoritmo, ya que hubo una presencia equilibrada de categorías del LCC: (4) medicina, (2) ciencias sociales, (3) ciencias y (6) tecnología. Por lo que no afecta a los objetivos de eliminar el sesgo en la elección e impedir que la muestra de análisis fuera construida con inclinaciones a algún área de la ciencia en particular

con la equivalencia de letras por dígitos, pero en lugar de una sola cifra se necesitan dos porque las letras de la sub categoría tienen un rango más amplio (A – Z). Para resolver esta cuestión tomé como referencia el orden que ocupan las letras del abecedario y las enumeré: *A* corresponde a 01 y *B* 02, así sucesivamente.

Con lo anterior se busca obtener cifras compuestas por las 27 letras del abecedario. El problema reside cuando los números aleatorios generados por el programa en línea son mayores al límite. El criterio establecido fue restar el número máximo (27) las veces que fueran necesarias hasta que –eayera" o estuviera en el rango marcado.

Por ejemplo: en el número aleatorio 2 77 372, la segunda y tercera cifra conforma 77, un número mayor al límite establecido. Si restamos 27 a 77 en dos ocasiones (77-27=53 y 53-27= 23), el resultado es la posición de una letra del abecedario [*Véase: Tabla 3.2. Posición numérica de letras del abecedario*], la cual determina la subcategoría. En esta ocasión la letra seleccionada fue la V (23 -> V). Para consultar el resultado final del número aleatorio 277372 revisar *Tabla 3.4. Ejecución y resultados generales para selección de revistas no predeterminadas*, apartado 2.

1. **G Geografía, Antropología**	**2. H Ciencias Sociales**
G Geografía en General	H Ciencias Sociales en General
GA Cartografía	HA Estadísticas
GB Geografía Física	HB Teorías Económicas, Demografía
GC Oceanografía	HC Historia Económica
GF Ecología Humana	HD Industrias, Economía Laboral y Agraria
GN Antropología	
GR Folklore	HE Transportación y Comunicaciones
GT Maneras y Costumbres	HF Comercio: Contabilidad, Mercadeo
GV Deportes y Recreación.	HG Finanzas
	HJ Finanzas Públicas
	HM Sociología: General y Teorías

	HQ Familia, Matrimonio, Hogar HT Sociología Urbana y Rural HV Criminología HX Socialismo, Comunismo, Anarquismo, Bolchevismo, Utopías
3. Q Ciencias Q Ciencias en General QA Matemáticas, Ciencias de Computadora QB Astronomía QC Física QD Química QE Geología QH Historia Natural, Biología QK Botánica QL Zoología QM Anatomía Humana QP Fisiología QR Microbiología	**4. R Medicina** R Medicina en General RA Aspectos Públicos de la Medicina RB Patología RC Medicina Interna, Psiquiatría, Neurología RD Cirugía RE Oftalmología RF Otorrinolaringología: Oídos, Nariz y Garganta RG Ginecología y Obstetricia RJ Pediatría RK Odontología RL Dermatología RM Terapéutica, Farmacología RS Farmacia y Materia Médica RT Enfermería RX Homeopatía RZ Otros Sistemas de Medicina: Quiropráctica, Osteopatía
5. S Agricultura S Agricultura en General SB Cultivo de Plantas SD Ciencia Forestal	**6. T Tecnología** T Tecnología en General TA Ingeniería General y Civil TC Ingeniería Hidráulica y Oceánica

SF Ganadería SH Acuacultura SK Caza, Manejo de Vida Silvestre, Vida al Aire Libre	TD Tecnología Ambiental, Ingeniería Sanitaria TE Ingeniería de Carreteras TF Ferrocarriles TG Construcción de Puentes TH Construcción de Edificios TJ Ingeniería Mecánica TK Ingeniería Eléctrica, Electrónica, Ingeniería Nuclear TL Vehículo Motor, Aeronáutica, Astronáutica TN Ingeniería Minera. Metalurgia TP Tecnología Química TR Fotografía TS Manufacturas TT Manualidades TX Economía Doméstica

Tabla 3.1. **Áreas temáticas del LCC**

Una vez que ya tenemos la categoría y sub categoría seleccionada, el último paso fue juntar las últimas tres cifras aleatorias. Su objetivo final será identificar el registro más cercano en la base de datos de SERIUNAM (más adelante se explicará a detalle el proceso).

3.1.2 Ejecución

El diseño de esta parte del análisis se divide en dos: el desarrollo del código (ubicar la categoría y sub categoría) y la búsqueda en la base de datos de SERIUNAM.

El primer paso para su realización es obtener los números aleatorios. Para generarlos es necesario ingresar a la página de *Nosetup*, http://nosetup.org/php_on_line/numero_aleatorio_2 y agregar los siguientes datos en los espacios vacíos:

Inicio: 0
Final: 699999 } Rango de posibles combinaciones de números de 6 cifras

La selección del primer número (6) se debe a que tenemos seis áreas del conocimiento que determinan la categoría del LCC (Geografía, Antropología; Ciencias sociales; Ciencias; Medicina; Agricultura; Tecnología), las cuales son propicias para el análisis con el Perfil. Los demás dígitos no tienen ningún otro tipo de regla o prohibición.

Número de veces: 6 } La cantidad de veces que se repite dicho conjunto

La razón de elegir esa cantidad de repeticiones fue arbitraria. Cualquier número seleccionado no afecta la veracidad ni la funcionalidad del algoritmo propuesto, sólo el sistema *Nosetup* lo pide como obligatorio.

Resultado: **486236**, **312 221**, 277372, 346625

Para explicar en detalle este proceso utilizaré como primer ejemplo el siguiente resultado del generador: 486236. El 4, la primera cifra, se va a intercambiar por una categoría del LCC enumerada previamente del 1 al 6 (1= G Geografía, antropología, 2= H Ciencias sociales, 3= Q Ciencias, 4= R Medicina, 5= S Agricultura, 6= T tecnología).

El **4** corresponde a **R**, es decir, a la categoría de **Medicina.**

Ahora; para determinar la sub categoría a través de la conversión de los dos números siguientes (posiciones 2 y 3 dentro de la sucesión numérica de los 6 dígitos aleatorios) a letras, se desarrollaron las siguientes reglas:

- **Si las dos cifras son mayores que 27:** Se resta el número 27, cifra máxima de letras del abecedario, las veces que sean necesarias para que el número resultante se localice entre 1 y 27. Se aplica la primera regla.

Siguiendo con el ejemplo 4**86**236, el segundo y tercer dígito forman 86 por lo que se resta en tres ocasiones 27 para obtener el número 5, el cual se encuentra dentro del rango del 1 al 27. La letra ubicada en la quinta posición del abecedario es la **E**. Al combinarse con el primer resultado (**RE**) se determina que el área de la ciencia del artículo por analizar es **Oftalmología**.

A	B	C	D	E	F	G	H	I	J	K	L	M	N	Ñ	O	P	Q	R	S	T	U	V	W	X	Y	Z
01	02	03	04	05	06	07	08	09	10	11	12	13	14	15	16	17	18	19	20	21	22	23	24	25	26	27

Tabla 3.2. **Posición numérica de letras del abecedario**

- **Si las dos cifras están dentro del rango del 01 al 27:** Se localiza el número en el lugar que le corresponde en el orden del abecedario. Un segundo caso que sirve como ejemplo es el número aleatorio 3**12** 221, se utiliza el 12: la letra del abecedario que se encuentra en esa posición es la L.

Para definir la categoría y sub-categoría se combina la primera letra resultante con la segunda y se revisa si la combinación existe en la *Tabla 3.1*. Áreas temáticas del LCC. En la primera prueba se unió la letra Q (3) con la L; QL en la clasificación de la biblioteca del congreso es **Zoología**.

Con el objetivo de ubicar las combinaciones construidas en la base de datos, se va a agregar al par de letras producidas (QL y RE) las últimas tres cifras arrojadas por el generador de números al azar *Nosetup*:

- **QL 221**
- **RE 236**

Paso 1. Número aleatorio	Paso 2. Elección de categoría general del LCC	Paso 3. Elección de sub- categoría del LCC	Paso 4. Base de datos	Resultado
486236	4= R Medicina	86-27= 59 59-27= 32 32-27=**5** **5= E** **RE Oftalmología**	486 236	**RE 236**
312 221	3= Q Ciencias	**12= L** **QL Zoología**	312 221	**QL 221**[60]

Tabla 3.3. **Proceso aleatorio de selección de revistas y artículos de investigación**

El siguiente paso del proceso, una vez que generado el código, es ingresar al motor de búsqueda en línea SERIUNAM. En el recuadro en blanco se escribe la clave obtenida en la primera parte del procedimiento para obtención de títulos de revistas (**RE236**); en clasificación se seleccionará la opción "*Clasificación LC*" y por "*Palabras*". Se debe marcar la opción "*Toda la base*". La búsqueda no se limita ni por idioma ni por año.

Fig. 3.4 **Página principal SERIUNAM [http://bibliotecas.unam.mx/index.php/catalogos]**

[60] Esta combinación no fue elegida dentro de los títulos que sirvieron para el análisis con el Perfil debido a que la revista obtenida no era de acceso gratuito y el convenio con la UNAM se había terminado.

Al dar clic en buscar, aparece una tabla de dos columnas *"No. Registros"* y otra en la que se ordena de menor a mayor los registros encontrados. Es probable que no aparezca tal cual la combinación RE236, pero se selecciona la que más se acerque. El registro con menor rango de diferencias es **re336.**

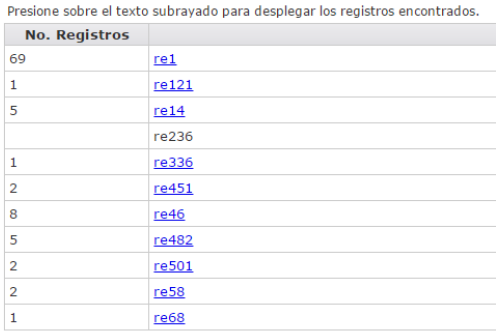
Presione sobre el texto subrayado para desplegar los registros encontrados.

No. Registros	
69	re1
1	re121
5	re14
	re236
1	re336
2	re451
8	re46
5	re482
2	re501
2	re58
1	re68

Fig. 3.5. **Lista de registros relacionados a RE236 en SERIUNAM**

Seleccionamos el registro y de inmediato aparece en la pantalla "Vista completa del registro" entre los datos que se proporcionan están el título, clave de la revista, datos de publicación, frecuencia actual, texto completo, etc. Empleando esta metodología, la revista resultante fue: ***Cornea (New York, N.Y. En línea)***[61]**.**

[61] Esta prueba fue realizada en Febrero del 2015, por lo que en caso de que el sistema de SERIUNAM o NOSETUP cambie es necesario realizar las adecuaciones pertinentes al trabajo a continuación propuesto.

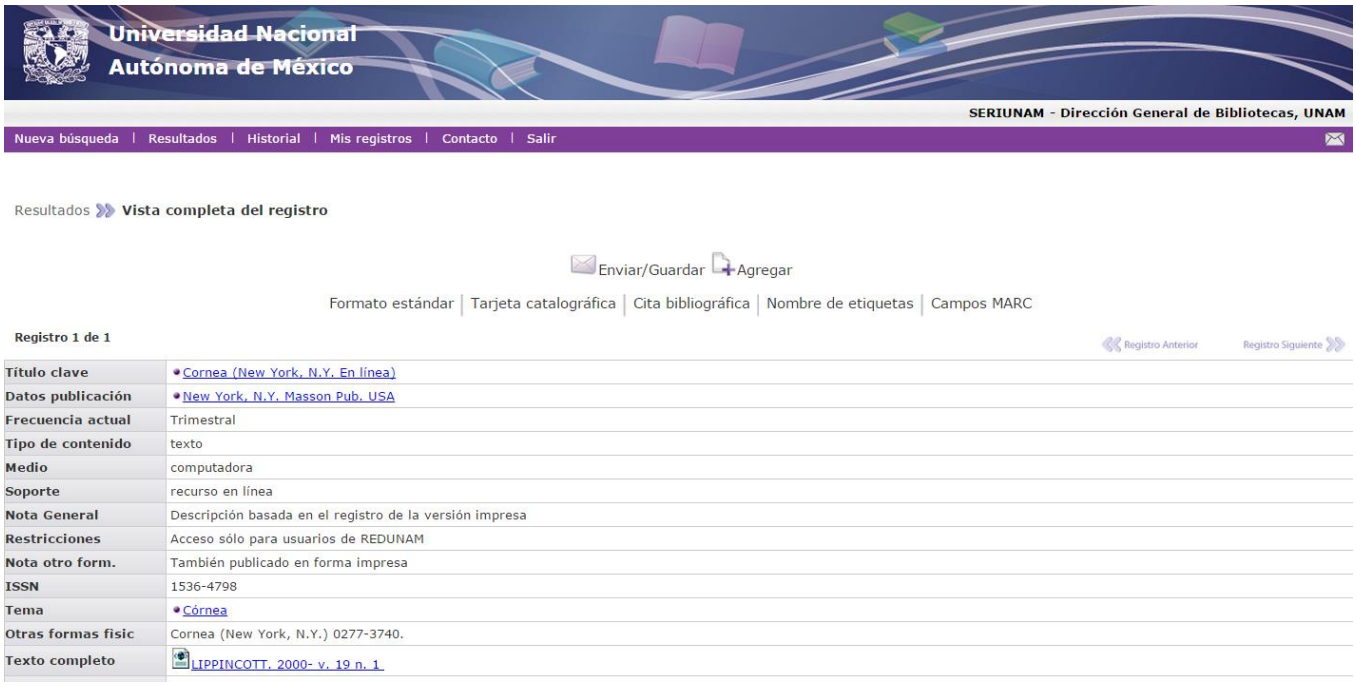

Fig. 3.6. **Vista completa del registro**

3.1.3 Resultados

El ejercicio se puede resumir en el siguiente esquema:

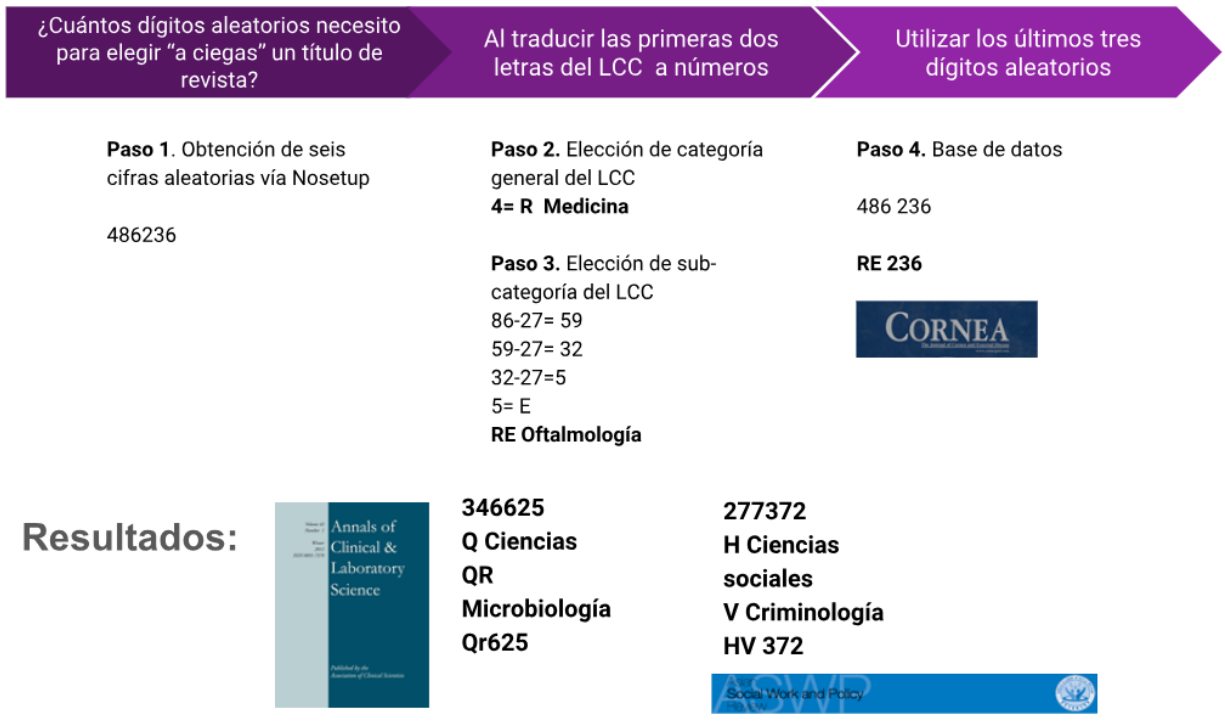

Para encontrar los títulos de las 4 revistas realicé este proceso en más de 25 ocasiones. Repetí algunos de los códigos porque las combinaciones de primeras dos letras no coincidían con ninguna categoría y sub-categoría del LCC, el idioma de la revista era distinto al inglés o español, eran revistas sin revisión de pares; o el acuerdo con la UNAM había terminado y era necesario pagar para obtener el acceso a los artículos más recientes.

Esta primera etapa se completa con la tabla de resultados generales:

Número aleatorio	**Categoría**	**Sub categoría**	**Combinación SERIUNAM**	**Resultado final**
1. 486236	4= R Medicina	86-27= 59 59-27= 32 32-27=5 5=E RE Oftalmología	re236/ re336	Cornea (New York, N.Y. En línea) http://journals.lww.com/corneajrnl/pages/default.aspx
2. 277372	2= H Ciencias sociales	77-27= 50 50-27= 23 23= V HV Criminología	hv372/	Asian social work and policy review http://onlinelibrary.wiley.com/doi/10.1111/aswp.2014.8.issue-1/issuetoc
3. 346625	3= Q Ciencias	46-27=19 19= R QR Microbiología	Qr625/ qr672	Annals of clinical and laboratory science http://www.annclinlabsci.org/site/misc/about.xhtml

Tabla 3.4. **Ejecución y resultados generales para selección de revistas no predeterminadas**

3.1.2 | Selección aleatoria de artículos científicos en revistas no predeterminadas

En la primera etapa se encontraron 4 diferentes títulos aleatorios de revistas: *Cornea, Asian social work and policy review, Journal of contaminant hydrology, Annals of clinical and laboratory science*[62].

A continuación, se buscó identificar localizar al azar títulos de artículos en dichas publicaciones. Por ello se desarrolló un método con el que se pudiera obtener un segundo algoritmo para encontrar la página dentro de un Número incierto que estuviera incluido en un volumen también incierto.

Al tener identificada la revista, la selección de un artículo específico dependía de encontrar tres elementos: volumen de la revista, número (*issue*) dentro de ese volumen y página dentro del rango de ese número.

Para lo cual se determinó obtener una combinación de seis cifras y determinar los tres elementos: dos para volumen [*Véase: 3.1.2.1, Volumen*], uno para el número [*Véase: 3.1.2.2, Número (issue)*] y tres para la página [3.1.2.3, Página]. Se utilizó el generador de números al azar *Nosetup,* con las siguientes especificaciones:

Ejemplo.

Inicio: 0
Final: 699999 } Rango de posibles combinaciones de números de **6 cifras**

Número de veces: 6 } La cantidad de veces que se repite dicho conjunto. La selección de esa cantidad de repeticiones fue arbitraria. Cualquier número

[62] Anterior al planteamiento de este proceso se estableció que se analizarían artículos científicos, es decir, no se incluirían editoriales, revisiones breves (*minireviews*), reportes de casos, comunicaciones cortas, porque el objetivo del trabajo fue examinar el Perfil de Ciencia en los artículos de investigación.

seleccionado no afecta la veracidad ni la funcionalidad del algoritmo propuesto, sólo el sistema lo pide como obligatorio.

Resultado: 401107

3.1.2.1| Volumen

Es necesario identificar en cuál de todas las ediciones publicadas a lo largo de los años se encuentra la página, es decir, determinar un volumen de la revista científica. Para localizar el volumen fue a partir de un número aleatorio; al preguntarse la cantidad de dígitos necesarios se estableció que debía de elegirse con base en el rango de inicio de la revista hasta su última edición en ese momento.

Por lo general, una publicación no supera los dos dígitos debido a que los documentos cambian de volumen cada año o seis meses. Por esa razón se estableció utilizar dos dígitos aleatorios, y en caso de que hubiera publicaciones con tres se aplicaría una regla correctiva.

Los lineamientos para determinar el volumen de las revistas se establecieron en base en prueba y error. Como resultado se encontraron tres combinaciones posibles: i) el número aleatorio coincide de inmediato con el volumen ii) el número aleatorio rebasa a los volúmenes existentes; o iii) la revista tiene un volumen de tres dígitos.

Si las dos cifras resultantes se ubican dentro del rango, se selecciona ese volumen para realizar la prueba. Por ejemplo, en *Annals of Clinical & Laboratory Science* los volúmenes van del 1 al 45; el número aleatorio fue **40** 1107 al separar las dos primeras cifras (40) se obtuvo directamente el volumen en el que se encuentra el artículo. En flujo esto es:

¿Existe $V_{45}= v_{40}$?

Sí, 40 es el volumen por analizar

Sin embargo, es posible que se presenten otras situaciones más complejas que el caso anterior, por ejemplo, si los dos números aleatorios rebasan el número máximo de volúmenes publicados hasta ese momento, se propuso aplicar el *Algoritmo 1*:

> Dado dos números, v_2 (el dividendo, las dos primeras cifras aleatorias) y V_2 (el divisor, el número total de volúmenes de la revista), el volumen será el residuo de la división.
>
> V_2: Número total de volúmenes de la revista
> v_2 Dos primeras cifras del número aleatorio

La revista *Cornea* hasta enero de 2015 tuvo 34 publicaciones. El número aleatorio fue 924905. Se tomaron las dos primeras cifras (92), como rebasó la cifra máxima de volúmenes publicados hasta ese momento, se dividió entre el último número editado (34). El resultado de la operación fue 2, el módulo (resto de la división) fue 24. La expresión es:

> ¿Existe $V_{34}= v_{92}$?
> No, 92 rebasa a 34
> Si no v_{92} mod (V_{34})
> 92 / 34= 2 mod (24)
>
> Nota: Si no hubiera un volumen idéntico, aun al aplicar esta regla se elegiría el último volumen de la revista publicado hasta el momento.

3.1.2.2| Número (*issue*)

Después de realizar este procedimiento para el volumen, ahora necesitábamos conocer en qué publicación individual dentro de todas las ediciones de ese año se encuentra el artículo. Para determinar el número de la revista se encontró que este elemento, en el caso de las revistas aleatorias predeterminadas, no superaba nueve en doce meses, por lo que se estableció que era necesario un dígito aleatorio para definirlo.

En caso de querer replicar esta propuesta, ahora con una publicación de doce números (uno por mes), los cuales equivalen a dos dígitos, se aplica la regla correctiva *Impar/par*: se agrega un 1 en caso de que el primer dígito del número aleatorio sea par, o un 2 si es impar.

Al querer obtener el número de la revista a partir de un dígito aleatorio y hacer una prueba con un elemento al azar, se descubrió que se pueden presentar dos escenarios: uno en el que coincide el resultado aleatorio con un número de la revista de ese año, y otro en el que el último número del rango sea rebasado por el obtenido con el generador.

Si la primera alternativa sucede, de inmediato se define el número de la publicación. Siguiendo con el ejemplo de *Annals of Clinical & Laboratory Science,* sus números publicados en un año van del 1 al 4; el número (*issue*) se selecciona utilizando la tercera cifra del proceso aleatorio, en ese caso fue 40 **1** 107. Se obtiene el número directamente.

En dado caso que esto no ocurra, tal como se ha realizado en ocasiones anteriores, se desarrolló el Algoritmo 2, el cual divide el rango máximo de Números de la publicación entre el dígito aleatorio, el residuo determinará en qué número se encuentra el documento por analizar con el Perfil. La representación es:

¿Existe $N_1 = n_1$?
Si no n_1 div (N_1),
R = N

Donde N_1 la cantidad total de números de la revista, y n_1 el número obtenido por las dos primeras cifras del dígito aleatorio. Si no coinciden: n_1 se convierte en el dividendo y N_1 en el divisor; el residuo o resto es el *issue* de la revista. El ejemplo de esta revista continuará como base para encontrar el número de página.

Por ejemplo, *Asian Social Work and Policy Review* publica hasta 3 números al año. El número aleatorio fue 24 **7** 544. La tercera cifra es 7 por lo que se divide entre 3. El residuo es 1, el cual será el número del artículo por analizar. La expresión es:

¿Existe N3 = n7?
No, n7 rebasa N3
Si no n7 div (N3),
7/3= residuo (1)

Para consultar el título del artículo final luego de resolver los algoritmos, consultar *Tabla 3.6.* Ejecución de algoritmos y resultados generales para selección de artículos en revistas no predeterminadas, apartado 2.

3.1.2.3| Página

El último elemento por identificar es la página que aloja el artículo. Este proceso se inspira en el acto de tener las hojas de una revista ordenadas en el suelo y tirar un dardo de espaldas para ver en cuál de ellas podría caer. Como no hay ninguna garantía de que el dardo va a descender en la primera hoja de un artículo valido para el análisis, se revisa el resultado, y en caso de que se encuentre dentro de los parámetros establecidos[63] se elige el título más cercano a un artículo válido.

Luego de una revisión al rango de páginas incluidas en las revistas aleatorias no predeterminadas y a un número indeterminado de publicaciones arbitradas, en ninguna de ellas se rebasaron las mil páginas de extensión por número. Con ello se estableció que se necesitaban **tres dígitos** producidos por el generador de números aleatorios para encontrar la hoja donde estaría el artículo por analizar.

Las posibles situaciones a las que nos enfrentamos con las combinaciones son: la página se encuentra dentro del rango del número generado aleatoriamente o el número aleatorio rebase el máximo de hojas de la revista.

[63] En diversas ocasiones en la página resultante no había un artículo de investigación (*Research article*) sino una reseña, un editorial, u otras secciones no adecuadas para verificar el Perfil, por lo que se utiliza el artículo más cercano a la página del resultado.

Al realizar esta prueba se presentó un cambio con respecto a las otras, si bien puede ocurrir que de inmediato los tres dígitos coincidan con una página de la revista, en otros casos las publicaciones inician en 1, o pueden comenzar con un dígito variable y no fijo. Por esa razón se necesitó plantear otro tipo de proceso para todos los casos.

Si los tres números aleatorios fueran mayores al máximo de hojas de la revista: se verifica que las páginas inician en *1* (P_1) y llevan un orden progresivo (1, 2, 3…). En ese escenario, se resuelve el siguiente algoritmo, en dónde $P_{3,}$ el divisor, es la cifra máxima de páginas contenidas en ese número y p_3, el dividendo, las últimas tres cifras aleatorias; el residuo que resulte de la operación es la página del artículo a analizar.

Lo anterior se expresa de la siguiente manera:

¿Existe $P_3 = p_3$?

Si no…

¿$P_1 = 1$?,

Sí es así, entonces p3 mod (P3)

En caso de que el número de la revista científica inicie con cualquier otra cifra diferente a *1* se realizó la siguiente prueba:

Se determina que $p_{3,}$ son las últimas tres cifras aleatorias; P_f es la página final del número de la revista; $P_{1,}$ la página en la que inicia y δp es el resultado de la resta de P_1 a P_f.

Después se dividirá P_3 por δp, el residuo de esta operación se utilizará en el siguiente paso. Ahora bien, en caso de que P_3 sea *mayor* que P_1 se restará el residuo a P_f, y si pasara lo contrario, es decir que los números aleatorios P_3 fueran *menores* que P_1, es necesario sumar el residuo a P_1. El resultado será la página en donde se encuentra el artículo por analizar

$\delta_P = Pf - Pi$

P+ ->Pf - res

p- -> pi + res

En toda división, el divisor es igual al dividendo multiplicado por el cociente (q), más el residuo (r); en nuestro caso:

(1) $PE = q(\delta p) + r$

Además, el residuo es siempre menor que el dividendo:

(2) $r < \delta p$,

Porque si no fuera así entonces $r > \delta p \Rightarrow r = \delta p + \delta p'$ y, en virtud de (1), $PE = q(\delta p) + r = q(\delta p) + \delta p + \delta p' = (q+1)(\delta p) + \delta p'$ y el cociente ya no sería q sino (q+1) y el residuo no sería r sino $\delta p'$, lo cual contradice la hipótesis inicial. Por tanto, $r < \delta p$.

Entonces, $r < \delta p \Rightarrow r < pf - pi \Rightarrow pi < pf - r < pf$

En conclusión, pf – r es un número que siempre cae en el rango que va de pi a pf, que es exactamente lo que andábamos buscando. Y como r es generado mediante operaciones aritméticas a partir de PE, que es aleatorio, entonces r conserva el carácter aleatorio de PE.

Página dentro del número

Para determinar la página del artículo se utilizan los tres últimos números de izquierda a derecha generados aleatoriamente. En el caso de que la página coincida dentro del rango de hojas que tiene la revista, se elige el artículo de investigación incluido en esa página.

Los tres últimos números aleatorios arrojados por el generador para la revista *Annals of clinical and laboratory science* fueron 107 (P_3); inicia con la página 1 (Pi) y finaliza en la 89 (P_f). La cifra, al ser menor que el número aleatorio, se expresa así:

$P_3 = 107$

$P_f = 89$

Pi= 1

89/107= 1

Residuo: **18**

En donde P_3 corresponde a los tres últimos números aleatorios (107), P_f la cifra final de páginas del número seleccionado (89) y P_1 (1) la página inicial. Se divide P_f y P_3 (89/107), y el residuo de esa operación (18) es la página del artículo.

Al final de este paso, ya con volumen, número y página de la revista seleccionados, el artículo resultó ser: *"Association of ATP7BMutation Detection Rate with Biochemical Characteristics in Korean Patients with Wilson Disease*".

Available online at www.annclinlabsci.org

Annals of Clinical & Laboratory Science, vol. 40, no. 1, 2010 15

Association of *ATP7B* Mutation Detection Rate with Biochemical Characteristics in Korean Patients with Wilson Disease

Hyung-Doo Park,[1] Hyun-Kyung Park,[2] Hae-Sun Chung,[1] Soo-Youn Lee,[1] Jong-Won Kim,[1] and Chang-Seok Ki[1]

[1]Department of Laboratory Medicine and Genetics, Samsung Medical Center, Sungkyunkwan University School of Medicine, Seoul; [2]Department of Laboratory Medicine, Seoul National University College of Medicine, Seoul, Korea

Abstract. Wilson disease (WD) is an autosomal recessive disorder caused by mutations in the *ATP7B* gene, yet many patients have either one mutation, or no mutation. We investigated whether the mutation detection rate is associated with any biochemical characteristics of WD. In a study of 71 patients, we used PCR-sequencing to screen for *ATP7B* mutations in 7 exons (exons 8, 10, 11, 14, 15, 16, and 18) covering 95% of known mutations in Korean patients with WD. We also investigated serum concentrations of various biochemical analytes. Data were analyzed by linear association test and one-way ANOVA. Based on the number of detected *ATP7B* mutations, a significant difference in serum ceruloplasmin concentration was found among the 3 groups ($p < 0.001$). Serum ceruloplasmin concentration averaged 3.32 ± 1.74, 10.8 ± 5.50, and 14.9 ± 3.88 mg/dl (mean ± SD) in the 25, 20, and 26 patients with two, one, and no *ATP7B* mutations, respectively. We observed 82.9% and 16.7% of mutant allele frequency in WD patients with ceruloplasmin concentration <10 mg/dl and 10-20 mg/dl, respectively ($p < 0.001$). Thus serum ceruloplasmin concentrations among WD patients differed according to the number of *ATP7B* mutations detected.

Keywords: Wilson disease, *ATP7B* mutation, ceruloplasmin

Introduction

Wilson disease (WD; MIM #277900) is a disorder of copper (Cu) metabolism [1]. Liver disease, neurologic presentations, and psychiatric disturbances are caused by an accumulation of Cu. The age of affected individuals varies from 3 to >50 yr. Worldwide prevalence of WD appears to be about 30 per 1 million, with a gene frequency of 0.56% and a carrier frequency of 1 in 90 [2,3]. However, the incidence of WD in Korea may be higher than that in Western populations, given the report of a Korean family with WD in two consecutive generations [4].

Address correspondence to Chang-Seok Ki, M.D., Ph.D., Department of Laboratory Medicine and Genetics, Samsung Medical Center, Sungkyunkwan University School of Medicine, 50 Ilwon-Dong, Gangnam-Gu, Seoul, 135-710, Korea; tel 82 2 3410 2709; fax 82 2 3410 2719; e-mail changski@skku.edu.

Diagnosis of WD usually depends on detection of low serum Cu and ceruloplasmin concentrations, increased urinary Cu excretion, presence of Kayser-Fleischer rings in the cornea, and/or increased hepatic Cu concentration. No single feature is completely reliable, but a diagnosis can usually be made provided that WD is suspected [2,3,5]. There is no worldwide consensus on a definitive diagnostic tool, but elevated liver Cu concentration is important for confirmation of WD [6,7]. WD is caused by mutations in the *ATP7B* gene, which encodes a Cu-transporting P-type ATPase. More than 379 probable disease-causing mutations from populations worldwide have been reported [8]. Because WD is an autosomal recessive disorder, most WD patients have two *ATP7B* mutations. Mutation analysis may be useful in cases with unclear liver disease [9]. However, many WD patients have either one *ATP7B* mutation

***Fig. 3.7* Association of ATP7BMutation Detection Rate with Biochemical Characteristics in Korean Patients with Wilson Disease**

Existe otra posibilidad que puede presentarse con respecto a la selección de página y es que *el número de la revista científica no inicie en 1 sino con cualquier otra cifra*. Para estos casos se hace lo que indica el siguiente ejemplo:

Por ejemplo, en la realización del trabajo para la revista *Cornea:*

P_3=905 P_f= 507 Pi= 369	Determinar P_3 por los tres números aleatorios, 905. La página final (P_f), 507 y la inicial (Pi) 369.

Pi – P_f= δP 507 – 369= 138	Restar la página en la que inicia el número de la página final: el resultado es δP.
p3/ δp = res 905/138 = 77	δP se divide entre los números aleatorios. Ubicar el residuo.
P+ ->pf– residuo 507-77= 430	Debido a que el número aleatorio 905 (P_3) es mayor a la primera página 369 (P_i), se resta el residuo 77 a la página fina (P_f) 507. El resultado, 430 es la página donde se encuentra el artículo a analizar.

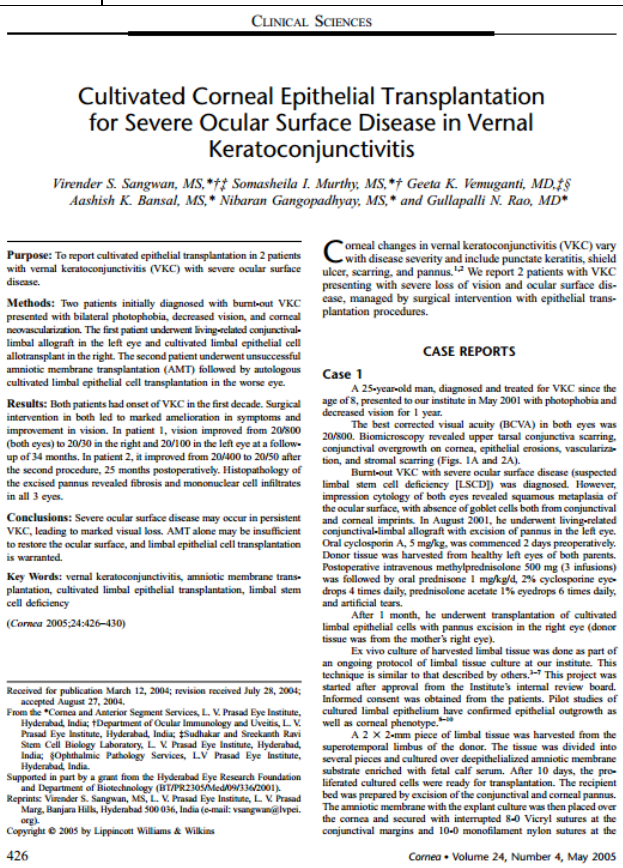

CLINICAL SCIENCES

Cultivated Corneal Epithelial Transplantation for Severe Ocular Surface Disease in Vernal Keratoconjunctivitis

Virender S. Sangwan, MS,†‡ Somasheila I. Murthy, MS,*† Geeta K. Vemuganti, MD,‡§ Aashish K. Bansal, MS,* Nibaran Gangopadhyay, MS,* and Gullapalli N. Rao, MD**

Purpose: To report cultivated epithelial transplantation in 2 patients with vernal keratoconjunctivitis (VKC) with severe ocular surface disease.

Methods: Two patients initially diagnosed with burnt-out VKC presented with bilateral photophobia, decreased vision, and corneal neovascularization. The first patient underwent living-related conjunctival-limbal allograft in the left eye and cultivated limbal epithelial cell allotransplant in the right. The second patient underwent unsuccessful amniotic membrane transplantation (AMT) followed by autologous cultivated limbal epithelial cell transplantation in the worse eye.

Results: Both patients had onset of VKC in the first decade. Surgical intervention in both led to marked amelioration in symptoms and improvement in vision. In patient 1, vision improved from 20/800 (both eyes) to 20/30 in the right and 20/100 in the left eye at a follow-up of 34 months. In patient 2, it improved from 20/400 to 20/50 after the second procedure, 25 months postoperatively. Histopathology of the excised pannus revealed fibrosis and mononuclear cell infiltrates in all 3 eyes.

Conclusions: Severe ocular surface disease may occur in persistent VKC, leading to marked visual loss. AMT alone may be insufficient to restore the ocular surface, and limbal epithelial cell transplantation is warranted.

Key Words: vernal keratoconjunctivitis, amniotic membrane transplantation, cultivated limbal epithelial transplantation, limbal stem cell deficiency

(*Cornea* 2005;24:426–430)

Received for publication March 12, 2004; revision received July 28, 2004; accepted August 27, 2004.

From the *Cornea and Anterior Segment Services, L. V. Prasad Eye Institute, Hyderabad, India; †Department of Ocular Immunology and Uveitis, L. V. Prasad Eye Institute, Hyderabad, India; ‡Sudhakar and Sreekanth Ravi Stem Cell Biology Laboratory, L. V. Prasad Eye Institute, Hyderabad, India; §Ophthalmic Pathology Services, L.V Prasad Eye Institute, Hyderabad, India.

Supported in part by a grant from the Hyderabad Eye Research Foundation and Department of Biotechnology (BT/PR2305/Med/09/336/2001).

Reprints: Virender S. Sangwan, MS, L. V. Prasad Eye Institute, L. V. Prasad Marg, Banjara Hills, Hyderabad 500 034, India (e-mail: vsangwan@lvpei.org).

Corneal changes in vernal keratoconjunctivitis (VKC) vary with disease severity and include punctate keratitis, shield ulcer, scarring, and pannus.[1,2] We report 2 patients with VKC presenting with severe loss of vision and ocular surface disease, managed by surgical intervention with epithelial transplantation procedures.

CASE REPORTS

Case 1

A 25-year-old man, diagnosed and treated for VKC since the age of 8, presented to our institute in May 2001 with photophobia and decreased vision for 1 year.

The best corrected visual acuity (BCVA) in both eyes was 20/800. Biomicroscopy revealed upper tarsal conjunctiva scarring, conjunctival overgrowth on cornea, epithelial erosions, vascularization, and stromal scarring (Figs. 1A and 2A).

Burnt-out VKC with severe ocular surface disease (suspected limbal stem cell deficiency [LSCD]) was diagnosed. However, impression cytology of both eyes revealed squamous metaplasia of the ocular surface, with absence of goblet cells both from conjunctival and corneal imprints. In August 2001, he underwent living-related conjunctival-limbal allograft with excision of pannus in the left eye. Oral cyclosporin A, 5 mg/kg, was commenced 2 days preoperatively. Donor tissue was harvested from healthy left eyes of both parents. Postoperative intravenous methylprednisolone 500 mg (3 infusions) was followed by oral prednisone 1 mg/kg/d, 2% cyclosporine eyedrops 4 times daily, prednisolone acetate 1% eyedrops 6 times daily, and artificial tears.

After 1 month, he underwent transplantation of cultivated limbal epithelial cells with pannus excision in the right eye (donor tissue was from the mother's right eye).

Ex vivo culture of harvested limbal tissue was done as part of an ongoing protocol of limbal tissue culture at our institute. This technique is similar to that described by others.[3–7] This project was started after approval from the Institute's internal review board. Informed consent was obtained from the patients. Pilot studies of cultured limbal epithelium have confirmed epithelial outgrowth as well as corneal phenotype.[8–10]

A 2 × 2-mm piece of limbal tissue was harvested from the superotemporal limbus of the donor. The tissue was divided into several pieces and cultured over deepithelialized amniotic membrane substrate enriched with fetal calf serum. After 10 days, the proliferated cultured cells were ready for transplantation. The recipient bed was prepared by excision of the conjunctival and corneal pannus. The amniotic membrane with the explant culture was then placed over the cornea and secured with interrupted 8-0 Vicryl sutures at the conjunctival margins and 10-0 monofilament nylon sutures at the

Tabla 3.5. **Ejecución algoritmo 3 revista *Cornea***

3.1.2.4| Ejecución y resultados

El ejercicio, a grandes rasgos, se puede resumir en el siguiente esquema:

Los resultados generales aparecen a continuación:

Número aleatorio	Volumen	Número	Página	Nombre del artículo
1. 924 905	92/34= 2 Residuo 24	4	P_3=905 P_f= 507 P_i= 369 δp= 138 p_3 / δp = res 905 / 138 = 77 P+ ->pf– residuo 507-77= **430**	*Cornea* *"Cultivated Corneal Epithelial Transplantation for Severe Ocular Surface Disease in Vernal Keratoconjunctivitis"* **Volumen 24, Número 4, pp. 426-430, May 2005** http://journals.lww.com/corneajrnl/toc/2005/05000
2. 247 544	24-8=16-8= 8	7/3= res1 Issue1	P_3= 544 P_f= 108 P_i= 1 108/544= 5	*Asian Social Work and Policy Review* *"Importance of Family Values DifferencesBetween Husbands and Wives in Determining Depression in Foreign Wives in Korean Multicultural Families: Examining theModerating Effect of Social Support"*

			residuo 4	**Volumen 8, Número 1, pp. 1-15, Feb. 2014** http://onlinelibrary.wiley.com/doi/10.1111/aswp.2014.8.issue-1/issuetoc
3. 401 107	40	1	P_3= 107 P_f= 89 P_i= 1 89/107= 1 Residuo**18**	*Annals of Clinical & Laboratory Science* *"Association of ATP7B Mutation Detection Rate with Biochemical Characteristics in Korean Patients with Wilson Disease*" **volumen 40, Número 1, pag.15-19, Enero 2010** **http://www.annclinlabsci.org/content/40/1.toc**
4. 411 768	41/9=4 Residuo 5	1	P_3= 768 Pf=72 Pi= 1 72/768= 10 Residuo **48**	*Cone-based placement for field programmable gate arrays* **Volumen 5, Número 2, p. 49 – 62, Enero 2011** http://digitalibrary.theiet.org/content/journals/10.1049/iet-cdt.2009.0058

Tabla 3.6. **Ejecución de algoritmos y resultados generales para selección de artículos en revistas no predeterminadas**

3. 3 | Selección de artículos científicos en revistas predeterminadas

3.3.1 | *Journals*

Las revistas científicas predeterminadas utilizadas para esta investigación fueron: *Nature*, Science, *The Proceedings of the National Academy of Sciences* (PNAS) y PLOS ONE. Estos *journals* fueron elegidos porque los artículos publicados en ellos abordan distintas ramas de la ciencia, lo que asegura la multidisciplinariedad en los textos por analizar, y debido a su trascendencia en la definición de la agenda periodística de ciencia de una gran cantidad de medios de comunicación.

Tan sólo en *The New York Times,* según los resultados de un análisis de contenido realizado a su sección de ciencia, se registró que durante el periodo de 1998 a 2012 se citaron 274 diferentes revistas indexadas, de las cuales *Nature* (171 citas), Science (126 citas) y *The Proceedings of the National Academy of Sciences* (PNAS) (99 citas) resultaron ser las revistas más referenciadas[64]. Entretanto PLOS ONE es el primer *journal* multidisciplinario de libre acceso con más de 140,000 artículos producidos hasta marzo de 2016.

Debido al prestigio, a la calidad de las investigaciones publicadas a lo largo de los años y a las estrategias que llevan a cabo las oficinas de comunicación de algunas de estas revistas, estos títulos se encuentran presentes regularmente en las redacciones que realizan coberturas sobre ciencia en México y en el mundo.

3.3.2 | Diseño de algoritmos para selección aleatoria de artículos científicos

Se estableció que el rango de tiempo en el que se encontraron los artículos en las publicaciones fuera de 2006 a 2015 debido a que PLOS ONE tuvo su primera edición en 2006. Esta regla aplica tanto para las revistas predeterminadas como las que fueron seleccionadas de forma aleatoria. Los detalles del trabajo se explican a continuación.

3.3.2.1 *Nature*

Nature es la revista científica interdisciplinaria más citada en el mundo, de acuerdo con el *Journal Citation Reports Science Edition 2013* (Thomson Reuters, 2014). Artículos (*Articles)* y Cartas (*Letters)* fueron los tipos de artículos analizados debido a que en estos apartados se muestran investigaciones originales.

En "artículos" las conclusiones representan un avance sustancial en la comprensión de un problema importante y éstas tienen implicaciones inmediatas y de gran alcance, su extensión no rebasa las 5 páginas ni se incluyen más de 50 referencias. Mientras que

[64] Kiernan, Vincent. *Source diversity among journals cited in Science Time*s. Public Understanding of Science. 2014. P. 201.

"cartas" son breves informes centrados en un hallazgo excepcional cuya importancia será de interés para los científicos de diversas disciplinas, y no abarca más de 4 páginas ni excede las 30 referencias[65].

Para este trabajo se decidió crear un algoritmo que resultara eficiente en la elección de los textos. El único requisito era utilizar la cantidad mínima de cifras producidas por el generador de números aleatorios *Nosetup* para encontrar los títulos.

El primer paso fue determinar que era necesario localizar el ―año", ―volumen", ―número" y ―página de la publicación", debido a que estos elementos contienen números que pueden ser seleccionados aleatoriamente, lo que permite identificar una publicación.

Al revisar los requerimientos se decidió que para *Nature* no era esencial encontrar ―número" y ―año", porque al ubicar ―volumen" se lograba obtener ―número", mientras que ―año" al encontrar la ―página". El proceso se describe a continuación:

Volumen

El número mínimo y máximo de volúmenes entre 2006 a 2015 publicador por *Nature*, van del 439 al 528. En un inicio se requerían tres dígitos, pero como el primero sólo puede ser 4 o 5 se estableció que era necesario encontrar dos dígitos y determinar un criterio para seleccionar cuál de las dos opciones debía de utilizarse. El procedimiento fue revisar cuál de las posibles combinaciones existía dentro del rango de los volúmenes[66] existentes.

4 o 5 + (Dos número aleatorios) = el ―volumen" en el que se encuentra el artículo

Ejemplo

Número aleatorio: **46** 283

[65] Nature. For Authors en *Manuscript formatting guide*. Consultado el 17 abril 2016 a las 18:54. http://www.nature.com/nature/authors/gta/index.html#a1.1

[66] Las combinaciones con el criterio y el número aleatorio que no aplicaron en este trabajo fueron 10 números: 429, 430, 431, 432, 433, 434, 435, 436,437, 438, debido a que no se ajustan con el rango establecido previo al inicio de este análisis. En el caso de que algunos de estos números salgan en el proceso, se deberá repetir la prueba.

V_2 : dos cifras (46)

Es decir,

Volumen con la combinación 546, no existe ⇒ intentar con 4, si coincide

Si no hubiera un volumen idéntico, la regla es utilizar el inmediato anterior

Se queda como ―volumen" seleccionado el **446**, el cual le corresponde el ―número" **7133**

Página

Si en un inicio las tres cifras aleatorias coinciden con alguna página existente, esa es la que se elige o se selecciona el artículo más cercano a esa combinación. En el caso de este ejercicio los cuatro números aleatorios coincidieron con alguna página de la publicación por lo que no fue necesario crear una regla correctiva.

Número aleatorio	**Nombre**	**Año**	**Volumen**	**Número**	**Página**
46 283	*A new eutriconodont mammal and evolutionary development in earlymammals*	2007	446	7133	283
21 191	*Neural dynamics for landmark orientation and angular path integration**	2015	521	7551	191
43 635	*A second class of chemosensory receptors in the olfactory epithelium**	2006	443	7103	635
73 580	*Linking synchronization to self-assembly using magnetic Janus colloids. (578-81)*	2011	473	7425	580

Tabla 3.6. Tabla de resultados - Proceso de selección aleatoria

3.3.2.2 *Science*

Esta revista también conocida como *Science Magazine,* es una publicación académica de la *American Association for the Advancement of Science AAAS* y se estima que es consultada por más de 500 mil personas alrededor del mundo cada semana[67].

Para iniciar este ejercicio fue necesario formular la pregunta base: ¿Cuántos dígitos aleatorios se requieren para elegir a ~~–e~~iegas" un artículo científico? Con la única condición de utilizar cantidad mínima de cifras producidas por el generador de números aleatorios *Nosetup* para determinar los títulos.

La lógica para responder este cuestionamiento fue: en *Science* se publican 4 volúmenes y por lo general, el número de páginas al año no excede a 1,800 pues por número se incluyen entre 150 a 200 páginas máximo. Por lo que se descubrió que al determinar ~~–v~~olumen" se lograba obtener ~~–a~~ño", mientras que la ~~–p~~ágina" va a dar el ~~–n~~úmero".

Como el rango de años de consulta de artículos es de 2006 a 2015, sólo se utilizó el listado de volúmenes del 300 al 351. Es decir, no era necesario utilizar otro número distinto al 3 por lo que se requirieron dos cifras aleatorias para encontrar volumen.

Ahora para determinar la página se revisó que el rango de hojas sólo va a ir entre 0 y menos de 2000 (1999), con lo cual el primer número de la página debe de tener 4 cifras pero la primera sólo va a ser entre 0 u 1, dando como resultado que ese primer dígito no fuera necesario generarlo de forma aleatoria porque se creó una regla: ~~–S~~i el número aleatorio anterior es par se agrega 0 y si es impar 1".

Por lo que la respuesta de cuántos dígitos aleatorios necesito es 5, dos para volumen y tres para página. La ejecución del ejercicio se puede consultar a continuación:

[67] AAAS, *2014 Science Media Kit.* P. 3.

Tabla de resultados - Proceso de selección aleatoria						
Número aleatorio	Ejercicio	Nombre	Año	Volumen	Número	Página
25 678	V: 325 Para la página 8 es par por lo que se agrega 0 (se queda igual) P: 678	The Last Glacial Maximum http://science.sciencemag.org/content/325/5941/710	2009	325	5941	pp. 710-714
38 481	V: 338 P: 1 (impar) 1481	Arthropod Diversity in a Tropical Forest http://science.sciencemag.org/content/338/6113/1481	2012	338	6113	pp. 1481 - 1484
34 193	V: 334 P: 3 (impar) 1193	Probing the Solar Magnetic Field with a Sun-Grazing Comet http://science.sciencemag.org/content/340/6137/1196	2013	340	6137	pp. 1196 - 1199
50 746	V: 350 P: 6 (par) 0746	A brain circuit that synchronizes growth and maturation revealed through Dilp8 binding to Lgr3 http://science.sciencemag.org/content/350/6262/aac6767	2015	350	6262	

3.3.2.3 *Proceedings of the National Academy of Sciences (PNAS)*

Al igual que en el proceso de selección de revistas, el primer paso es determinar 5 cifras aleatorias utilizando el generador de números al azar Nosetup.

Ejemplo:

Inicio: 0 -> Rango de posibles combinaciones de números de 5 cifras

Final: 99999

Número de veces: 5 -> La cantidad de veces que se repite dicho conjunto. La selección de esa cantidad de repeticiones fue arbitraria. Cualquier número seleccionado no afecta la veracidad ni la funcionalidad del algoritmo propuesto, sólo el sistema lo pide como obligatorio

Resultado: 48174, 50787, 51068, 71120, 74052

El periodo de tiempo en que se trabajo fue entre 2006 a 2015 para asegurar uniformidad con las otras revistas predeterminadas[68].

200**6**
200**7**
200**8**
200**9**
201**0**
201**1**
201**2**
201**3**
201**4**
201**5**

pqrst

Año ⟶ A (6, 7, 8, 9, 1, 2, 3, 4, 5)

p ⟶ Modulo 3 (0, 1,2)

En PNAS durante un año las páginas de la revista oscilan entre 1 a 20 mil. Para determinar la página se debe de realizar módulo 3 para que la primera cifra del número aleatorio sea 0, 1 y 2.

[68] *Plos One* existe desde 2006

Para realizar el módulo de un X número siempre se restará 3; por ejemplo, si la primera cifra es 4 se restará 3 y quedará 1. El resultado sustituirá a la cifra aleatoria y se unirá a los siguientes números para determinar la página.

Resultados generales						
4 P (página) p p(mod. 3) 4-3= **1**	8 Q	1 R	7 S	4 A(año)	Resultado Página: 18174 Año: 2014	Direct measurements of methane emissions from abandoned oil and gas wells in Pennsylvania. PNAS | December 23, 2014 | vol. 111 | no. 51 | 18173–18177
1 P (página) p p(mod. 3)	1 Q	1 R	7 S	5 A(año)	Resultado Página: 11175 Año: 2015	Geometrically controlled snapping transitions in shells with curved creases PNAS | September 8, 2015 | vol. 112 | no. 36 | 11175–11180
4 P (página) p p(mod. 3) 4 – 3 = 1	9 Q	9 R	1 S	1 A(año)	Resultado Página: 19911 Año: 2011	Friction mechanism of individual multilayered Nanoparticles PNAS **|** December 13, 2011 **|** vol. 108 **|** no. 50 **|** 19901–19906
6 P (página) p p(mod. 3) 6 – 3 = 3 3 – 3 = 0	6 Q	2 R	4 S	0 A(año)	Resultado Página: 6240 Año: 2010	Lethal protein produced in response to competition between sibling bacterial colonies PNAS **|** April 6, 2010 **|** vol. 107 **|** no. 14**|** 6258–6263

3.3.2.4 *Public Library of Science (PLOS One)*

Esta revista arbitrada, a diferencia de las anteriores revistas predeterminadas, es de libre acceso. Esta característica hace que sea una revista sin una publicación impresa y sólo pueda ser consultada en línea.

Al contar con la característica de un DOI ordenado de forma consecutiva y cronólogica resulto más sencillo definir los parámetros aleatorios en la selección del material. La forma en como es ordenada responde al siguiente modelo:

10.1371/journal.pone.0xxxxx

Por lo que fue necesario identificar:

10.1371	**journal.pone.**	**0xxxxxx**
DOI general de PloS	*pone* corresponde a PloS ONE	**0000001** corresponde al primer artículo publicado (2006)
		0146294 artículo asignado a la última publicación encontrada del 31 de diciembre del 2015
		0155282 última publicación al 4 de mayo de 2016

El resultado general fue:

Resource Competition May Lead to Effective Treatment of Antibiotic Resistant Infections	**http://journals.plos.org/plosone/article?id=10.1371/journal.pone.0080775**
Fetal Radiation Exposure Induces Testicular Cancer in Genetically Susceptible Mice	**http://journals.plos.org/plosone/article?id=10.1371/journal.pone.0032064**
CD46 Protects against Chronic Obstructive Pulmonary Disease	**http://journals.plos.org/plosone/article?id=10.1371/journal.pone.0018785**
A Feature Fusion Based Forecasting Model for Financial Time Series	**http://journals.plos.org/plosone/article?id=10.1371/journal.pone.0101113**

3. 3 | Identificación de categorías

3.3.1 |Proceso de lectura a detalle

Una vez que determiné los títulos de los artículos científicos, se procedió a leerlos de principio a fin con el propósito de identificar la frecuencia de aparición de las categorías con las que el Perfil caracteriza la ciencia de cada artículo. El ejercicio consistió en detectar y subrayar en el texto – impreso o en digital – las categorías de la herramienta conforme se presentaban. Para asegurar una mayor precisión en la ejecución de esta tarea traté de apegarme lo más posible a las definiciones propuestas [*Véase: Tabla 2.1. Perfil de Ciencia*].

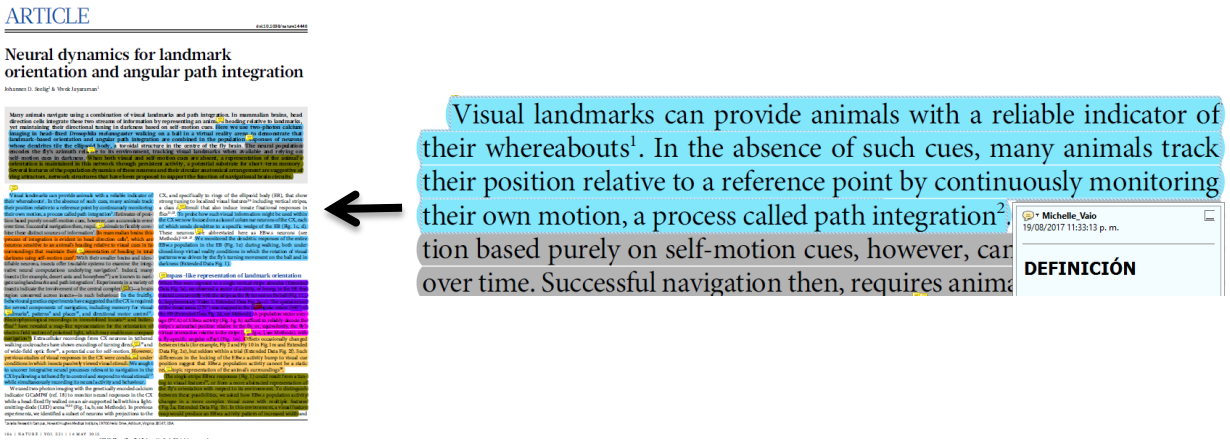

Fig 3.8. Selección de categorías del Perfil de Ciencia en el artículo Neural dynamics for landmark orientation and angular path integration

Luego, se estableció un formato para llevar el registro de cada una de las apariciones:

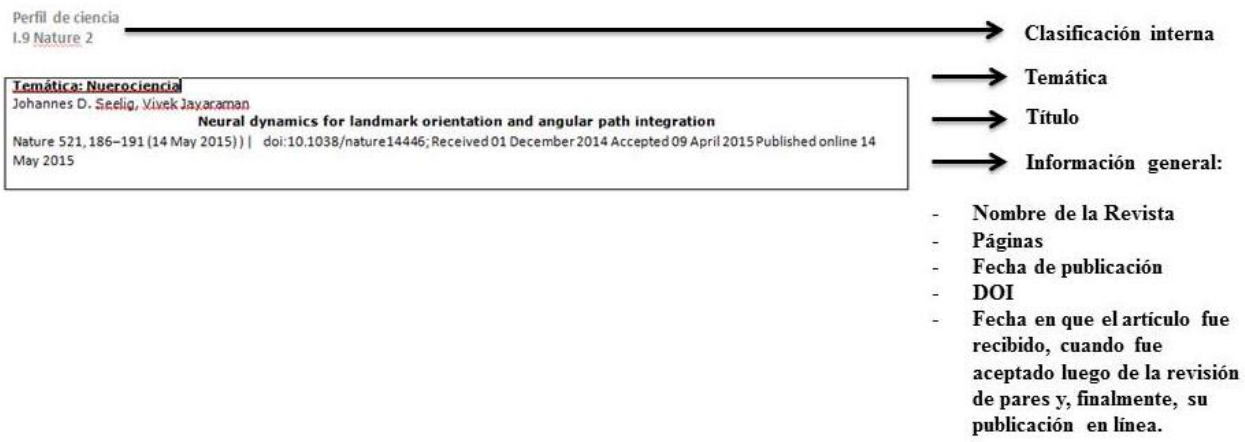

Fig 3.9. Ejemplo de tabla de información general de los registros XX. Componentes de la tabla de registros

Este formato se utilizó para todos los artículos científicos. El ejercicio resulto ser un gran reto, ya que fue un primer acercamiento a la literatura especializada en ciencia y toda la muestra se encontraba escrita en un inglés avanzado, lo cual, en primera instancia, pudo influir en la calidad del proceso de decisión al momento de localizar cada una de las categorías y conseguir una interpretación precisa del texto.

3.3.2 | Ejemplos de la interpretación de los rasgos

Definición	
Ejemplos del corpus	Interpretación de dos rasgos centrales: *significado, concepto*
[I.9] Nature2. Neural dynamics for landmark orientation and angular path integration	*Concepto:* Integración de rutas *Significado:* [cuando]… animales rastrean su posición relativa a un punto de referencia mediante el monitoreo continuo de su propio movimiento
[F.6] PNAS 3. Geometrically controlled snapping transitions in shells with curved creases	*Concepto:* Curvatura geodésica *Significado:* $\kappa g = \kappa \cos\psi$ *Concepto:* Curvatura normal *Significado:* $\kappa N = \kappa \sin\psi$ Ambas proyecciones respectivas de la curvatura del espacio sobre la Tangente (^ u +, Fig. 1B) y normal (^ n +, Fig. 1B) de la superficie media de la concha.

Magnitud	
Ejemplos del corpus	Interpretación de dos rasgos centrales: *dimensión, importancia*
[D.4] PNAS 1. Direct measurements of methane emissions from abandoned oil and gas wells in Pennsylvania	*Dimensión:* Según los cálculos de los investigadores las emisiones de metano en los pozos de petróleo y gas abandonados en Pensilvania fue de 0.03-0.05 CH4 por año *Importancia:* Esto representa del 4 al 7% de las emisiones causadas por el conjunto de efectos producidos por las actividades humanas estimadas para 2014

[**M.13] Science** 2 Arthropod Diversity in a Tropical Forest	*Dimensión:* Establecimos una colaboración que involucraba a 102 investigadores con experiencia abarcando toda la gama de filogenias y modos de alimentación presentes entre los artrópodos (20). Este consorcio invirtió un total de 24,354 días de trampas (o personas) muestreando el bosque de San Lorenzo (SLPA) en Panamá utilizando protocolos estructurados (figura S1). Identificamos 129,494 artrópodos que representan 6144 especies focales (Fig. 1 y tabla S1) de 0,48 ha de bosque maduro muestreado intensivamente. *Importancia:* Proporcionar una estimación global de la riqueza de especies de artrópodos en una selva tropical
Evidencia empírica	
Ejemplos del corpus	Interpretación de dos rasgos centrales: *¿Qué afirman?, lo saben por…*
[E.5] PNAS 2 Lethal protein produced in response to competition between sibling bacterial colonies	*¿Qué afirman?:* Se encontró que el material extraído de agar cerca de regiones inhibidas por la subtisilina contenía una proteína del mismo tamaño (12 kDa) detectada en la respuesta a la competencia entre colonias de bacterias hermanas de dos colonias (Fig. 1D Right Lane) *Lo saben por:* La identidad se confirmó mediante análisis de la secuencia de aminoácidos.
[A.1] Aleatorio 1 Cultivated Corneal Epithelial Transplantation for Severe Ocular Surface Disease in Vernal Keratoconjunctivitis	*¿Qué afirman?:* [Se presentaron] cicatrices de la conjuntiva tarsal superior, sobre crecimiento conjuntival en la córnea, erosiones epiteliales, vascularización y cicatrices del estroma (Figuras 1A y 2A)” 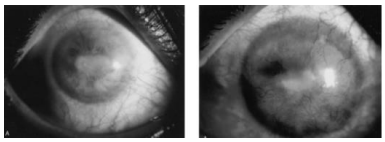 *Imagen 2.2. Figura 1A y 2ª Trasplante Epitelial Corneal Cultivado para Enfermedad de Superficie Ocular Grave en Queratoconjuntivitis Vernal* *Lo saben por:* La biomicroscopía
Incertidumbre	

Ejemplos del corpus	Interpretación de dos rasgos centrales: *Seguridad en mediciones y conclusiones (limitaciones)*
[D.4] PNAS 1 Direct measurements of methane emissions from abandoned oil and gas wells in Pennsylvania	*Seguridad en mediciones:* Estimamos que el efecto combinado de las diversas fuentes de incertidumbres en las estimaciones de la tasa de flujo dará lugar a errores dentro de un factor de 2 de nuestra estimación. Este error es pequeño en relación con la variación de siete órdenes de magnitud en los caudales medidos. Además, la mayoría de las fuentes de incertidumbre de medición sesgarían los caudales medidos a ser más bajos que sus números reales.
[R.18] PLOS 3 Resource Competition May Lead to Effective Treatment of Antibiotic Resistant Infections	*Conclusiones (limitaciones*): El conocimiento derivado del presente análisis está limitado por la capacidad de implementar efectivamente las condiciones antiR y por las suposiciones hechas por el modelo (Ecuación 1). Por ejemplo, una condición antiR obtenida mediante el uso de un fármaco de interacción supresora ocurre solo en un rango limitado de concentraciones de fármaco, que puede no ser fácilmente controlable para la aplicación de tratamiento.
Hipótesis	
Ejemplos del corpus	Interpretación de dos rasgos centrales: *Sospechan, Aún no*
[L.12] Science 1. The Last Glacial Maximum	*Sospechan:* Es probable que la desglaciación tardía ocurrida en el Tibet fuera resultado de la fuerte influencia que tuvo el monzón de Asia oriental en dicho territorio. *Aún no:* Durante todo el Máximo Glacial (LGM por sus siglas en inglés) el Tibet permaneció invariable, no se presentó una reducción de humedad suministrada al glaciar, sin embargo, se debilitó de forma abrupta hace 17. 5 miles de años sin tener una razón clara por la cual haya sucedido dicho fenómeno.
[Q.17] PLOS A Feature Fusion Based Forecasting Model for Financial Time	*Sospechan:* Creemos que las posibles razones se encuentran en las dos siguientes explicaciones. (1) Cuanto menor es la dimensionalidad, mayor es la relación de ruido a información útil contenido en las características.

Series	En este caso, la función de fusión fortalecerá el ruido para afectar el rendimiento predictivo. (2) Para el algoritmo CCA, el componente de las características extraídas no está correlacionado, pero no es independiente, lo que significa que los componentes no tienen influencia entre sí en el sentido del promedio estadístico. *Aún no:* Sin embargo, no se puede visualizar de manera visible cuando los componentes son insuficientes.
Explicación	
Ejemplos del corpus	Interpretación de dos rasgos centrales: *¿Qué?,¿Por qué/¿Cómo?*
[E.5] PNAS 2 Lethal protein produced in response to competition between sibling bacterial colonies	*¿Qué?:* Aumento de la densidad bacteriana y, en consecuencia, el estrés nutricional de la bacteria. *¿Por qué?* La expansión de una colonia está limitada por la tensión superficial, no puede expandirse lo suficientemente rápido como para crear un nuevo espacio para la bacteria reproductora, lo que causa un aumento en la subtilisina, una serina proteasa secretada por P. dendritiformis la cual puede detectarse alrededor de colonias individuales de cada una de las bacterias.
Desarrollo matemático	
Ejemplos del corpus	Interpretación de dos rasgos centrales: *Formulación y solución de ecuaciones; cálculos algebraicos; inferencia estadística; aproximaciones y simplificaciones.*
[F.6] PNAS 3. Geometrically controlled snapping transitions in shells with curved creases	Un cálculo directo (véase la información de apoyo) obtiene la curvatura media de la cáscara cerca del pliegue, $H=\frac{1}{2}\left(\kappa_N+\frac{\mathcal{K}+(\partial_s\psi+\tau)^2}{\kappa_N}\right),$ Donde τ es la torsión del pliegue, que mide la velocidad que el plano osculador gira alrededor de la bisagra y, por lo tanto, la noplanaridad de la bisagra (32).

[B.2] A2 Importance of family values differences between husbands and wives in determining depression in foreign wives in Korean multicultural families: examining the moderating effect of social support	**Table 1** Descriptive statistics Variables / Mean / SD / *n* / % Age gap between husband and wife: 8.46 / 7.06 Wife's education: 11.59 / 2.86 Household income per month No income: 4 / 1.7 <500,000 won: 2 / 0.8 500,000–1 million won: 10 / 4.1 1–1.5 million won: 38 / 15.8 1.5–2 million won: 64 / 26.6 2–2.5 million won: 58 / 24.1 2.5–3 million won: 22 / 9.1 3–4 million won: 32 / 13.2 4–5 million won: 7 / 2.9 More than 5 million won: 4 / 1.7 Wife's working status Currently not working: 179 / 74.3 Currently working: 62 / 25.7 Wife's language ability Not good: 97 / 40.2 Good: 144 / 59.8 Use of broker agency No: 199 / 82.6 Yes: 42 / 17.4 Social support Family support: 0.28 / 0.51 Friend support: 0.62 / 0.68 Formal support: 1.27 / 2.58 Family values difference: 6.70 / 3.62 Depression: 3.38 / 4.31
Predicción	
Ejemplos del corpus	Interpretación de dos rasgos centrales: *¿Qué afirman?, Verificaciones previas*
[**M.13**] **Science** 2 Arthropod Diversity in a Tropical Forest	*Verificaciones previas:* Sus hallazgos sugieren que, al contrario de lo que se pensaba antes, es posible lograr la comprensión a gran escala de los artrópodos tropicales que existen en un hábitat determinado. Sus datos indican que una muestra exhaustiva de 1 hectárea de selva podría revelar casi dos tercios de todas las especies de artrópodos presentes en un área mucho más grande. *¿Qué afirman?:* Para determinar la diversidad de especies de un bosque tropical lluvioso no es necesario que la superficie total muestreada sea muy extensa, siempre y cuando el diseño de muestreo cubra adecuadamente

	tanto los micro hábitats como las especies de plantas.
[**S.19] PLOS 4** Fetal Radiation Exposure Induces Testicular Cancer in Genetically Susceptible Mice	*¿Qué afirman?:* El feto masculino de mujeres expuestas a la radiación a las 5-6 semanas de embarazo podría tener un mayor riesgo de desarrollar cáncer testicular. *Verificaciones previas*: Los pesos de los testículos y el porcentaje de tumores que fueron teratomas confirmados, (un tipo de tumores que pueden contener varios tipos diferentes de tejidos, como pelo, músculo y hueso en su interior) los cuales resultaron ser más altos en los ratones irradiados que en el grupo de control, lo que indica que la irradiación indujo tumores más agresivos y/o que fueran más propensos a desarrollarse en cada testículo durante el periodo de tiempo en el que fueron expuestos.

Tabla 3.7. Ejemplos de la interpretación de los rasgos del Perfil de Ciencia

3.3.3 | Código cromático de certidumbre

En esta investigación se detectó que las selecciones de las interpretaciones presentan un alto grado de subjetividad al depender de la habilidad del monitor. En 2015, al comienzo del trabajo esta tesista contaba con una experiencia limitada en lectura de artículos científicos, su práctica con este tipo de literatura se circunscribía a un par de trabajos escolares solicitados en la materia optativa de Periodismo de ciencia. Durante el transcurso de esta tesis trabajaba como Coordinadora de Vinculación en una Organización de la Sociedad Civil (OSC), en donde no utilizaba literatura especializada en su rutina diaria, lo que me hacía poco experimentada en la lectura de estos documentos.

Otra característica respecto a las posibles incertidumbres del trabajo fue la curva de aprendizaje para entender y aplicar el Perfil de Ciencia en la metodología. El entendimiento de la herramienta fue gradual, y se presentó un cambio entre la lectura del primer artículo al octavo.

Ante un posible problema con respecto a la validez de las interpretaciones por los motivos ya señalados fue que se planteó crear una herramienta para evaluar el nivel de confianza de todo el análisis.

Esta propuesta fue el Código Cromático de Certidumbre (CCC), una solución parcial ante la falta de otros monitores que junto conmigo pudieran realizar el mismo ejercicio [*Véase: Proceso de lectura a cabalidad*] para poner a prueba el Perfil.

Esta herramienta proporciona información que permite conocer la Incertidumbre en términos expresados en los objetivos específicos, que son:

a. Obtener el grado de certeza de cada una de las interpretaciones
b. Explorar las limitaciones del Perfil de Ciencia para ser usado por reporteras sin preparación científica más allá de la educación preparatoria
c. Proponer una síntesis para entender el Perfil de Ciencia en el marco de la aplicación del CCC

Para ello se analizaron del orden de 1,187 interpretaciones con dicha herramienta. El ejercicio consistió en –calificar" cada una de las selecciones con alguno de los siguientes tres colores y su significado:

Ninguna o muy pocas dudas ->
Algunas dudas en la interpretación ->
Serias dudas en la interpretación ->

Con el propósito de facilitar la aplicación del CCC, busqué dos conceptos clave de cada rasgo.

Definición	**¿Qué significa este término?** Proviene del latín definitio, que significa delimitar. Conjunto de palabras que expresan con claridad y precisión la significación de un concepto, palabra o frase. Ayuda a generar la comprensión del término y delimita lo que es para distinguirlo con respecto a lo que no es. En ciencia, las definiciones tienden a ser monosémicas (i.e., con un solo significado).	**Conceptos clave**	
		Concepto	***Significado***
Magnitud	**¿Cuáles son las dimensiones de este fenómeno?** Da idea de la grandeza y la importancia, absoluta o relativa, de forma cuantitativa o cualitativa. Cuando el fenómeno es percibido como "problema", importan las magnitudes de: i) el problema; ii) la intervención; y iii) los efectos de la intervención.	**Da idea de la *importancia* del fenómeno**	**Se muestran las *dimensiones* de forma cuantitativa y/o cualitativa**

<table>
<tr><td>Hipótesis</td><td>¿Qué sospechan que sucede y por qué? Del griego (proposición), es la base de un argumento aún por sustanciar. Relación de causa-efecto (A=>B) respecto de la cual hay razones para creer que es cierta, pero que aún no ha sido plenamente demostrada.</td><td>¿Qué sospechan que sucede?</td><td>¿Por qué lo creen?</td></tr>
<tr><td>Evidencia Empírica</td><td>¿Cómo saben lo que afirman? De la raíz indoeuropea per- (poner a prueba, arriesgar), es conocimiento producido mediante actos de ciencia que buscan "ver" en un sentido amplio: mediciones, experimentos, observaciones, simulaciones por computadora, pruebas clínicas, encuestas, etc.; y suele presentarse en forma de tablas, gráficas, esquemas, fotografías, animaciones, material audiovisual, etc.</td><td>¿Qué es lo que afirman?</td><td>¿Cómo lo saben?</td></tr>
<tr><td rowspan="2">Incertidumbre</td><td rowspan="2">¿Qué seguridad tienen de los valores numéricos encontrados y las aseveraciones propuestas? Toda medición lleva asociado un rango en cuyo interior se encuentra, con la mayor probabilidad, el valor de la variable medida. (Cuanto más ancho es ese intervalo, menor es la precisión de la medida.)
Los reportes científicos suelen señalar</td><td colspan="2">Seguridad en:</td></tr>
<tr><td>¿En qué rangos tienen certeza sobre los valores numéricos?</td><td>¿Qué limitaciones de la investigación influyen sobre lo reportado?</td></tr>
</table>

	las limitaciones de la investigación; éstas sirven para estimar la incertidumbre no cuantitativa de sus conclusiones.		
Explicación	**¿Por qué y cómo suceden las cosas de cierta forma?** Del latín explanare (hacer plano, claro), expone las razones de los fenómenos mediante la secuencia en que las causas siguen a los efectos.	**¿Qué sucede?**	**¿Por qué / cómo?**
Desarrollo Matemático	Formulación y solución de ecuaciones; cálculos algebraicos; inferencia estadística; aproximaciones y simplificaciones.		
Predicción	**¿Qué afirman que sucederá?** Relación de causa-efecto para la cual se tiene un alto nivel de convicción con base en un buen número de verificaciones previas. Suele formularse como una relación causal en que, si la casa ocurre en el presente, el efecto se manifestará, consecuentemente, en el futuro.	**¿Qué afirman?**	**Verificaciones previas**

Tabla 3.8. Síntesis para entender Perfil de Ciencia en la aplicación del código cromático

En este ejercicio sólo se analizaron con el CCC las selecciones de las primeras lecturas a detalle, otras partes del texto que no fueran interpretaciones previas del Perfil fueron omitidas.

A partir de la aplicación de este método se redujeron de las 1,187 interpretaciones resultado del primer análisis a 1,140, es decir 47 selecciones fueron desechadas al no cumplir con alguna de las características mínimas de la caracterización de los rasgos para formar parte del grupo final de interpretaciones del Perfil de Ciencia contabilizadas en resultados.

Capítulo 4

Resultados

De los diecinueve artículos que fueron analizados los rasgos: Magnitud, Evidencia empírica e Hipótesis aparecieron en todos los artículos científicos, mientras que en un 95 por ciento de los textos analizados (18 de un total de 19) localicé los rasgos Incertidumbre, Explicación y Predicción en por lo menos una ocasión en el contenido del artículo científico.

Las categorías que menos se presentaron fueron: Definición y Desarrollo Matemático. El rasgo Definición aparece en el 80% de los artículos analizados, mientras en el segundo caso aparece en un 58%.

				Definición			Magnitud			Evidencia empírica			Incertidumbre			Hipótesis			Explicación			Desarrollo matemático			Predicciones		
	Categoría	Nombre del artículo	Temática	Primera aplicación Perfil	Resultado general código cromático	Resultado por color	Primera aplicación Perfil	Resultado general código cromático	Resultado por color	Primera aplicación Perfil	Resultado general código cromático	Resultado por color	Primera aplicación Perfil	Resultado general código cromático	Resultado por color	Primera aplicación Perfil	Resultado general código cromático	Resultado por color	Primera aplicación Perfil	Resultado general código cromático	Resultado por color	Primera aplicación Perfil	Resultado general código cromático	Resultado por color	Primera aplicación Perfil	Resultado general código cromático	Resultado por color
1	A1	Cultivated Corneal Epithelial Transplantation for Severe Ocular Surface Disease in Vernal Keratoconjunctivitis	OFTALMOLOGÍA	0	0	0 0 0	7	7	5 2 0	21	20	18 2 0	2	2	2 0 0	5	5	4 1 0	0	0		0	0		9	9	5 3 1
2	A2	Importance of family values differences between husbands and wives in determining depression in foreign wives in Korean multicultural families: examining the moderating effect of social support	TRABAJO SOCIAL	8	5	3 2 0	7	6	4 2 0	5	5	3 2 0	2	2	2 0 0	11	10	8 2 0	1	1	1 0 0	2	2	2 0 0	3	2	2 0 0
3	A4	Association of ATP7B Mutation Rate with Biochemical Characteristics in Korean Patients with Wilson Disease	GENÉTICA	3	3	1 2 0	15	10	8 0 2	19	14	14 0 0	3	0	0 0 0	5	6	4 2 0	7	2	1 0 1	3	3	2 1 0	5	5	2 3 0
4	PNAS 1	Direct measurements of methane emissions from abandoned oil and gas wells in Pennsylvania	CIENCIAS AMBIENTALES	4	3	3 0 0	13	11	9 2 0	9	8	7 0 1	5	7	6 1 0	4	2	2 0 0	4	4	4 0 0	0	1	1 0 0	9	9	9 0 0
5	PNAS 2	Lethal protein produced in response to competition between sibling bacterial colonies	CIENCIAS BIÓLOGICAS	3	2	1 1 0	15	12	1 1 10	32	32	29 2 1	3	3	1 1 1	18	16	11 5 0	7	8	7 0 1	0	2	2 0 0	5	5	2 2 1
6	PNAS 3	Geometrically controlled snapping transitions in shells with curved creases	FÍSICA APLICADA	11	10	8 1 1	11	11	5 3 3	26	21	20 0 1	3	1	1 0 0	8	7	5 0 2	7	7	4 1 2	7	7	5 2 0	6	6	4 2 0
7	PNAS 4	Zbtb20 is essential for the specification of CA1 field identity in the developing hippocampus	NEUROCIENCIAS	15	15	3 3 3	13	13	9 3 1	30	30	18 9 3	2	3	1 1 1	16	16	14 0 2	11	11	5 5 1	0	0		5	5	3 2 0
8	Nature 1	A new eutriconodont mammal and evolutionary development in early mammal	PALEONTOLOGÍA	2	1	0 0 1	14	12	5 4 3	16	16	11 5 0	1	1	0 1 0	10	9	8 2 1	9	7	4 1 2	0	0		1	1	0 1 0
9	Nature 2	Neural dynamics for landmark orientation and angular path integration	NEUROCIENCIAS	2	2	1 0 1	12	11	5 4 2	21	17	16 0 1	6	4	2 1 1	14	14	9 1 4	7	5	1 1 3	0	0		4	4	3 0 1
10	Nature 3	Linking synchronization to self-assembly using magnetic Janus colloids	FÍSICA APLICADA	2	3	2 1 0	9	7	2 3 3	13	13	12 1 0	0	0	0 0 0	9	9	6 1 0	3	3	2 1 0	0	2	2 0 0	1	1	1 0 0
11	Nature 4	TA second class of chemosensory receptors in the olfactory epithelium	NEUROCIENCIAS	2	1	0 1 0	20	15	8 7 0	22	17	16 1 0	9	10	7 1 3	19	20	18 1 1	2	2	1 0 0	0	0		0	0	
12	Science 1	The Last Glacial Maximum	CIENCIAS ATMOSFÉRICAS	3	3	2 1 0	8	9	4 3 2	25	23	20 1 2	4	4	3 1 0	25	24	22 2 0	12	11	9 1 4	0	0		2	2	2 0 0
13	Science 2	Arthropod Diversity in a Tropical Forest	ECOLOGÍA	0	0	0 0 0	13	11	10 1 0	12	10	9 1 2	6	6	2 1 3	3	3	3 0 0	2	2	2 0 0	0	3	2 0 1	6	6	6 0 0
14	Science 3	Probing the Solar Magnetic Field with a Sun-Grazing Comet	ASTRONOMÍA	3	3	1 0 2	7	6	6 0 0	18	18	14 4 0	5	5	4 1 0	10	10	7 1 3	7	7	4 2 1	1	1	1 0 0	5	5	2 1 2
15	Science 4	A brain circuit that synchronizes growth and maturation revealed through Dlgap4 binding to Ig23	NEUROCIENCIAS	1	0	0 0 0	17	16	10 3 3	61	54	40 6 8	9	9	6 0 3	21	21	19 2 0	18	16	12 2 2	0	0		6	6	4 1 1
16	Plos 1	CD46 Protects against Chronic Obstructive Pulmonary Disease	MEDICINA	1	1	1 0 0	11	10	6 4 0	19	19	16 3 0	6	6	1 2 3	6	6	5 0 1	7	7	6 1 0	1	2	2 0 0	3	3	2 1 0
17	Plos 2	A Feature Fusion Based Forecasting Model for Financial Time Series	ECONOMÍA	8	7	7 0 0	16	16	5 5 6	12	12	12 0 0	3	2	2 0 0	8	7	5 2 0	8	8	5 2 1	16	16	16 0 0	3	3	2 1 0
18	Plos 3	Resource Competition May Lead to Effective Treatment of Antibiotic Resistant Infections	MEDICINA	5	4	4 0 0	13	13	12 1 0	16	16	16 0 0	8	8	6 1 1	7	6	5 0 1	10	10	7 1 2	5	5	5 0 0	9	9	5 3 1
19	Plos 4	Fetal Radiation Exposure Induces Testicular Cancer in Genetically Susceptible Mice	MEDICINA	0	0		9	9	5 3 1	9	9	8 0 1	6	6	5 1 0	5	5	3 2 0	2	2	2 0 0	0	0		4	4	3 0 1

Fig 4.1. Resultados generales luego de la aplicación del Perfil de Ciencia

Para facilitar la lectura y consulta de la anterior figura se muestra en cuatro partes:

Categorías	Definición			Magnitud		
	Primera aplicación Perfil	Resultado general código cromático	Resultado por color	Primera aplicación Perfil	Resultado general código cromático	Resultado por color
A1	0	0	0 0 0	7	7	5 2 0
A2	8	5	3 2 0	7	6	4 2 0
A4	3	3	1 2 0	15	10	8 0 2
PNAS 1	4	3	3 0 0	13	11	9 2 0
PNAS 2	3	2	1 1 0	15	12	1 1 10
PNAS 3	11	10	8 1 1	11	11	5 3 3
PNAS 4	15	15	3 3 9	13	13	9 3 1
Nature 1	2	1	0	14	12	5

			0			4
			1			3
Nature 2	2	2	1	12	11	5
			0			4
			1			2
Nature 3	2	3	2	9	7	1
			1			3
			0			3
Nature 4	2	1	0	20	15	8
			1			7
			0			0
Science 1	3	3	2	8	9	4
			1			3
			0			2
Science 2	0	0	0	13	11	10
			0			1
			0			0
Science 3	3	3	1	7	6	6
			0			0
			2			0
Science 4	1	0	0	17	16	10
			0			3
			0			3
Plos 1	1	1	1	11	10	6
			0			4
			0			0
Plos 2	8	7	7	16	16	5
			0			5
			0			6
Plos 3	5	4	4	13	13	12

			0			1
			0			0
Plos 4	0	0		9	9	5
						3
						1

Categorías	Evidencia empírica			Incertidumbre		
	Primera aplicación Perfil	Resultado general código cromático	Resultado por color	Primera aplicación Perfil	Resultado general código cromático	Resultado por color
A1	21	20	18	2	2	2
			2			0
			0			0
A2	5	5	3	2	2	2
			2			0
			0			0
A4	19	14	14	3	0	0
			0			0
			0			0
PNAS 1	9	8	7	5	7	6
			0			1
			1			0
PNAS 2	32	32	29	3	3	1
			2			1
			1			1
PNAS 3	26	21	20	3	1	1
			0			0
			1			0

PNAS 4	30	30	18	2	3	1
			9			1
			3			1
Nature 1	16	16	11	1	1	0
			5			1
			0			0
Nature 2	21	17	16	6	4	2
			0			1
			1			1
Nature 3	13	13	12	0	0	0
			1			0
			0			0
Nature 4	22	17	16	9	10	7
			1			1
			0			3
Science 1	25	23	20	4	4	3
			1			1
			2			0
Science 2	12	10	9	6	6	2
			1			1
			2			3
Science 3	18	18	14	5	5	4
			4			1
			0			0
Science 4	61	54	40	9	9	6
			6			0
			8			3
Plos 1	19	19	16	6	6	1
			3			2
			0			3

Plos 2	12	12	12	3	2	2
			0			0
			0			0
Plos 3	16	16	16	8	8	6
			0			1
			0			1
Plos 4	9	9	8	6	6	5
			0			1
			1			0

Categorías	**Hipótesis**			**Explicación**		
	Primera aplicación Perfil	**Resultado general código cromático**	**Resultado por color**	**Primera aplicación Perfil**	**Resultado general código cromático**	**Resultado por color**
A1	5	5	4	0	0	
			1			
			0			
A2	11	10	8	1	1	1
			2			0
			0			0
A4	5	6	4	7	2	1
			2			0
			0			1
PNAS 1	4	2	2	4	4	4
			0			0
			0			0
PNAS 2	18	16	11	7	8	7
			5			0

			0			1
PNAS 3	8	7	5 0 2	7	7	4 1 2
PNAS 4	16	16	14 0 2	11	11	5 5 1
Nature 1	10	9	6 2 1	9	7	4 1 2
Nature 2	14	14	9 1 4	7	5	1 1 3
Nature 3	9	9	6 3 0	3	3	2 1 0
Nature 4	19	20	18 1 1	2	2	1 1 0
Science 1	25	24	22 2 0	12	11	6 1 4
Science 2	3	3	3 0 0	2	2	2 0 0
Science 3	10	10	7 1 3	7	7	4 2 1
Science 4	21	21	19 2	18	16	12 2

			0			2
Plos 1	6	6	5 0 1	7	7	6 1 0
Plos 2	8	7	5 2 0	8	8	5 2 1
Plos 3	7	6	5 0 1	10	10	7 1 2
Plos 4	5	5	3 2 0	2	2	2 0 0

Categorías	**Desarrollo Matemático**			**Predicción**		
	Primera aplicación Perfil	**Resultado general código cromático**	**Resultado por color**	**Primera aplicación Perfil**	**Resultado general código cromático**	**Resultado por color**
A1	0	0	 	9	9	5 3 1
A2	2	2	2 0 0	3	2	2 0 0
A4	3	3	2 1 0	5	5	2 3 0
PNAS 1	0	1	1	9	9	9

			0 0			0 0
PNAS 2	0	2	2 0 0	5	5	2 2 1
PNAS 3	7	7	5 2 0	6	6	4 2 0
PNAS 4	0	0		5	5	3 2 0
Nature 1	0	0		1	1	0 1 0
Nature 2	0	0		4	4	3 0 1
Nature 3	0	2	2 0 0	1	1	1 0 0
Nature 4	0	0		0	0	
Science 1	0	0		2	2	2 0 0
Science 2	0	3	2 0 1	6	6	6 0 0
Science 3	1	1	1	5	5	2

			0			1
			0			2
Science 4	0	0		6	6	4
						1
						1
Plos 1	1	2	2	3	3	2
			0			1
			0			0
Plos 2	16	16	16	3	3	2
			0			1
			0			0
Plos 3	5	5	5	9	9	5
			0			3
			0			1
Plos 4	0	0		4	4	3
						0
						1

Tabla 4.1. Resultados dividida por categorías luego de la aplicación del Perfil de Ciencia en todas sus etapas

4.1| Análisis cuantitativo: frecuencia de apariciones generales por artículo

Los rasgos con más apariciones en promedio fueron Evidencia empírica con 19, Magnitud con 11 e Hipótesis con 10, los cuales consistentemente aparecen en cada uno de los 19 artículos científicos que fueron analizados.

En contraste, los rasgos que aparecieron con menor frecuencia fueron Desarrollo matemático con 2 apariciones en promedio, Definición en 3 ocasiones e Incertidumbre y Magnitud con 4, respectivamente.

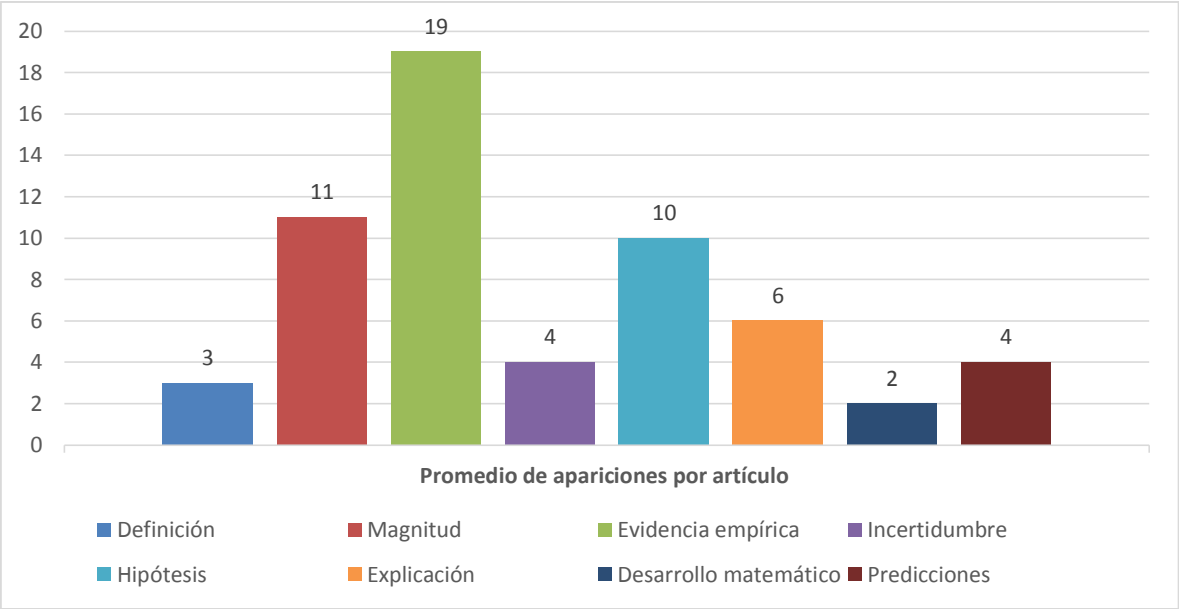

Gráfica 4.1. Promedio de apariciones por artículo

4.2| Análisis cuantitativo: frecuencia de apariciones por disciplina científica

Los 19 artículos se agruparon por composición disciplinaria, utilizando la clasificación del Sistema Nacional de Investigadores[69]:

Área I: Físico Matemáticas y Ciencias

Área II: Biología y Química

Área III: Medicina y Ciencias de la Salud

Área IV: Humanidades y Ciencias de la Conducta

Área V: Ciencias Sociales

Área VI: Biotecnología y Ciencias Agropecuarias

Área VII: Ingenierías

[69] Criterios SNI.CONACYT https://www.conacyt.gob.mx/index.php/sni/convocatorias-conacyt/convocatorias-sistema-nacional-de-investigadores-sni/marco-legal-sni/criterios-sni

En esta etapa fue necesario revisar las temáticas de cada uno de los *papers* para luego agruparlos con base en la propuesta del SNI. De los artículos analizados no se identificó ninguno correspondiente a las áreas VI y VII.

Área I: Físico Matemáticas y Ciencias:

1. PNAS 1 Direct measurements of methane emissions from abandoned oil and gas wells in Pennsylvania
2. PNAS 3 Geometrically controlled snapping transitions in shells with curved creases
3. Nature 3 Linking synchronization to self-assembly using magnetic Janus colloids
4. Science 1 The Last Glacial Maximum
5. Science 3 Probing the Solar Magnetic Field with a Sun-Grazing Comet

Área II: Biología y Química

1. A4 Association of ATP7B Mutation Rate with Biochemical Characteristics in Korean Patients with Wilson Disease
2. PNAS 2 Lethal protein produced in response to competition between sibling bacterial colonies
3. Nature 1 A new eutriconodont mammal and evolutionary development in early mammal
4. Science 2 Arthropod Diversity in a Tropical Forest
5. Science 4 A brain circuit that synchronizes growth and maturation revealed through Dilp8 binding to Lgr3

Área III: Medicina y Ciencias de la Salud

1. A1 Cultivated Corneal Epithelial Transplantation for Severe Ocular Surface Disease in Vernal Keratoconjunctivitis

2. PNAS 4 Zbtb20 is essential for the specification of CA1 field identity in the developing hippocampus
3. Nature 2 Neural dynamics for landmark orientation and angular path integration
4. Nature 4 TA second class of chemosensory receptors in the olfactory epithelium
5. Plos 1 CD46 Protects against Chronic Obstructive Pulmonary Disease
6. Plos 3 "Resource Competition May Lead to Effective Treatment of Antibiotic Resistant Infections"
7. Plos 4 "Fetal Radiation Exposure Induces Testicular Cancer in Genetically Susceptible Mice"

Área IV: Humanidades y Ciencias de la Conducta

1. A2 Importance of family values differences between husbands and wives in determining depression in foreign wives in Korean multicultural families: examining the moderating effect of social support

Área V: Ciencias Sociales

1. Plos 2 A Feature Fusion Based Forecasting Model for Financial Time Series

Luego de asociar los artículos a la categoría que le correspondía, se obtuvo el promedio de apariciones de cada rasgo del Perfil; en la siguiente gráfica se muestra los resultados en orden ascendente:

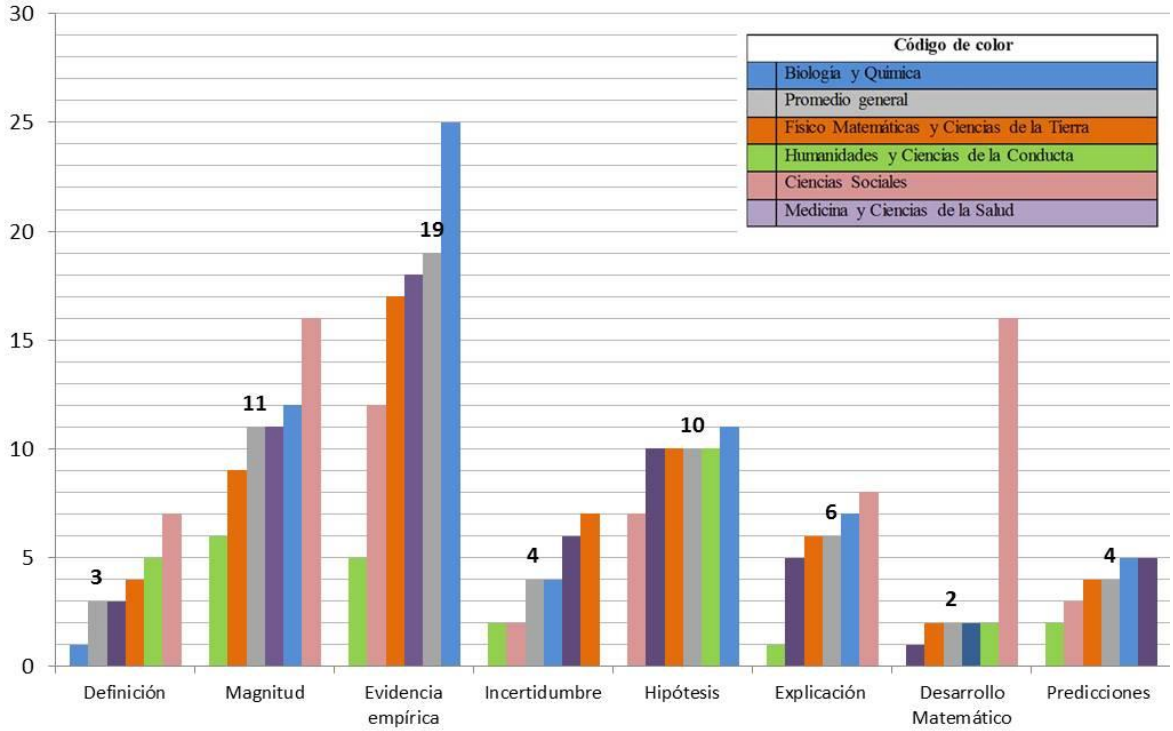

Gráfico 4.2. Promedio general por aparición de categorías del Perfil de Ciencia clasificado según el Sistema Nacional de Investigadores

En este gráfico se observan más apariciones del rasgo Definición en el Área V (Ciencias Sociales) que en Área II (Biología y Química), con una diferencia de 6 entre una y otra.

Para Magnitud el Área V (Ciencias Sociales) fue la que tuvo más apariciones, 16 en total; en contraste, en el Área IV (Humanidades y Ciencias de la Conducta) hubo seis.

En el caso de Evidencia empírica, el Área II tiene el mayor número de apariciones, con un promedio de 25, mientras en el Área IV fue el rasgo que registró menos, con 5. Esta disparidad entre un rasgo y otro es de 20 apariciones, es la diferencia más grande entre todas las que se presentaron a lo largo de esta identificación de apariciones del Perfil de Ciencia.

El rasgo Incertidumbre se localizó en 7 ocasiones en el Área I: Físico Matemáticas y Ciencias de la Tierra; posicionándose como el grupo de disciplinas con más apariciones, caso contrario sucedió en el Área IV, con 2.

Hipótesis fue el rasgos del Perfil que menos variaciones presentó entre una y otra área, es decir, en tres disciplinas científicas (área I, III, IV) encontré 10 apariciones, sólo hubo discrepancias en ciencias sociales que tuvo 7 y en biología y química con 11 apariciones.

En el caso de Explicación, ciencias sociales fue el área en el que más identifiqué esta categoría del Perfil, mientras que en humanidades y ciencias de la conducta sólo localicé una.

Desarrollo Matemático, rasgo que en promedio tuvo menos apariciones que todas las demás categorías, resultó tener mayor presencia en el Área V: Ciencias Sociales con 16 y sólo una aparición en promedio en los artículos del Área III: Medicina y Ciencias de la Salud.

En cambio para Predicción, en el área de Medicina y Ciencias de la Salud, fue en la que se identificaron 5 apariciones en promedio, y el área de Humanidades y Ciencias de la Conducta tuvo 2, esto posiciona a dicha área como la que tuvo menor número de apariciones en un 62.5 por ciento del total de los rasgos del Perfil de Ciencia.

4.3| Análisis cualitativo: resultados de la aplicación del código cromático de certidumbre

Durante la revisión cromática, la cual consiste en indicar el nivel de certidumbre de las interpretaciones a partir de ~~–e~~alificarlas" con tres colores: verde, ninguna o muy pocas dudas; amarillo, algunas dudas; y rojo serias dudas en la interpretación, si lo que se consideró en el primer análisis cumplía con las características de alguno de los 8 rasgos del Perfil [*Véase: Tabla 2.1. Perfil de Ciencia Cruz, Morelos, Gómez, Quiroz, 2017*]

Luego de la aplicación del código cromático, del total de las 1,140 interpretaciones, en un 69% de los casos resultaron estar dentro del parámetro muy segura (787), en un 20% segura (228) y en 11% poco segura (125). En particular se detectó menor seguridad en la selección de rasgos como Definición y Magnitud, en contraste, se presentaron menores dudas en las identificaciones de los rasgos Evidencia empírica, Predicción y Desarrollo Matemático.

La identificación de ninguna o muy pocas dudas en las interpretaciones de las áreas: I, III, IV y V del Sistema Nacional de Investigadores, a excepción del Área II: Biología y Química, donde se puede observar un menor grado de certidumbre son algunos de los resultados reconocidos en esta parte de la investigación.

Capítulo 5

Interpretaciones generales

En este trabajo se da a conocer el conjunto de los 8 rasgos que caracterizan al Perfil, una herramienta que pretende ayudar a alcanzar uno de los requerimientos centrales del periodismo de ciencia: la verificación como disciplina de trabajo.

El análisis pretendió revisar si los rasgos del Perfil representan a la ciencia publicada en revistas arbitradas. La literatura especializada juega un papel clave en el periodismo de ciencia al fungir como su fuente primaria, debido a que la consulta de un artículo científico se propone como esencial para la investigación periodística.

5.1 | ¿Por qué un retrato de la argumentación científica como herramienta?

Facilitar el ―viaje" de los artículos científicos a las historias periodísticas, sin que ello implique perder calidad y el rigor en la interpretación, es una labor compleja pero fundamental si se busca entender y profundizar sobre un tema de ciencia desde su origen.

El periodista que tuvo su último contacto formal con áreas de estudio como las físico matemáticas y/o biología o química en cursos pre universitarios se enfrenta a un reto a la hora de escribir textos con contenido científico verificado.

Esta problemática no se limita a las personas que estudiaron la licenciatura en comunicación y quieren publicar un texto sobre ciencia; esto también es aplicable para aquellos que pretenden escribir sobre un tema alejado de su área de especialización.

Además, las condiciones laborales de las periodistas son poco favorables y algunas de las reporteras que en la actualidad ejercen el periodismo de ciencia o medio ambiente en la Ciudad de México reciben poca preparación complementaria[70,71]

Ante este panorama es vital brindar diferentes opciones e instrumentos para que el periodista pueda ser crítico y sea capaz de estar a la par, como profesional, con funcionarios públicos e incluso con los mismos científicos a la hora de, por ejemplo, encontrarse en una entrevista con ellos.

El Perfil de Ciencia tiene como fin ayudar a las reporteras a enfrentarse a tales retos al permitirles identificar con rapidez la ciencia contenida en un artículo científico y jerarquizarla a la hora de querer utilizarla en su trabajo periodístico. Para tener confianza de que es así, tuvimos que poner a prueba la hipótesis, observando si los rasgos del Perfil representan la ciencia en artículos especializados.

La presente investigación representa el primer eslabón para conocer la validez de la herramienta. La manera en que se hizo fue rastreando los rasgos que componen al Perfil a partir de la aplicación de un proceso de lectura en una muestra de 19 artículos.

Todos los textos se eligieron de forma aleatoria con el objetivo de impedir que el corpus fuera construido con inclinaciones a algún área de la ciencia en particular. El máximo grado de rigor de mis conclusiones dependía de que no hubiera sesgos.

5.2 | La Ciencia sí es reconocible

El resultado de esta investigación fue la presentación de evidencia empírica a favor de la representatividad de la ciencia a través del Perfil. Esto se sustenta en que 6 de los 8 rasgos

[70] Flores Gonzáles, Denisse Joana. *Op Cit*, 2018, P.102.
[71] En la investigación de Flores se mencionan los factores que afectan la calidad de la cobertura, por ejemplo, la intensificación de la inmediatez, la falta de transparencia en la conformación de equipos de investigación y la limitación de los periodistas a secciones específicas, entre otras. Además, según resultados de la *Encuesta para identificar a los periodistas de ciencia en la Ciudad de México,* el 56% del total de periodistas encuestados no había tomado ningún curso o capacitación enfocados al periodismo de ciencia en los 3 años previos a la encuesta.

(Magnitud, Evidencia empírica, Hipótesis, Incertidumbre, Explicación y Predicción) aparecieron en más del 95% de los artículos analizados, mientras que Definición aparece en el 80% y Desarrollo Matemático en un 58%, y por lo menos 3 rasgos (Magnitud, Evidencia empírica e Hipótesis) aparecieron en todos los textos.

Entre las consideraciones generales se encontró que conforme avanzaba en el proceso de lectura resultaba más sencillo identificar los rasgos del Perfil en los artículos científicos. Desde mi percepción, hubo un cambio en la velocidad de la aplicación del análisis en los últimos 8 artículos (a partir del 11 al 19), de 20 horas se disminuyó a 12 por texto. Se cree que dicha reducción de tiempo se debe a la práctica constante de lectura de artículos científicos y discutir las interpretaciones tanto con el asesor de este proyecto de investigación como con las tesistas que junto conmigo utilizaban al Perfil como herramienta de análisis.

Esta evidencia anecdótica expone la utilidad de fomentar espacios de enseñanza del Perfil para que otras estudiantes de periodismo o reporteras en activo interesadas en aplicar la metodología sepan que a pesar de que existirá una curva de aprendizaje, al cabo de cierto entrenamiento, serán capaces de leer y utilizar artículos científicos de forma más rápida y eficiente

Durante el ejercicio de aplicar la herramienta en los 19 artículos científicos se detectaron 1,140 interpretaciones de los ocho rasgos que la componen. Se cree que a pesar de las posibles incertidumbres [*Véase: 5.4 Limitaciones*] dicho número podría modificarse pero no de forma abrupta, tal como se muestra en los resultados del Código Cromático de Certidumbre en los cuales en un 90% me encuentro entre segura y muy segura de mis selecciones iniciales.

En esta experiencia, Magnitud, Evidencia empírica, Definición e Hipótesis fueron los rasgos más sencillos de comprender y aplicar en los artículos científicos debido a que

durante mi formación en la licenciatura como científica social y periodista me enfrenté en otras ocasiones a identificar y trabajar con estos rasgos.

Caso contrario fue Explicación, elemento que a pesar de aparecer en un 95% de los artículos científicos, resulto ser el más difícil de identificar. Los conflictos que se detectaron durante el ejercicio fueron que la forma en cómo se caracterizó el rasgo en el modelo no coincidió con la manera en que los científicos lo mostraron en los artículos que formaron parte de este corpus, cada autor eligió su propio estilo al presentar explicaciones, no existió una caracterización universal.

Lo que se encontró en este trabajo de investigación apoya la hipótesis de que el Perfil de Ciencia permitirá a las periodistas identificar la ciencia contenida en artículos especializados y justifica su utilización como herramienta de análisis de contenido en coberturas periodísticas de temas que incluyen ciencia.

5.3 | Utilidad periodística de los rasgos del Perfil

La reportera de ciencia, quien además de entender el tema debe sintetizarlo a ~~–~~diez mil caracteres redactados en buen castellano, amables, comprensibles y sustanciosos"[72], requiere pistas que le ayuden a facilitar este trabajo. Durante mi análisis detecté que los rasgos del Perfil pueden servir para conseguir información valiosa de un artículo científico. Esta investigación arrojo las siguientes recomendaciones:

Si se compara con el promedio general de interpretaciones identificadas de otros rasgos, Evidencia empírica apareció en un mayor número de ocasiones. [*Véase: Análisis cuantitativo: frecuencia de apariciones generales por artículo*]. Este resultado es coherente con lo que afirma Karl Popper respecto al papel central que juega la evidencia en la

[72] Crúz *Mena*, J. ~~–~~La ciencia del periodismo de ciencia" en *Antología de la Divulgación de la Ciencia en México.* P. 114.

ciencia[73], el cual nos ayuda a "probar hipótesis y teorías, […] (la evidencia) es el núcleo del proceso de la ciencia"[74].

Sin duda, en un trabajo formal de investigación es indispensable este rasgo para dar rigor y veracidad a los datos obtenidos, mientras que, en el ámbito periodístico, es necesario hacer un proceso de selección de la evidencia esencial para contar una historia. Se aconseja poner mayor atención en la discriminación de las interpretaciones de este rasgo cuando una reportera use como fuente un artículo de ciencias exactas, pues según los resultados de esta investigación dichas disciplinas tienden a incluir un gran número de Evidencias.

En el caso de Magnitud, segundo rasgo con más apariciones en promedio, una de sus principales características es que ayuda a entender la dimensión e importancia de algún suceso o fenómeno, lo cual puede ser uno de los primeros pasos para fortalecer o identificar un ángulo original de una historia.

Por otro lado, las periodistas deben tener en mente que una de las principales motivaciones de los científicos de escribir artículos especializados es querer dar a conocer sus resultados a sus pares y deben de comunicarlo de forma concisa. El que aparezca Definición como uno de los rasgos que menos presencia tiene en los artículos analizados podría indicar que los investigadores dan por hecho que sus colegas conocen ciertos términos técnicos por lo que tienden a no detenerse a definirlos pues sus documentos no están dirigidos para que los consulten periodistas. Por lo anterior se aconseja que el reportero tenga en cuenta que es probable no encontrar definiciones en artículos especializados.

Asimismo, otro punto de partida para determinar una historia puede ser a partir de identificar la Predicción de una problemática o un fenómeno tratado en el artículo, este rasgo aparece en casi todos los artículos científicos analizados, por lo que se considera que esta tendencia podrá replicarse en otros textos. La caracterización de Predicción podría

[73] Popper, Karl R. *The Logic of Scientific Discovery"*, P. 127.
[74] U.S.*Testing scientific ideas.* Consultado el 31 de mayo de 2018 en: https://undsci.berkeley.edu/article/0_0_0/howscienceworks_06

generar nuevos ángulos o identificar una idea valiosa a partir de conocer qué dicen los investigadores que sucederá.

5.4 | Limitaciones

El Código Cromático de Certidumbre funcionó como un indicador de las dificultades de la interpretación respecto al primer análisis, ocasionadas por una experiencia limitada en lectura de artículos científicos de la monitora cabe recordar que su práctica con este tipo de literatura se circunscribía a un par de trabajos escolares solicitados en la materia optativa de Periodismo de Ciencia.

Esta herramienta ayudo a responder si el CCC es apto para ser usado por reporteras sin formación científica. Luego de este análisis, resultó que en un 89% se encontró entre segura y muy segura de sus selecciones iniciales. No obstante, en Definición y Magnitud se detectó mayor desconfianza en la interpretación que en otros rasgos [*Véase: Tabla 4.1. Resultados dividida por categorías luego de la aplicación del Perfil de Ciencia en todas sus etapas*] por ejemplo, se seleccionaron en 204 ocasiones Magnitud y en 23 ocasiones confundió este rasgo con elementos de la metodología, esto sucedió al suponer que cualquier parámetro cualitativo relativo a una medición demostraba la relevancia, absoluta o relativa, de la investigación.

La forma en que pude remediar esta confusión fue con la práctica constante de la herramienta y la discusión de los rasgos del Perfil de Ciencia con otros colegas y en congresos en los que fueron presentados resultados parciales de la investigación.

Otra imprecisión detectada luego de aplicar el código cromático de certidumbre fue en el rango Explicación, un concepto que en un inicio resultaba difícil de entender y luego de revisar cada interpretación, se lograron identificar 16 nuevas explicaciones.

Estas incertidumbres en el análisis apelan a favor de realizar una validación más completa del Perfil de Ciencia en artículos científicos, ahora haciendo un control cruzado entre otros

monitores con niveles de experiencia en lectura de literatura especializada distintos (avanzado, intermedio y principiante) para contrastar resultados.

Lo anterior no se pudo llevar a cabo en este proyecto de investigación debido a que no se contó con los suficientes recursos humanos y financieros. La idea es que los monitores analicen y repliquen el proceso de evaluación realizado en esta tesis al Perfil de Ciencia. Se propone que luego de la ejecución del ejercicio se calcule un índice numérico del acuerdo entre los codificadores, esta práctica se conoce como confiabilidad del monitor (*intercoder reliabilit*[75]*y*) y es usada para la validación de investigaciones de diversos temas.

Se considera que el CCC es un buen indicador debido a que hizo explícito el nivel de seguridad en las interpretaciones. Se tiene la hipótesis que a pesar de que puedan salir distintos resultados en otros ejercicios no serán radicalmente diferentes a los ya señalados.

[75] Lombard, Matthew, et al. *Content Analysis in Mass Communication Assessment and Reporting of Intercoder Reliability*. 2002.

Conclusiones

La investigación arrojó los siguientes resultados:

→ Se validó al Perfil de ciencia al comprobarse la hipótesis de que es posible caracterizar la ciencia en artículos arbitrados a través de una serie de rasgos identificables con relativa facilidad por reporteras.

→ Se mostró evidencia empírica a favor de la representatividad de la ciencia en los artículos especializados a través del Perfil de Ciencia. Esto se sustenta en que 6 de los 8 rasgos (Magnitud, Evidencia Empírica, Hipótesis, Incertidumbre, Explicación y Predicción) aparecieron en más del 95% de los artículos analizados.

En el caso de Definición apareció este rasgo en el 80% de los textos revisados y Desarrollo Matemático en un 58%. Magnitud, Evidencia Empírica e Hipótesis aparecieron en todos los artículos.

→ Se concluyó que el modelo tiene potencial para ser usado por reporteras sin preparación científica más allá de la educación preparatoria. En las 1,190 interpretaciones luego de la aplicación del Código Cromático de Certidumbre, en un 89% de los casos se encontraron entre ninguna o muy pocas dudas al respecto de las interpretaciones calificadas.

→ El Perfil de Ciencia enriquece la variedad de herramientas que ayudan a la reportera a incorporar la ciencia en sus textos y puede servir como instrumento para la planeación de trabajos en periodismo de ciencia.

Bibliografía

- Alvarado Cruz, R. (2013). *Diagnóstico de contenidos de ciencia en noticiarios televisivos nacionales a través del protocolo sobre cambio climático y del modelo de funcionalidad del periodismo: conferencia de las partes (COP 16)* México, FCPyS-UNAM, Tesis de licenciatura. Recuperado en http://ru.ameyalli.dgdc.unam.mx/handle/123456789/510.
- Antonio, L. (2013). Periodistas V.S científicos ¿se llevan o no se aguantan? en el *Primer Foro de Periodismo de la Ciencia*, FCPyS.
- Arboleda, T. (2015)*; Ciencia y Tecnología en los telediarios colombianos: sobre lo que se cubre y no se cubre* en Ensaio Pesquisa em Educação em Ciências (Belo Horizonte). Recuperado en http://www.scielo.br/scielo.php?pid=S1983-21172015000100208&script=sci_abstract&tlng=es
- Biblioteca Universidad de Sevilla (2018). *Factor de Impacto: Journal Citation Reports (JCR).* Recuperado en http://guiasbus.us.es/factordeimpacto
- Blanco Altozano, P. (2012). *El artículo científico: puntualizaciones acerca de su estructura y redacción*. Recuperado en http://www.ub.edu/doctorat_eapa/wp-content/uploads/2012/12/El-art%C3%ADculo-cient%C3%ADfico_aspectos-a-tener-en-cuenta.pdf.
- Clark, F. (2006) *A Longitudinal Study of the New York Times Science Times Section*. Science Communication.
  Colombia. Recuperado en http://www.redalyc.org/pdf/817/81722411.pdf
- Criterios SNI. *CONACYT* Recuperado en https://www.conacyt.gob.mx/index.php/sni/convocatorias-conacyt/convocatorias-sistema-nacional-de-investigadores-sni/marco-legal-sni/criterios-sni
- Cruz Mena, J. (2003). Las universidades como fuentes de información científica en crisis sociales: La epidemia del SARS como caso de estudio en *Primer Congreso Iberoamericano de Comunicación Universitaria*, México.
- Cruz Mena, J. (2010). Cómo elegir (y comprender) las fuentes en el periodismo de ciencia en *Jornalismo e ciência: uma perspectiva ibero-americana. /Coordenação: Luisa Massarani*. Rio de Janeiro: Fiocruz / COC / Museu da Vida.
- Crúz, J (2001). La ciencia del periodismo de ciencia en Antología de la Divulgación de la Ciencia en México.

- Cruz, M. (2016) Un modelo de formación universitaria en Periodismo de Ciencia presentado en Simposio PCST Costa Rica *Comunicación científica como profesión: Formación, responsabilidades y roles*.
- Estupinyà, P. (2014). El periodismo científico en América Latina ha mejorado en los últimos 5 años en *El rastreador científico en español.*
- Flaste Richard (1992), the New York Times Book of Science Literacy, *The New York Times*, USA, P.3.
- Flores Gonzáles, D. (2018). *La cobertura de la contingencia ambiental (2016) en portales digitales de la ciudad de México. un estudio desde la sociología de producción de noticias*. Universidad Iberoamericana. México, Tesis de maestría, 2018, P.102.
- Flores González, D. (2015). *Análisis de la cobertura de la pandemia de influenza A (H1N1) en revistas y televisión mexicana desde el punto de vista de la función social del periodismo de ciencia*. México, FCPyS-UNAM, Tesis de licenciatura. Recuperado en http://132.248.9.195/ptd2014/mayo/302149519/Index.html.
- García Rojo, María Keninseb. *Evaluación de la calidad del periodismo de ciencia en la prensa mexicana desde un modelo de funcionalidad. La cobertura del brote de influenza A (H1N1) en abril y mayo de 2009 como caso de estudio* [Tesis en progreso].
- Guevara, M. (2008*). Revisión por pares: ¿Qué es y para qué sirve?* Universidad del Norte
- Iglesias, S. (1981). *Principios del método de la investigación científica*. Editorial Tiempo y Obra.
- Jeff, J. (2013). How to read and understand a scientific paper: a guide for non-scientists en *Violent Metaphors*. Recuperado en https://violentmetaphors.com/2013/08/25/how-to-read-and-understand-a-scientific-paper-2/
- Kovach, B. (2012), Tom. *Los elementos del periodismo*. Editorial Aguilar
- Lystbæk, G. (2011). *From journal to headline: the accuracy of climate science news in Danish high quality newspapers*. JCOM | The Journal of Science Communication.
- Mosterín, J. Et al. Diccionario de Lógica y Filosofía de la Ciencia. 2002. P. 609.
- Nature. For Authors en *Manuscript formatting guide*. Recuperado en https://www.nature.com/nature/for-authors/formatting-guide#a1.1
- Popper, K. (1992). *The Logic of Scientific Discovery,* Recuperado en http://strangebeautiful.com/other-texts/popper-logic-scientific-discovery.pdf
- Revueltas, G (2010). *Fuentes de información en periodismo científico: congresos, revistas y press releases* en Jornalismo e ciência: uma perspectiva ibero-americana. /Coordenação: Luisa Massarani. Rio de Janeiro: Fiocruz / COC / Museu da Vida, 2010, P. 54.

- Rojas Soriano, R. (2013). *Guía para realizar investigaciones sociales*. México. Plaza y Valdes Editores. Recuperado en https://raulrojassoriano.com/cuallitlanezi/wp-content/themes/raulrojassoriano/assets/libros/guia-realizar-investigaciones-sociales-rojas-soriano.pdf
- Rosen Ferlini, C. (2008) *Análisis de la cobertura periodística del cambio climático en 2001 desde un modelo de funcionalidad. México*, FCPyS-UNAM, Tesis de licenciatura, 2008 P. 140. Recuperado en http://ru.ameyalli.dgdc.unam.mx/handle/123456789/523.
- Rueda, A (2007). *La síntesis como herramienta en el periodismo de ciencia. un análisis comparativo con su uso en la literatura infantil*. México, FCPyS-UNAM, Tesis de licenciatura. Recuperado en: http://ru.ameyalli.dgdc.unam.mx/123456789/490.
- SciDev (2008) *How do I write a scientific* paper Recuperado en http://www.scidev.net/global/publishing/practical-guide/how-do-i-write-a-scientificpaper-.html
- Somedicyt. (2016) Encuesta para identificar a los periodistas de ciencia en la Ciudad de México Reporte de Resultados.
- Stanton, Liz (2017). *Last Week Tonight with John Oliver*. HBO. Recuperado en https://www.youtube.com/watch?v=0Rnq1NpHdmw
- Understanding Science project, *U.S. Testing scientific ideas*. Recuperado en https://undsci.berkeley.edu/article/0_0_0/howscienceworks_06
- Veneu, F, Massarani, L. (2008). *Science journalism in Latin America: how the scientific information from a scientific source is accommodated when it is transformed into a journalistic story*, JCOM | The Journal of Science Communication.

NOTAS INFORMATIVAS

- Rueda, A. (21 de junio de 2015). Latinoamérica… ¿el patito feo del periodismo de ciencia? En *RedMPC*. Recuperado en https://redmpc.wordpress.com/2015/06/21/latinoamerica-el-patito-feo-del-periodismo-de-ciencia-parte-ii/
- Red Mexicana de Periodistas de Ciencia (13 de enero 2016). *Crean formalmente la red mexicana de periodistas de ciencia (REDMPC).* Recuperado en https://redmpc.wordpress.com/2016/01/13/crean-formalmente-la-red-mexicana-de-periodistas-de-ciencias-redmpc/.

ANEXOS

Anexo 1. Interpretaciones generales

DEFINICIÓN				
Consecutivo	**Clasificación**	**Apariciones**	**Consecutivo del paper**	**Color**
1	**A1**		**0**	
2	**A2**	Family values are political and social beliefs reflecting cultural and historical characteristics of society (Kim, 1998). At the same time, family values are reflective of individual characteristics, explaining different value systems among members of the same family.	**1**	
		Familism, often understood to be the opposite of individualism, refers to the form in which ―the interests of the individual are subordinated to those of the family" (Hellier, 1970, pp. 73).	**2**	
		Caring for elderly parents is also another subcategory of the value system, which refers to the values one holds in regards to adult children's responsibility in caring for elderly parents.	**3**	
		Social support usually refers to the aid given to individuals in stressful situations by others, including material, financial, informational, emotional, and instrumental aids (House & Kahn, 1985)	**4**	
		The family values scale (Ok, 1989) measures individuals' value systems in regards to family and family life including individuals' propensity to consider family's needs more than his or her own and their attitudes towards the roles women and men have to assume within the family.	**5**	
3	**A4**	Wilson disease (WD; MIM #277900) is a disorder of copper (Cu) metabolism [1]. Liver disease, neurologic presentations, and psychiatric disturbances are caused by an accumulation of disorder of copper Cu.	**1**	
		Wilson disease (WD) is an autosomal recessive disorder caused by mutations in the ATP7B gene, yet many patients have either one mutation, or no mutation.	**2**	
		WD is caused by mutations in the ATP7B gene, which encodes a Cu-transporting P- type ATPase. Because WD is an autosomal recessive disorder, most WD patients have two ATP7B mutations.	**3**	
4	**PNAS 1**	Orphaned wells can be defined as abandoned wells with no responsible party available, other than the state.	**1**	
		Mass flow rates, in units of mass per time per well, beginning from the moment of chamber deployment, were calculated using linear regression in MATLAB on the concentration data, c [mass/volume], over time. where dc=dt is the slope of the fitted line for cðtÞ and Ve is the effective chamber volume. For control locations, F is scaled based on the land area covered by the chamber for the control and the nearest well location.	**2**	
		Mass flow rates, in units of mass per time per well, beginning from the moment of chamber deployment, were calculated using linear regression in MATLAB on the concentration data, c [mass/volume], over time.	**3**	
5	**PNAS 2**	Bacterial cannibalism, some bacterial prespores secrete a molecule that kills their neighbors, while inducing an immunization system that ensures their own survival.	**1**	

		The antimicrobial compounds secreted during cannibalism or fratricide (2 – 6) are called bacteriocins, and usually have a narrow spectrum of activity as they kill only closely related bacteria, which compete for the same resources.	**2**	
6	**PNAS 3**	We consider a crease to be a long but narrow region of locally weak material introduced, for example, through a local thinning of the shell.	**1**	
		If the osculating plane makes an angle ψ with respect to the shell (Fig. 1B), we can define the geodesic curvature, κg =κcosψ, and the normal curvature, κN =κsinψ, as the respective projections of the space curvature onto the tangent (^u+, Fig. 1B) and normal (^n+, Fig. 1B) of the shell‘s midsurface.	**2**	
		A straightforward calculation (see the Supporting Information) obtains the mean curvature of the shell near the fold, where τ is the torsion of the fold, which measures the rate that the osculating plane twists around the hinge and, hence, the nonplanarity of the hinge (32).	**3**	
		In this case we may use the definition of the geodesic curvature to solve for the angle ψ, which yields ψ =±cos−1ðκg=κÞ.	**4**	
		The bending energy density of a folded surface, in the vicinity of the fold, is EB =B=2ðH −H0Þ2,whereB is a bending modulus and H0 is the background shell curvature	**5**	
		Bending along an asymptotic curve, defined to have κN = 0	**6**	
		Define the normalized crease radius as α=Rt=Rs (Fig. 4A).	**7**	
		EP ~Yðt=RsÞ5=2r3, with Y as the Young‘s modulus of the material.	**8**	
		Hence the total energy (ET) for deformation scaled by B can be expressed as: where γ is the Föppl–von Kármán number γ ≡ ^YR2s=B, with ^Y as the stretching modulus of the material (plotted schematically in Fig. 5A).	**9**	
		FIG. 5A	**10**	
7	**PNAS 4**	The hippocampus is an archicortical structure located at the medial-temporal edge of the neocortex. It can be divided into distinct cytoarchitectonic regions: the CA1 and CA3 of Ammon‘s horn, and the dentate gyrus (DG) (1). All three regions consist of a principal layer of densely packed neurons—pyramidal cells in the CA1 and CA3, and granule cells in the DG.	**1**	
		The subiculum and the transitional neocortex (also known as mesocortex) lie between Ammon‘s horn and the neocortex. The subiculum comprises a principal cell layer of large, less-compact pyramidal neurons, whereas the cytoarchitecture of the transitional neocortex is distinct from the archicortex in that the principal laminae comprise several subsets of relatively less compact neurons organized into deep and upper layers (2).	**2**	
		Mannosidase 1 alpha (Man1α), a specific marker of mature CA1 neurons (17)	**3**	
		Sox5 (a layer V, VI, and subplate marker) (19)	**4**	
		Tshz3 (a marker of all neocortical layers) (20)	**5**	
		Id2 (a layer II–III, V–VI, and subplate marker) (21)	**6**	
		Neurotrophin 3 (NT3, a transient marker for upper layer in cingulate and retrosplenial cortices) (5)	**7**	
		ER81 (a layer V marker) (22)	**8**	
		Cux2 (a layer II–IV marker) (23)	**9**	
		Mef2c (a layer I–VI marker) (24)	**10**	

		Fibronectin1 (a marker for subiculum)	**11**	
		Calretinin, which is indicative for the axons of mossy cells in the IML (7).	**12**	
		Axin2, an intracellular negative regulator of Wnt signal transduction and a known downstream target of canonical Wnt signaling	**13**	
		Nr4a2 (a marker for subiculum and deep layer projection neurons) (27)	**14**	
		BDNF (a survival factor of hippocampal progenitors) (28)	**15**	
8	**Nature 1**	Yanoconodon allini gen. et sp. nov. Yan is for the Yan mountains in Northern Hebei Province; conodon is Latin for ‗cuspate tooth', a common suffix for mammalian taxonomic	**1**	
9	**Nature 2**	In the absence of such cues, many animals track their position relative to a reference point by continuously monitoring their own motion, a process called path integration.	**1**	
		we now focused on a class of columnar neurons of the CX, each of which sends dendrites to a specific wedge of the EB (Fig. 1c, d). These neurons are abbreviated here as EBw.s neurons (see Methods)13,23-27.	**2**	
10	**Nature 3**	Janus colloids, micronsized spherical particles with different surface chemistry on their opposing hemispheres	**1**	
		However, at higher h, synchronization criteria set in. The larger the tube diameter, the smaller the coupling strength e and the larger the friction ftube, leading to lower dissociation angle hc. For example, with increasing h in Fig. 2c we saw fewer (550) microtubes and none above hc (which is about 25u for this structure).	**2**	
		Here ω***free* is the** angular velocity of free particles under the same condition, and *ςr* and *ςtube* **are** the rotational friction coefficients of the single particle and the entire tube, respectively.	**3**	
11	**Nature 4**		**0**	
		Vomeronasal organ — an olfactory structure with receptors that differ from odorant receptors	**1**	
12	**Science 1**	The Last Glacial Maximum (LGM) is conventionally defined from sea-level records as the most recent interval in Earth history when global ice sheets reached their maximum integrated volume.	**1**	
		In evaluating insolation, we include the summer energy index, defined as the sum of insolation at a given latitude on days when a threshold insolation value corresponding to 0°C is exceeded.	**2**	
		FIG. 4. Constraints on changes in sea level and deep ocean temperature. The vertical purple bar represents the time of LGM as defined from the RSL data, whereas the vertical gray bar represents the earliest interval when sea level began to fall to the LGM lowstand, corresponding to the time when the first ice-sheet LLGM were reached	**3**	
13	**Science 2**		**0**	
14	**Science 3**	solar corona (~1 to 2 solar radii, RS, measured from Sun center).	**1**	
		—standard" coronal conditions (r < 1.2 RS, electron number density ne ~ 108 cm–3, electron temperature Te ~ 1.5 MK):	**2**	
		that is, vi → vi,macro = (vi · b)b = vpb, where vp is the speed parallel to the field direction, b = B=B / |B|. where B is the local magnetic field vector.	**3**	

15	**Science 4**		**0**	
16	**Plos 1**	[T regulatory cells (Treg)] Tregs are CD4 + CD25 + T cells, they express FOXP3, secrete IL10, suppress cytotoxic (Tc) and helper (Th1) T cells. Tregs are produced by coupling of CD3 with CD46; they are able to regulate the responses adaptive.	**1**	
17	**Plos 2**	X(t)=AS(t) s(t) =Wx(t) Where *A* is called mixing matrix, is a separati is an unknown mixture coefficient. From the formula (1), we can see linear combination of the independent random signals . That is,	**1**	
		F(X) = <Wq(x)>+b where, is the weight vector, is constant, and represents a kind of nonlinear function that maps x from the input space to the high dimensional space in order to transform the nonlinear problem into a linear one.	**2**	
		(6)(6)where is a precision parameter which represents the tube size of the SVR.	**3**	
		Information fusion is a new, high-level technology which collects different information from multi-sensors of the same object and removes redundant information or noise from mutual information. Commonly, there are three different fusion levels: data level fusion, feature level fusion, and decision level fusion [52].	**4**	
		Table 1. Variables used as inputs.	**5**	
		where a and b are the eigenvector of eigenfunction, respectively. The projection matrix Ad~fa1,a2, ,adg and Bd~fb1,b2, ,bdg is composed of the eigenvectors corresponding to the first d largest eigenvalues of function (15). After Ad and Bd are calculated, the fusion feature of x and y can be obtained by the following equation.	**6**	
		Table 2. Measure indicators.	**7**	
18	**Plos 3**		**0**	
		The pathogens are composed of sensitive (represented by the subscript S) and resistant (represented by the subscript R) strains. The abundance of pathogens, B=BS+BR, is limited to a carrying capacity l?k [43–45], giving rise to a logistic growth. The growth rate, lS or lR, is the difference between the division (d) and the mortality (m) rate. The model also considers the effect of the immune system, represented by the number of phagocytes (P) and their killing rate (c), and assumes that the populations of pathogens and phagocytes are well mixed.	**1**	
		where a indicates the rate at which resistance is attenuated (resistance-decaying rate) and B0 the abundance of resistant pathogen at a reference time.	**2**	
		the maximum abundance of resistant pathogen that guarantees an effective antibiotic treatment (which we call h0).	**3**	
		where Dl = lS - lR is the difference in growth rate of sensitive and resistant strains. Dl<0 when no treatment is applied and it increases under antiR conditions.	**4**	
19	**Plos 4**		**0**	

MAGNITUD

Consecutivo	Clasificación	Apariciones	Consecutivo del paper	Color
1	A1	In patient 1, vision improved from 20/800 (both eyes) to 20/30 in the right and 20/100 in the left eye at a follow- up of 34 months. In patient 2, it improved from 20/400 to 20/50 after the second procedure, 25 months postoperatively.	1	
		The best corrected visual acuity (BCVA) in both eyes was 20/800. Biomicroscopy revealed upper tarsal conjunctiva scarring, conjunctival overgrowth on cornea, epithelial erosions, vascularization, and stromal scarring (Figs. 1A and 2A).	2	
		At the 3-month postoperative visit in November 2001, his vision had improved to 20/60 in both eyes. The corneal clarity had improved, with no recurrence of conjunctivalization or neovascularization (Figs. 1B and 2B)	3	
		Her BCVA was 20/400 in the right eye and 20/25 in the left.	4	
		Three months later, vision in her right eye had improved to 20/50.	5	
		Her BCVA was 20/50 and 20/25 in the right left eyes, respectively	6	
		We have reported 2 cases of VKC with severe ocular surface disease successfully managed with surface reconstruction.	7	
2	A2	As the age gap between husbands and wives also tends to be rather large, with an average of 12.1 years compared with 2.2 years among Korean couples (Statistics Korea, 2011), it is also possible that foreign wives are more likely to struggle with values differences as their spouses are much older with stronger patricentric values.	1	
		For analyses, the 2006 Gyeonggi Province International Marriage Data were used. Gyeonggi Province is a heavily populated area for marriage migrants with over 24% of all multicultural families residing in the region (Kim et al., 2009). The samples (husbands and wives) were recruited from four metropolitan areas, two industrial areas, and four rural areas using systematic random sampling (Chung et al., 2007).	2	
		The data contain responses from 810 foreign wives and 425 Korean husbands. Researchers excluded families without a child; thus, the final sample size was 241 marriage migrant women and their husbands.	3	

		In this sample, husbands were 8.46 years older than their wives on average, ranging from 5 (wife was 5 years older than her husband) to 40. Thus, it was consistent with the previous findings that the age gap between the husband and the wife in multicultural families is greater than that between Korean couples, which is 2.8 years on average (Kwon, 2010).	**4**	
		The mean years of education were 11.59 (SD = 2.86) so we can assume that the marriage migrant women had some high school education. Monthly household income was approximately 2 million won per month.	**5**	
		Approximately 75% of wives were in the workforce at the time of the interview and almost 60% of them answered they do not have difficulties understanding Korean. Those who used a broker agency for the current international marriage constituted 17.4%.	**6**	
3	**A4**	In a study of 71 patients, we used PCR-sequencing to screen for ATP7B mutations in 7 exons (exons 8, 10, 11, 14, 15, 16, and 18) covering 95% of known mutations in Korean patients with WD.	**1**	
		Direct sequencing of all 21 ATP7B exons and their adjacent introns from 120 Korean WD patients showed a mutation detection rate of 75.0% (180/240), and about 95% of mutations were identified within 7 exons (exons 8, 10, 11, 14, 15, 16, and 18) [10].	**2**	
		About 25% of mutant alleles had not been previously identified in Korean patients with WD [10,11].	**3**	
		Seventy-one patients were recruited for the present study (median age 21.0 yr, range 4~49 yr). Sixty-nine patients were unrelated and two were sisters of two patients.	**4**	
		Mutation screening was performed for 7 exons (exons 8, 10, 11, 14, 15, 16, and 18) representing 95% of exons containing mutations found in Korean patients with WD [10].	**5**	
		However, even the most sensitive and specific laboratory tests are secondary to astute clinical suspicion in the search for WD [16].	**6**	
		About 85% of 516 Korean patients with WD have demonstrated hepatic symptoms [17], similar to the results of the present study.	**7**	
		Cu chelation requires life-long compliance; therefore, prompt, accurate diagnosis of WD is important.	**8**	

		However, ceruloplasmin deficiency is a key finding in the diagnostic approach to WD because there is no single definitive test for diagnosis of WD.	**9**	
		demonstrated a ceruloplasmin concentration of <10 mg/dl in 72.7% of patients with WD, but the ceruloplasmin concentration in 9.1% of patients with WD was >21 mg/dL [21].	**10**	
4	**PNAS 1**	A total of 42 and 52 direct measurements were made at wells and at locations near the wells (“controls”) in forested, wetland, grassland, and river areas in July, August, October 2013 and January 2014, respectively.	**1**	
		Three out of the 19 measured wells were high emitters that had methane flow rates that were three orders of magnitude larger than the median flow rate of 1.3 × 10−3 kg d well.	**2**	
		We scaled methane emissions from our direct measurements of abandoned wells in Pennsylvania and calculate that they represent 4–7% of current total anthropogenic methane emissions in Pennsylvania.	**3**	
		To characterize abandoned oil and gas wells‘ potential as a significant methane source, we made first-of-a-kind direct measurements of methane flow rates from 19 wells in various locations across McKean and Potter counties in Pennsylvania (PA) (Fig. 1). The measured wells were selected mainly based on logistical and legal access (Supporting Information). As of January 17, 2014, only 1 of the 19 wells was on the PA Department of Environmental Protection‘s (DEP ‘s) list of abandoned and orphaned wells.	**4**	
		Fig. 1. The 19 measured wells are located in McKean County and Potter County in Pennsylvania. There are 12,127 abandoned, orphaned, and plugged wells on the Pennsylvania DEP‘s website (as of January 17, 2014), with 4,273 in McKean County and 188 in Potter County. The map shows the DEP wells that are in the region of our field study. Note that only the western portion of Potter County is shown in the detailed map.	**5**	
		The DEP database provides information on the well status (abandoned, plugged, or orphan) and well type (gas, oil, combined oil and gas, or undetermined) but does not provide other information such as well age and depth. No additional information on the measured wells is available. This is indicative of the general scarcity of available information on this class of old wells in PA. This work provides previously unavailable data on methane leakage rates and other emissions from abandoned oil and gas wells.	**6**	

		A comparison of the methane δ13C values to that of known thermogenic and microbial sources (20) indicates that most of the methane flow rates from wells are thermogenic or a mixture of microbial and thermogenic sources. Only 3 of the 26 measurements at wells had methane δ13C values in the microbial range. The methane δ13C values of the measured wells ranged from −71‰ to −21‰.	**7**	
		This range is broader than published methane δ13C values of thermogenic methane in natural gas in the northern Appalachian basin, which range from −47.9‰ to −30.7‰ (21). The methane δ13C values at controls ranged from −85‰ to 756‰, indicating control sources were more likely to be of primarily microbial origin.	**8**	
		Only 3 of the 26 measurements at wells had methane δ13C values in the microbial range.	**9**	
		Using these numbers, we estimate methane emissions from abandoned oil and gas wells in PA to be 0.03–0.05 Mt CH4 per year, which corresponds to 4–7% of estimated total anthropogenic methane emissions in PA for 2010 (22) (Supporting Information).	**10**	
		Assuming the mean flow rate found here is representative of all abandoned wells in Pennsylvania, we **scaled** the methane emissions to be 4–7% of estimated total anthropogenic methane emissions in Pennsylvania.	**11**	
5	PNAS 2	The highest identity (57%) was found with a protein of unknown function of the Geobacillus sp. Y412MC10 (9). There was also identity (53%) with an uncharacterized protein IRC4 (increased recombination center) associated with recombination in yeast (10), but no other insights into function were obtained from analysis of the protein sequence.	**1**	
		However, no growth was detected even at very low subtilisin level on the 1.7% agar gel. (ii) At a lower agar concentration (1.5%), high subtilisin levels were found to inhibit growth, trigger secretion of the third protein and cause cell death (Fig. 1E). However, if surfactant (0.0006% Brij 30) was initially added to the medium (11), the colony expanded; high subtilisin levels were found to promote colony growth, and the third protein was not detected.	**2**	
		Twelve mL of molten agar was poured into8.8 cm diameter Petri dishes, which were dried for 4 d at 25 °C and 50% humidity until the weight decreased by 1 g.	**3**	

		The bacteria are maintained at−80°C in Luria Broth (Sigma) with 25% glycerol.	**4**	
		Polyacrylamide gel electrophoresis on 1 mm NuPAGE 4–12% Bis-Tris gels (Invitrogen).	**5**	
		The Blotting buffer contains 20% methanol and dichlorodiphenyltrichloroethane.	**6**	
		The precipitated proteins were resuspended in 1 ML water and placed in dialysis tubing with a 12–14 kDa cutoff	**7**	
		Column: 0.8×250mm C18 column. Buffer A: 0.1% TFAin water (LC-grade). Buffer B: 100% acetonnitrile (LC-grade),ca.0.8% TFA	**8**	
		Flow rate 200μL⁄min. Absorption was measured for 2 wavelengths: 214 nm(absorption of peptide bonds) and 280 nm (for detecting aromatic aminoacids residues).	**9**	
		Following induction for 2 h at 37 °C, cells were harvested and lysed by sonication in buffer containing 20 mM	**10**	
		Sodium phosphate, 500 mM NaCl, 30 mM imidazole, 1 mM PMSF and450mg⁄L lysozyme	**11**	
		he His-tag protein waseluted from the nickel column using 500 mM Imidazole.	**12**	
6	PNAS 3	While the well-known rules and mechanisms behind folding a flat surface have been used to create deployable structures and shape transformable materials, folding of curved shells is still not fundamentally understood.	**1**	
		Because our proposed design principle arises purely from geometry, it does not rely on special materials or anisotropy to generate rapid snap-through transitions; in practical applications, this enables one to harness the instability for fast actuations purely by design, thereby providing a simple method for the design of rapidly actuating structures from a wide range of elastic materials.	**2**	
		For creased cylinders with a small fd,θg=f2.8 mm,6.6°g, we note that the effective stiffness of the shell is much lower for small displacements, but that the indentation profile matches the increased shell for large indentation.	**3**	
		For creases with larger,θg=f11.4 mm,12.8°g, the localized stretching energy can be focused entirely in the crease, so that the energy landscape is modified to allow for a fast snap.	**4**	

		Upon indentation, for an uncreased shell (Rs =35 mm, α=0) we observe a monotonically increasing load response similar to previous studies (1, 38, 45) (Fig. 4B).	**5**	
		In a similar fashion to the cylinder, we observe a local minimum in force for lower values of α (=0.5) devoid of a stable folded state, but indenting a creased shell with higher α (=0.6) leads first to an unstable, nonaxisymmetric snap, soon followed by a well-defined stable snap (Fig. 4B, Insets and Movie S3).	**6**	
		The energy for this state has a bending energy contribution from the inverted bulge that scales as EB ~Bðr=RsÞ2, whereas the ―Pogorelov ridge," acting as an elastic boundary layer, contains all of the stretching energy (35, 47).	**7**	
		Although material asymmetry is a proven mechanism for creating this bifurcation of stability, for the case of a creased shell, the inherent geometry itself serves as a barrier to folding.	**8**	
		Our results provide a purely geometrical mechanism for designing multistable structures, thus circumventing the need for complex materials or fabrication methods in creating structures with fast dynamics.	**9**	
		While inhomogeneous shells have already been predicted to serve as a template for constructing tunable shapes (49), and used to design next-generation substances such as lock-and-key colloids (50) or controllably collapsible capsules (39), our geometric design principle adds further insight into controlling the mechanics of thin shells.	**10**	
		The ability to introduce tunable bistability into a curved shell via structural inhomogeneity represents a major step in generating programmable materials with rapid actuation capabilities.	**11**	
7	**PNAS 4**	Zbtb20 mRNA was first detected by in situ hybridization in the hippocampal primordium as early as embryonic day (E) 12.5, and was greatly increased by E13.5 (Fig. 1Aand Fig. S1A).	**1**	
		To further define the expression distribution of Zbtb20, we pulse labeled with bromodeoxyuridine (BrdU) at E15.5 for 1 h, the stage at which the generation of pyramidal cells in Ammon's horn is most active (4).	**2**	

		This transformation became progressively more conspicuous during early postnatal development, when both the hippocampus and transitional neocortex gradually acquire their mature features (Fig. S2 E–H).	**3**	
		However, compared with the wild-type control, the mutant DG was obviously smaller at E18.5 (Fig. S2 C and D), and exhibited shorter blade like structure during postnatal development, with the external blade (DGe) even much shorter (Fig. S2 E–H).	**4**	
		From P0 through P21, however, there was a remarkable increase in the number of apoptotic cells in the mutant hippocampus (Fig. S3 I–K). At P7, for example, there was a 10-fold increase in TUNEL positive cells in mutant hippocampus compared with control.	**5**	
		NP2 and EphA4 are normally expressed in the entire hippocampus from early embryonic development (15, 16), but were greatly reduced in the mutant CA1 field at E16.5, 2 days before the onset of the cytoarchitectonical abnormalities we observed (Fig. S4 A–D).	**6**	
		Furthermore, at more caudal levels, the expression domain of Fibronectin1 (a marker for subiculum), normally located between CA1 and retrospenial cortex in wild type (http://www.brain-map.org/), was ectopically present adjacent to the lateral border of the CA3 (Fig. 4 K and L).	**7**	
		After placing DiI in the DG of P14 mice, the mossy fibers were clearly visualized in the stratum lucidum of wild-type CA3, but absent in the mutant (Fig. S6 A and B). Similarly, Schaffer collaterals, which extend from CA3 to CA1, were present in the wild types rather than the mutants after placing DiI in the CA3 and DG (Fig. 6 E and F). Taken together, the tracing results show the remarkable defects in hippocampal neuronal network in Zbtb20 mutant mice.	**8**	
		It turned out that there were a total 153 up-regulated and 192 down-regulated unique probe sets that exhibited a minimum 2-fold change and reached statistical significance.	**9**	
		Notably, it was recently reported that down-regulation of Zbtb20 expression by RNA interference from E15 results in the loss of Calbindin-D28k expression by CA1 neurons (29), although their cell fate was not elaborately determined.	**10**	
		Another intriguing finding in this study is the field-dependent manner in which Zbtb20 controlled hippocampal development.	**11**	

		Our study showed that the loss of Zbtb20 did not cause any notable alterations to the expression and activity of both canonical and noncanonical Wnt signaling components in the hippocampal region at embryonic stages. These observations suggest that Wnt signaling alone is not sufficient to induce archicortex differentiation.	**12**	
		Taken together, this study establishes a critical role for Zbtb20 in the specification of CA1 field identity and in the maintenance of neuronal survival in the developing hippocampus, and provides insight into the regulation of corticogenesis.	**13**	
8	**Nature 1**	Detachment of the three tiny middle ear bones from the reptilian mandible is an important innovation of modern mammals.	**1**	
		The connected ear and jaw structure is similar to the embryonic pattern in modern monotremes (egg-laying mammals) and placental mammals, but is a paedomorphic features retained in the adult, unlike in monotreme and placental adults.	**2**	
		Equivalent beds in the western Liaoning Province were dated to 125 to 122 million years ago	**3**	
		Yanoconodon is preserved with the middle-ear bones (except the stapes), an ossified Meckel‘s cartilages, and the associated (although disarticulated) hyoid elements (Fig. 1; also Supplementary Information).	**4**	
		The malleus has a manubrium that is similar to (although more robust than) that of the adult monotreme Ornithorhynchus17–19, and the goniale element (_prearticular‘) is also present (Fig. 3).	**5**	
		Yanoconodon is similar to gobiconodontids but different from closely related Jeholodens in having these primitive features. Similar to many cynodonts and some mammaliaforms, the anterior seven lumbar vertebrae have mobile ribs, several with an expanded proximal portion of the rib as in (but less developed than) the plated lumbar ribs of many cynodonts and the docodont Castorocauda.	**6**	
		Yanoconodon and Repenomamus36 have 26 thoracolumbar vertebral segments, an exceptional number if com- pared to the 22 thoracolumbars of Jeholodens, and 19 or 20 thoraco- lumbars in most Tertiary and modern mammals.	**7**	
		The homology of post-dentary elements of non-mammalian tetrapods with the mammalian middle-ear bones has long been established. Long before the current fossil evidence was discovered, it was hypothesized that the migration of middle-ear bones from the mandible in cynodont–mammal evolution underwent an intermediate stage in which these bones would be anteriorly connected to the lower jaw, but suspended medial to (and free of) the mandibular pterygoid region (ref. 43 and Fig. 28.11 of ref. 44).	**8**	

		Yanoconodon‘s middle ear shows a paedomorphic resemblance to the embryonic pattern of modern mammals	**9**	
		Yanoconodon and Repenomamus both have 26 thoracolumbar vertebrae, and these eutriconodontans represent a high variation for the highly conserved 19 to 20 thoracolumbar vertebrae of crown Mammalia.	**10**	
		By contrast, Jeholodens lost lumbar ribs and achieved a distinctive boundary between the thoracic and lumbar regions (Fig. 4: node 2); its 15 thoracic and 7 lumbar vertebral counts are more comparable to modern mammals.	**11**	
		Reciprocally, homoplastic thoraco-lumbar characters within eutriconodontans and symmetrodontans provide two cases for extrapolating the Hox gene patterning of laboratory mice to early mammal phylogeny on a grand evolutionary scale.	**12**	
9	**Nature 2**	Many animals navigate using a combination of visual landmarks and path integration	**1**	
		Visual landmarks can provide animals with a reliable indicator of their whereabouts.	**2**	
		We sought to uncover integrative neural processes relevant to navigation in the CX by allowing a tethered fly to control and respond to visual stimuli while simultaneously recording its neural activity and behavior.	**3**	
		Consistent with EBw.s activity representing orientation by flexibly locking to a single landmark, the resulting EBw.s representation again involved a single bump (Extended Data Fig. 4b-f; Supplementary Video 3), with the same mapping of the visual scene onto the EB as before (Extended Data Fig. 4g)	**4**	
		Figure 2 | b, Mean and s.d. of number of bumps across trials for each of 9 flies.	**5**	
		Persistent activity in the CX can maintain compass information when the fly is standing in darkness for 30 seconds — two orders of magnitude longer than might be explained by calcium sensor decay kinetics18.	**6**	
		Direct experimental evidence in support of these models has been difficult to obtain in mammals due to the distributed nature of the underlying circuits.	**7**	
		Taken together, these data are consistent with a function for the EBw.s population as an internal compass that adaptively represents the fly‘s orientation relative to visual landmarks.	**8**	

		We studied the activity dynamics of a complete population of identified CX neurons in tethered walking flies and found that this network uses information from both landmark-based and angular path integration systems to create a compass-like representation of the animal's orientation in the environment.	**9**	
		Figure 4 | Experiments with flies walking in total darkness. b, Mean and s.d. of number of bumps across trials for each of 11 flies.	**10**	
10	**Nature 3**	Synchronization occurs widely in the natural and technological worlds, from the rhythm of applause and neuron firing to the quantum mechanics of coupled Josephson junctions, **but has not been used to produce new spatial structures**.	**1**	
		A short period of chaotic clapping, applause often becomes rhythmic—everyone claps with the same phase and tempo. This illustrates fundamental elements of synchronization: the individual units display periodic motion, they display adjustable phase and frequency, and they couple.	**2**	
		Thin nickel films (18 nm or 21 nm) were directionally deposited onto one hemisphere of 3-mm spherical silica particles7,8. The magnetic response of these particles is smaller along the Janus director (red arrow in Fig. 1a) and larger in the plane perpendicular to it (Supplementary Fig. 2), yielding a discoid symmetry.	**4**	
		Hence, for most experiments we employed a fixed frequency f (20 Hz) and field strength (5 mT), leaving h as the control parameter. Although composed of Brownian particles, the system was deterministic, with interactions around 104 times the thermal energy.	**6**	
		We considered a (330) structure in its **lowest-energy configuration** in a static field, with each sphere‘s director pointing to the central axis. Once the processing field was switched on, the constituent particles rotated with respect to the tube and adopted an average orientation that deviates from inward-pointing by an angle y defined in Fig. 3b.	**7**	
		This dynamics-induced transition offers interesting possibilities for structural selection (Fig. 2c) that would not be possible with conventional static energy minimization.	**8**	
		The path is also clear to extend these approaches using patterned arrays of external driving sources to achieve spatially resolved reconfigurable structures.	**9**	

11	**Nature 4**	Odorants are detected in the nasal olfactory epithelium by the odorant receptor family, **whose 1,000 members** allow the discrimination of a myriad of odorants.	**1**	
		Genes encoding these receptors, called _trace amine-associated receptors‘ (TAARs), **are present in human**, mouse and fish.	**2**	
		Notably, **at least three mouse** TAARs recognize volatile amines found in urine: one detects a compound linked to stress, whereas the other two detect compounds enriched in male versus female urine: one of which is reportedly a pheromone	**3**	
		Mammals have **as many as** 1,000 different odorant receptors that vary in protein sequence	**4**	
		On the basis of genome sequence data, this family **has 15 members in mouse and 6 in human**, and is also found in fish	**5**	
		TAARs are unrelated to odorant receptors, with their closest relatives being receptors for biogenic amines such as serotonin and dopamine. For example, mouse **TAAR1 is 33% identical to the mouse 5-hydroxytryptamine (serotonin) receptor 4, but only 16% identical** to the most closely related mouse odorant receptor (OLFR461), and it lacks sequence motifs characteristic of odorant receptors.	**6**	
		Zebrafish **reportedly has 57 intact** taar genes, only one of which—taar9—is listed as such at the NCBI. Interestingly, UniGene lists three ESTs for zebrafish taar9, all of which are from olfactory rosettes—the location of the fish olfactory epithelium.	**7**	
		Figure 1|Digoxigenin-labelled antisense RNA probes for the mouse Taar genes indicated were hybridized to coronal sections of mouse olfactory epithelium. Each Taar probe hybridized to mRNA in a small percentage of OSNs scattered in selected olfactory epithelial regions. The Taar7d probe hybridizes with 5 different Taar7 subfamily members and labels more OSNs, as well as more olfactory epithelial regions, than the other probes. Scale bar, 1 mm.	**8**	
		Figure 2| qPCR analysis was performed in triplicate (^s.d.) using primers specific for nine mouse Taar genes, two mouse odorant receptor genes (OR-M5 (Olfr139) and OR-EG (Olfr73)), and the mouse beta-Actin gene with cDNAs prepared from different mouse tissues (A, heart; B, spleen; C, intestine; D, liver; E, brain; F, vomeronasal organ; G, olfactory epithelium; H, taste papillae; I, olfactory bulb; J, testis; K, olfactory epithelium (repeat)). cDNAs were prepared with (solid bars) or without (empty bars) reverse transcriptase	**9**	

		In mutant mice that express the odorant receptor MOR28 (Olfr1507) in 50–90% of OSNs26, **only 0.8% (2 in 250), rather than 50–90%**, of neurons that hybridized to Taar6 or Taar7f probes were co-labelled by a MOR28 probe (Fig. 3d).	**10**	
		Analyses of Taar-positive cells within the same zone as odorant receptor-positive cells **showed that 0 out of 174** Taar-positive cells were M49-positive, **and only 6 out of 1,617 Taar-positive cells were K20-positive**.	**11**	
		The latter is fivefold fewer than the ,30 out of 1,617 predicted to be positive for odorant receptor expression if each Taarpositive neuron randomly selected 1 out of 250 intact odorant receptor genes for expression in the K20 expression zone. Among odorant receptor-positive neurons, 2,577 out of 2,583 (99.8%) did not hybridize to Taar probes.	**12**	
		In addition, mTAAR5 was potently activated by trimethylamine, but not by the related compounds methylamine, dimethylamine and tetramethylammonium chloride, **which failed to activate mTAAR5 even at 1,000-fold higher** concentrations (Fig. 4b).	**13**	
		Nonetheless, mTAAR5 responded robustly to highly diluted urine from male mice, but not female mice or humans (Fig. 5a), **with the EC50 corresponding to a 30,000-fold dilution of male urine**. Higher concentrations of female urine elicited a much weaker response, which was equivalent to that seen with male urine **diluted 30-fold more** (Fig. 5c). The urine of males did not activate mTAAR5 until the males had reached puberty at about one month of age (Fig. 5b).	**14**	
		Figure 2| Note that for actin, the scale of the y-axis is 200 times greater than for the other genes.	**15**	
12	**Science 1**	We used 5704 14C, 10Be, and 3He ages that span the interval from 10,000 to 50,000 years ago (10 to 50 ka) to constrain the timing of the Last Glacial Maximum (LGM) in terms of global ice-sheet and mountain-glacier extent.	**1**	
		the timing of regional variability in ice-sheet maxima is also important for understanding ice-sheet sensitivity to regional and global climate change, as well as in establishing ice-sheet–climate feedbacks.	**2**	
		Resolving the timing of regional variability in ice-sheet maxima is also important for understanding ice-sheet sensitivity to regional and global climate change, as well as in establishing ice-sheet–climate feedbacks.	**3**	

		In particular, key questions that remain widely debated are what initiated the last deglaciation of the global ice sheets and what was their sub- sequent role during deglaciation in climate change, questions that are best assessed from the record of individual ice sheets rather than the integrated sea- level record.	**4**	
		We drew on 4271 14C ages and 475 terrestrial cosmogenic nuclide (TCN) ages that span the interval from 10,000 to 50,000 years ago (10 to 50 ka) to constrain the timing of maxima in global ice-sheet extent (Fig. 1). For all but the Barents- Kara and Greenland Ice Sheets, the spatial distribution of ages is sufficient to evaluate regional variability in the timing of maxima for different sectors of individual ice sheets.	**5**	
		We have also documented specific ice-sheet contributions to several key events in the evolution of the integrated global sea-level record into and out of the LGM, including a Northern Hemisphere ice-sheet source for the 19-ka MWP and a significant Antarctic ice-sheet contribu- tion to MWP-1A.	**6**	
		Insofar as these two MWP‘s represent a substantial flux of freshwater into the surrounding ocean, the geographic sources of these events are consistent with inducing the ocean and climate changes that occurred at these times (12, 24).	**7**	
		Our constraints in support of an extended LGM sea-level lowstand provide important insights into the origin of the carbonate d18O signal measured in benthic foraminifera (d18Oc), which is often used directly as a proxy for sea-level change.	**8**	
		We emphasize that the LR04 stack does not capture regional variability in d18OT and that Skinner and Shackleton (25) argued that the Atlantic temperature minimum leads that of the Pacific, as is apparent from the d18Oc records shown in Fig. 4B.	**9**	
13	**Science 2**	Most eukaryotic organisms are arthropods. Yet, their diversity in rich terrestrial ecosystems is still unknown. Here we produce tangible estimates of the total species richness of arthropods in a tropical rainforest	**1**	
		The whole **6000-hectare forest** reserve most likely sustains **25,000** arthropod species.	**2**	
		Notably, just 1 hectare of rainforest yields >60% of the arthropod biodiversity held in the wider landscape.	**3**	

		Most eukaryote species are terrestrial arthropods (1), and most terrestrial arthropods occur in tropical rainforests (2). However, considerably greater sampling effort is required in tropical arthropod surveys to yield realistic estimates of global species richness (3–7). A basic hindrance to estimating global biodiversity lies in a lack of empirical data that establish local biodiversity, which can be scaled up to achieve a global estimate.	**4**	
		Although many studies reported species richness for selected groups of well-studied insect taxa, **no satisfactory estimate of total arthropod species richness exists** for a single tropical rainforest location to date.	**5**	
		The unstructured collection and small-scale survey of tropical arthropods **cannot yield convincing estimates** of total species richness at a specific forest.	**6**	
		Where such structured estimates are made, it is invariably for insect herbivores on their host plants (5). However, species accumulation rates may differ markedly for nonherbivore guilds, which include more than half of all described arthropod species.	**7**	
		To provide a comprehensive estimate of total arthropod species richness in a tropical rainforest, we established a collaboration involving 102 re- searchers with expertise encompassing the full breadth of phylogenies and feeding modes present among arthropods (20). This consortium invested a total of 24,354 trap- (or person-) days sam- pling the San Lorenzo forest (SLPA) in Panama using structured protocols (fig. S1). **We identified 129,494 arthropods representing 6144 focal species** (Fig. 1 and table S1) from 0.48 ha of intensively sampled mature forest.	**8**	
		This allowed us to extrapolate focal arthropod species richness to a larger forest area with unprecedented power, through a series of best-informed species richness estimates derived from six competing models for each of 18 focal data sets.	**9**	
		Because this study targeted the full spectrum of arthropods, **it offers a comprehensive test of previous estimates of species richness based only on selected guilds or taxa**. Reassuringly, our well- resolved estimates of tropical arthropod species richness are of the same order of magnitude as prior estimates (table S3), adding credence to recent estimates of tropical arthropod diversity.	**10**	
		On a global scale, our results have implications for current estimates of total species richness, which have been weakened by the lack of knowledge regarding the strength of association between vascular plant species and nonherbivore guilds.	**11**	

14	**Science 3**	In December 2011, one such opportunity came in the form of a naturally occurring celestial explorer: Sun-grazing Kreutz-family (2) comet C/2011 W3 (Lovejoy), **the first Sun-grazer observed** to survive its approach and reemerge from the corona (3), **and the second comet observed within the** corona at extreme ultra-violet (EUV) wavelengths.	**1**	
		With a perihelion of 1.2 RS, comet Lovejoy **came within 140,000 km of the visible solar surface**. At heliocentric distances of 1.2 to 2.0 RS, which are above the typical usable heights for stereoscopic or tomographic reconstructions of the coronal magnetic field and plasma state (5, 6), this passage was imaged from multiple viewpoints by three space-based EUV-imaging telescopes.	**2**	
		Fig. 1. The yellow scale bar in each panel **indicates** a length of 100 Mm (105 km) in the plane of the sky (POS), the Sun-centered plane normal to the spacecraft.	**3**	
		A thorough description of how EUV emission can occur from cometary material injected into the corona was given by Bryans and Pesnell (7), who modeled the comet tail as a cylinder along the orbit path and used ion outflow velocities of 10 to 100 km s–1 as plausible limits on the overall width.	**4**	
		To do so, we used a state-of-the-art three-dimensional (3D) thermodynamic magnetohydrodynamic (MHD) model of the global corona, tailored to best approximate the corona during perihelion (9). This massively parallel computation involved **solving for the full 3D magnetic field and plasma state (flow, magnetic field, temperature, and density) in a global spherical domain from 1.0 to 20 RS**	**5**	
15	**Science 4**	Animals have a remarkable capacity to maintain a constant size, even in the face of genetic and environmental perturbations.	**1**	
		The Drosophila insulin-like peptide Dilp8 **has been shown** to mediate homeostatic regulation.	**2**	
		As Lgr3 outputs, the modulation of these neuronal populations according to Dilp8 **levels is critical to delay maturation and promote growth** compensation in a manner that stabilizes body size.	**3**	
		Without adequate Dilp8-Lgr3 signaling, **the brain is incapable of stabilizing** size between the distinct body parts, and we see left-right asymmetries and size variations that are greater than usual, reflecting developmental instability	**4**	
		Body-size constancy and symmetry are signs of developmental stability. Yet, it is unclear exactly how developing animals buffer size variation.	**5**	

		The impressive consistency and fidelity in the size of developing organisms (1–3) reflect both the robustness of genetic pro- grams and the developmental plasticity necessary to counteract the variations in size arising from genetic noise, erroneous morphogenesis, disease, or injury.	**6**	
		Recently, the secreted peptide Dilp8, a mem- ber of the insulin/relaxin-like family, has been identified as a factor that mediates homeostatic control in Drosophila melanogaster.	**7**	
		In addition, Dilp8 orchestrates hormonal responses that stabilize body size**. This includes (i) inhibiting the production of the steroid hormone** ecdysone by the prothoracic gland (PG) until the elements or organs affected are re- composed and also **(ii) slowing down growth rates** of undamaged tissues to ensure that affected organs catch up with normal tissues so that the adult flies reach a normal body size and maintain body proportions and symmetry.	**8**	
		Our data identify the insulin genes, dilp3 and dilp5, the JH, and the ecdysone hormone **as central for developmental size stability**	**9**	
		Collectively, **these findings unveil a homeostatic circuit that forms** a framework for studying how the brain stabilizes body size without constraining the adaptability of the system to reset body size in response to changing needs.	**10**	
		Ubiquitous expression of UAS-RNAi transgenes (several lines were tested) against each of the fly relaxing receptors reveals **whether they are required for developmental** delay resulting from dilp8 overexpression.	**11**	
		Tissue-specific knockdown of lgr3 further showed that **Lgr3 is required in the nervous system** (tub-dilp8 elav>lgr3-IR) (Fig. 1E) and not in the ring gland (using retnR9F04-Gal4)	**12**	
		Thus, similarities in the phenotypes of dilp8 (12) and lgr3 loss—as well as the prevention of Dilp8-induced developmental delay, growth-rate reduction, and excess body weight through the loss of lgr3—**strongly suggest that Lgr3 acts as a Dilp8 receptor.**	**13**	
		In this sense, the dense pre- synaptic sites of Lgr3 neurons indicate strong connectivity between these neurons and the PTTH neurons and IPCs. Thus, to detect direct connections, we used GRASP (GFP reconstitu- tion across synaptic partners) analysis, which s based on the expression of two nonfluorescent split-GFP fragments (spGFP1-10 and spGFP11) tethered to the membrane in two neuronal populations (40).	**14**	

		Because JH titer is normally determined by its rate of biosynthesis by the larval CA gland, as well as its rate of degradation, we used qRT-PCR to measure the expression of a gene encoding a key biosynthetic enzyme [juvenile hormone acid methyltransferase (JHAMT)] (43) and the direct target of JH that encodes a transcription factor that transduces the actions of JH [kruppel-homolog- 1 (kr-h1)] (46, 47).	**15**	
		Communication in neuronal networks is essential for synchronization and efficient performance. Notably, although most neurons have only one axon, Lgr3-responding neurons display exten- sive axonal arborizations reminiscent of hub neurons (39).	**16**	
		This was a multicenter effort to study **eighty-seven subjects** (Table 1) with and without COPD and emphysema […] These subjects were further subdivided in different groups for microarray, flow cytometry or autoimmunity testing as detailed bellow.		
		Microarray. Thirteen non-atopic ex-smokers enduring medically necessary lung surgery, due to lung volume reduction (LVRS) or small peripheral carcinoma		
		four subjects of age 78(6), were used as control (control group), which had no to mild obstruction according to their pulmonary function test (PFT), forced expiratory volume in one second (FEV1) percentage of predicted, average (SD), 80(24) and no emphysema as shown by their computed tomography (CT) scan; five patients of age 71(7) with mild to moderate emphysema and COPD 65(15) FEV1% (emphysema group); four patients age 65(5) with severe emphysema and COPD (end-stage group) shown by a FEV1% 34(9) and high resolution computed tomography (HRCT), and/or conventional CT scan performed as previously described [5] was used to classify on the presence or the absence of centrilobular, paraseptal or panlobular emphysema [22–24].		
		The patients had no history of allergy or asthma and had not received oral/systemic or inhaled corticosteroids during the last six months. At the time of study, all patients were free of acute symptoms suggestive of upper or lower respiratory tract infection in the 6 weeks preceding the study.		

		Autoimmunity to elastin. Forty-nine participants were entered into this study, serum from twenty-one individuals were chosen because of their early onset of COPD (EO-COPD) is likely to be caused by an autoimmune disease; they had average age of 50(3) with severe emphysema and end-stage COPD as shown by pulmonary function test (FEV1%) 21(5). Twenty-eight subjects with matching age 49(11) and no obstruction/emphysema according to their FEV1% 95(8) were used as control.		
		All participant had a smoking history of 50(3) pack per year (PPY) for EO-COPD and 21(15) PPY for control, 18 of the EO-COPD and 14 of the control group were ex-smokers all with similar quitting time (QT).		
		There are 18 protective genes expressed in healthy ex-smokers		
		Thus, we also verified a significant decreased of CD95 that was associated with the CD46 down regulation (Fig. 4B), which has an important role in the down-regulation of immune responses; since severe autoimmunity is developed in human and mice with deficiency in the Fas pathway [16,18].		
		Most importantly, a positive association among CD4 + T cell depletion and CD46 reduction was also **proven to be significantly linear (r =0.896, p =0.006, Fig. 4C)** indicating that selective depletion of Tregs with disease progression was associated with down regulation of CD46.		
		In summary, CD46 plays a protective role against emphysema/ COPD by restraining the CD8 + T cells proliferation and the complement cascade through production of Tregs that regulates the ratios of CD4+/CD8+ T cells and simultaneously regulating C3b deposition favoring apoptosis over necrosis, thus, protecting this subjects from autoimmunity and chronic inflammation.		
17	**Plos 2**	Predicting the stock market has become an increasingly interesting research area for both researchers and investors, and many prediction models have been proposed.	**1**	
		In this paper, a prediction model is constructed to forecast stock market behavior with the aid of independent component analysis, canonical correlation analysis, and a support vector machine.	**2**	
		Detecting financial time series trends is a decision support process, and stock data is typically representative of a financial time series.	**3**	
		Regarding prediction tools, some soft computing methods, such as Artificial Neural Networks (ANNs) and Support Vector Machine (SVM), have become popular methods for stock market forecasting due to their excellent nonlinear regression performance.	**4**	

		ICA and SVR are used under the multivariable regression framework, also called MICA-SVR in [27], [28] and [29]. Both of them apply ICA to extract the feature from the raw data and use SVR to predict the future price.	**5**	
		In this study, a data driven model named ICA-CCA-SVR is proposed, which predicts stock closing price considering the influence of both historical closing price and current technical variables by combining ICA, Canonical Correlation Analysis (CCA), and SVR.	**6**	
		Among these algorithms, the fixed-point algorithm has become a very popular way to implement ICA, due to the fast convergence speed and good stability. For details of fixed-point algorithm,	**7**	
		The AICA-SVR model only focuses on the effect of the closing price itself, and does not pay attention to other related factors. In other words, this model behaves as if all the related factors can be reflected by the closing price of the stock, so the historical closing price decides the future trends.	**8**	
		However, it is not reasonable to treat the stock closing price as coequal with other technical variables. In fact, the history values of stock closing price plays the most important role in impacting the future of the closing price.	**9**	
		Both the AICA-SVR and the MICA-SVR models can be regarded as pattern recognition systems. For this type of problem, the feature of the input is a key factor in impacting the prediction accuracy. AICA-SVR focuses on the closing price movement as the influence for the historical price, while MICA-SVR is more concerned about the influence of other technical variables.	**10**	
		On balance volume combines price and volume to show how money may be flowing into or out of a stock. Bollinger band shows the upper and lower limits of normal price movements based on the standard deviation of prices.	**11**	
		Emotional index is the most important index to measure the power changes of the straddle	**12**	
		To evaluate the performance of the ICA-CCA-SVR model, we performed experiments on two real-world datasets: the Shanghai stock market index and the Dow Jones index. Comparison was made with the AICA-SVR and the MICA-SVR models	**13**	

		The Shanghai stock market index data collected from January 4, 2003 to December 31, 2005 are used in this experiment. The overall data includes 1180 trading days' data, which are split into two parts: January 4, 2003 to December 31, 2004 and January 1, 2005 to December 31, 2005. The former, which includes 726 trading days' data, is used as the training set, and the latter, which includes 242 trading days' data, is used as the testing set.	**14**	
		To test the robustness of the model, we selected three years' worth of data from the Dow Jones index, which includes two years of data for the training set and one year of data for the testing set. The Dow Jones index data were collected from January 2, 2003 to December 31, 2005 for use in this experiment.	**15**	
		Experimental results on the Shanghai stock market index and on the Dow Jones index show that the ICA-CCA-SVR model proposed in this paper obtains better performance than both the AICA-SVR and MICA-SVR models.	**16**	
18	**Plos 3**	Drug resistance is a common problem in the fight against infectious diseases. Recent studies have shown conditions (which we call antiR) that select against resistant strains. However, no specific drug administration strategies based on this property exist yet. Here, we mathematically compare growth of resistant versus sensitive strains under different treatments (no drugs, antibiotic, and antiR), and show how a precisely timed combination of treatments may help defeat resistant strains.	**1**	
		Drug resistance is an important problem during infection treatment, particularly in intensive care units [1]. Cases of resistance have been described in infections caused by different types of pathogens, such as viruses, bacteria, fungi and protozoa [2–5] and the increasing incidence has made resistance a major public health issue [6].	**2**	
		This fact can be exemplified by, but it is not exclusive to, infections caused by the methicillin-resistant Staphylococcus aureus (MRSA), whose incidence rate has almost doubled (city of Atlanta) or tripled (city of Baltimore) in a period of three years, from 2002 to 2005 [6]. The relevance of those numbers is evident when compared to infectious diseases that are caused by other bacteria also common in the human respiratory tract and skin, such as Streptococcus pneumonia and Haemophilus influenzae.	**3**	

		The number of MRSA infection cases was about twice and 30 times the numbers for S. pneumonia and by H. influenza, respectively, in the calendar year of 2005 and was associated with about 18000 deaths [6]. Also, MRSA is associated with over 20% of S. aureus infections in Europe [7]. This alarming situation highlights the need for alternatives to reduce the incidence of resistance. Two common potential strategies for this purpose are drug restriction and multiple-drug therapy.	**4**	
		A special case of restriction is drug cycling, in which restrictions to specific classes of drugs are alternated over some time interval. A review on the topic identified only four references rigorously investigating drug cycling [13]. Three of them reported cycling to be effective in reducing the incidence of resistance and one did not find any statistical significance. They also reported lack of standard procedures, which makes it hard to obtain a conclusive valuation of policies.	**5**	
		Resistant strains would not be so alarming if we were able to control them. In order to do so, one would have to find conditions (which we call antiR) in which sensitive strains are able to grow faster than resistant ones. Under these conditions, resistant strains would have a selective disadvantage and decrease in population size. The antiR conditions can be applied to reduce resistance, turning an infection susceptible to antibiotic treatment. The effectiveness of this strategy depends on a precise timing schedule for the application of antiR and antibiotic treatment.	**6**	
		Modifications caused by chemical decay may cause an antibiotic to be no longer effective, while maintaining its capacity to activate the genes for resistance. Under these conditions, the modified antibiotic is not effective and the activation of the efflux pumps is not associated with any benefit for the bacteria. Thus, it only increases the cost of carrying and expressing the genes for resistance, favoring growth of sensitive strains.	**7**	
		In spite of the growing knowledge about antibiotic resistance, there is still not a standard way to control it. The use of drug combinations can lead to multi-resistant strains [35–38]. Specific strategies to turn antiR conditions into therapeutic plans have not been proposed yet. Drug restriction is not a well-established intervention, with limited studies available on the topic [14,36].	**8**	

		In this paper, we use a mathematical model [42] to quantitatively study antibiotic therapy and the effect of an antiresistance treatment in a single-host model (Fig. 1A-B). We simulate a case where antibiotic treatment is not effective and show how the application of antiR conditions could provide an effective treatment.	**9**	
		We studied the effect of an antiR treatment in the infection dynamics and examined how it could help to fight resistant nfections. The application of an antiR treatment reduces the abundance of resistant pathogens (Fig. 2). Interestingly, the intensity of this resistance attenuation increases when the abundance of sensitive pathogen is close to the carrying capacity and indicates a change in fitness when both strains have to compete for resources	**10**	
		Figure 7. Schematic representation of a host population models that includes the possibility of resistance loss. A modified implementation of a previous host population model [40] under a combination of two drugs a and b (Equation S6 and S7 in File S1) takes into account the possibility of resistance loss. Hosts can be infected by pathogens of four different types: wild type, a-resistant, bresistant and a,b-resistant.	**11**	
		In addition to exploring in detail the behavior of a single host model under conditions that induce resistance attenuation, we asked ourselves whether resistance attenuation in host population models could affect infection dynamics at an epidemiological level.	**12**	
		In the battle against antibiotic resistance, the use of mathematical models is important for transforming the cumulative understanding of the mechanisms for acquisition and loss of resistance [27,75,76] into potential strategies to treat infection caused by resistant pathogens. While our work does not suggest an immediate and practical protocol to fight resistant infection, it highlights simple quantitative aspects of resistance attenuation that could eventually translate into novel strategies to fight resistant infections.	**13**	
19	**Plos 4**	The prevalence of testicular germ cell tumors (TGCT), a common solid tissue malignancy in young men, has been annually increasing at an alarming rate of 3%. Since the majority of testicular cancers are derived from germ cells at the stage of transformation of primordial germ cell (PGC) into gonocytes, the increase has been attributed to maternal/fetal exposures to environmental factors.	**1**	

		We examined the effects of an estrogen (diethylstilbestrol, DES), an antiandrogen (flutamide), or radiation on the incidence of testicular germ cell tumors in genetically predisposed 129.MOLF-L1 (L1) congenic mice by exposing them to these agents on days 10.5 and 11.5 of pregnancy.	**2**	
		Testicular germ cell tumors (TGCT) are the most common malignant tumor in Caucasian men aged between 15 and 40 years. Human TGCTs are mainly classified histologically into seminomas, which resemble the primordial germ cells (PGCs), and non-seminomas, which are either undifferentiated (embryonal carcinoma) or differentiated showing embryonic (teratoma) or extra-embryonic (yolk sac) patterning	**3**	
		Teratomas are characterized by the differentiation to a diverse array of cell and tissue types. The median age of onset of various tumor types differs with seminomas arising at about 35 years, most nonseminomas at 25 years, and most teratomas and yolk sac tumors at around 1.5 years.	**4**	
		There has been an annual increase of 3% in the incidence of TGCTs in young Caucasian men throughout the world in the past 50 years [4], but the reasons are elusive. Elucidation of the cause of this increase is important for possible prevention or reversal of this increase.	**5**	
		Ionizing radiation, a known carcinogen [8], that increases the incidence of childhood and other adult cancers in individuals exposed during fetal development [9,10], has received little study. One case-control study did show that exposure to ionizing radiation during pregnancy increased the risk of testicular cancer in male offspring	**6**	
		In the current study, we employed the 129.MOLF-L1 (L1) congenic strain, with a reported 30% incidence of TGCTs, to maximize the power of the study. We used this mouse model to test the effect of estrogen, antiandrogen and ionizing radiation exposure on TGCT incidence.	**7**	
		We examined the effects of treatments with an estrogen (diethylstilbestrol, DES), an antiandrogen (flutamide), or irradiation on the incidence of TGCT in an animal model. We exposed pregnant L1 females to the agents at days 10.5 and 11.5 of pregnancy.	**8**	

		In the present study we unequivocally demonstrated that fetal radiation exposure during E10.5–E11.5 induces testicular germ cell cancers, most of which show the multiple dermal origins typical of teratomas, in a genetically susceptible mouse model.Ts is the first demonstration of induction of testicular cancer byan environmental agent when exposed during embryonic period.	**9**	

EVIDENCIA EMPÍRICA				
Consecutivo	**Clasificación**	**Apariciones**	**Consecutivo del paper**	**Color**
1	**A1**	Both patients had onset of VKC in the first decade. Surgical intervention in both led to marked amelioration in symptoms and improvement in vision. In patient 1, vision improved from 20/800 (both eyes) to 20/30 in the right and 20/100 in the left eye at a follow-up of 34 months. In patient 2, it improved from 20/400 to 20/50 after the second procedure, 25 months postoperatively.		
		The best corrected visual acuity (BCVA) in both eyes was 20/800. Biomicroscopy revealed upper tarsal conjunctiva scarring, conjunctival overgrowth on cornea, epithelial erosions, vascularization, and stromal scarring (Figs. 1A and 2A).	**2**	
		At the 3-month postoperative visit in November 2001, his vision had improved to 20/60 in both eyes. The corneal clarity had improved, with no recurrence of conjunctivalization or neovascularization (Figs. 1B and 2B)	**3**	
		He presented in February 2002 with complaints of decreased vision and pain in both eyes. Examination showed edema of the temporal limbal allograft and adjacent cornea in the left eye with epithelial defect	**4**	
		At the last follow-up in June 2004, visual acuity was 20/30 and 20/100. The central corneal clarity was maintained in the right eye (Fig. 4B); the left eye, however, showed residual deep stromal scarring (Fig. 4A). He continued on oral cyclosporine and topical loteprednol etabonate 0.5% eyedrops and carboxymethylcellulose sodium 1% eyedrops.	**5**	
		Her BCVA was 20/400 in the right eye and 20/25 in the left.	**6**	
		The corneas showed perilimbal thickening, superficial vascularization, and conjunctival overgrowth. Corneal scarring and superficial punctate erosions were present in both eyes (right more than the left) (Fig. 5)	**7**	

		However, there was recurrence of superficial vascularization in 1 quadrant.	**8**	
		Four months later, her vision had decreased to 20/80	**9**	
		… vascularization had now recurred in 3 quadrants (Fig. 6).	**10**	
		Two months postoperatively, she complained of redness and itching in both eyes. Examination showed reactivation of VKC with upper tarsal papillary hypertrophy and gelatinous limbal thickening (Fig. 7B).	**11**	
		Her BCVA was 20/50 and 20/25 in the right left eyes, respectively	**12**	
		The right eye showed improved corneal clarity and decreased vascularization (Fig. 8A) and the left eye was asymptomtics.	**13**	
		FIGURE 8. Patient in case 2. At 2-year follow-up, there is no recurrence of vascularization in the right eye (A), and the left eye	**14**	
		Conjunctival pannus from all 3 eyes showed squamous metaplasia with keratinization of the entire epithelium, with few to no goblet cells.	**15**	
		The underlying stroma revealed lymphocytes, plasma cells, and mast cells along with fibrosis and dilated lymphatics.	**16**	
		The corneal pannus in all 3 eyes showed regenerating changes with marked hyperplasia and keratinization.	**17**	
		The corneal stroma contained lymphocytes, plasma cells, and fibrosis. Occasional eosinophils were seen in both the conjunctival and corneal pannus in case 2.	**18**	
		All these individuals subsequently underwent cultured limbal epithelial cell transplantation with restoration of ocular surface postoperatively.	**19**	
		While a positive cytology confirms the diagnosis, a negative report should be interpreted in the light of the clinical features	**20**	
2	**A2**	Findings showed that family values differences affected the wives' depression and family support had a significant moderating effect.	**1**	
		Marriage migrant women tended to receive support more from friends than family or formal sources. The mean score of depression among marriage migrant women was 3.38 (SD = 4.31).	**2**	
		we found that age gap between couples and use of a broker agency were significantly related to depression in marriage migrant women. Interestingly, as a couple's age gap increased, depression in marriage migrant women decreased. In addition, wifes who used a broker agency for their marriage had a higher level of depression. While use of a broker agency was significant in models 1 and 2, it became insignificant in the full model. Family values difference between husband and wife significantly affected depression in wives.	**3**	
		the finding that only 20% of the wives reported having close relationships with their family also shows that the majority of the women are still at risk of experiencing depression, not having family members to discuss and/or mitigate the difficulties experienced in marriage due to value differences.	**4**	

		The findings of this study also support the criticism that what determines psychological wellbeing of spouses does not depend entirely on how acculturated the women are, but also on the extent to which they share and exchange their values, culture, and cus- toms with their husbands.	**5**	
3	**A4**	Based on the number of detected ATP7B mutations, a significant difference in serum ceruloplasmin concentration was found among the 3 groups ($p < 0.001$).	**1**	
		We observed 82.9% and 16.7% of mutant allele frequency in WD patients with ceruloplasmin concentration <10 mg/dl and 10-20 mg/dl, respectively ($p < 0.001$). Thus serum ceruloplasmin concentrations among WD patients differed according to the number of ATP7B mutations detected.	**2**	
		Serum ceruloplasmin concentration averaged 3.32 ± 1.74, 10.8 ± 5.50, and 14.9 ± 3.88 mg/dl (mean ± SD) in the 25, 20, and 26 patients with two, one, and no ATP7B mutations, respectively.	**3**	
		at least two positive findings were observed for the following characteristics: presence of Kayser- Fleischer rings in the cornea, increased Cu concentration in 24-hr urine or liver tissue, and decreased serum ceruloplasmin.	**4**	
		In addition, many patients presented with hepatic symptoms, signs of increased serum alanine aminotransferase (ALT) or aspartate aminotransferase (AST) activities, and neurologic symptoms, such as movement disorders.	**5**	
		We identified 70 ATP7B mutations in Korean patients with suspected WD. When patients were classified into three groups according to the number of ATP7B mutations, 25 patients had two mutations (homozygous or compound heterozygous), and 20 had one mutation.	**6**	
		The other 26 patients had no mutation in 7 ATP7B exons (Table 1).	**7**	
		Table 1. Biochemical findings in patients with suspected Wilson Desease	**8**	
		With the exception of ceruloplasmin, other clinical or biochemical characteristics among the three groups were not significantly different. Significant differences were observed in serum ceruloplasmin concentrations among the three patient groups ($p < 0.001$) (Fig. 1).	**9**	
		Fig 1. Serum ceruplasmisnconcentrationsin WD patients	**10**	
		Table 2. The ATP7B mutant allelefrequency was associated with serumceruplasmin concentration in WD patients.	**11**	
		In the present study, all WD patients with two ATP7B mutations had serum ceruloplasmin concentrations <10 mg/dL.	**12**	
		These patients presented with ceruloplasmin reduction and no other condition.	**13**	
		In summary, we investigated the relationship between biochemical and molecular characteristics in WD patients. Ceruloplasmin concentrations differed significantly, depending on the number of ATP7B mutations, and mutation detection rate was associated with ceruloplasmin concentration.	**14**	

4	**PNAS 1**	The mean methane flow rates at these well locations were 0.27 kg/d/well, and the mean methane flow rate at the control locations was 4.5 × 10−6 kg d location	**1**	
		Methane flow rates from abandoned wells were found to be significantly higher than methane flow rates observed at controls (Fig. 2). The mean flow rate at well locations was 11,000 mg/h/ well (0.27 kg/d/well), and the mean flow rate at control locations was 0.19 mg h location (4.5 × 10−6 kg d location). The median flow rate at well locations was 56 mg/h/well (1.3 × 10−3 kg d well), which is still higher than both the mean and median flow rate at control locations. The median flow rate at controls was 0 mg/h/location (or 0 kg d location) considering all values, and 6.7 × 10−3 mg h location (1.6 × 10−7 kg d location) considering nonzero values only. Positive methane flow rates were observed at all 19 wells with values, averaged over multiple sampling events, ranging from 6.3 × 10−1 to 8.6 × 104 mg/h/well. Average methane flow rates over multiple sampling events at control locations ranged from −1.2 × 10−1 to 4.2 mg/h/location.	**2**	
		Methane flow rates at wells were based on good linear fits with 88% of the flow rates having R2 values greater than 0.8 (Supporting Information).	**3**	
		Methane flow rates at well locations appeared to be unaffected by land cover, which included forest, grassland, river, and wet l and. In contrast, we found that methane fluxes at control locations were dependent on land cover. A large proportion of flow rates from controls in forests and grasslands were negative (i.e., methane sinks) and ranged from −1.2 × 10−1 to 1.8 mg h location, and the flow rates from controls in wetlands were consistently positive and relatively high, ranging from 1.6 × 10−2 to 4.2 × 101 mg h location.	**4**	
		We found that methane flow rates from plugged wells were not necessarily lower than methane flow rates at unplugged wells. For example, in the grassland area, both the largest and the second lowest methane fluxes originated from plugged wells.	**5**	
		We found that the samples collected at wells were likely to be more enriched in 13C than those collected at controls (Fig. 4).	**6**	
		Fig. 4 also shows that locations with larger methane flow rates emitted methane that was more enriched in 13C. Wells with methane flow rates that were greater than 103 mg/h/well were likely to be emitting methane of thermogenic origin; and wells with flow rates in the order of 100 to 101 mg/h/well emitted meth- ane of microbial, thermogenic, or mixed thermogenic/microbial origin.	**7**	

		Fig. 3 Average alkane ratios ([C2H6]/[CH4], [C3H8]/[CH4], and [n-C4H10]/ [CH4]) (A) and proportions of samples with alkane ratios greater than 0.01 (B) at control and well location with detectable ethane, propane, and n-butane concentrations are calculated for samples collected in July, August, and October 2013 and January 2014.	**8**	
5	**PNAS 2**	Analysis of secretions reveals the presence of subtilisin (a protease) and a 12 kDa protein, termed sibling lethal factor (Slf).	**1**	
		Purified subtilisin promotes the growth and expasion of P. dendritiformis colonies, whereas Slf is lethal and lyses P. dendritiformis cells in culture.	**2**	
		The 20 kDa recombinant protein was produced and found to be inactive, but exposure to subtilisin resulted in cleavage to the active, 12 kDa form.	**3**	
		Below a threshold concentration, subtilisin promotes colony growth and expansion. However, once it exceeds a threshold, as occurs at the interface between competing colonies, Slf is then secreted into the medium to rapidly reduce cell density by lysis of the bacterial cells.	**6**	
		Here we analyze the proteins secreted by competing sibling P. dendritiformis colonies **and show** that they include subtilisin, which stimulates cell growth and reproduction, and a lethal protein.	**7**	
		Protein bands **were detected** at 32, 30, and 12 kDa (Fig. 1B). In contrast, extracts from the agar surrounding single growing colonies (Fig. 1C) **showed only** two protein bands, 32 and 30 kDa(Fig. 1D,Left Lane).	**8**	
		The Blast analysis **resulted** in one perfect match between each of the partial protein sequences and a corresponding gene in the P. dendritiformis genome.	**9**	
		Fig. 1. Colonies of P. Dendritiformis (T morphotype) grown for one week on 1.5% agar with 2g⁄ L peptone, and analysis of proteins released into the medium.	**10**	
		Flagellin had no effect on colony growth or morphology, but subtilisin (both theP. dendritiformisprotein andthe commercial one) inhibited growth, and only dead cells were found in the inhibited area (Fig. 1E).	**11**	
		Material extracted from agar near subtilisin-inhibited regions **was found** to contain a pro-tein of the same size (12 kDa) detected in the region between two colonies (Fig. 1D Right Lane); the identity was confirmed by amino acid sequence analysis	**12**	
		Very high subtilisin levels (Fig. 3A,Lower Line**) resulted** in cell death at the inhibited interface. In low-nutrient liquid medium, subtilisin stimulated growth, even at the maximum concentration (20 mg in 3 mL of culture) tested(Fig. 3B	**13**	
		HPLC ***indicated that*** no other inhibiting compounds, including proteins or small peptides, were present in the dialyzed extract (SI Text).	**14**	
		The extracted Slf placed near a single growing colony inhibited growth (Fig. 3C). This protein **was found to be** inhibitory only; no growth stimulation was found even at low levels of the protein (SI Text).	**15**	
		In addition, when Slf was added to liquid cultures before the liquid was inoculated, no growth **was detected**.	**16**	
		For grown liquid cultures, high levels of Slf lysed bacterial cells. More importantly, evidence of cell lysis was visible at the edge of inhibited colonies (see faint region in the magnified image in Fig. 3C).	**17**	

		The P. dendritiformis bacteria were unaffected by the 20 kDa protein, but the 12 kDa fragment lysed growing colonies, ***as observed for*** the 12 kDa protein that was extracted from the area of inhibition between colonies (Fig. 3C)	**18**	
		Fig. 4C shows the profile of the bacteria, nutrient, subtilisin, and Slf concentrations immediately after Slf was produced.	**19**	
		This, in turn, increases the expansion rate of the colony, and the bacteria at the front move farther away from the location of the subtilisin maximum. Subsequently, subtilisin levels at the front decrease. An opposite chain of events happens at low subtilisin concentrations.	**20**	
		Fig. 4. Numerical simulationof colony competition	**21**	
		As explained previously, the bacteria at the front get closer to the location of the subtilisin maximum, and ***as a result***, the reproduction rate becomes faster than the ability of the colony to expand (11).	**22**	
		Slf is secreted into the environment and ***can be*** isolated from the agar between competing colonies. N-terminal sequencing of the purified protein and comparison of the amino acid sequence with the genome identified the dfsB gene	**23**	
		This secreted form of the protein is biologically active and causes lysis of P. dendritiformis on surfaces or in liquid medium.	**24**	
		The present analysis and testing of factors secreted by P. dendritiformis ***indicates that it*** is a second factor, subtilisin, which triggers the threshold response.	**25**	
		On the surface of relatively low-nutrient agar, the bacteria are actively motile and spread outward, forming highly branched colonies. Subtilisin is secreted into the environment and its proteolytic activity may break down proteins to provide more easily used nutrient sources to the bacteria.	**26**	
		As the edges of neighboring colonies approach each other, the local concentration of subtilisin increases sharply, and exceeds the threshold for regulated colony growth (compare to Fig. 4A)	**27**	
		This results in secretion of the active form of Slf (Fig. 4A, Red Curve), which lyses cells in the zone between the two colonies and prevents either colony from invading the other‘s territory	**29**	
		Both Slf and these toxins kill sibling cells, pointing to a possible similar mechanism.	**30**	
		It is likely that this phenomenon is not restricted to P. dendritiformis. Bioinformatics analyses of the full-length, 20 kDa, DfsB protein revealed that it is a member of a large family of conserved hypothetical genes found in a wide range of Gram-positive bacteria such as Geobacillus sp. Y412MC10 (9).	**31**	
		A close homolog (designated IRC4) is found in the yeast Saccharomyces cerevisiae, where it has been implicated in recombination (10). However, the gene is not found in other yeasts or in any of the other sequenced eukaryotic genomes	**32**	
6	PNAS 3	When these conditions are violated we show, using experiments and simulations that shells undergo rapid snapping motion to fold from one stable configuration to another.	**1**	
		In particular, folding a curved surface along a crease often leads to large deformations of the shell. However, despite these nonlinear deformations, we show that the local geometry of the crease alone creates a large energy barrier that leads to a snapping transition in a sufficiently thin shell.	**2**	
		Figura 1	**3**	

		Therefore, the three types of Gaussian curvature naturally divide the shell behavior under folding into one of three types. When K > 0 (such as on a sphere), there are no asymptotic curves so all creases can generate a snap-through instability. When K = 0, however, the shell is either completely flat, or has a single di-rection at each point with κN = 0.	**4**	
		Finally, surfaces with K<0 pose a further interesting case— having two directions at each point along which κN = 0, neither of which need be straight (41). Consequently, one can have both kinds of κN = 0 curves on a K < 0 surface: planar and nonplanar, as we discuss here on a helicoid. All of these κN = 0 curves are marked in white on respective geometries in Fig. 1C.	**5**	
		For the helicoid specifically, one family of curves is given by the generating lines, whereas the other is given by a family of helices that have nonzero curvature and torsion.	**6**	
		On the other hand, creases with finite κNon a cylinder can be created by intersecting the surface with a plane at an oblique angle (θ) at a distance (d) from the apex, as shown in Fig. 3 and Materials and Methods.	**7**	
		As indicated in Fig. 3B(Movie S2), a transition to an antisymmetric mode is observed before snapping completely into the mirror reflection isometry. Notably, stability of the isometric state and the presence of an antisymmetric mode in our experiments is consistent with finite-element analysis (FEA, performed using ABAQUS, Dassault Systemes).	**8**	
		Figura 2	**9**	
		Figura 3	**10**	
		Indenting an increased cylinder near the free edge produces a deformation pattern that is composed of two parts: a region of mirror isometry that contains only bending, and a localized ridge (1, 33, 37, 42). The localized region, which acts as an elastic boundary layer, contains all of the stretching energy of the deformation.	**11**	
		Here, we observe that for lower values of fd, θg the bending energy cost of the mirror isometry is large enough that the energy gain from creasing is insufficient to result in bistability, whereas larger fd, θg values lower the cost of the ridge sufficiently to induce bistability.	**12**	
		Unlike previously discussed geometries, due to the symmetry of the sphere these creases have constant κN over the whole surface, allowing analytically tractable solutions.	**13**	
		There is a well-known nearly isometric deformation of a sphere seen for displacements larger than the thickness but smaller than the crease size (33, 46).	**14**	
		However, for small values of α the monotonically increasing bending energy overcomes the energy gain from thinning the shell at the crease, and the folded state remains unstable.	**15**	
		As shown schematically in Fig. 5A, for a creased spherical shell there is a local minimum in the Pogorelov energy centered at r = Rt that generates an energy barrier that competes with bending energy.	**16**	
		We report the total energy for axisymmetric solutions with γ =104 (corresponding to the elastomeric hemispheres discussed here) as a function of the indenter displacement (h) and the normalized crease radius (α) in Fig. 5B.	**17**	
		We find that, beyond a critical crease radius, there is a bifurcation of stability and the energy curves develop a well-defined local minimum (solid) and maximum (dashed), with the region between these curves denoting a basin of attraction for the folded state.	**18**	

		Through numerical simulations, we find that for increasing thickness, larger values of the crease radius are required to create a stable snap.	**19**	
		Moreover, we conduct a series of experiments on spherical shells with a range of γ and α, and identify the stability of the folded state. These reveal a boundary between bistability and monostability that is in excellent agreement with our numerical calculations.	**20**	
		Further bolstering this, for some samples we observe the presence of folded states that are temporarily stable (for times on the order of seconds)—the proximity of these samples to the predicted phase boundary further demonstrates the agreement between experiments and simulation.	**21**	
7	**PNAS 4**	We found that Zbtb20 expression was initially activated in the hippocampal anlage at the onset of corticogenesis, and persisted in immature hippocampal neurons.	**1**	
		Targeted deletion of Zbtb20 in mice did not compromise the progenitor proliferation in the hippocampal and adjacent transitional ventricular zone, but led to the transformation of the hippocampal CA1 field into a transitional neocortex-like structure, as evidenced by cytoarchitectural, neuronal migration, and gene expression phenotypes.	**2**	
		Correspondingly, the subiculum was ectopically located adjacent to the CA3 in mutant.	**3**	
		Although the field identities of the mutant CA3 and dentate gyrus (DG) were largely maintained, their projections were severely impaired.	**4**	
		The hippocampus of Zbtb20 null mice was reduced in size, and exhibited increased apoptotic cell death during postnatal development.	**3**	
		Anti-Zbtb20 immunostaining revealed that Zbtb20 protein was expressed within the E13.5 hippocampal primordium, but was excluded from the cortical hem and neocortical region (Fig. 1B).	**4**	
		By E14.5, when immature pyramidal cells from Ammon's horn start to migrate out of the proliferative ventricular zone (VZ) to form the cortical plate (CP) (12), Zbtb20 expression was observed in presumptive postmitotic pyramidal cells in the CP and, to a much less extent, in the VZ (Fig. 1C). In addition, robust Zbtb20 expression was detected in the dentate migratory path and the DG anlage at E16.5 (Fig. S1B).	**5**	
		We found that the majority of BrdUpositive cells in the hippocampal VZ were colabeled with anti-Zbtb20, and the majority of Zbtb20-positive cells located outside the VZ were not labeled with BrdU, indicating that these were postmitotic cells (Fig. 1 D–F).	**6**	
		In summary, Zbtb20 transcripts are detected in the hippocampal primordium as early as E12.5, and thereafter Zbtb20 is expressed specifically in progenitor cells and postmitotic neurons of the developing hippocampus.	**9**	
		FIG. 10	**10**	
		Found that, though it did not differ noticeably from wild-type or heterozygous littermate controls with respect to its size, cell density, and cellular distribution pattern before E16.5 (Fig. S2 A and B), morphological defects became apparent by E18.5.	**11**	
		At this developmental time point, the wild-type hippocampal anlage has a thin and compact CP that is clearly distinguishable from the intermediate zone (IZ) and the CP of the adjacent transitional neocortex. In contrast, the E18.5 CA1 region of Zbtb20− − mice was wider and less dense, and the reticular IZ was thinner than that in control and thus appeared very similar to the adjacent transitional neocortex (Fig. S2 C and D).	**12**	

		In addition to the CA1, the CA3 and DG also exhibited severe morphological defects in Zbtb20 knockout mice. At E18.5, the mutant CA3 began to exhibit a wider and more loosely packed CP than in wild type (Fig. S2 C and D). In contrast to the mutant CA1, the mutant CA3 maintained a single pyramidal layer comprising morphologically homogenous neurons during postnatal development (Fig. 2 A and B and Fig. S2 E–H).	**13**	
		To determine the apoptotic cell death of hippocampal neurons, we performed TUNEL labeling. At E18.5, a few TUNEL-positive cells were detected in the mutant hippocampus, with no significant difference from the wild-type control (Fig. S3G–I).	**14**	
		At E16.5, the expression domains of Sox5 (a layer V, VI, and subplate marker) (19), Tshz3 (a marker of all neocortical layers) (20), and Id2 (a layer II–III, V–VI, and subplate marker) (21) were found to expand ventrally in mutants (Fig. S5 A–F) and were present in the E18.5 CA1 (Fig. 4 A–D and Fig. S5 G and H).	**15**	
		Moreover, the expression domain of neurotrophin 3 (NT3, a transient marker for upper layer in cingulate and retrosplenial cortices) (5), was also expanded ventrally in mutants at E18.5 (Fig. S5 I and L), and NT3-positive neurons were distributed throughout the upper layer of the mutant CA1 region at P7 (Fig. 4 I and J).	**16**	
		Fig. 3	**17**	
		Fig. 4	**18**	
		Consistent with previous reports (12), most wild-type CA1 neurons born at E16.5 still remained within the IZ at E18.5 and P1, which resulted in a compact IZ (Fig. 5 A and C). In contrast, some of the mutant CA1 neurons born at E16.5 had crossed the IZ and reached the CP by E18.5 (Fig. 5B), and the majority of them had penetrated the CP by P1 (Fig. 5D).	**19**	
		Consistent with previous reports (26), we found that in wild-type mice the Wnt receptor Frizzled 5 (Fzd5) and secreted frizz led related protein 1 (SFRP1) were expressed in the transitional/ neocortical VZ, whereas SFRP3 was expressed in the hippocampal and transitional VZ, but excluded from the neocortex (Fig. S7 A–F).	**20**	
		In addition, by immunohistochemistry analysis, we did not find any remarkable change of the activating status of the signaling components of TGF-β, BMP, or FGF in the mutant hippocampal and adjacent transitional VZ (Fig. S7 M–R).	**21**	
		Notably, the increased expression of Tshz3, NT3, Mef2c, and Id2 in knockout hippocampus is consistent with their ectopic expression in mutant CA1 (Fig. 4 C–F, I, and J and Fig. S5 C–J).	**22**	
		FIG. 5	**23**	
		FIG. 6	**24**	
		In this study, we examined the role of Zbtb20 in hippocampal development. Our findings provide compelling evidence that Zbtb20 is essential for the specification of CA1 field identity and the postnatal survival of hippocampal neurons.	**25**	
		Although Zbtb20− − CA1 progenitor cells seemed to proliferate normally in the hippocampal primordium, they migrated rapidly to the CP, pausing for an abnormally short period in the IZ, in a manner similar to that of transitional neocortex progenitors. The CA1 fields of Zbtb20− − mice lacked the typical compact and homogeneous composition of the pyramidal cell layer and instead developed deep and upper cortical layers reminiscent of the transitional neocortex.	**26**	
		Remarkably, Zbtb20− − CA1 neurons failed to express or expressed reduced levels of CA1 markers, such as NP2, EphA4, EphA6, and Man1α, but maintained Oct6 expression, which is normally expressed in CA1 and transitional neocortex.	**27**	

		Furthermore, the mutant CA1 field ectopically expressed many transitional neocortex- specific markers, including the transcription factors Sox5, Tshz3, Id2, Mef2c, ER81, Cux2, and the trophic factor NT3. In addition, the expression domain of Fibronectin1, a subiculumspecific marker, was shifted laterally and located adjacent to mutant CA3.	**28**	
		This CA1-specific effect of Zbtb20 was also observed when Zbtb20 was ectopically expressed in transitional neocortex (29).	**29**	
		Our study also indicates that Zbtb20 is required for the postnatal survival of hippocampal neurons. We found that increased apoptosis occurred throughout the entire region of Zbtb20 null hippocampus during postnatal development.	**30**	
8	**Nature 1**	Here we describe a Mesozoic eutriconodont nested within crown mammals that clearly illustrates this transition: the middle ear bones are connected to the mandible via an ossified Meckel‘s cartilage	**1**	
		The last molariform in the holotype of Yanoconodon has partially erupted (Fig. 3b), similar to the condition in Jeholodens.	**2**	
		However, the exposed interior of the lower and upper jaws shows no replacement at any tooth loci and its functional teeth (including the last tooth) are all permanent. The holotype is either a late-stage subadult or an adult with a delayed eruption of the last molar.	**3**	
		It differs from gobiconodontids in the absence of replacements at the anterior molariform loci, although it shares this delayed eruption of the ultimate molariform with older gobiconodontid individuals	**4**	
		By comparison to Yanoconodon, we recognize that an ossified Meckel‘s cartilage is also preserved, although it is detached from the mandible in Jeholodens.	**5**	
		The Meckel‘s cartilage is similar to those preserved in several gobiconodontids (Fig. 3e, 3f)9–12	**6**	
		FIG. 1	**7**	
		The anterior (mandibular) limb and the posterior (tympanic) limb ofMeckel‘s cartilage are twisted and curved relative to each other at the mid-length of the cartilage (red arrow in Fig. 3).	**8**	
		The midlength twist and curvature of Meckel‘s cartilage made it feasible for the anterior limb of the cartilage to be nestled in the Meckel‘s groove on the mandible9–11, while the tympanic limb of the cartilage and its associated ectotympanic and prearticular are separated mediolaterally from the pterygoid region of the mandible (Fig. 3f, g), as postulated by Allin.	**9**	
		The middle ear and the ossified Meckel‘s cartilage in late-stage subadult or adult of Yanoconodon (Fig. 3g) show a similar structural pattern to the embryos of monotreme (Fig. 3i) and placental mammals.	**10**	
		FIG. 11	**11**	
		In Yanoconodon and gobiconodontids (and by inference also Jeholodens), the former step of mediolateral separation of the middle ear from the mandible has already occurred. But reabsorption of Meckel‘s cartilage did not happen, resulting in the retention in Yanoconodon of the middle-ear connection to the mandible, otherwise seen only in the early embryonic or fetal stage of extant mammals.	**12**	
		The paedomorphic connection of the middle ear to mandible of eutriconodonts and mammaliaforms is consistent with their lack of the long-bone epiphyses for terminating skeletal growth, as seen in modern mammals.	**13**	
		Homeotic changes in vertebral identities, such as shift of the thoracolumbar boundary or gradational transition, are now correlated with the loss and gain of Hox genes function in mice.	**14**	
		FIG. 3	**15**	

		FIG. 4	**16**	
9	**Nature 2**	Here we use two-photon calcium imaging in head-fixed Drosophila melanogaster walking on a ball in a virtual reality arena to demonstrate that landmark-based orientation and angular path integration are combined in the population responses of neurons whose dendrites tile the ellipsoid body, a toroidal structure in the centre of the fly brain.	**1**	
		When both visual and self-motion cues are absent, a representation of the animal‘s orientation is maintained in this network through persistent activity, a potential substrate for short-term memory.	**2**	
		When flies were exposed to a single vertical stripe stimulus (Extended Data Fig. 1a), we observed a sector of activity, or bump, in the EB that rotated concurrently with the stripe as the fly turned on the ball (Fig. 1f, j, k; Supplementary Video 1, Extended Data Fig. 2a-c). The spatial extent of the visual arena (270°) was mapped to the full angular extent (360°) of the EB (Extended Data Fig. 2d, see Methods).	**3**	
		Fig 1.	**4**	
		Figure 1 | Ellipsoid body activity tracks azimuth of visual cue. a, Schematic of setup. Inset, close-up of fly on air-supported ball (modified from ref. 20). b, Schematic of fly central brain and CX: ellipsoid body (EB), fan-shaped body (FB), protocerebral bridge (PB), paired noduli (NO), lateral accessory lobe (LAL) and gall (Gall). MB: mushroom body.	**5**	
		Instead, consistent with EBw.s activity representing the fly‘s orientation, we observed a single bump of similar width (Fig. 2a–c, Supplementary Video 2, Extended Data Fig. 3a–c), the spatial extent of the arena was once again mapped onto the EB (Extended Data Fig. 3d), and the PVA estimate of the fly‘s azimuth remained accurate (Fig. 2d–g, Extended Data Fig. 3e, f).	**6**	
		We observed that EBw.s activity transitioned from one offset to another relative to the visual cues (Extended Data Fig. 5a–c, Supplementary Video 4), potentially reflecting the ambiguity inherent in determining landmark-guided orientation in an environment with multiple indistinguishable visual landmarks.	**7**	
		FIG. 2	**8**	
		Instead, we observed that EBw.s. population activity moved to match the cue shift, preserving the initial offset between the EBw.s bump and visual cue azimuth (Extended Data Fig. 6a, b, Fig. 3b; Supplementary Video 5).	**10**	
		Consistent with this, the relationship between walking rotation and EBw.s bump movement was strongly dependent on closed-loop gain (Fig. 3h), whereas the relationship between visual cue movement and rotation of the EBw.s bump scaled only slightly with gain (Fig. 3i). Nevertheless, we occasionally observed examples of EBw.s activity being more influenced by the animal's rotation than cue movement, particularly in situations of low gain (Extended Data Fig. 6d-f).	**11**	
		Specifically, we examined EBw.s activity during epochs when the fly stopped walking while in the dark. In almost all such cases, the EBw.s population maintained a representation of the fly's orientation (Fig. 4e-i; Extended Data Fig. 10a-f; Supplementary Video 7 and 8).	**12**	
		FIG. 3	**14**	
		Combining landmark orientation with information about the animal's movement effectively creates an internal reference frame for the animal in its surroundings.	**15**	

		Consistent with this notion, the EBw.s activity bump largely remained tethered to the position of one landmark even in the presence of another identical landmark in front of the fly (Extended Data Fig. 4i). The bump also did not always shift instantaneously following an abrupt displacement of visual landmarks, as if temporarily retaining the original orientation reference before locking on to its new position (Extended Data Fig. 6b).	**16**	
		FIG 4	**17**	
		we have observed several of the expected features of ring attractor models37,39,40 in the dynamics of this population of CX neurons: organization of activity into a localized bump, movement of the bump to neighboring wedges based on self-motion, drift in bump location in darkness, persistent activity, and both abrupt jumps and gradual transitions of the activity bump when triggered by strong visual input.	**18**	
10	**Nature 3**	In optical images they appeared like the phases of the moon, owing to the dark metal coating.	**1**	
		The resulting dynamics, which resembled a gyroscope‘s nutation, are quantitatively captured by the equations of motion (Methods). Notably, the rotation and oscillation frequencies can be controlled by the precession angle θ.	**2**	
		FIG. 1	**3**	
		Once synchronized, the particles‘ rotation slowed slightly, while their geometric centres started to rotate around a common central axis. Their spatial positions are staggered head-to-tail owing to the Janus feature, which is captured in simulation by a point dipole moment shifted from the particle‘s geometric centre.	**4**	
		We observed frequency locking even when particles had different coating thicknesses and hence different inherent frequencies.	**5**	
		At low precession angle h, we observed a family of long, defect-free microtubes forming spontaneously (region I in Fig. 2a). Structurally, unlike the chiral helices observed in amphiphilic self-assembly14 or magnetic assembly directed by steric hindrance15, these microtubes wereachiral and can be interpreted as staggered stacks of regular polygons with k edges (Fig. 2b).	**6**	
		Initially, zigzag chains approached and wrapped around one another randomly, then short ordered (kk0) strands nucleated, and finally nuclei propagated to _zip up‘ a corresponding structure. Once formed, these structures rolled on the substrate.Within region I of the dynamic state diagram, the distribution of microtubes changed with θ (Fig. 2c): increasing θ shifted the distribution towards smaller k.	**7**	
		On exceeding a threshold h only zigzag chains **were observed** (region II) and subsequent increase of h transformed them in known ways, into hexagonal sheets oriented perpendicular to the precession axis (region III, Fig. 2d). The synchronization-induced structural transitions of interest here occurred at relatively low h where the frequency dependence is small.	**8**	
		Distorting the lowest-energy configuration, this generated a restoring torque dE/dy (incorporating all many-body interactions) that rotated the tube while slowing the constituent particles.	**9**	
		FIG. 2	**10**	
		However, at higher h, synchronization criteria set in. The larger the tube diameter, the smaller the coupling strength e and the larger the friction ftube, leading to lower dissociation angle hc. For example, with increasing h in Fig. 2c we saw fewer (550) microtubes and none above hc (which is about 25u for this structure).	**11**	
		The abundance of mediumdiameter structures such as (330) thus first increased at the expense of thicker structures and dominated at some angles. This agrees qualitatively with the trend seen in simulation (Supplementary Fig. 13).	**12**	

		Consistent with simulations from random initial conditions, **we also observed** (kk2k) and chiral structures when we coated the same nickel films onto paramagnetic spheres (Supplementary Video 9).	**13**	
		These experiments indicated that all mouse Taar genes, except Taar1, are expressed in the olfactory Epithelium	**1**	
		They further showed that the expression levels of individual Taar genes in the olfactory epithelium resemble those of odorant receptor genes.	**2**	
		we obtained no evidence for Taar gene expression in any tissue—including the brain—apart from the olfactory epithelium, even though **we detected** high-level expression of genes encoding several biogenic amine receptors in the brain.	**3**	
		Using the zebrafish Taar9 protein to search ESTs translated in silico by TBLASTN, we found a large number of zebrafish ESTs encoding related proteins, with 33 of the 37 highest matches being sequences from a zebrafish olfactory epithelium cDNA library (NIH_ZGC_14).	**4**	
		The labelled neurons were confined to certain olfactory epithelial zones, which varied among the Taar genes, another feature characteristic of odorant receptor gene expression	**5**	
		Expression of each Taar, except Taar1, was seen in both male and female mice by qPCR as well as RNA in situ hybridization. Quantification of OSNs labelled by individual Taar probes in every fortieth section along the anterior–posterior axis of the olfactory epithelium (eight sections per probe) gave average counts of 214, 658 and 343 labelled cells for Taar2, Taar6 and Taar9 probes, respectively.	**6**	
		Tabla 1	**7**	
		Results consistent with the findings in the transgenic mice were obtained when non-transgenic olfactory epithelial sections were double-labelled with Taar probes (Taar6, Taar7e or a mix of all Taar probes) and OR-M49 or OR-K20 (Olfr142) odorant receptor probes, which should hybridize with two and five intact odorant receptor genes (and one odorant receptor pseudogene each), respectively (Fig. 3e).	**8**	
		In contrast, OSNs labelled with probes for Taar2, Taar6, Taar7f or Taar9 showed the same double-labelling with a Gaolf probe (Fig. 3f) as those labelled with an odorant receptor probe.	**9**	
		FIG. 3	**10**	
		FIG. 4	**11**	
		Consistent with reports that hTAAR1 and rat TAAR4 respond to small organic amines23, we identified several previously unknown TAAR ligands, all of which were amines.	**12**	
		Together, these experiments identified ligands for mTAAR1, mTAAR3, mTAAR4, mTAAR5 and mTAAR7f (Fig. 4a). The mTAARs **responded similarly with or without the rho tag**, except for mTAAR4, which required the tag for function, and mTAAR3, which only responded without the tag.	**13**	
		In these experiments, mTAAR3 responded to several primary amines, including isoamylamine (EC50 ¼ 10 mM) (Fig. 4a). In contrast, mTAAR5 and mTAAR7f both responded to tertiary amines: mTAAR5 to trimethylamine (EC50 ¼ 0.3 mM) and N-methylpiperidine, and mTAAR7f to N-methylpiperidine (EC50 ¼ 20 mM) (Fig. 4a). Consistent with previous reports that hTAAR1 and rat TAAR4 both recognize b-phenylethylamine23, this compound activated hTAAR1, mTAAR1 (EC50 ¼ 0.1 mM) and mTAAR4 (EC50 ¼ 1 mM) (Fig. 4a).	**14**	
		FIG. 5	**15**	

		These studies show that at least four TAARs expressed in the mouse olfactory epithelium recognize small-molecule amines and, furthermore, that each of these receptors detects a unique set of amine ligands.	**16**	
		In addition, we found that the mouse TAAR that recognizes trimethylamine is activated by extremely dilute mouse urine from sexually mature males, but not females or prepubescent males.	**17**	
12	**Science 1**	Growth of the ice sheets **to their maximum positions occurred between** 33.0 and 26.5 ka in response to climate forcing from decreases in northern summer insolation, tropical Pacific sea surface temperatures, and atmospheric CO2	**1**	
		The onset of deglaciation of the West Antarctic Ice Sheet occurred between 14 and 15 ka, **consistent with evidence that this was the primary source** for an abrupt rise in sea level ~14.5 ka.	**2**	
		We find that in the prediction for Barbados, peripheral bulge dynamics and, to a lesser extent, the continental (lithospheric) levering effect dominate the anti-syphoning effect during the LGM (7), leading to a net sea-level fall of ~3 m. In contrast, the remaining four sites lie well outside the peripheral bulges, and the sea-level rise due to anti-syphoning dominates; **the net result is** a ~4- to 5-m rise in sea level at these sites.	**3**	
		across the LGM period, **when the modeled** ice history shows no change in the ice volume, the differential sea-level change between Barbados and the other sites approaches 10 m (Fig. 2 and fig. S1).	**4**	
		Over the next 2500 years, the remaining ice sheets [and sectors of the Laurentide Ice Sheet (LIS)] **continued to grow**, so that by 26.5 ka, nearly all ice sheets had attained their maximum extents, corresponding to the onset of the LGM sea-level lowstand (Fig. 3C).	**5**	
		Fig. 1.	**6**	
		This evidence for widespread ice-margin retreat occurring between 19 and 20 ka **indicates that** the 19-ka meltwater pulse, which represents a rapid 10-m rise in sea level from the LGM lowstand some- time between 19 and 20 ka (Fig. 3C) (8, 12), originated from these Northern Hemisphere ice sheets.	**7**	
		Moreover, the earlier retreat of Northern Hemisphere mountain glaciers is synchronous, within error, with retreat from most Northern Hemisphere LLGM ice-sheet margins at ~19 ka.	**8**	
		We have shown that the duration of the LGM sea-level low- stand (26.5 to 19 ka) is in excellent agreement with the duration of maximum extent of most of the global ice sheets.	**9**	
		Comparison of the reasonably well- established global sea-level record for the past 35,000 years (35 ky) (Fig. 4A) with several benthic d18Oc records from the Pacific and Atlantic basins (Fig. 4B) **clearly demonstrates that** the d18Osw signal has been compromised by these other effects, and that their relative contribution varies between sites.	**10**	
		Fig. 2. Sea-level predictions for New Guinea (blue line) and Barbados (purple line) compared to RSL data with depth uncertainty for the interval from 10 to 50 ka from New Guinea (blue circles) (4, 52, 53), Barbados (purple triangles) (5, 54), the Bonaparte Gulf (green half-pluses represent- ing age and depth uncertainty) (8), and the Sunda Shelf (blue half-pluses) (55). Eustatic sea-level time series are shown as a gray line. The vertical gray bar indicates the time of the LGM as defined from the RSL data	**11**	

		Fig. 3 Summary of glacier and ice- sheet chronologies for LLGM with RSL data constraining the time of the LGM. The vertical purple bar represents the time of the LGM as defined from the RSL data, whereas the vertical gray bar represents the earliest interval when sea level began to fall to the LGM lowstand, corresponding to the time when the first ice-sheet LLGM were reached.	**12**	
		Summary of the timing of the LLGM for each of the ice-sheet sec- tors and ice sheets shown in figs. S2 and S3, with the small horizontal purple bars with gray bars on either end representing the time of the LLGM and associated error, respectively	**13**	
		The initial phase of sea-level lowering toward the LGM lowstand, accompanied by the time of earliest LLGM ice- sheet maxima (33 to 29 ka), **occurred at the same time that northern summer insolation began to decline** (Fig. 5B) and as summer energy was de- creasing, particularly at 45°N, where ablation rates along the southern LIS margin would have been most sensitive to this index (Fig. 5A), thus supporting a northern latitude insolation control on ice-sheet growth.	**14**	
		FIG. 4. Constraints on changes in sea level and deep ocean temperature. The vertical purple **bar represents the time** of LGM as defined from the RSL data, whereas the vertical gray bar represents the earliest interval when sea level began to fall to the LGM lowstand, **corresponding to the time when** the first ice-sheet LLGM were reached	**15**	
		RSL data for the interval from 10 to 50 ka (Fig. 3), converted to d18Osw by scaling the glacial-interglacial d18Osw change of 1.0 T 0.1‰ (27) to the corresponding sea-level change	**16**	
		The red line shows our estimate of global average deep sea temperature derived by subtracting the sea-level component of seawater in the RSL data (Fig. 4A) from the LR04 benthic d18O stack (28) (Fig. 4B), with the residual d18O converted to temperature using a relation of 0.28‰ °C−1. The green line shows the modeled changes in deep ocean temperature from (29)	**17**	
		Temporal relation between the LGM and various climate-forcing factors. **The vertical purple bar represents the time** of the LGM as de- fined from the RSL data, whereas the vertical gray bar represents the earliest interval when sea level be- gan to fall to the LGM lowstand, cor- responding to the time when the first ice-sheet LLGM were reached	**18**	
		ummer energy for 45oN (red line, t = 400) and 65oN (purple line, t = 400). (B) 21 June–20 July inso- lation for 45oN (red line) and 65oN (purple line) (58). (C) Atmospheric CO2 from the Dome C ice core (light purple circles) (59) and Byrd ice core (dark purple circles) (60). (D) The 500-year average NINO3 index from the Zebiak-Cane model forced with orbital-scale solar variations (gray line) (37) compared to SST records from the tropical Pacific [deep yellow, RC13-110 (34); ruby red, ODP 846B (35); light orange, TR163-19 (31); magenta, MD98-2176 (40); red, MD98-2181 (40)]. (E) The 20-year-resolution d18O record from the Greenland NGRIP ice core (61) (blue line) and the SD of that record calculated with a centered, 3-ky sliding window	**19**	
		SST records from the western equatorial Pacific indicate that surface waters in the warm pool had already cooled to LGM values by ~60 k.	**20**	
		We used these simulations to estimate the possible sea-level response to a cooling of the tropical Pacific. **For example, in the case** of an intermediate-sized (MIS 3) LIS, cooling of the tropical Pacific induces a mass balance increase of 0.17 m year−1 (38), which integrated over the area of the ice sheet for 6500 years (33.0 to 26.5 ka) results in a global sea-level fall of ~24 m.	**21**	

		In contrast to the multiple controls that may have induced ice-sheet growth, our geochronology for the LGM **clearly demonstrates that** only northern insolation led the termination and was thus the primary mechanism for triggering the on- set of Northern Hemisphere deglaciation.	**22**	
		When considering the onset of the LGM, **we note that most Northern Hemisphere LGM ice sheets were in equilibrium** (mass balance) as long as summer insolation was within 10 W m−2 (or 0.2 GJ m−2 for summer energy) of the minimum value.	**23**	
13	**Science 2**	Using a comprehensive range of structured protocols, we sampled the phylogenetic breadth of arthropod taxa from the soil to the forest canopy in the San Lorenzo forest, Panama**. We collected 6144 arthropod species from 0.48 hectare and extrapolated total species richness to larger areas on the basis of competing models**.	**1**	
		Although individual estimators adjusting for different aspects of sampling design offered slightly different estimates (Fig. 1B**), the total species richness for the entire San Lorenzo forest (~6000 ha) was consistently quantified at between 18,000 and 44,000 species** (including focal and nonfocal species).	**2**	
		A relatively large proportion of the expected species richness of the forest was recovered for most of our focal taxonomic groups (Fig. 2). For example, high proportions of all ant species and of the parasitoid species targeted in our study were collected from our 12 sites, whereas fungal feeders would require more intensive sampling to achieve adequate coverage.	**3**	
		Beta diversity of all arthropods (in the broad sense of species turnover among sites) increased roughly linearly with cumulative area surveyed ($F_{1,3} = 2422.5$, $P < 0.001$). With increasing sampling effort, sample coverage [an unbiased measure of sample completeness, see (20)] was high and accumulated at significantly different rates across different arthropod orders and guilds, and across the various guilds comprised by beetles (Fig. 3).	**4**	
		Despite idiosyncrasies in the rate of increase in sample completeness across insects groups, the high proportion of overall species richness detected at small spatial scales (Figs. 2 and 3) has a remarkable consequence. Based on a general relationship between species numbers and area**, we estimate that almost two-thirds (64%) of all species in SLPA occur in a single hectare of rainforest**.	**5**	
		FIG. 1	**6**	
		The implications of the results observed on a local scale are clear. For every species in the well-known vascular flora (1294 species), avifauna (306 species), and mammalian fauna (81 species) of SLPA, we estimate that there will be a mini- mum of 17, 71, and 270 arthropod species, respectively (based on lower bound of species richness) and most likely as high as 20, 83, and 312 arthropod species, respectively	**7**	
		FIG. 3. Accumulation of species richness with area at SLPA (20). For all groups, **a high proportion of overall species richness was detected at small spatial scales.** (A) Partitioning of species richness within arthropod guilds at different spatial scales (a: single site of 0.04 ha; b3: three sites spaced apart totaling 0.12 ha; b6: six sites totaling 0.24 ha; b12: 12 sites totaling 0.48 ha; bha: 1.0 ha; bSLPA: 6000 ha; means T SEM are shown for a, b3, and b6). (B) Species-area models for the main arthropod groups and large data sets	**8**	
		Average sample coverage [TSEM; error bars, see methods (20)] **plotted against the cumulative number of sites surveyed, for the main** (A) arthropod guilds and orders and (B) beetle guilds. For the sake of clarity, SEMs are omitted in (A).	**9**	

		Based on the close association observed here between floristic diversity and both herbivore and nonherbivore species richness, we tentatively conclude that the most recent estimate of global tropical arthropod species [6.1 million arthropod species (24)] does not require drastic correction to account for differential scaling rela- tionships of nonherbivore taxa	**10**	
14	**Science 3**	Imaged from multiple perspectives, extreme ultraviolet observations of Lovejoy's tail **showed substantial changes in** direction, intensity, magnitude, and persistence.	**1**	
		The observed tail motions reveal the inhomogeneous magnetic field of the solar corona.	**2**	
		We show how these motions constrain field and plasma properties along the trajectory, **and how they can be used to** meaningfully distinguish between two classes of magnetic field models.	**3**	
		Fig. 1. Base ratio processed 171 Å EUV **observations from multiple viewpoints are shown**; the white enhancements highlighted by short red arrows indicate the emitting comet tail.	**4**	
		UVI-A and EUVI-**B images that show** the apparent ~~–~~wiggles" out of the orbital path observed during the closest approach.	**5**	
		An AIA **image before perihelion (ingress) with arrows indicating** the southwest tail motion and other relevant directions.	**6**	
		The long-lasting portions of the tail are highlighted, with a time sequence of post- perihelion AIA images (egress) **that show a separation** of approximately 5.5 and 15.5 min, respectively.	**7**	
		AIA observations before perihelion (ingress, Fig. 1B**) show that** the comet tail motion was markedly in the southwest direction.	**8**	
		Fig.2. The top two rows show a comparison between 171 Å imaging observations and synthesized emission from the model solution. The bottom rows show the local magnetic field along the comet trajectory.	**9**	
		The local magnetic field along the comet trajectory gives a sense of the complex local magnetic geometry encountered by the comet, **which is used to infer** the initial direction and magnitude of comet tail ion velocity, $(vc\cdot b)b$.	**10**	
		Fig. 3. Comparison of the magnetic field (left), initial tail velocity $(vc\cdot b)b$ (center), and resulting comet tail flow (right) predicted by the thermodynamic MHD model (top row) and the PFSS field model (bottom row) for the AIA ingress observations.	**11**	
		Fig. 4. MHD model overlays of electron temperature (left), electron density (center), and the lifetime estimate, $t_{OV;OVI}$ (right), over the AIA egress observations. **The MHD data along the trajectory are shown** as a wide color contour placed above the orbit line.	**12**	
		Note that the comet trajectory is interspersed with closed- field regions (blue lines) where the field orientation is changing rapidly in the comet frame, which similarly modifies $(vc\cdot b)b$ over short time periods.	**13**	
		To fully link the MHD solution with the observations, we probed the comet tail evolution by approximating the deceleration of cometary ions along the magnetic field as an exponential decay with time constant td = 150 s plus flow and diffusion terms. This reduced the comet tail dynamics to the ballistic tracking of test particles within a 3D vector field and inhomogeneous medium (10).	**14**	
		There is an overall global resemblance between the thermodynamic MHD and PFSS solutions, which is not unexpected for regions with low relative electric currents.	**15**	

		Because the curvature of the field on the east side of the streamer region (blue lines, lower left) differs between the two models, **the comet flow prediction is in the opposite** (northeast) direction for the PFSS model during this time period.	**16**	
		In any case, this comparison **highlights the capability of the comet tail observations** to corroborate or invalidate portions of global field models—an otherwise nontrivial task fraught with ambiguity.	**17**	
		Using the MHD model values to compute tOV,OVI, **we find that** this time scale is considerably lengthened relative to ~~–~~typical" (ne = 108 cm–3) coronal conditions for the later half of the view, **which is qualitatively consistent** with the transition from short to long lifetime in the tail observations (albeit broader and slightly offset)	**18**	
		We found that Dilp8 binds to and activates the relaxin leucine-rich repeat– containing G protein–coupled receptor Lgr3 to mediate homeostatic control through a pathway dependent on adenosine 3′,5′-monophosphate.	**1**	
		We show that Dilp8-Lgr3 balances growth against the extended growth period by dampening the production of dilp3 and dilp5 by insulin- producing cells (IPCs) in the brain and inhibiting synthesis of the juvenile hormone (JH)	**2**	
		We also identify two pairs of dorsomedial neurons in the pars intercerebralis that are necessary and sufficient to mediate the effects of Dilp8.	**3**	
		These neurons have extensive axonal arborizations, and genetic and green fluorescent protein reconstitution across synaptic **partners show that these neurons connect with** the insulin-producing cells and prothoracicotropic hormone–producing neurons to attenuate growth and maturation	**4**	
		By employing a candidate approach and bio- chemical assays, we demonstrate that the orphan relaxin receptor Lgr3 acts as a Dilp8 receptor.	**5**	
		We identify the neuronal population molecularly defined by the lgr3 enhancer fragment R19B09 (24) and show that it is necessary and sufficient to mediate such homeostatic regulation.	**6**	
		Using tools for circuit mapping and an adenosine 3′,5′-monophosphate (cAMP) sensor as an indicator of Lgr3 receptor activation in vivo**, we determined that** a pair of these Lgr3 neurons is highly sensitive to Dilp8.	**7**	
		When the lgr3, but not lgr4, gene was silenced (tub-Gal4 UAS-dilp8 UAS-lgr3- RNAi, hereafter tub>dilp8>lgr3-IR), Dilp8-induced developmental delay was fully suppressed (Fig. 1, B and C). Depletion of lgr3 accelerated pupar- iation by ~8 hours (Fig. 1C), as in dilp8 mutants (13). **We verified the efficiency of** the lgr3-RNAi transgene by quantitative real-time polymerase chain reaction.	**8**	
		The delay in pupariation induced by Dilp8 **resulted in normal-sized adults**, owing to Dilp8-induced growth compensation. Yet, the extra time the tub-dilp8 larvae spent in the feeding period led to overweight adults (12, 13). Knockdown of lgr3 also prevented the dilp8-overexpressing animals [tub-dilp8, daughterless (da)-Gal4 UAS-lgr3-RNAi] from being overweight.	**9**	
		Knockdown of lgr3 in neurons, but not in the ring gland, also **prevented the Dilp8- induced reduction of growth rate** (fig. S1, F and G). Further, neuronal depletion of lgr3 using elav-Gal4 (elav>lgr3-IR) **produced** adults that displayed greater fluctuations in asymmetry, as evidenced by significantly larger left-right variations in the size of adult wings (Fig. 1F).	**10**	

		The underlying mechanism **may involve** direct Dilp8 sensing in neurons expressing PTTH or IPCs, the two prominent yet separate neural circuits that regulate ecdysone production in the PG and/or overall growth rates during larval development. **Alternatively**, the receptor may transduce Dilp8 signals in a novel neuronal population or directly in endocrine cells.	**11**	
		The underlying mechanism **may involve** direct Dilp8 sensing in neurons expressing PTTH or IPCs, the two prominent yet separate neural circuits that regulate ecdysone production in the PG and/or overall growth rates during larval development. **Alternatively**, the receptor may transduce Dilp8 signals in a novel neuronal population or directly in endocrine cells.	**12**	
		Only cells transfected with the lgr3- expressing plasmid responded to a 30-min ex- posure to Dilp8 (50 nM) with an increase in cAMP levels, from 213.8 ± 67.94 fmol/5 × 104 cells to 1.612.36 ± 302.6 fmol/5 × 104 cells (Fig. 2A and materials and methods).	**13**	
		Indeed, we detected a strong colocalization of Dilp8 at the surface of Lgr3-expressing cells (Fig. 2C and fig. S2).	**14**	
		When the endogenous expression of the lgr3 gene was quantified (fig. S1A) (27), it appeared to be expressed only very weakly. **Not surprisingly, attempts to map** lgr3-expressing neurons by conventional immunological approaches using anti- bodies against the Lgr3 protein (materials and methods**) were unsuccessful**.	**15**	
		Using the Gal4/UAS system to coarsely map functionally relevant neurons, **we found that** Lgr3 is not required within the IPCs themselves (dilp3- Gal4), the neuropeptide F-expressing cells (npf-Gal4), the circadian clock neurons (pdf-Gal4 and per-Gal4), the PTTH neurons (ptth-Gal4), or he ventral nerve cord (VNC) [teashirt (tsh)-Gal4]	**16**	
		We found that using the R19B09-Gal4 enhancer to deplete lgr3 (Fig. 3B) fully suppressed the Dilp8- induced delay and did so with the same magnitude as when lgr3 was ubiquitously depleted by tub-Gal4 (Fig. 1B). No other Gal4 enhancer lines prevented the Dilp8-induced delay (Fig. 3B).	**17**	
		We also found that overexpression of the UAS- lgr3 transgene in R19B09-labeled neurons was sufficient to evoke a ~12-hour delay in pupariation (Fig. 3D), but this process was not delayed when expressed under control of the other lgr3 genomic fragments.	**18**	
		FIG. 2. cAMP **measurement in untreated** Drosophila Kc cells (5 × 104 cells per culture) transiently transfected with the indicated Lgr plasmids and the empty plasmid or treated with either 5 or 50 nM Dilp8 peptide for 30 min.	**19**	
		Dilp8- **stimulated dose-dependent cAMP production** by Kc cells expressing Lgr3. The concentration of Dilp8 ranged from 0 to 250 nM. Kc cells were transiently transfected with the lgr3, lgr4, or lgr2 plasmids, and an EC50 value of 6.31 T 0.1277 nM was obtained for Lgr3.	**20**	
		Dilp8 and Lgr3 colocalization assessed **by** confocal immunofluorescence. Kc cells expressing the extracellular domain of Lgr3-ECD::3xHA were incubated with medium containing Dilp8-Flag (materials and methods)	**21**	

		However, Lgr3 dis- plays high levels of constitutive activity only when expressed in a heterologous system [human embryonic kidney 293 cells (27)]; this high constitutive activity is not observed in Drosophila cells (Fig. 2A) or in vivo in neurons (see below). Moreover, **Lgr3 activity is greatly increased in the presence of Dilp**8 (Fig. 2, A and B, and be- low).	**22**	
		Together with the observations made for the tsh-Gal4 line (Fig. 3A), which typically labels all neurons in the VNC (33), we conclude that a set of ~12 central neurons per hemisphere, molecularly defined by R19B09-Gal4**, reflects the Lgr3 neurons that are necessary and sufficient to control size and developmental timing in response to Dilp8.**	**23**	
		Other lgr3 genomic fragments (e.g., R17G11-Gal4) (fig. S5) **that did not suppress the Dilp8-induced delay failed to produce levels of Dilp8-induced cAMP** comparable to those found in R19B09-labeled neurons (fig. S5, A and B), in agreement with their inability to prevent Dilp8-induced delay (Fig. 3B).	**24**	
		FIG. 3. **Puparion time of** animals with brain-region– specific knockdown of lgr3, using RNAi and the indicated Gal4.	**25**	
		Cumulative **puparion time of** animals over- expressing UAS-lgr3, using R19B09-Gal4 (D), or with electrical hyperexcitation of neurons labeled by R19B09-Gal4, using the UAS-NaChBac ion channel	**26**	
		The intensity of luciferase in other Lgr3-independent cells in the elav-Gal4 brains was not generally altered (fig. S5D), indicating that the loss of CRE-F-luc signal in the dorso- medial and dorsolateral neurons **was not due to nonspecific effects of** the lgr3-RNAi.	**27**	
		Brainbow-assisted analysis and the pre- and postsynaptic markers **revealed that** Lgr3 neurons in the dorsomedial region extend both ipsilateral and contralateral axon projections (Fig. 5, D to D″), with thin dendrites descending into the VNC (Fig. 5, B and C, and movie S3)	**28**	
		Fig. 4. **Expression of** UAS- DsRed in neurons defined by the R19B09-Gal4 enhancer (see fig. S4 for the expression of the other lgr3-Gal4).	**29**	
		Higher-magnification views of central neurons in the dorsomedial region stained with anti-Luc (red) and the neuroblast marker anti-Mira (green).	**30**	
		Knockdown of lgr3 (elav-Gal4/UAS-Flp; tub-dilp8/+; CRE-F-luc/UAS-lgr3- IR) inhibits the Dilp8-induced cAMP response detected by luciferase driven by the CRE-F-luc construct, reflecting Lgr3 activation and probing specificity of the UAS-lgr3-IR transgene.	**31**	
		Confocal sections of the control brains (F) elav-Gal4/UAS-Flp; tub-dilp8/+; CRE-F-luc/+ and (G) elav-Gal4/UAS-Flp; +/+; CRE- F-luc/+. Scale bars, 75 mm in (A) and (C) [also applies to (C′) and (D)]; 40 mm in (E) [also applies to (F) and (G)].	**32**	
		We detected unre- constituted GFP, using immunofluorescence result-ing from expression of the spGFP1-10 fragment at the PTTH soma and axons (compare panels C and F in fig. S6). Immunofluorescence staining of PTTH neurons and signals of GRASP between IPCs and Lgr3 revealed probable synaptic con- tact sites in the circuit.	**33**	

		Thus, we tested the effect of hyperpolarization of the membrane of PTTH neurons by expressing the potassium channel mKir2.1, which has proven to be a highly effective approach for shunting neuronal activity in excitable neurons (42). Expression of UAS-mKir2.1 in the PTTH neurons using ptth-Gal4 produced a larval-pupal transition delay of 12 hours compared with WT controls (Fig. 5I and see Fig. 5K for measurement of ecdysone signaling).	**34**	
		IPCs **modulate growth systemically via** circulating insulin-like peptides (such as Dilp2, -3, and -5) and via endocrine mechanisms, such as direct regulation of JH synthesis in the CA (23, 43), which was also recently shown to instructively regulate larval growth in Drosoph- ila (44, 45).	**35**	
		The levels of dilp3 and dilp5, which are known to respond to nutrition and stress (16) (Fig. 6B), and of JHAMT and kr-h1 in JH biosynthesis and signaling (Fig. **6C) were also significantly down-regulated in tub-dilp8 larvae,** and their expression was restored to almost-normal levels by specific knockdown of lgr3 in R19B09 neurons. This non–cell-autonomous effect was specific because the expression of dilp2 was not altered (fig. S8).	**36**	
		The tub>dilp8 larvae **reach the correct pupal size and adult size** [as assessed by measuring pupal vol- ume and adult wing size and shape (12)]. In contrast, tub>dilp8 larvae fed with the JH analog (JHA) methoprene produced significantly larger pupae (~25%) than did control animals (Fig. 6D).	**37**	
		Our data provide strong evidence that Dilp8 signals for organismal and organ homeostatic size regulation are transduced via the orphan relaxin receptor Lgr3 and that activation of Lgr3 in molecularly defined neurons mediates the necessary hormonal adjustments for such homeostasis. Human insulin/relaxin-like peptides are transduced through four GPCRs: RXFP1 to -4.	**38**	
		Additionally, as for Lgr3 (this study), activation of RXFP1 and -2 by their cognate ligand **binding stimulates increased cAMP production**	**39**	
		Our study shows that without lgr3,thebrain is unable to detect growth disturbances and, more importantly, cannot adjust the internal hormonal environment to allocate additional developmental time for restoring affected parts or catching up on growth.	**40**	
		FIG. 5. Lgr3 neurons with soma in the dorsomedial region and a prominent response to Dilp8 detected by DsRed (R19B09-Gal4>DsRed) ensheathed PTTH dendritic fields and axons (anti-PTTH, blue) and densely innervated IPCs (anti-Dilp2, green).	**41**	
		Single confocal optical sections of larval brains of R19B09-Gal4 driven presynaptic (UAS-syt::GFP, green) and post- synaptic (UAS-DenMark, red) markers	**42**	
		UAS-dBrainbow reveals that projections from distinct neural subpopulations labeled by R19B09-Gal4 converge on the dorsomedial Lgr3 neurons (green neurons, arrowheads).	**43**	
		Positive, robust signals of GRASP **revealed extensive connections** between Lgr3 (R19B09-LexA>spGFP11) and IPCs (dilp3-Gal4>spGFP1-10>mCD8::RFP). Brains were counterstained with anti-DE-Cad (blue).	**44**	
		GRASP signals (arrowheads) between Lgr3 neurons (R19B09-LexA>spGFP11) and PTTH-producing neurons their contralateral limbs, nor do we understand how limbs maintain proportion with other body parts, even when faced with perturbations (this statement is also applicable to other bilaterally abnormalities. Our study shows that without lgr3, the brain is unable to detect growth disturbances and, more (ptth-Gal4>spGFP1-10) are detected with immunofluorescence (green)	**45**	

		Brains stained with anti-PTTH (blue) could detect potential contact sites (asterisks) of the circuit. GRASP signals (green) were contributed by connections between Lgr3 (R19B09-LexA>spGFP11) and IPCs (red) (dilp3- Gal4>spGFP1-10>mCD8::RFP).	**46**	
		Dilp8- induced delay in puparion formation is prevented by the constitutive active PTTH receptor torsoRL3 mutation. (I) Electrical silencing of PTTH neurons (ptth-Gal4 UAS-mKir2.1) delays pupariation, as compared with controls.	**47**	
		PTTH neuronal silencing does not evoke growth compensation and results in larger pupae, as compared with controls.	**48**	
		Expression of Eip75B at 100 hours AEL in control larvae (ptth-Gal4) and larvae with electrically silenced PTTH neurons (ptth>mKir2.1). ***P < 0.001 (unpaired t test)	**49**	
		Our study also identifies the Lgr3-expressing neurons necessary and sufficient to respond to Dilp8. Moreover, using a cAMP sensor, we have identified a pair of neurons that are highly sensitive to Dilp8.	**50**	
		GRASP analyses show that Lgr3 neurons are broadly connected with the IPCs and, to a lesser extent, with PTTH neurons, linking (Dilp8) inputs to the neuronal populations that regulate the key hormonal outputs modulating larval and imaginal disc growth.	**51**	
		FIG. 6. **Expression of** Eip75B (A), dilp3 and dilp5 (B), JHAMT [(C), left] and kr-h1 [(C), right] genes analyzed by qRT-PCR in mRNA isolated from ~10 larvae for each genotype and age	**52**	
		Model for plastic and homeostatic regulation of body size. If the growth rate is fixed, an extension of the developmental time results in larger adults (plastic regulation)	**53**	
		Model of Lgr3 circuit and output pathways. Dilp8 produced by peripheral tissues conveys information about overall growth status	**54**	
16	**Plos 1**	After reports of CXCR3 positive T cells indicating a T helper 1 (Th1) type of immune response [4] we found CXCR3 on macrophages [5] and showed that cross-talk among T cells and macrophages through the binding of interferon gamma (INFc) inducible protein 10 (IP10), secreted by T cells, to the CXCR3 receptor on macrophages macrophage-metalloprotease 12 (MMP12) was induced, showing a feed forward loop that destroyed the ECM through a non-antigenic cross talk [5].	**1**	
		We identified CD46 as protective gene that plays a pivotal role between the immune response adaptive and innate; down regulation of CD46 was associated with CD4+ T cell depletion, CD95 down regulation, and C3b accumulation with increased C5a in the lung. All together these data indicates a key role of CD46 in inflammation clearance and homeostasis of the immune response.	**2**	
		Table 1. Clinical and Demographic Characteristics of Participants.	**3**	
		Table 2. Protective genes.	**4**	
		Figure 1. Quantification of CD46 levels	**5**	
		Figure 2. Inflammation in the murine smoking model	**6**	

		Focusing our analysis on those genes that were consistently present only in control patients and not in diseased patients; we found 18 gene products that we called protective genes, listed in Table 2, and verified 5 of them by quantitative RT-PCR.	**7**	
		The results show a significantly higher expression of CD46 on T cells of control patients, without variation on macrophages or neutrophils (Fig. 1A), this data is further supported by the in vivo experiments.	**8**	
		Using the smoke-exposed murine model of COPD, we observed a significant decrease in CD46 expression in the lung (Fig. 2A) that was accompanied by significantly increased accumulation of C3b on the lung tissue, which co-precipitated with elastin (Fig. 2B)	**9**	
		Since C3b is required for the cleavage of C5 into C5a and C5b we quantified the protein down-stream, C5a. Furthermore, the inflammation caused by cigarette smoke (Fig. 3A) in the acute stage (1 week) resulted in a significant increase of IL12 secretion, which biased the immune system to Th1 and was suppressed by C5a up-regulation at the 4th week (Fig. 3B) of inflammation but this response was significantly impeded in C5aR knockout mice at 1 and 4 weeks of cigarette exposure (p =0.03, n =3 and n =5 for Wt) (Fig. 3A).	**10**	
		After the initial bias to Th1 occurred these cells secrete IP10 that binds to the CXCR3 receptor on macrophages inducing MMP12, and secretion of perforin and granzymes from CD8+ T cells that kill epithelial cells [28] releasing large amounts of elastin and causing cell death.	**11**	
		Decreased expression of CD95 indicates failure to eliminate Tc by Treg	**12**	
		Figure 3. Kinetic of the inflammation in murine smoking model.	**13**	
		Top plot show significantly less IL12 (average 6 SD) secretion in C5aR 2/2 (*, p,0.001, n = 3) compared to Wt, while (B) CXCR32/2 shows significantly decrease C5a secretion (**, p = 0.02, n = 3) at 4 weeks smoke and (C) decreased IL10 (1, p = 0.03, and n = 3) relative to Wt (n = 6). P values were calculated using T student test, two tails.	**14**	
		Thus, we inferred the pattern of T cells proliferation with disease progression through the analysis of the total lymphocytes in lung parenchyma; we verified that the increment in CD8T cells was at expenses of the CD4+ T cells population (Fig. 4 B) that directly correlated with the lung function decay (CD4/CD8 vs FEV1, Fig. 4B, bottom right corner).	**15**	
		We identified a region of the elastin protein that had more immunogenic properties; the different level of IgG binding to this region among the responders, which were classified as such if their OD was above the threshold set at the highest background, was of (9,9) and no responders (19,12), for control and EO-COPD respectively. EO-COPD group showed a significantly higher (86%) titer of IgG to elastin then normal controls (p= 0.0308 determined by Mann-Whitney test, Fig. 4D). According to these results the sensitivity of the ELISA test used is 43% and the specificity 68%.	**16**	

		In this study we searched for genes that protect ex-smoker from developing severe emphysema and COPD. We found that exsmokers without emphysema had higher expression of CD46 in their lungs compared to emphysema/COPD patients, that also occurred in vivo in the murine smoking model of COPD where CD46 down regulation was accompanied with accumulation of C3b co-precipitated with elastin and increased C5a which in return suppressed secretion of IL12, from macrophages, stimulated by the cigarette smoke.	**17**	
		Figure 4. Molecular cross-talk of the protective genes	**18**	
		From the kinetic of the inflammatory process seen in the animal model we learn that acute exposure to cigarette smoke initially triggers the Th1 bias inducing IL12 from macrophages [42], which is repressed later by the complement system with the increase of C5a [43,44].	**19**	
17	**Plos 2**	The proposed model is applied to the Shanghai stock market index and the Dow Jones index, and experimental results show that the proposed model performs better in the area of prediction than other two similar models.	**1**	
		Experimental results in the Shanghai stock market index and the Dow Jones index show that the ICA-CCA-SVR model performs better than AICA-SVR and MICA-SVR.	**2**	
		Figure 1. The input and output data of AICA-SVR model.	**3**	
		Figure 4. Multi-variable ICA regression model (MICA-SVR).	**4**	
		Figure 5. ICA-CCA regression model (ICA-CCA-SVR).	**5**	
		Figure 6. Shows the r curve versus the variation of dimensions and the proposed method consistently outperforms the other methods in the Shanghai stock market index.	**6**	
		Figure 7. Shows the r curve versus the variation of dimensions and the proposed method consistently outperforms the other methods in the Dow Jones index.	**7**	
		Figure 8. The actual Shanghai stock market index and its predicted values from ICA-CCA-SVR, MICA-SVR, and A ICA-SVR.	**8**	
		Figure 9. The actual Dow Jones index and its predicted values from ICA-CCA-SVR, MICA-SVR, and AICA-SVR.	**9**	
		The curves between r and Dim on the Shanghai stock index and Dow Jones index are displayed in the Figs. 6 and 7, respectively. From these figures, we can not only find the optimal dimensionality, but also illustrate the validity of the selected features of the three models. Figs. 6 and 7 give a comparison in terms of r using AICA-SVR and MICA-SVR, and ICA-CCA-SVR, respectively. The number Dim in the X-axis of figures refers to the dimensionality of features using different feature selection models.	**10**	
		One possible underlying reason is that the single variable does not contain sufficient information whereas the multi-variable does. On the Shanghai stock market index, when dimensionality is smaller than 5, the r of the AICA-SVR model is higher than that of the MICA-SVR model. However, when the dimensionality is more than 8, the r of the MICA-SVR model is much higher than that of AICA-SVR.	**11**	

		The performance of the ICA-CCA-SVR model is superior to both MICA-SVR and AICA-SVR with the increase of Dim. On the Shanghai stock market index, all plots of the ICA-CCA-SVR model are higher than MICA-SVR and AICA-SVR, although the first two plots have no distinct advantages and are even lower than AICA-SVR, due to the prediction information not being sufficient at lower dimensionality.	**12**	
		The highest r of the ICA-CCA-SVR model is 0.95174, which is also much bigger than that of AICASVR and MICA-SVR. At the same time, as the Dim increases, the ICA-CCA-SVR model shows stable predictive performance compared to the other models. On the Dow Jones index, when dimensionality is smaller than 5, the r of the ICA-CCA-SVR model is lower than that of the MICA-SVR model, and even is lower than AICA-SVR when Dim is equal to 3, 4 and 5. However, when the dimensionality is increased to 6, the r of the ICA-CCASVR model is much higher than that of AICA-SVR and MICASVR. The ICA-CCA-SVR model obtains the highest r of 0.87446 among the three models.	**13**	
		The actual Shanghai stock market index and predicted values from all three models are illustrated in Fig. 8 and Fig. 9 is the same curve for the Dow Jones index. It can be observed from Fig. 8 that the predicted values obtained from the proposed ICA-CCA-SVR model are closer to the actual values than those of the MICA-SVR and AICA-SVR models. From Fig. 9, we can see that the predicted values on the Dow Jones index of all three models are not fitted as well as they are on the Shanghai stock market index. Even so, the ICA-CCA-SVR model remains superior to the other two models.	**14**	
		Table 3 demonstrates the comparisons of the forecasting results of three models for Shanghai stock market index. It can be seen from the table that the ICA-CCA-SVR model shows much better performance than the other two models. All the measure indicators of the ICA-CCASVR model are significantly improved after feature fusion. For example, the indicators MAPE, RMSE, MAE and MSE values of the ICA-CCA-SVR model reach 0.011, 16.54, 12.638 and 273.56 respectively, which is much less than those of the AICA-SVR and MICA-SVR models. The indicators R2 and r values of ICA-CCASVR model reach 0.9486 and 0.95174, which is much bigger than those of the AICA-RVR and MICA-SVR models. Comparing the MICA-SVR model with the AICA-SVR model, the MICA-SVR model shows better performance than the AICA-SVR model.	**15**	
		From the above results, we can draw the conclusion that the ICA-CCA-SVR model performs well and surpasses the AICASVR and MICA-SVR models. The predicted stock price is influenced both by its the historical price and by related technical variables.	**11**	
		We also notice that the performance of ICA-CCA-SVR is no better than that of AICASVR AICASVR and MICA-SVR models, when the projecting dimensionality is low, that is, less than 3 for the Shanghai stock market index and 6 for the Dow Jones index.	**12**	
18	**Plos 3**	Based on this model, we estimate treatment schedules that would lead to a complete elimination of both sensitive and resistant strains. In particular, we derive an analytical expression for the rate of resistance loss, and hence for the time necessary to turn a resistant infection into sensitive (tclear). This time depends on the experimentally measurable rates of pathogen division, growth and plasmid loss.	**1**	

		We simulated infection dynamics when no treatment is applied to determine the key parameters responsible for resistance attenuation. We observed that the stability of the genes for resistance (represented by the plasmid loss rate) as well as the parameters related to growth rate play a key role in resistance attenuation when the sensitive population is close to carrying capacity (Fig. 3).	**2**	
		Figure 2. Resistance attenuation is boosted when the population of sensitive pathogens approaches carrying capacity.	**3**	
		Figure 3. Resistance attenuation occurs in the in the absence of antibiotic treatment when the abundance of sensitive pathogen is saturated.	**4**	
		The possible outcomes of treatment can be visualized by a schematic phase plane representation (Fig. S3). Note that, according to this schematic representation, no single treatment is effective at treating an infection for all ranges of pathogen populations. However, an effective treatment is possible for any combination of pathogen populations, using a multi-treatment therapy.	**5**	
		The infection dynamics for a multi-treatment therapy can be visualized by plotting the phase plane for each individual treatment in a tri-dimensional representation (Figure 5). This representation helps choose the correct strategy to combat infection based on pathogen abundances.	**6**	
		It also helps visualize necessary conditions for an effective treatment. In particular, an effective treatment for a full range of pathogen populations requires that the antibiotic treatment is effective even if the abundance of sensitive pathogen is at carrying capacity (Text S4 in File S1 and Fig. S2). A medically relevant outcome of this analysis is that it provides a potential explanation for the prevalence of high-resistant infection in immunosuppressed patients [49,50] (see Text S4 in File S1).	**7**	
		Figure 4. AntiR treatment boosts resistance attenuation and leads to total healing.	**8**	
		Figure 5. Schematic representation of a phase space shows possible paths for an effective therapy.	**9**	
		The applicability of the outlined strategy to fight resistance depends on the ability to realistically estimate the resistancedecaying rate (Equation 4). Experimental measurements of the r and dR parameters can be obtained using the method described in [52], while the parameter Dl can be measured as shown in [53].	**10**	
		Empirical data for an antiR condition was obtained from [33]. The authors measured the ratio of doxycycline-sensitive to doxycycline-resistance Escherichia coli after 24 hours under control and antiR treatment, which was 1.4 and 150, respectively. From those values, we obtain Dlctrl = 0.34d21 and DlantiR = 5.01d21, where the index indicates, respectively, control and antiR conditions.	**11**	
		We show that the optimal duration of the antiR administration (tclear) depends on the resistance-decaying rate, a constant that can be estimated from experimentally measurable parameters [33,52].	**12**	
		Figure 6. Resistance attenuation is influenced by the nature of antiR treatment and by the plasmid loss rate.	**13**	
		Figure 8. A host population model that takes into account resistance loss leads to different conclusions on the strategies to combat resistance.	**14**	
		One of the assumptions of the model described in Figure 1 is that the genes for resistance can be transferred and lost. This assumption is consistent with the integration and excision properties of mobile genetic elements [57–60]. De Gelder and colleagues performed experimental measurements that show that plasmid loss due to recombination plays a key role in resistance attenuation [51];	**15**	

		By introducing a resistance-decaying rate into a previous host population model [40] we found significant changes in the predicted optimal strategy.	**16**	
19	**Plos 4**	Neither flutamide nor DES produced noticeable increases in testis cancer incidence at 4 weeks of age. In contrast, two doses of 0.8-Gy radiation increased the incidence of TGCT from 45% to 100% in the offspring. The percentage of mice with bilateral tumors, weights of testes with TGCT, and the percentage of tumors that were clearly teratomas were higher in the irradiated mice than in controls, indicating that irradiation induced more aggressive tumors and/or more foci of initiation sites in each testis. This radiation dose did not disrupt spermatogenesis, which was qualitatively normal in tumor-free testes although they were reduced in size.	**1**	
		There was no effect of flutamide, DES or irradiation on the reproductive ability of the dams (Table 1). This was confirmed by the similar percentages of mice producing progeny after successful mating and the comparable litter sizes in the treated and respective control dams.	**2**	
		Testes were harvested from the male offspring and many of them contained visible tumors (Figure 1A and B). Histological examination confirmed that most of these were teratomas with tissues from multiple dermal origins, but some contained only neuroepithelial cells (Figure 1C and D). Flutamide did not significantly increase the incidence of total TGCTs (30% of testes had tumors vs. 21% in control). However, it did slightly increase the incidence of TGCTs that were confirmed to be teratomas by the presence of multiple dermal origin cell types (24% of testes vs. 14% in control, P = 0.04)	**3**	
		Table 1. Breeding efficiency in 129.MOLF-L1 congenic mice with or without in utero flutamide, DES, or radiation treatment.	**4**	
		Figure 1. Morphology and histology of the testes in 4-week-old 129.MOLF-L1 male mice irradiated in utero with two doses of 0.8 Gy and controls.	**5**	
		In contrast, irradiation of the males during fetal development with two doses, each of 0.8 Gy, led to TGCTs in 80% of the testes (compared to 28% in control) and in 100% of the male offspring (Table 2). The numbers of mice with unilateral and bilateral tumors in all groups were binomially distributed, confirming a previous report that the occurrence of a tumor in each testis was an independent event	**6**	
		When mouse PGCs arrive in the gonad at E10.5, they are potentially pluripotent. However, by day 15.5, they are gonocytes and have uppressed expression of pluripotency genes (Oct4, Nanog, Sox2), undergone cell cycle arrest, are expressing germ cell genes (Nanos3, Dazl, Dnd1, Mvh) [22,23], and are committed to the germ cell self-renewal and differentiation pathway [12]. Between days E10.5 & 11.5 they undergo epigenetic changes that include both global DNA demethylation which involves single-strand breaks (SSBs) and activation of the base-excision repair pathway with chromatin localization of the proteins involved, as well as chromatin remodeling involving loss and replacement of histones and changes in their modifications	**7**	
		A recently described inbred, congenic mouse strain, 129.MOLFL1 [19], referred to as L1 was used. These were originated from crosses between the 129 (129S1/SvImJ) strain andMOLF/Ei inbred mice of the Mus m. molossinus mouse subspecies. To create L1 mice 129 consomic mice with MOLF-Chr19 mice were backcrossed to 129, selecting for a 7.6 Mb region from the MOLF chromosome 19, and then made homozygous for MOLF-derived region by intercrossing the progeny.	**8**	

		Timed matings were performed with pairs of L1 mice. Pregnant females on days 10.5 and 11.5 of their pregnancy were treated with two daily doses of the chemical or physical agent as described below. In some cases females were used for a second or third round of treatments during consecutive pregnancies with a waiting period of a few weeks between pregnancies. In such cases of multiple treatments, pregnant females received either the same agent or they received control treatment in each pregnancy	**9**	

INCERTIDUMBRE				
Consecutivo	**Clasificación**	**Apariciones**	**Consecutivo del paper**	**Color**
1	**A1**	However, clinical diagnosis of LSCD in our cases was not supplemented by cytologic evidence. Impression cytology is one of the useful methods of diagnosis of LSCD but was inconclusive here.	**1**	
		Undoubtedly, response to treatment alone is insufficient to confirm a diagnosis of LSCD. It must be emphasized that overdiagnosis of LSCD, especially in the event of bilateral disease, can lead to unnecessary surgery and long-term immunosupression with systemic cyclosporine.	**2**	
2	**A2**	First several important predictors of depression in marriage migrant women are omitted in this study due to the use of secondary data. For example, the length of relationship including marriage as well as the acculturation level other than language ability may be important predictors of mental distress; however, these variables were not available in the dataset used in this study.	**1**	
		Also, the data failed to differentiate those who do not have friend support because they do not have friends at all from those who have friends but do not receive support from them. Furthermore, as this study used cross-sectional data, the interpretation of the findings warrants caution. For example, it may be the case that those who are more depressed tend to experience more different values from their husbands.	**2**	
3	**A4**			
4	**PNAS 1**	Sources of uncertainty included flux chamber design, deployment, sampling, laboratory analysis of samples, and data selection for regression analysis (Supporting Information).	**1**	
		We estimate that the combined effect of the various sources of uncertainties in flow rate estimates will lead to errors within a factor of 2 of our estimate. This error is small relative to the seven orders of magnitude* variation in measured flow rates. Furthermore, most of the sources of measurement uncertainty would bias the measured flow rates to be lower than their actual	**2**	
		Fig. 3 The error bars in A represent the SDs of the dataset.	**3**	

		It is difficult to quantitatively assess the ability of our measurements to capture the distribution from all abandoned wells in PA and the representativeness of the mean flow rate for all wells in PA remains uncertain.	**4**	
		We found seasonal effects were present in controls, with lower methane fluxes observed in the January 2014 sampling round. Although there is no evidence of significant seasonal effects in the methane flow rates from wells, additional measurements are needed to reach a firm conclusion.	**5**	
		We also did not find a consistent ratio for wells or controls and obtained alkane ratios ranging from 1 × 10−5 to 0.8. The high variability in alkane ratios may be a result of mixing between various microbial and thermogenic (deeper) sources.	**6**	
		We acknowledge that the sample may not be representative of all wells in PA and the denominator used to determine the percentage in terms of total anthropogenic methane emissions is uncertain (Supporting Information). (Also, recall that the measurement error in flow rates is estimated to be up to a factor of 2.)	**7**	
5	**PNAS 2**	The above results leave several unanswered key questions. In particular, why is Slf produced by neighboring colonies (or when subtilisin is added near single colonies), but not by a single colony?	**1**	
		suitable genetic systems are not yet available for P. dendritiformis	**2**	
		The plates were mounted on a rotating stage inside a $1m^3$ chamber maintained at 30.0 (más º– menos) 0.5°C and 90 (más – menos) 2% humidity, as described previously (7).	**3**	
6	PNAS 3	An important exception to the previous analysis arises when the crease has zero normal curvature everywhere.	**1**	
7	**PNAS 4**	Whether Zbtb20 accordingly plays a role in the projections of CA1 neurons remains to be defined.	**1**	
		It has been implied that Zbtb20 may also be involved in corticogenesis (11), but its physiological role in hippocampal development has not been defined.	**2**	
		At present, we do not have data to distinguish between these two possibilities.	**3**	
8	**Nature 1**	but adds new information on its structural connection with the middle-ear bones, which are as yet unknown in gobiconodontids.	**1**	

		Interestingly, the bump did not always move instantaneously. In response to the first landmark shift in Extended Data Fig. 6b (see also Supplementary Video 5), for example, the bump rapidly tracks the shifted visual landmark, but the second abrupt displacement of the landmark elicits a much slower response.	**1**	
		It is unknown how this information is converted into an abstract and flexible representation of the animal's orientation relative to landmarks	**2**	
		Although the EBw.s population tracks the fly's rotational movements in darkness, we do not yet know where and how translational motion — an important component of a complete navigational system — is incorporated. Additionally, while the calcium sensor we chose for our imaging experiments has the temporal resolution necessary to capture EBw.s representations of the fly's angular rotation (see Methods), it lacks the precision necessary for us to determine whether EBw.s activity represents the fly's predicted future orientation or its estimate of current orientation	**3**	
		Estimates of position based purely on self-motion cues, however, can accumulate error over time. Successful navigation then, requires animals to flexibly combine these distinct sources of information.	**4**	
10	Nature 3		**0**	
11	**Nature 4**	It could be that TAARs are expressed in small subsets of brain neurons **below the detection level** of these assays (,100 copies of mRNA per cell in 60,000 brain cells).	**1**	
		Every Taar probe, except a Taar1 probe, labelled a small subset of OSNs that were scattered in the olfactory epithelium **in a seemingly random fashion (Fig. 1).**	**2**	
		Each Taar probe was specific for one Taar gene (see below) except the Taar7 and Taar8 probes, **which are likely to hybridize with all of the highly related members** of the Taar7 (Taar7a, b, d, e and f) or Taar8 (Taar8a, b and c) subfamilies, respectively.	**3**	
		It is difficult to completely exclude coexpression of odorant receptors and TAARs in nontransgenic olfactory epithelium, because each odorant receptor gene is typically expressed in only ,1 in 1,000 OSNs, or ,1 in 250 in the odorant receptor‘s expression zone.	**4**	

		No TAAR responses were seen to five mouse pheromones (each at 0.2 mM) or to an MHC peptide (at 0.5 mM). **However, it cannot be excluded that** some TAARs respond to these molecules, but, like many odorant receptors, those TAARs cannot be functionally expressed in HEK293 cells.	**5**	
		Unfortunately, mouse urine generally inhibited responses in the SEAP assay when diluted even 100-fold, making it difficult or impossible to detect TAAR responses to lowabundance urinary compounds.	**6**	
		Figuere 5| The activating substance in male mouse urine was not evident until after puberty (day 29; b).	**7**	
		Future studies should clarify whether all TAAR ligands are biogenic compounds produced in mammals, and, if so, how they are synthesized in vivo	**8**	
		qPCR reactions with 50-fold more mouse brain cDNA (detection threshold, ,100 copies of mRNA per cell in 1,200 cells) also failed to reveal the expression of either Taar1 or Taar9 in mouse brain (data not shown).	**9**	
		Future studies should provide information on the ligands of additional TAAR family members and illuminate the functional roles played by individual TAARs.	**10**	
12	**Science 1**	Within uncertainties, the earliest maxima were reached by several ice sheets (or sectors of ice sheets) sometime between 29 to 33 ka (Fig. 3B and figs. S2 and S3). This early re- sponse included large and small ice sheets at mid- and high northern latitudes, as well as the West Antarctic Ice Sheet (WAIS) in the Southern Hemisphere.	**1**	
		Disentangling global changes in seawater d18O (d18Osw) fromregional changes in seawater temperature (d18OT) and water-mass d18O, however, remains largely unresolved (25–27), adding considerable uncertainty in interpreting the phase relationship of this proxy to other climate parameters.	**2**	
		RSL data with depth uncertainty for the interval from 10 to 50 ka from New Guinea (blue circles) (4, 52, 53), Barbados (purple triangles) (5, 54), the Bonaparte Gulf (green half-pluses representing age and depth uncertainty) (8), and the Sunda Shelf	**3**	
		Whether these changes in CO2 and **SSTs were induced by** deglaciation of Northern Hemisphere ice sheets (12) **or** high southern latitude insolation (40, 41), however, **remains an open question**.	**4**	
13	**Science 2**	In particular, the most likely lower bound of species richness was estimated to be at least 21,833 **species [95% confidence level (CL)** = 18,665, 29,420; model a1 in Fig. 1B], **and the biologically and statistically best- supported estimate of richness** (criteria outlined in table S2) was 25,246 species **(95% CL** = 19,721, 33,181, model B+S in Fig. 1B). Accord- ing to our estimates, a single hectare of rain- forest will be inhabited by an average of 18,439 species.	**1**	

		Beta diversity of all arthropods (in the broad sense of species turnover among sites) increased roughly linearly with cumulative area surveyed (**F1,3 =2422.5, P < 0.001**).	**2**	
		However, despite the high sample coverage values, we cannot discount the possibility that there were some vanishingly rare species that may not have been discovered with the sampling proto- cols used in this study.	**3**	
		r plant models predicted total arthropod richness in the San Lorenzo **forest to a precision of 1% (correlation between richness estimates** provided by the plant model and best estimates: r = 0.992, P < 0.0001, N = 18;	**4**	
		Plot of the percentage error between all arthropod species observed and estimated by the plant model against cumulative number of sites. Shaded boxes indicate means and 95% CL.	**5**	
		However, this does not imply that most arthropod species have self-supporting populations in small forest areas or fragments.	**6**	
14	**Science 3**	Although our understanding of the corona has greatly improved with sophisticated remote sensing techniques and modeling methods**, models and extrapolations explicitly depend on** photospheric magnetic field observations (**which provide only a partial constraint on the extended field**) as a boundary condition. Because of the extremely harsh near-Sun environment, even the most advanced near-Sun exploration mission planned to date—Solar Probe Plus (1), which will take a spacecraft within 8.5 RS of the solar surface— **leaves a crucial measurement gap between** the base of the solar atmosphere and the extended solar wind.	**1**	
		observable tail emission nearer to the Sun (left half) had a relatively short lifetime **(t ≤ 5 min)** while the portion located farther out remained much longer **(t ≥ 15 min)**.	**2**	
		This molecule will quickly be photodissociated (t ~ 2.9 s) and the free neutral O atom is rapidly ionized via charge exchange with coronal protons and collisions with coronal electrons **(t ≤ 0.07 s for O → O+).**	**3**	
		Unlike the thermodynamic MHD calculation, the PFSS **solution assumes that the** domain is current-free at all heights up to a source surface radius where the field becomes radial (typically 2.5 RS). However, PFSS **solves only for the minimum energy state** of the coronal field distribution, and therefore **does not capture structures energized** through sustained motions and thermodynamic forces.	**4**	
		Neither the MHD model nor the PFSS model reproduced the southwestern motion between 23:45 and 23:48 UT, which passes through the cusp of the closed-field region. The exact location of this feature is more sensitive to model parameters as well as the boundary conditions, **which lack the most recent photospheric observations** on this side of the Sun (because of solar rotation).	**5**	

15	**Science 4**	However, the receptor that transduces Dilp8 signals and **its site of action remained unknown**	**1**	
		Knockdown of lgr3, but not of lgr4, prevents the pupariation delay induced by dilp8 overexpression. tub> indicates tubulin-Gal4. Error bars indicate SD. (C) Average puparion time of the indicated genotypes, exposing acceleration or delay relative to their controls. Error bars (SD) are invisible when the three replicates coincide. Approximately 60 pupae per genotype were scored, and the graph shows data pooled from three independent experiments. ***P < 0.001 (two-tailed unpaired t test). n.s., not significant. (D) Knockdown of lgr3 prevents excess body weight induced by dilp8 (tub-dilp8 da>lgr3-IR). ***P < 0.001; significant difference from all controls (two-tailed unpaired t test). Data are mean T SD. n = 25 age-synchronized adult males in each genotype. (E) Tissue- specific knockdown of lgr3, using UAS-lgr3-IR and the indicated Gal4 lines. The graph shows data pooled from three independent experiments, and each data point is mean T SD. A total of 60 pupae were scored per genotype. ***P < 0.001 (two-tailed unpaired t test). (F) Fluctuating asymmetry index of left-right wings of males of the indicated genotypes and rescued animals. Numbers indicate pairs of wings scored. **P < 0.01; ***P < 0.001 (F test).	**2**	
		… increase in cAMP levels, from 213.8 ± 67.94 fmol 5 × 104 cells to 1.612.36 ± 302.6 fmol/5 × 104 cells (Fig. 2A and materials and methods).	**3**	
		(EC50) of 6.31 ± 0.12 Nm. As a reference, the cAMP levels in Kc cells transfected with the empty vector alone were 132.69 ± 66.71 fmol/5×104 cells and 127.73 ± 77.19 fmol/5 × 104	**4**	
		For example, the Lgr3719-733 antiserum readily detected the Lgr3 protein ectopically expressed using the GAL4 UAS system (fig. S2, G to G′′), confirming the specificity of our antisera**, yet it could not detect endogenous lgr3 expression**, supporting the weak expression of the Lgr3 protein.	**5**	
		Data are shown as mean T SD (n = 3 inde- pendent repeats), and the asterisks indicate that the cAMP level was statistically different from un- treated controls, ***P < 0.001 (t test).	**6**	
		In (A) and (B), data are mean T SD and are pooled from three independent experiments; 60 pupae were scored per genotype. **Error bars are invisible** when the three replicates coincide. ***P < 0.001 (two-tailed unpaired t test).	**7**	
		Approximately 60 pupae were scored per genotype. Each data point is mean T SD (n = 3 independent repeats).	**8**	
		Less is known about how the brain stabilizes body size to ensure that developing organisms reach the correct, genetically determined size. **We also do not know how** limbs grow to precisely match the size of their contralateral limbs, nor do we understand how limbs maintain proportion with other body parts, even when faced with perturbations (this statement is also applicable to other bilaterally symmetric traits.	**9**	
16	**Plos 1**	The reason why this destructive mechanism is not suppressed after the initial smoke injury is removed remains unclear.	**1**	

		Percent FEV1c (Average +- 6 SD) 84615 63615 2866*C. Percentage of Forced expiratory volume (FEV1) in one second is *significantly different ($p<0.05$) for the end-stage group compared to the control group.	**2**	
		*, $p<0.0001$; {, $p<0.001$; {, $p<0.01$; 1, $p<0.05$.	**3**	
		Cumulative values for lymphocytes showed a significative decrease (control, n = 6; emphysema, n = 7, end-stage n = 6, p,0.05) more patient were included with the same lung characteristics. (B) Gene expression of Casp 8, on the same patients, determined by qRT-PCR (median+-SD) on emphysema patients with (n = 5) and without cancer (n = 4) shows no different expression level due to cancer away from the emphysemic region (p = 1).	**4**	
		Data are expressed as the mean value 6 SD unless otherwise indicated. Statistical significance was determined using Mann-Whitney no parametric test, two tails, for human data comparison, and student‘s t-test (two-tailed distribution with a two sample equal variance) for animal work.	**5**	
		However, the fact that in patients with severe COPD there is persistent down regulation of CD46 mRNA after the noxious irritant has been removed, indicates dysregulation at the transcriptional level, perhaps due to polymorphisms or latent viral infections such as measles or adenovirus [41].	**6**	
17	**Plos 2**	The selection of C, e and kernel parameter s is an open problem, and a cross-validation method is commonly used in some research fields.	**1**	
		However, ICA can obtain the high order statistic characteristic hiding in the signal. Moreover, PCA application to the signal analysis is that the original data should be satisfied with a normal distribution. Unfortunately, this condition cannot be satisfied in a practical application such as stock market analysis.	**2**	
		Although the proposed model provides many insights, it also has minor weaknesses. The forecasting accuracy of the model is not particularly high; for example, the highest correlation coefficient is 0.95174 for the Shanghai stock market index and 0.87446 for the Dow Jones index.	**3**	

18	**Plos 3**	The model also assumes that the genes for resistance are carried by mobile genetic elements (referred to in what follows as plasmids, see also Discussion). The resistance-carrying mobile genetic elements can be transferred to a sensitive strain, due to horizontal gene transfer, at a rate t, and be lost during replication, with a probability r [47].	**1**	
		This phenomenon depends on the simple assumption that the resistance plasmid can be lost: the population of sensitive pathogens could then spontaneously rise to high levels from a high abundance of resistant pathogen.	**2**	
		An optimal treatment depends on the precise timing of the application of antibiotic and antiR conditions. If the infection is already sensitive, antibiotic treatment should be used from the beginning of therapy. On the other hand, if the infection is resistant, antiR should be applied first in order to reduce the load of resistant pathogen. When the abundance of resistance is low enough, the infection becomes sensitive and an effective treatment can be achieved after antibiotic application.	**3**	
		We did not find an analytical solution for h0 in terms of the model parameters, but this value can be estimated numerically and visualized in the phase plane representation (Fig. S3B).	**4**	
		The numbers of individuals infected are correspondingly represented by variables yw, ya, yb, and ya,b. The original model [40] considered only the possibility of acquiring resistance (black arrows). In our modified host population model, motivated by our findings in the single host model, we assume that a nonzero resistance-decaying rate can cause loss of resistance (red arrows).	**5**	
		The insight derived from the present analysis is limited by the capacity to effectively implement antiR conditions, and by the assumptions made by the model (Equation 1). For example, an antiR condition obtained through the use of a suppressive interacting drug occurs only at a limited range of drug concentrations, which might not be easily controllable for treatment application.	**6**	
		In addition, a pathogen could adapt to an antiR treatment by developing a second resistance Further important aspects of the way pathogens may cope with antibiotics, such as persistence, compensatory mutations, the development of secondary resistance involving alternative biological mechanisms, as well as a simultaneous application of antibiotic and antiR treatment, are not part of the current investigation, but would be interesting subjects for future expansions.	**7**	
		however the rate of transfer and loss of mobile genetic elements is still an under-explored topic [61,62]. Estimating the extent to which this assumption is true requires specific measurements that are not available in current reports	**8**	

19	**Plos 4**	The dose of DES given was effective in acting on the embryo as it caused cryptorchidism in 16% of the testes. However, there was no indication that it induced cancer (only 3 of 24 testes analyzed contained TGCTs). Similarly in a study involving treatment of pregnant 129 mice, a dose of ethinyl estradiol that increased cryptorchidism in the offspring did not induce a significant change in the incidence of teratomas [21].	**1**	
		Further characterization of the model to determine the optimal exposure time or intervals, the dose-response, and the effects on less susceptible mouse strains is needed to initiate mechanistic studies and risk estimation.	**2**	
		Cohort studies are unlikely to be able to test whether there is an association between such exposure and testis cancer since X-ray doses in diagnostic procedures have been declining [9], the numbers of pregnant women in populations exposed to radiation are small [10], there is likely a limited developmental window of sensitivity, the incidence of testis cancer in human is low, and several decades elapse between exposure and appearance of tumors. Nevertheless, there is one report of an association between maternal ionizing radiation exposure during pregnancy and testicular cancer in their offspring	**3**	
		About 30% of the L1 males were reported to develop spontaneous testicular tumors and the MOLF genes contributing to this high tumor incidence are not yet known [19].	**4**	
		The in utero exposed and control male offspring in the flutamide arm were euthanized at the age of 4–5 weeks; the exposed and control males in the radiation and DES arms were euthanized at the age of 4 weeks.	**5**	
		The data are presented as mean 6SEM. The significance of differences between the testis weights from mice of the same age was evaluated by a Student‘s t-test. The significance of the differences in the frequency of TGCTs between treated and control mice was determined using the Chi-square test.	**6**	

HIPÓTESIS				
Consecutivo	**Clasificación**	**Apariciones**	**Consecutivo del paper**	**Color**
1	**A1**	Severe ocular surface disease may occur in persistent VKC Leading to marked visual loss	**1**	
		We suspect that in both our patients, chronic limbal inflammation may have precipitated LSCD	**2**	
		In our patients with long-standing VKC, we hypothesize that chronic limbal inflammation Might have affected the microenvironment of the stem cells, resulting in poor stromal support	**3**	

		Patients with long-standing VKC there could have been direct damage to the stem cells by the toxic products of eosinophils and other inflammatory cells in the vicinity.	**4**	
		(One could consider response to treatment (successful outcome of stem cell transplantation in case 1 and failure of the amniotic membrane transplant in case 2) his could also merely signify that the new healthy tissues are more resistant to the disease process than the previous compromised surface.	**5**	
2	**A2**	Researchers recommended that practitioners should be attentive to values differences between the spouses when working with multicultural families.	**1**	
		This study therefore seeks to understand how potential differences in family values between the spouses may affect the mental health of foreign wives	**2**	
		This study also examines the role of social support as a potential protective factor, buffering the effect of family values differences on depression. Specific research questions are as follows: Do family values differences between the husband and the wife affect the wife‘s depression? Does social support have a moderating effect on the relationship between family values differences between spouses and the wife‘s depression?	**3**	
		With an increasing divorce rate among these couples (Chung & Han, 2009; Seol et al., 2005) as well as proliferating mental health issues among spouses, understanding differences between spouses, such as family values, is critical in designing intervention plans to work with these families at risk.	**4**	
		With such scarcity of literature examining the importance of values differences, this study thus fills the void by expanding the current understanding of family life and mental health status of the foreign wives.	**5**	
		In other words, women who are younger and have low marital and life satisfaction, low income, no children, great discrepancy of spouse information, high acculturative stress, and low social support tend to be more depressed than their counterparts.	**6**	
		Though services for women and multicultural families have expanded in the past few years, This may be due to the shortage of counselors with expertise with multicultural families, as well as a lack of bilingual workers who can provide services in different languages. Thus, services providing systematic intervention for family affairs and counseling for couples remain lacking and only a small number of women have reported using these services (Kim et al., 2009).	**7**	

		The women have support from their family, friends, neighbors, and others, the stress derived from differences in family values between the spouses may be reduced, which in turn lessens the likelihood of experiencing mental distress such as depression. In other words, having social support may mitigate the effect of having great differences in values on likelihood of experiencing depression.	**8**	
		Among social support factors, family support was significantly related to depression in wives. Also, there was a moderating effect of family support only; for those with a higher level of family support, the slope of family values difference against depression was gentle. Thus, they felt less depressed while family values difference increased, compared with those who had a lower level of family support. Friend support and formal support were not statistically significant moderators.	**9**	
		In other words, the greater the difference in values between the spouses, the more likely the wives are to experience depression. An age gap between spouses is also signifi- cantly related to depression in marriage migrant women. Among social support factors, family support has a significant moderating effect on the relationship, mitigating the effect of family values differences on the wives' depression.	**10**	
3	**A4**	Diagnosis of WD usually depends on detection of low serum Cu and ceruloplasmin concentrations, increased urinary Cu excretion, presence of Kayser-Fleischer rings in the cornea, and/or increased hepatic Cu concentration. No single feature is completely reliable, but a diagnosis can usually be made provided that WD is suspected [2,3,5].	**1**	
		Mutation analysis may be useful in cases with unclear liver disease [9].	**2**	
		However, there is no evidence of a large deletion or duplication in WD patients with either one ATP7B mutation or no mutation (unpublished data).	**3**	
		In particular, we found a wide distribution of serum ceruloplasmin concentrations in 20 patients with one ATP7B mutation. In these patients, WD may be attributed to a point mutation in an uncovered exon or to another pathogenic mechanism.	**4**	
		Because only a limited number of patients were studied, these results contribute little to the use of ceruloplasmin for screening purposes. However, these findings suggest that another mechanism may be the cause of WD in patients with less than two ATP7B mutations. Further study will be necessary to confirm or refute this hypothesis.	**5**	
		However, these findings suggest that another mechanism may be the cause of WD in patients with less than two ATP7B mutations.	**6**	
4	**PNAS 1**	Millions of abandoned wells exist across the country and some are likely to be high emitters.	**1**	

		Carbon isotope information provides additional evidence suggesting that the source of methane from the wells is likely to represent a mixture of microbial and thermogenic sources. In general, methane originating from ther- mogenic sources is more enriched in 13C; whereas, methane originating from microbial sources is relatively depleted in 13C.	**2**	
5	**PNAS 2**	The presence of genes encoding homologs of dendritiformis sibling bacteriocin in other bacterial species suggests that this mechanism for self-regulation of colony growth might not be limited to P. dendritiformis.	**1**	
		The release of DNA from lysed cells (allolysis) may increase genetic diversity when there is variation in the population.	**2**	
		A. Indeed, when two colonies are competing, there is faster expansion at the facing fronts at the early stages of growth (SI Text), likely because of the added low level of subtilisin from the neighboring colony.	**3**	
		The hypothesis are subtilisin is a growth promoter	**4**	
		Consequently, bacteria become overpopulated, which likely triggers the production of the 12 kDa protein, reducing the number of bacteria.	**5**	
		By answering this question we could potentially show the evolutionary advantage of bacteria dying in the inhibited region in the presence of another colony, rather than simply sporulating (P. dendritiformis spores are shown in SI Text).	**6**	

		In this paper we suggest an approach in which bacteria, nutrients, prespores, subtilisin, and Slf are modeled as continuous fields, and the outer effective envelope of the colony is given by a smooth, time-dependent curve (which is in accord with the experimental observation that the bacteria swim in a lubrication layer (12) that has a sharp, well-defined edge).	**7**	
		Assuming that subtilisin increases bacterial reproduction, we find that high subtilisin levels at the front increase bacterial density.	**8**	
		It is suggested that to ensure survival the bacteria must quickly reduce the population level.	**9**	
		However, Slf had no effect on the closely related species Bacillus subtilis. This suggests that Slf has a narrow spectrum of activity, similar to other bacteriocins (15, 16).	**10**	
		An approach to assessing the role of Slf and subtilisin could be the construction of knockout mutations and the corresponding complemented strains in each gene of interest.	**11**	
		Using these methods, we have shown that inhibition is due to secretion of a lethal protein, Slf. This protein has no homology to any known bacteriocin or toxin and may represent a new class of antibacterial factors.	**12**	
		The gene is annotated as a conserved hypothetical, predicted to encode a protein of 20.4 kDa. The protein is apparently processed and cleaved between lys-71 and pro-72, and the secreted form is the 12 kDa carboxy terminus of the protein.	**13**	
		Subtilisin is secreted into the environment and its proteolytic activity may break down proteins to provide more easily used nutrient sources to the bacteria.	**14**	
		The concentration of subtilisin is proportional to the cell density and may serve as a quorum sensor to control the growth of cells at the edge of the colony.	**15**	

		The position of the gene, at the end of a S. cerevisiae chromosome in a region that is not syntenic with other yeast, suggests that it may have been acquired from a bacterial source at some point in the evolution of S. cerevisiae.	**16**	
6	PNAS 3	This deformation between preprogrammed states can be tuned to be either continuously foldable or snap discontinuously.	**1**	
		A. An advantage of this decomposition is that, if in-plane strains in the shell vanish, B. the geodesic curvature of the fold must remain unchanged after folding (30, 31), C. yielding the relationship κNðsÞ=κgðsÞtanψðsÞ.	**2**	
		The coexistence of this set of curves makes the helicoid an ideal surface on which to validate the design rule.	**3**	
		According To our hypothesis, we expect the cylinder to undergo a snapping transition when deformed along this crease.	**4**	
		By weakening the material through creasing, the stretching cost for the ridge can be dramatically lowered, and the folded state may become stable.	**5**	
		Along the lines of argument we presented for stability of creased cylinders, a spherical shell poses a system which can be solved analytically.	**6**	
		Evidently, for larger values of α, this gain surpasses the bending energy of the shell, resulting in bistability due to the presence of a local minimum in total energy. Thus, we infer that the stability of creased shells is governed by the competition between bending energy of the undeformed shell and stretching energy contained in the creased region.	**7**	
7	**PNAS 4**	It has been implied that Zbtb20 may also be involved in corticogenesis (11), but its physiological role in hippocampal development has not been defined.	**1**	
		However, the subiculum appeared to be located adjacent to CA3 region in mutant, as shown by the appearance of a single principal cell layer with relatively large, loosely packed neurons (2) (Fig. 2 C and D and C′ and D′). Taken together, these findings suggest that Zbtb20 ablation leads to the transformation of the CA1 field into a transitional neocortex-like structure and the corresponding translocation of subiculum adjacent to the CA3.	**2**	
		Beginning at P3, the hippocampus of Zbtb20 null mice was smaller and less compact than in wild-type and heterozygous littermates, and the density of cells progressively decreased during postnatal development (Fig. 2 A and B and Fig. S2 E–H). This reduction could be due to a decrease in cell proliferation, an increase in cell death, and/or neuronal disorganization.	**3**	
		These data suggest that the reduced hippocampus in Zbtb20− − mice is mainly caused by the increased postnatal apoptosis of hippocampal neurons.	**4**	
		These observations, together with the loss of CA1-specific markers, suggest that the neurons in mutant CA1 region have acquired a transitional neocortex-like identity. Interestingly, none of these genes were ectopically expressed in the CA3 and DG fields	**5**	

		Given the apparently normal cell proliferation of the progenitors in hippocampal and transitional VZ, the cytoarchitectonical transformation is most likely caused by the misspecification of the mutant CA1 precursors.	**6**	
		Similarly, KA1 expression in the CA3, and Prox1 in the DG was reduced in mutant mice from E16.5 onward (Fig. 3 I–L and Fig. S4 G–L). These suggest that in the absence of Zbtb20, the specification of CA3 and DG neurons is largely maintained, although their differentiation is impaired.	**7**	
		In addition, the accelerated migration may partly explain the appearance of a less-compact mutant CA1 IZ at E18.5 (Fig. S2 C and D).	**8**	
		Furthermore, the β-catenin activity at E13.5, detected broadly in the telencephalic VZ and the cortical hem, was similar between Zbtb20 knockouts and wild-type mice (Fig. S7 K and L). These data suggest that loss of Zbtb20 does not lead to significant alterations of canonical Wnt signaling in hippocampal primordium	**9**	
		Our findings suggest that the hippocampal CA1 field from the mice lacking Zbtb20 is transformed into a transitional neocortexlike structure and the subiculum is correspondingly shifted into the lateral border of mutant CA3.	**10**	
		Explant culture experiments have suggested that the hippocampal primordium is well established by E12.5 (3), supporting a ―protomap" model, which posits that embryonic patterning cues act on cortical progenitor cells to specify the different areas of the mature cortex (8).	**11**	
		During the initial phase of hippocampal development (before E12.5), Wnts from the cortical hem are critical for the expansion of, and most likely the selection of, a pool of hippocampal progenitor cells (5, 6).	**12**	
		Alternatively, Zbtb20 may be an obligate downstream target of Wnt signaling in the specification of CA1 cell fates.	**13**	
		However, to determine the exact roles of Zbtb20 in progenitor cells and postmitotic neurons, experiments would need to be conducted wherein Zbtb20 expression is temporally controlled in hippocampal precursors and postmitotic neurons, respectively.	**14**	
		This supports the hypothesis that hippocampal subfields are patterned by unique mechanisms (18). Early differentiation of the CA1 and CA3 regions begins at the two hippocampal poles respectively, and progresses inwards, suggesting that the signals that specify the two CA field identities are derived from organizers close to each pole (18).	**15**	
		Interestingly, we observed that the expression domain of transitional neocortex markers encroached into the CA1 region of Zbtb20 mutants gradually, from dorsal to ventral and eventually expanding to, but not beyond, the CA1/CA3 boundary. This phenomenon suggests that, although Zbtb20 is expressed in the CA3 region from E12.5 and into postnatal development, this subfield relies on separate mechanisms to suppress the expression of transitional neocortex patterning genes.	**16**	
8	**Nature 1**	This suggests that reversal to (or retention of) this premammalian ancestral condition is correlated with different developmental timing (heterochrony) in eutriconodonts.	**1**	
		This is similar to the effect of homeobox gene patterning of vertebrae in modern mammals, making it plausible to extrapolate the effects of Hox gene patterning to account for homoplastic evolution of vertebral characters in early mammals.	**2**	

		By contrast, eutriconodonts lacked a similar mechanism for terminating skeletal growth that would presumably slow down (although not stop completely) in the adult, because of the absence of the epiphyseal growth plates.	**3**	
		The tympanic membrane suspended by the ectotympanic ring and malleus manubrium would be re oriented more mediodorsally (see red arrows in b-1 and b-2 of Fig. 3b), similar to the ectotympanic‘s migratory path during ontogeny in the marsupial Monodelphys, leaving a space between the pterygoid region of the mandible and the tympanic membrane for access of the external auditory meatus and for pterygoid muscle.	**4**	
		The triple knockout of Hox10 paralogues can alter the thoracic versus lumbar boundary, and triple knockout of Hox11 can alter lumbar versus sacral vertebral identities.A loss of Hox10 gene function can regenerate the lumbar ribs and a more gradational thoraco-lumbar transition in laboratory mice (Fig. 4)	**5**	
		These derived lumbar features of Jeholodens evolved from within eutriconodontans, convergent to those in theriiform mammals (node 1 in Fig. 4), and may be hypothesized as an independent activation of Hox10 gene patterning.	**6**	
		Given that the regeneration of lumbar ribs in mutant mice is correlated with loss of function of Hox10 paralogues (Fig. 4b), it is plausible that a similar mutation (that is, triple knockout of Hox10 paralogues or a similar developmental event) was correlated with the ‗reappearance‘ of lumbar ribs in Akidolestes, whose immediate relatives in success 3ive ranks of theriiform mammals (node 1 in Fig. 4) all lack lumbar ribs.	**7**	
		The homology of post-dentary elements of non-mammalian tetrapods with the mammalian middle-ear bones has long been established. Long before the current fossil evidence was discovered, it was hypothesized that the migration of middle-ear bones from the mandible in cynodont–mammal evolution underwent an intermediate stage in which these bones would be anteriorly connected to the lower jaw, but suspended medial to (and free of) the mandibular pterygoid region (ref. 43 and Fig. 28.11 of ref. 44).	**8**	
		This developmental mechanism for evolutionary homoplasy of thoracolumbar structure is mutually compatible with one of the two functional interpretations: either the lumbar ribs in Akidolestes had a function similar to that in primitive mammals and cynodonts with similar ribs23–25, or the separate loss of lumbar ribs in Jeholodens was an adaptation convergent to most theriiform mammals.	**9**	
9	**Nature 2**	Several features of the population dynamics of these neurons and their circular anatomical arrangement are suggestive of ring attractors, network structures that have been proposed to support the function of navigational brain circuits.	**1**	
		Electrophysiological recordings in immobilized locusts12 and butterflies13 have revealed a map-like representation for polarized light E-vector orientations that may enable sun-compass navigation	**2**	

		Offsets occasionally changed between trials (for example, Fly 2 and Fly 10 in Fig. 1m and Extended Data Fig. 2e), but seldom within a trial (Extended Data Fig. 2f). Such differences in the locking of the EBw.s activity bump to visual cue position suggest that EBw.s population activity cannot be a static retinotopic representation of the animal's surroundings20.	**3**	
		The single-stripe EBw.s responses (Fig. 1) could result from a tuning to visual features20, or from a more abstracted representation of the fly's orientation with respect to its environment.	**4**	
		To distinguish between these possibilities, we asked how EBw.s population activity changes in a more complex visual scene with multiple features (Fig. 2a; Extended Data Fig. 1b). In this environment, a visual feature map would produce an EBw.s activity pattern of increased	**5**	
		If EBw.s responses arise from self-motion cues rather than landmark orientation, the abrupt shift in landmark azimuthal position should not by itself induce matching shifts in EBw.s activity.	**6**	
		If EBw.s activity is determined by the fly's orientation relative to the landmark, the bump should move in lockstep with landmark rotation rather than with the fly's turning movements. Indeed, in almost all cases, activity in the EBw.s population faithfully followed the visual cue (Fig. 3d-g, Extended Data Fig. 6c).	**7**	
		Previous studies have described static visual maps in the CX12,13,20. Such maps may allow navigating insects to maintain a sun-compass-based heading direction.	**8**	
		Here we found that EBw.s neurons track the fly's orientation relative to visual landmarks in a variety of different visual environments (Fig. 1, Fig. 2), suggesting that the CX dynamically adapts to estimate the fly's orientation within its visual surroundings (Extended Data Fig. 2d, Extended Data Fig. 3d, Extended Data Fig. 4g).	**9**	
		Subsets of ring neurons likely bring information about spatially localized visual features20 to specific rings of the ellipsoid body	**10**	
		Many of the CX's proposed functions in directed locomotion11,15, visual place learning10, and action-selection34 may rely on this internal reference.	**11**	
		Our observation that EBw.s activity was maintained in the absence of self-motion suggests that internal dynamics play a significant role in shaping neural activity in the fly brain, much as they do in the brains of larger animals.	**12**	
		In the CX, this activity may allow the fly to retain a short-term orientation memory even when landmarks are temporarily out of sight8.	**13**	
		Cell-intrinsic mechanisms could also underlie some of these features, including, for example, persistent activity	**14**	
10	**Nature 3**	This requirement leads to a synchronization-induced structural transition that offers various applications based on the potential to form, disintegrate and fine-tune self-assembled in- motion structures in situ.	**1**	
		Furthermore, it offers a generalizable method of controlling structure using dynamic synchronization criteria rather than static energy minimization, and of designing new field-driven microscale devices in which components do not slavishly follow the external field.	**2**	
		Therefore, **our findings could in principle** scale up to macroscopic systems.	**3**	

		This dynamic requirement is the keyto understanding the structural stability. We analysed this systemignoring interactions between microtubes, which is a valid assumption for a broad range of volume fractions.	**4**	
		Equation (1) has the same mathematical form as the classical Adler equation for synchronization, **so we can** apply all the general analyses of this equation.	**5**	
		On the basis of their capacity for in situ assembly, disassembly and reconfigurability, the structures demonstrated in **this study suggest** various potential applications, such as selective cargo uptake and transport inside these hollow microtubes and fluid flow control with the known high efficiency of synchronized states.	**6**	
		These synchronization criteria **suggest a materials** selection method complementary to the conventional equilibrium approach of energy minimization.	**7**	
		To dynamically destabilize structures that compete with targeted ones **could benefit** the current trend of designing selfassembly of anisotropic building blocks26–28 (which tend to form multiple possible structures), and **may stimulate** related consideration of other dynamical systems, both smaller (molecular) and larger (granular) than considered here.	**8**	
		The required phase-free dynamics **can be** achieved by designing shapes more complex than the simple spheres considered here or more generally via a driving frequency so high that building blocks cannot track the field.	**9**	
11	**Nature 4**	The evolutionary conservation of the TAAR family suggests a chemosensory function distinct from odorant receptors.	**1**	
		Ligands identified for TAARs thus far suggest a function associated with the detection of social cues.	**2**	
		The evolutionary conservation of the TAAR family suggests a chemosensory function distinct from odorant receptors.	**3**	
		These features of the odorant receptor family would seem to account easily for the odorant recognition abilities of mammals and are used combinatorially to detect different odorants and encode their unique identities	**4**	
		However, a small percentage of OSNs lack Gaolf, the G protein through which odorant receptors signal, suggesting that they might express another class of chemosensory receptor.	**5**	

		proteins can stimulate some OSNs, suggesting that those OSNs might express a class of receptor that detects peptides rather than small volatile odorants	**6**	
		responses to some mouse pheromones involve the olfactory epithelium, raising the possibility that the olfactory epithelium also contains a dedicated class of pheromone receptors.	**7**	
		To explore whether there might be other types of chemosensory receptors in the olfactory epithelium, we initiated a search for additional G protein-coupled receptors (GPCRs) expressed by mouse OSNs.	**8**	
		Together, these data suggest that TAARs may be expressed primarily or exclusively in the olfactory epithelium	**9**	
		The olfactory epithelium ESTs included 24 different taar gene sequences, suggesting that numerous different TAARs are expressed in the fish olfactory epithelium.	**10**	
		Figure 2| All of the Taar genes, except Taar1, seem to be selectively expressed in the olfactory epithelium (red bars).	**11**	
		This suggests that, like odorant receptors12, TAARs may transduce signals by coupling to Gaolf, and thereby elevate intracellular cAMP levels.	**12**	
		The results described above suggested that there are multiple subsets of OSNs that use different TAAR family members rather than odorant receptors for the detection of chemosensory stimuli.	**13**	
		Urine samples from BALB/c and C57BL/6 male mice were both effective**, suggesting that** the ligand is not an MHC-linked individuality cue (Fig. 5a).	**14**	
		The mTAAR5 activator **seemed to be** highly volatile as it strongly activated several adjacent wells in a multiwell plate containing mTAAR5-expressing cells. The activator may well be trimethylamine,	**15**	
		In addition, NMR analysis indicates that trimethylamine is elevated in male compared with female mouse urine33, and in mouse urine compared with human urine36. Using mTAAR5, mice could, in principle, determine the gender and sexual status of other mice.	**16**	
		TAARs, are expressed in a small subpopulation of neurons that seem to lack odorant receptors, **suggesting that** these neurons use TAARs rather than odorant receptors to detect chemosensory stimuli.	**17**	
		These findings, together with the relatedness of TAARs to biogenic amine receptors, suggest that TAARs may specifically function as a family of chemosensory receptors for amines.	**18**	
		Together, **these findings suggest that** at least some murine TAARs detect social cues that may elicit innate behaviours or physiological responses. This idea is consistent with observations that the olfactory epithelium is involved in some pheromone responses14–17, and that certain pheromone responses may involve dual signals from the olfactory epithelium and vomeronasal organ16.	**19**	

		Evidence that fish TAARs are also expressed in the olfactory epithelium suggests that TAARs are likely to serve as olfactory receptors in diverse organisms, including humans. The evolutionary conservation of the TAAR family suggests that it may serve a function distinct from the odorant receptor family. The findings presented here suggest that this function may be associated with the detection of social cues such as pheromones.	**20**	
12	**Science 1**	Our compilation of radiometric ages **suggests that** there is considerable regional variability in the timing of when ice sheets (and various sectors of ice sheets) first reached their local last glacial maxima.	**1**	
		Although the onset of Greenland Ice Sheet (GIS) retreat from the LLGM is poorly constrained by exist- ing 14C and TCN ages (fig. S3B), **marine records of GIS runoff suggest that** GIS retreat may have commenced ~20 ka.	**2**	
		Stratigraphic relations of 14C ages to ice-margin history **suggest an onset of retreat** from the WAIS maximum extent in the Ross Sea between 13.9 and 15.2 ka (7) which, within dating uncertainties, corresponds to the rapid rise in sea level ~14.5 ka referred to as meltwater pulse 1A (MWP-1A).	**3**	
		There is information suggesting that in many places, mountain glaciers were near or at their maximum extent by ~30 ka, which is broadly contemporaneous with the in- terval when global ice sheets first began to reach their maxima.	**4**	
		Within uncertainties (7), the TCN-based geochronology **suggests** that mountain glaciers in western North America, Europe, and the tropics began to retreat from their LLGM positions before those in Tibet and the mid-latitudes of the Southern Hemisphere.	**5**	
		The retreat of tropical glaciers **may also be** synchronous, but **because the differences in scaling factors are greatest** in the tropics (fig. S4**), it is equally likely that** tropical-glacier retreat occurred earlier.	**6**	
		suggesting that most of the global ice sheets were in near-equilibrium with climate during this 7500-year interval.	**7**	
		In doing so, we adopt ice-sheet model **results that suggest that** the d18O of global ice sheets that contributed to glacial-interglacial sea-level changes was relatively homogenous and thus did not cause any significant temporal changes in this relation	**8**	
		We interpret the residual d18O signal (d18Oc – d18Osw) as recording the change in mean deep ocean temperature (d18OT) (Fig. 4C). Based on a relation of 0.28 ‰ °C−1**, this analysis suggests a maximum** cooling of the mean deep ocean temperature of 3.25 T 0.55°C, which, for a current mean deep ocean temperature (>2000 m) of 1.3°C (30), would place the average temperature of deep ocean waters (–2.2°C) near the freezing point, similar to previous data analyses (1, 26, 27) and model results.	**9**	
		In contrast, however, these same d18Oc **records indicate that** there are no substantial regional phase offsets in the evolution of temperature leading into and during the LGM**, suggesting a more uniform** change in the global ocean heat budget during this time.	**10**	
		A combination of these three forcing mechanisms **appears to explain** the growth phase of ice sheets to their LLGM positions.	**11**	
		This insolation control **may have been augmented** by additional radiative forcing from a small (~15 parts per million) de- crease in atmospheric CO2 (Fig. 5C).	**12**	
		There is also a strong temporal relationship between SST changes in the eastern equatorial Pacific and ice growth, **which suggests** that the 2° to 4°C cooling that occurred between 38 and 30 ka (Fig. 5D) (31, 34, 35) may have played a role in ice-sheet growth.	**13**	

		suggesting that the decrease in SSTs in the eastern equatorial Pacific between 38 and 30 ka reflects a decrease in the equatorial zonal SST gradient, resulting in a more La Niña– like SST field. A model of the response of the NINO3 index (the SST anomaly averaged over 150°W to 90°W and 5°S to 5°N) to orbital forcing indicates that this cooling **may have been** caused by changes in low-latitude precession-related insolation.	**14**	
		It is likely, however, that as the LIS expanded, the additional ice-sheet area added mass as well. **Assuming that a similar mass balance increase** (0.17 m year−1) applied to the LIS expanding in area at an average rate of 611 km2 year−1 results in a sea-level fall of ~31 m.	**15**	
		This analysis thus indicates that tropical Pacific SST cooling probably played an important role in causing the 32 to 38 m of sea-level fall associated with the growth of the LIS to its LLGM extent that we estimated from area-volume scaling relations.	**16**	
		GCM simulations further show that other Northern Hemisphere ice sheets responded similarly to tropical Pacific cooling (38) and **may have caused an additional** 13 m of sea-level fall in the 6500-year growth interval.	**17**	
		Moreover, the fact that ice sheets of all sizes, as well as Northern Hemisphere mountain glaciers, began to retreat at approximately the same time (19 to 20 ka) (Fig. 3, A and B) **suggests that the** primary insolation control on initial deglaciation was through increased summer ablation, which can substantially reduce the long response times of large ice sheets by enabling dynamical pro- cesses that lead to rapid mass loss.	**18**	
		The maximum ice sheets **may themselves have reinforced** this equilibrium condition by maintaining near-constant freshwater fluxes to the oceans and high albedo and orography, thereby reducing their role in causing climate variability.	**19**	
		Simulated precessional forcing of tropical SSTs (37) **suggests that** the warming of the eastern tropical Pacific should have occurred 4 to 5 ky earlier than it actually began (Fig. 5D**), indicating modulation** of the SST response to precession by some other mechanism.	**20**	
		At the same time, this extra- tropical forcing associated with glacial boundary conditions **may have directly caused** cooler tropical SSTs (44), thus changing the sensitivity of the tropical Pacific to precessional forcing	**21**	
		The onset of deglaciation of some ice sheets and mountain glaciers from their maxima was delayed until after 19 ka (Fig. 3), **suggesting the existence of** regional controls on glacier mass balance that modulated their response to insolation	**22**	
		The onset of retreat of the WAIS ~14.5 ka was substantially later than the start of regional warming throughout much of the Southern Hemisphere ~18 to 19 ka (48, 49), and its large contribution to MWP-1A (19) **suggests a nonlinear response** to this warming, perhaps through the collapse of buttressing ice shelves.	**23**	
		One possible explanation for the delayed deglaciation in Tibet is that it was due to the strong influence of the East Asian monsoon, which remained unchanged throughout the LGM until it abruptly weakened ~17.5 ka (50). This weakening may have resulted in a reduction in moisture delivered to the glacier, causing a shift to negative mass balance.	**24**	
13	**Science 2**	As the degree of host specificity (effective specialization) of other guilds **can be** much lower than that of insect herbivores, or **may be** driven by different factors (18, 19), global estimates based on herbivores alone are questionable.	**1**	

		Consequently, extensive cross-taxon surveys with structured protocols at reference sites **may be the only effective approach** toward estimating total arthropod species richness in tropical forests.	**2**	
		As arthropods are notoriously labor-intensive to survey, such an ~~–~~umbrella" approach **may be an efficient way forward.**	**3**	
14	**Science 3**	The apparent ~~–~~wiggles" out of the orbital path observed by EUVI-A and EUVI-B (Fig. 1A**) suggest a** rapid change in the way in which comet tail ions are either channeled by or influence the ambient coronal medium.	**1**	
		Assuming a locally fixed magnetic field, the newly felt Lorentz force will cause the ion to gyrate about the magnetic field, effectively eliminating perpendicular flow on a macroscopic scale while leaving the parallel component un- modified.	**2**	
		This scenario opens up the possibility of testing one or more model coronae	**3**	
		Examining each view, **we gain a sense for how** the field orientation implies non-radial and nonorbital directions for tail motion, as well as rapid switching in some regions due to the changing 3D magnetic field structure.	**4**	
		However, because this MHD model resolves thermodynamic forces that become non-negligible in regions where the magnetic field is weak relative to the plasma pressure, the details of the closed-field streamer regions, and hence the precise comet tail dynamics, **are expected to differ.**	**5**	
		This mismatch in tail motion **may be due to** missing forces in the PFSS model, although a PFSS model with a lower source surface might perform better.	**6**	
		A rough lifetime estimate for O4+ and O5+ ions, and hence their emission time scale in a coronal plasma, tOV,OVI , **can be calculated** from the electron impact ionization rates **under the assumption that** they scale with the local electron density	**7**	
		The longer time scales can also help to explain the relative constancy of emission from the long-lasting portions of the tail. Extensions to the parallel flow model.	**8**	
		Extensions to the parallel flow model, such as the inclusion of perpendicular ion flow mechanisms, drifts, or coronal field modifications [e.g., (14**)], could provide deep insight into the** two- way coupling of the comet to the coronal field itself. Such a scenario is likely needed to explain the slow but conspicuous backward-projected motion of a portion of the tail around 00:01 UT during ingress.	**9**	
		This bolsters the exciting prospect that coronal observations of comet flybys can offer a unique and complementary avenue toward understanding the solar atmosphere.	**10**	
15	**Science 4**	Larvae that lack lgr3 in neurons alone do not respond to Dilp8, **indicating that** the homeostatic system is centered in the brain.	**1**	

		This previously unrecognized circuit **suggests how growth and maturation rate are matched** and co-regulated according to Dilp8 signals to stabilize organismal size.	**2**	
		Two models can be envisioned to establish such homeostatic regulation: (i) a central mech- anism that dictates coordinated adjustments in both the duration and rate of growth and (ii) an endocrine mechanism that involves sensing and processing Dilp8 signals directly by hormone- producing cells.	**3**	
		Thus, the receptors that transduce the Dilp8 signals of growth status **may act directly or may communicate with** neurons that produce the prothoracicotropic hormone (PTTH).	**4**	
		These observations may explain how environmental and internal influences operate through individual IPCs or PTTH neurons to enable body-size variation and plasticity in developmental timing that can be vital for survival in changing environments.	**5**	
		However, the origin of developmental stability and invariant body size **may require different or more complex** neural mechanisms from those involved in adaptive size regulation.	**6**	
		These neurons display extensive axonal arborizations and **appear to connect** with IPCs and PTTH neurons to form a brain circuit for homeostatic body-size regulation	**7**	
		These data also suggest a central mechanism for systemic homeostatic size regulation although other lgr3-expressing peripheral tissues, such as the larval fat body (27), could also contribute.	**8**	
		Next, we used biochemical assays to investigate the interaction of Dilp8 and Lgr3. Human relaxin receptors largely activate cytosolic cAMP (25); thus, **we tested whether** the response of Dro- sophila Kc cells transiently expressing lgr3 to synthetic Drosophila Dilp8 peptides (materials and methods) was coupled to cAMP.	**9**	
		On the basis of structural homology of LGRs to glycoprotein hormone receptors (25, 31), the extracellular domain of the Lgr3 **is expected to** be soluble and to bind cognate ligands.	**10**	
		Collectively, these data suggest that Lgr3 encodes a functionally relevant Dilp8 receptor that is coupled to cAMP signaling like the human relaxin receptors RXPF1-2 (25).	**11**	
		Activation of R19B09 neurons by expressing the UAS-NaChBac ion channel transgene (35) was sufficient to trigger a delay of ~18 hours (R19B09>NaChBac) (Fig. 3E), **which suggests that** Dilp8-stimulated Lgr3 activation excites these neurons electrically.	**12**	
		The number and position of cells that activated de novo luciferase in response to tub-dilp8 in CRE-F-luc brains expressing the UAS-Flp panneuronally (Fig. 4F) matched the cells identified using the R19B09-Gal4 line, **which suggests that** the neurons labeled by this intronic lgr3 en- hancer represent the majority of cells sensitive to Dilp8 signals.	**13**	
		Brainbow analysis **also suggests that** a dialogue is maintained between the distinct cell subpopulations defined by R19B09-Gal4 and that this converges on the synaptic sites of the Lgr3 dorsomedial neurons (green neurons in brainbow image; Fig. 5, D and D″).	**14**	
		GRASP signals were observed for IPCs (Fig. 5E and fig. S6, A and B). GRASP signals **also suggest possible connections** be- tween Lgr3 and PTTH neurons, as detected by immunofluorescence (anti-GFP, Invitrogen) (Fig. 5F) as in (40).	**15**	
		These data suggest that Lgr3 neurons link Dilp8 input to IPCs and/or PTTH neurons to form a homeostatic circuit for synchronizing growth with maturation timing for body-size regulation.	**16**	
		It is possible that the release of PTTH at the larval-pupal transition might additionally require disinhibition of inhib- itory input(s), as proposed for the secretion of GnRH from hypothalamic neurons at the onset of puberty.	**17**	

		Thus, the coupled control of the growth rate **probably involves** the other branch (the IPCs) of the Lgr3 neuronal circuit.	**18**	
		Ablation or electrical silencing of IPCs produces adults that are much smaller than normal (9, 16), **suggesting that** size compensation via Dilp8 is unlikely to affect insulin signaling globally or completely.	**19**	
		RXFP3 is distinctly different in structure from fly Lgr3 (25), and its biochemical properties are also distinct, but RXPF3 is analogous to fly Lgr3 in the sense that it is found in highest abundance in the brain, **suggesting important central functions** for relaxin 3/RXFP3 (48, 49).	**20**	
		Furthermore, the information flow from Lgr3 neurons to IPCs and PTTH may explain how the brain matches growth with maturation in response to Dilp8 (Fig. 6F). This brain circuit provides the basis for studying how the brain copes with genetic and environmental perturbations to stabilize body size, pro- portions, and symmetry, all of which are vital for survival.	**21**	
16	**Plos 1**	From the gene array analysis of ex-smokers with and without emphysema/COPD (Table 1) we identified genetic deficiencies that may underlie the Treg cell deficiency and chronic inflammation in COPD, and/or elastin-specific autoimmunity.	**1**	
		Defective expression or polymorphism in these genes (Table 2) may be a predisposing factor for chronic inflammation that leads to COPD.	**2**	
		We thought that if elastin peptides were bound to C3b because they were presented as an auto-antigen, activating T cells, then we should also find IgG to elastin in the serum of patients that manifested early on-set of COPD (EO-COPD), we included for this study a total of 49 participants, 21 EO-COPD and compared them to 28 control, normal subjects.	**3**	
		The proliferation of CD8 + T may be due to elastin that is being presented as an auto-antigen, since 43% of COPD patients with early onset of the disease had IgG binding to elastin in their serum.	**4**	
		Free radicals may react in random manner with the cell surface proteins leaving them un-functional or even cleaving them, depletion of this receptor may be underlying the T cell dysregulation and increased cells death associated with cigarette smoke; nevertheless after smoke cessation normal individuals up-regulate CD46 and recover the immunological homeostasis, even some of their lung function.	**5**	
		However, the presence of IgG binding to elastin in only 43% of the early onset COPD indicates either the existence of other antigen that may be causing the remaining 57% EO-COPD to develop severe emphysema or, considering the disparity of reports in this matter [6–9], it is possible that a abridged sensibility of the tests and/or divergent COPD variants tested may cause dispersion in the results.	**6**	
17	**Plos 2**	ICA may use higher order statistical information for separating the signals, rather than the second-order information of the sample covariance as used in PCA. ICA can therefore reveal some underlying structure in the data, giving a fresh perspective to the problem of understanding the mechanisms that influence the stock market data.	**1**	

		Yeh et al [26] proposed the auto regression model based on ICA and SVR for time series prediction. Here, we call it the AICASVR model. Fig. 2 gives the stock market forecasting framework into which the model is applied. We can see that the model contains three stages: (1) the slide window is used to prepare the input data, (2) data pre-processing by ICA, and (3) forecast by SVR.	**2**	
		In this paper, we propose a stock market predictive framework based on feature fusion. In this framework, an auto regression module extracts feature A from the history data of the closing price, and a multi-variable regression extracts feature B from related technical variables. The feature fusion module combines feature A and B to create a union feature by using certain fusion methods.	**3**	
		The third stage of the model is the SVR used to predict the future value of the closing price. After the fusion feature is obtained, it can be used to train the stock market prediction model based on SVR. Its first step is to choose the kernel function. Different kernel function may yield different performances.	**4**	
		In this section, we give an intuitive analysis for the ICA-CCASVR model. The advantage of the proposed model may lie on the following reasons.	**5**	
		We believe that the possible reasons lie in the two following explanations. (1) The lower the dimensionality, the greater the ratio of noise to useful information is contained in the features. In this case, the fusion feature will strengthen the noise to impact the predictive performance. (2) For the CCA algorithm, the component of extracted features is uncorrelated but not independent, which means that the components have no influence over each other in the sense of statistical average. However, it cannot be visibly displayed when the components are insufficient.	**6**	
		We believe the main reason is that the proposed model has a certain sensibility to the data. Another weakness is that the optimal feature dimensionality of the ICA-CCA-SVR model may sometimes be higher than that of the other models, due to the serial features fusion method. To solve this problem, utilization of a more effective method as the parallel fusion method will be investigated through further study.	**7**	
18	**Plos 3**	Our analysis is based on a previously developed model of infection and immunity in which a costly plasmid confers antibiotic resistance. As expected, antibiotic treatment increases the frequency of the resistant strain, while the plasmid cost causes a reduction of resistance in the absence of antibiotic selection. Our analysis suggests that this reduction occurs under competition for limited resources.	**1**	
		Finally, we estimated tclear for a specific case, using available empirical data, and found that resistance may be lost up to 15 times faster under antiR treatment when compared to a no treatment regime. This strategy may be particularly suitable to treat chronic infection. Finally, our analysis suggests that accounting explicitly for a resistance-decaying rate may drastically change predicted outcomes in hostpopulation models.	**2**	
		Moreover, the implementation of drug restriction policies beyond a single hospital is challenging. In the case of cycling, lack of standard procedures and arbitrary definition of cycle duration are central issues [13,14,17], making strategies inconclusive. Mathematical models could help to improve strategies. However, most models [39–41] predict that antimicrobial cycling is not helpful in reducing resistance while most experimental investigations suggest benefits for cycling [14]. Such divergence encourages the search for the principles necessary to develop accurate models and highlights the importance of more experimental evidence.	**3**	

		Finally, our single-host model suggests that antibiotic resistance may be attenuated over time. We show that the incorporation of a similar resistance attenuation term into host-population models may change the current perspective on optimal strategies to reduce incidence of antibiotic resistance.	**4**	
		Throughout this work, we use a specific fixed value for each parameter and we assume that antibiotic treatment has equal access to each pathogen cell. These assumptions make it easier to understand the model principles and do not affect the conclusions of our analysis. A sensitivity analysis shows that our results are robust to a varying range of parameters	**5**	
		This phenomenon suggests that competition for resources might also direct resistance attenuation under no treatment conditions. Notably, resource competition has recently been shown, both in terms of mathematical simulations and experimental data, to play a major role in the duration of inflammatory reaction caused by virulent pathogen [48].	**6**	
		Our analysis illustrates a case where a resistant infection could be potentially cured based on the specific timing of two treatments: antibiotic and antiR. An antiR condition can reduce the abundance of a resistant strain by exploiting the cost of resistance.	**7**	
19	**Plos 4**	Since testicular cancer cells are derived from primordial germ cells (PGCs) or gonocytes [2] the increase has been attributed to maternal and fetal exposures to environmental factors, with most attention given to endocrine disruptors such as estrogens and antiandrogens	**1**	
		These examples suggest that this mouse teratoma model may be relevant to the adult forms of human testicular cancer as well, although there are reservations about such an extrapolation	**2**	
		The two radiation doses of 0.8 Gy did not disrupt spermatogenesis, which was qualitatively normal in testes that did not contain teratoma (Figure 1E and F). However, these tumor-free testes from irradiated mice had reduced weights compared to those from controls (Table 2), suggesting that irradiation had caused some loss or inhibition of proliferation of PGCs and/or somatic cells.	**3**	
		Ionizing radiation itself induces larger numbers of SSBs and produces damaged bases. This radiationinduced damage might perturb signaling pathways involving endogenous SSBs and base-excision repair regulating this epigenetic transformation and allow the cells to retain pluripotency as embryonic stem-like cells that subsequently form the TGCTs.	**4**	
		Although the extrapolation of the teratomas in mice to the sporadic testicular tumors in young adult human males is still debatable, the present results on in utero irradiation of mice suggest that the male fetus of women exposed to radiation at about 5–6 weeks of pregnancy might be at an increased risk of developing testicular cancer.	**5**	

Explicación

Consecutivo	Clasificación	Apariciones	Consecutivo del paper	Color
1	**A1**		**0**	
2	**A2**	Marriage migrant women face multiple layers of challenges from the moment of their arrival. They not only have to adjust to a new culture, language, and surroundings, but also have to adjust to sharing life with their husbands as well as taking on new roles as wives, daughters-in-law, mothers, and many more (Lee, 2013). ↓ With the short period of time available to build a relationship prior to marriage, coupled with language barriers and a lack of knowledge about each other‘s culture, practice, and customs, ↓ it is often difficult for couples to learn about each other before marriage, and such a lack of knowledge and understanding of each other often results in marital conflict. ↓ In addition, with values and cultural difference (Bang, 2010; Han, 2006; Lee, 2005), these spouses experience a rather severe level of mental distress in the course of their marriage (Seol et al., 2005). ↓ Some studies also found that women‘s mental health problems often also lead to family dissolution (Jang & Park, 2009; Kwon & Cha, 2006; Park, 2007).	**1**	
3	**A4**	We observed 82.9% and 16.7% of mutant allele frequency in WD patients with ceruloplasmin concentration <10 mg/dl and 10-20 mg/dl, respectively (p <0.001). Thus serum ceruloplasmin concentrations among WD patients differed according to the number of ATP7B mutations detected.	**1**	
		If left untreated, WD is a potentially lethal disorder. Early diagnosis of WD is important, because early administration of D-penicillamine can prevent the need for transplantation in most cases.	**2**	

4	**PNAS 1**	The presence and concentration of ethane, propane, and n-butane are useful for identifying the methane source as thermogenic or microbial ↓ Because ethane is not coproduced during microbial methanogenesis, the presence of ethane-to-methane ratios greater than 0.01 indicates gas of largely thermogenic origin (14, 19).	**1**	
		Ratios of ethane, propane, and n-butane relative to methane were more frequently greater than 0.01, and at higher values, for wells than for controls (Fig. 3). ↓ Nonetheless, the presence of these non methane hydrocarbons in controls indicates that ↓ there may be subsurface horizontal gas flow away from the well and subsequent emissions to the atmosphere	**2**	
		Methane emitted from most control locations is in the microbial range; however, one measurement reveals that methane emitted from control sources can contain thermogenic sources of methane as well. If we consider the integrated fluxes from all these wells, the methane emitted is primarily of thermogenic origin because the high-emitting wells would represent a large fraction of the total methane emitted from abandoned wells.	**3**	
		The measured wells presented in this paper are likely to be half a century old or older, and the positive flow rates measured at these wells indicate that the methane emissions from these wells may have been occurring for many decades and possibly more than a century. Therefore, the cumulative emissions from abandoned wells may be significantly larger than the cumulative leakage associated with oil and gas production, which has a shorter lifetime of operation.	**4**	

5	**PNAS 2**	A. If regulation is interrupted by the presence of another colony, the number of bacteria increases locally; B. This triggers the secretion of the lethal protein to rapidly reduce bacterial density	**1**	
		This suggests that: A. high subtilisin levels B. trigger secretion of this third protein, which is involved in the inhibition process and cell death	**2**	
		A. A colony‘s expansion is limited by surface tension (11); it cannot expand fast enough to create new space for the reproducing bacteria. B. Thus, an increase in subtilisin results in an increase of bacterial density and consequently nutrient stress.	**3**	
		A. One of the key features of the profile is that inside the colony, subtilisin concentration exceeds a critical threshold. B. This does not trigger production of Slf because the motile bacterial concentration in this region is low	**4**	
		A. Combining the two effects we find that subtilisin levels for a single colony reach a steady state in which the concentration of bacteria is close to maximal. B. Thus, subtilisin concentration at the front of the colony is regulated. This also accounts for the constant expansion rate of the colony (7).	**5**	
		a. When the local nutrient supply is exhausted, b. A proportion of the bacteria cease growing and initiate sporulation, allowing the colony to survive unfavorable conditions. However, when the bacteria are faced with invasion by a competing colony, a more drastic response occurs.	**6**	

		Subtilisin, a serine protease, is secreted by P. dendritiformis and can be detected around single colonies. The concentration at the front of converging colonies is higher, and this appears to lead to the secretion of Slf. This behavior can be modeled mathematically, and as predicted by the model, exposure of a single colony of P. dendritiformis to a high concentration of subtilisin results in Slf secretion and death. Taken together, the data suggest that subtilisin and Slf are part of a complex system to regulate population spread and density in response to environmental conditions.	**7**	
		A. A fundamental requirement for boundary formation is the ability to discriminate between self and nonself. In our case, Slf was found to be lethal to P. dendritiformis but not to other bacteria, even closely related ones. B. These observations support the idea that the Slf acts as a sibling bacteriocin that is secreted for killing bacteria of the same strain and not for general killing of other competing species.	**8**	
6	PNAS 3	A. An unfolded shell has κN of the same sign on either side of the crease, and thus matches the preferred curvature H0. However, the bending energy density of a shell which has been folded (Fig. 1B) is not zero B. because κN will be negative on one side and positive on the other; thus, only one side of the hinge can match the preferred curvature of the shell H0.	**1**	
		This occurs trivially on flat paper inscribed with a curved fold because ψ′ðsÞ, τðsÞ, and K vanish individually. In this case, the surface can be folded with a monotonically increasing energy mediated by the bending energy alone (31, 40).	**2**	

		Deforming these shells along the κN≠0 crease generates a discontinuous motion characteristic of a snap-through instability as predicted (Movie S1and Fig. 2A). Hence, the purely geometric nature of our design rule offers a way to understand the continuity or discontinuity of folding even without a detailed understanding of the complex shell mechanics	**3**	
		Remarkably, despite the introduction of a crease, the free cylinder displays a global bending deformation instead of snapping (Movie S2) Such Global deformations arise because cylinders have k=0, and thus can bend without stretching, so that there is a pathway accessible to the shell that costs less energy than snapping but still satisfies the constraints imposed by the indenter.	**4**	
		Given their axisymmetry, spherical shells are well suited to quantitative analytical, computational, and experimental analysis. Because the spherical geometry is devoid of any κN = 0 curves, we expect that intersecting a spherical surface with a plane to create a crease with finite κN will result in a snap.	**5**	
		Evidently, for larger values of α, this gain surpasses the bending energy of the shell, resulting in bistability due to the presence of a local minimum in total energy. Thus, we infer that the stability of creased shells is governed by the competition between bending energy of the undeformed shell and stretching energy contained in the creased region.	**6**	
		Because the speed of the snap arises from stretching in the shell, inertia mediates the transition at the speed of sound in the material (Movies S1–S3), and crucially, the snap is unimpeded by poroelasticity or hydraulic damping as displayed in many natural snapping systems (51).	**7**	
		At P7, many DG neurons in mutant were still present in the DG migratory path from dentate VZ to DG anlage, whereas few were observed in the wild-type counterpart. At P21, only a residual of DG was left in mutant (Fig. 2 A and B). These data indicate the severe defects of DG development in the absence of Zbtb20.	**1**	

		After 1 h of pulse, the frequency of BrdU-labeled cells both in the E14.5 hippocampal and transitional VZ and in the E18.5 DG were comparable between Zbtb20 mutant and wild-type embryos (Fig. S3 A–F), which indicate that Zbtb20 ablation does not alter the precursor proliferation in the hippocampal or adjacent transitional VZ.	**2**	
		Furthermore, Mannosidase 1 alpha (Man1α), a specific marker of mature CA1 neurons (17), was totally absent from the Zbtb20− −CA1 region at P21 (Fig. 3 Gand H). In contrast to its homogenous expression in wild-type CA1, Oct6 was detected in some neurons scattered in the mutant CA1 region, with a pattern reminiscent of that in transitional neocortex (Fig. S4 E and F) (18). These findings strongly indicate that the neurons in the mutant CA1 region have lost their CA1 identity.	**3**	
		Thus, both histological and genetic evidence strongly indicates that Zbtb20 ablation leads to the ventral expansion of transitional neocortex and a shift of subiculum position at the expense of the CA1 region.	**4**	
		These findings revealed that the mutant CA1 neurons migrated more rapidly through the IZ to the CP than their wild-type counterparts, at a rate similar to transitional neocortex neurons (12). Therefore, the altered migratory behavior also supports the notion that the mutant CA1 neurons have acquired the identity of transitional neocortex neurons.	**5**	
		To distinguish two possibilities of either abnormal penetration of entorhino hippocampal projections into the IML or loss of the IML in Zbtb20 mutant DG, we examined expression of Calretinin. Calretinin-positive fibers were densely distributed in wild-type IML, but absent in mutant DG (Fig. 6 C and D), indicating the loss of IML in mutant DG.	**6**	
		The up-regulation of Tbr1 and the orphan nuclear receptor Nr4a2 (a marker for subiculum and deep layer projection neurons) (27) and down-regulation of the trophic factor BDNF (a survival factor of hippocampal progenitors) (28) in mutant hippocampus were confirmed by RT-PCR (Fig. S6C), the latter may partly account for the increased apoptosis of the mutant hippocampal neurons. Taken together, these findings indicate that Zbtb20 orchestrates the expression of key factors for hippocampal development.	**7**	
		When the results of this study are placed in context with previous work that mis expression of Zbtb20 induces a CA1-like transformation of the transitional neocortex and subiculum (11, 29), *we conclude* that Zbtb20 is essential for the specification of CA1 field identity in the developing hippocampus.	**8**	

		Our study showed that the loss of Zbtb20 did not cause any notable alterations to the expression and activity of both canonical and noncanonical Wnt signaling components in the hippocampal region at embryonic stages. These observations suggest that Wnt signaling alone is not sufficient to induce archicortex differentiation.	**9**	
		Given that Zbtb20 is activated in the hippocampal anlage at E12.5, before the onset of CA1 differentiation (which begins at E15.5), and is expressed by both proliferating and postmitotic hippocampal progenitor cells, we reason that Zbtb20 is necessary to maintain archicortical potential in the presumptive CA1 subpopulation of multipotent cortical progenitors, and/or to maintain CA1 area identities in postmitotic neurons by suppressing transitional neocortex and subiculum differentiation regimes.	**10**	
		This increase was not likely to be an indirect effect of global metabolic dysfunction (9), because the majority of Zbtb20− − mice appeared normal and indistinguishable from wild-type controls before P10, although they later developed hypoglycemia.	**11**	
8	**Nature 1**	Yanoconodon has a triangular outline of the scapula, and a gracile and slightly curved clavicle that lacks a rigid articulation to the interclavicle, it therefore has a mobile and ‗therian-like' shoulder girdle (Fig. 1).	**1**	
		Yanoconodon is far more derived than mammaliaforms (Fig. 3a)5,6,22 in that its middle-ear bones are mediolaterally separated from the pterygoid part of the mandible (Fig. 3b, 3h), despite the plesiomorphic similarity in retaining the Meckel's connection to the mandible.	**2**	
		Owing to the curvature of Meckel's cartilage, the basicranial articulation of the incus is nearly co-axial with the fulcrum for movement around the dentarysquamosal jaw hinge, so the jaw movement had little impact on the middle ear function.	**3**	
		The heterochronic (‗premature') ossification of Meckel's cartilage in eutriconodonts is the immediate cause for this paedomorphic connection of middle ear and mandible, and is why there is an overall homoplastic distribution among therians (with DMME), eutriconodonts (without DMME), monotremes (with DMME) and pre-mammalian relatives (without DMME) (triangles in Fig. 2).	**4**	
		Modern mammals have a highly conserved pattern of vertebral identities: seven cervical, 13 to 14 thoracic, and five or six lumbar vertebrae (without separate lumbar ribs) for a combined 19 or 20 thoracolumbar vertebrae. These regional vertebral identities are patterned by homeobox genes	**5**	

		Homoplasy of mobile lumbar ribs also occurs in symmetrodonts (Fig. 4)33. The presence of primitive lumbar ribs in Akidolestes is best hypothesized as an atavistic reversal because its related spalacotheroids show the derived therian condition without lumbar ribs.	**6**	
		Shifts in the thoracolumbar boundary and homoplasy of their vertebral identities are primarily correlated with mutation in Hox genes for their patterning. This provides a plausible mechanism for the evolutionary patterns in lumbar ribs and the thoracolumbar transition in Mesozoic mammals (Fig. 4).	**7**	
		With their smaller brains and identifiable neurons, insects offer tractable systems to examine such navigational neural computations	**1**	
		All the cues used thus far provided the fly with landmarks that uniquely define its orientation in the environment. An activity bump could thus represent either the fly‘s angular position within the visual scene or its orientation relative to a specific landmark within it.	**2**	
		Such persistence was also a feature of EBw.s dynamics when the fly remained standing in a visual environment (Extended Data Fig 10g-r), extending beyond durations that elicit adaptation in early visual circuits29. Thus, even in the absence self-motion cues, EBw.s population activity maintains a stable representation of the fly's orientation in its environment with or without visual landmarks.	**3**	
		This representation persisted even when EBw.s calcium activity was low, as evident in the fact that renewed bouts of movement caused a bump to reappear in exactly the wedges expected based on the last orientation of the fly (Fig. 4h and Extended Data Fig. 10a, c, e, Supplementary Videos 7 and 8).	**4**	
		With initial sensory input, such a circuit can generate and sustain a localized activity bump. The bump's position on the circle corresponds to the animal's heading which is then updated by directional drive from self-motion signaling neurons.	**5**	
10	**Nature 3**	Phase freedom, a consequence of the discoid magnetic symmetry, allows interacting spheres to adjust their phases. For example, two particles (Fig. 1c) initially attract and approach until stopped by electrostatic repulsion at a separation of about 200 nm. Only at this close separation does the magnetic field created by one particle generate an appreciable torque on the other particle. Although small, this torque gradually drove the two particles to an antiphase steady state in both a and Q, regardless of the initial state.	**1**	

		This unsynchronized state ultimately dissociated into a loose aggregate of zigzag chains with lower average energy. Because ω_{free} depends monotonically on θ a critical ω_{free} translates into a critical θc.	**2**	
		Figure 3b confirms the coupling between the loss of synchronization, characterized by the difference Dv in rotational frequency of the constituent particles and the entire structure, and the structural transition, reflected by the sharp decrease of the positional order parameter S (defined in Methods). This process explains the boundary between regions I and II of Fig. 2a.	**3**	
11	**Nature 4**	In response to odorants, olfactory sensory neurons (OSNs) transmit signals to the brain, thereby ↓ generating odour perceptions	**1**	
		Notably, three ligands identified for mTAARs are natural components of mouse urine, a major source of social cues in rodents. mTAAR4 recognizes b-phenylethylamine, a compound whose elevation in urine is correlated with increases in stress and stress responses in both rodents and humans30–32, and both mTAAR3 and mTAAR5 detect compounds (isoamylamine and trimethylamine, respectively) that are enriched in male versus female mouse urine. Furthermore, isoamylamine in male urine is reported to act as a pheromone, accelerating puberty onset in female mice by one criterion34 (although not by another).	**2**	
12	**Science 1**	Nearly all ice sheets were at their LGM positions from 26.5 ka to 19 to 20 ka, **corresponding to minima in** these forcings. The onset of Northern Hemisphere deglaciation 19 to 20 ka was induced by an increase in northern summer insolation**, providing the source for** an abrupt rise in sea level	**1**	
		Because sea level is an integrated signal, however, it does not distinguish between globally synchronous ice-sheet maxima that may have been in equilibrium throughout this interval and temporally variable regional ice-sheet maxima that combined to produce a millennia- long sea-level lowstand.	**2**	
		Because ice-sheet extent scales with ice volume (2), our constraints on regional variability in ice-sheet maxima **allow us to evaluate** the temporal evolution of individual ice-sheet contributions to global sea-level change	**3**	

		Because mountain glaciers are highly sensitive to climate change, we used an additional 172 ^{14}C ages and 786 TCN ages to constrain mountain- glacier fluctuations from five widely distributed regions of the world (Fig. 1), allowing a more comprehensive assessment of the response of the cryosphere to climate change.	**4**	
		The sea-level change at these sites will differ from the eustatic change **because of the spatially varying** gravitational, deformational, and rotational perturbations in sea level driven by the ice-ocean mass transfer.	**5**	
		In the context of the global sea-level record, **we find that this expansion of ice sheets to their maximum extent can explain** much of the global sea-level fall from intermediate levels during marine isotope stage (MIS) 3 to the LGM lowstand	**6**	
		In those bars, the vertical purple segment and associated horizontal gray segment **represent the mean age** and the 1s age range for the onset of deglaciation based on the scaling factor that delivers the oldest age for the region, whereas the vertical blue segment and associated area outlined in gray represent the mean age and the 1s age range for the onset of deglaciation based on the scaling factor that delivers the youngest age for the region	**7**	
		Within the context of the LGM, however, **two additional features of this analysis stand out: Average** deep ocean temperatures must have warmed by nearly 1°C during the interval when ice sheets were reaching their maximum extent, followed by a cooling trend through the LGM that culminated in maximum cooling occurring well after the LGM.	**8**	
		The WAIS also reached its LLGM extent early in this growth interval (Fig. 3B), **with its growth explaining much of the remaining sea-level fall** to the LGM lowstand. In this case, recent analyses have shown that local changes in austral spring insolation control (40) or the duration of summer at high southern latitudes (41) **may have induced** climate changes that favored ice-sheet growth.	**9**	
		The initial retreat of Southern Hemisphere mountain glaciers, on the other hand, **is consistent with** the onset of Southern Hemisphere warming.	**10**	

		Although the lead-lag relationships established here by the timing of the LGM point to northern latitude insolation as the primary trigger of initial deglaciation of most Northern Hemisphere ice sheets and glaciers, subsequent increases in atmospheric CO2 and tropical Pacific SSTs (Fig. 5, C and D) **demonstrate the importanc**e of carbon cycle and ocean feedbacks in amplifying the deglacial response and causing global warming.	**11**	
13	**Science 2**	Although the scope for direct comparison is limited because of regional differences in sampling effort, lowland tropical forest in Panama **seems to support 2.1 to 8.4 times as many** arthropod species as observed in temperate forests (table S3). While this supports the obvious truism that tropical arthropods are indeed more diverse than their temperate counterparts (22**), the magnitude of that difference is far lower than many previous estimates would suggest**	**1**	
		Based on the dominance of arthropod species in the tropical fauna (table S3), **we may then argue that** conservation planning for biodiversity should be largely determined by the spatial scaling of arthropod diversity.	**2**	
14	**Science 3**	The Sun‘s magnetic field is of primary importance in solar and heliospheric physics. **It is the energy source for** solar activity**, and it defines the structure of** the solar corona and of the solar wind, which is largely determined in the low solar corona.	**1**	
		This motion corresponded neither to radial motion, **which would be expected if** the tail motion were dominated by solar wind outflows or radiation pressure, **nor to** motion tangential to the comet orbit, **which would be expected if** the medium had no influence at all.	**2**	
		After perihelion (egress, Fig. 1C), observable tail emission nearer to the Sun (left half) had a relatively short lifetime ($t \leq$ 5 min) while the portion located farther out remained much longer ($t \geq 15$ min). In some of these longer- lasting regions, the projected tail emission **continued to evolve anisotropically, forming** contrasted linear features not aligned with the orbital path.	**3**	
		Molecule containing O that was originally part of the solid comet body (the largest contributor being water ice) is sublimated via insolation from the comet surface with some outflow velocity.	**4**	
		The relative size and color of the arrows **is proportional to** the magnitude of (vc·b)b in km s–1	**5**	

		Because the “tail,” as seen in the EUV, is simply a tracer for the location of emitting ions as they interact with the medium, the apparent motion of the **tail can thus be** approximated by considering the motion and subsequent deceleration of cometary ions flowing parallel to the coronal magnetic field.	**6**	
		Unlike the thermodynamic MHD calculation, the PFSS **solution assumes that the** domain is current-free at all heights up to a source surface radius where the field becomes radial (typically 2.5 RS). However, PFSS **solves only for the minimum energy state** of the coronal field distribution, and therefore **does not capture structures energized** through sustained motions and thermodynamic forces.	**7**	
15	**Science 4**	Therefore, immature animals must employ homeostatic **mechanisms to counteract** substantial size variations and withstand developmental growth perturbations caused by genetic errors, disease, environmental factors, or injury. **Such mechanisms ensure that**, despite inevitable variations, the appropriate final body size is attained.	**1**	
		When growth is disturbed, Dilp8 is strongly activated and sexual maturation is postponed until the affected elements are recomposed; simultaneously, the growth of other organs is retarded during this process. **This compensatory mechanism allows** the growth of the affected tissues to catch up.	**2**	
		GRASP analyses demonstrate that these neurons are connected to both the IPCs and PTTH neurons critical for adjusting growth and maturation rate, respectively. Thus, through their extensive axonal arborizations, Lgr3 neurons function like a “neuronal hub”	**3**	
		They route peripheral information about growth status to other neuronal populations, **thereby synchronizing** damaged tissues and other (un- damaged) ones and allocating additional development time so that each organ attains the correct size and maintains proportionality and symmetry.	**4**	
		Lgr3 **neurons that respond to Dilp8 signals directly input on the** insulin-producing cells and the PTTH-producing neurons.	**5**	
		FIG. T**he brain detects growth status and anomalies via** Dilp8 activation of the Lgr3 receptor in two pairs of symmetric neurons. **These neurons distribute this information** to IPCs and PTTH neurons, which then trigger the hormonal responses that stabilize size	**6**	
		Most animals initiate a pubertal transition **only after the critical size** and body mass have been achieved and, generally, in the absence of tissue damage or growth abnormalities (5, 8–11). However, the mechanisms underlying such homeostatic regulation have yet to be fully defined.	**7**	

		During the larval (growth) stage, the expression of dilp8 de- clines as maturation proceeds, whereas its expression is activated when growth is disturbed (12, 13). **Hence**, fluctuating Dilp8 levels provide a reliable read-out of overall growth status (e.g., deficit) and the time needed to complete growth.	**8**	
		Accordingly, in the absence of dilp8, mutant flies **are incapable** of maintaining such strict control over their size, as reflected by the exaggerated variation in terms of overall proportionality and imperfect bilateral symmetry.	**9**	
		In Drosophila, **several anatomically separate neural populations regulate** growth and maturation time by imping- ing directly on the ring gland [which is made up of the PG and the juvenile hormone-producing corpus allatum (CA)]	**10**	
		In- sect PTTH neurons, **which are** analogous to the gonadotropin-releasing hormone (GnRH) neurons in mammals (5, 10), signal the commitment to sexual reproduction by stimulating the production of ecdysone in the PG to terminate growth.	**11**	
		Similarly, manipulations of the PTTH neuropeptide and neurons **result in adult fly size variations, leading to flies that are larger or smaller than normal** due to an extension or acceleration of the larval period.	**12**	
		The insulin receptor also directly activates synthesis of the juvenile hormone (JH) (a hormone that promotes growth and juvenile development) in the CA (23) and production of the steroid prohormone ecdysone in the PG (14), again augmenting the variation in normal adult size.	**13**	
		Because most G protein–coupled receptors (GPCRs) **display some level of constitutive activity** [two-state model of GPCR function (34)] in the absence of agonist ligands, delayed pupariation due to increased levels of endogenous lgr3 via overexpression in R19B09-labeled neurons might reflect an increased response to a low concentration of endogenous Dilp8 or constitutive activity.	**14**	
		The Lgr3 receptor response to **Dilp8 is strongly coupled to** cAMP stimulation (Fig. 2, A and B), enabling us to precisely determine the Lgr3- responding neurons via a cAMP biosensor. We used the CRE-F-luciferase (luc) construct (CRE, cAMP response element) (Fig. 4B) that has already been characterized in vivo (36). **Thus**, by combining the CRE-F-luc construct with UAS-Flp and R19B09-Gal4, we could assay specific cAMP responses in a physiological context (R19B09 neurons and tub-dilp8 background).	**15**	

		Paired organs **are controlled by** an identical genetic program and grow in the same hormonal environment, yet small deviations in size can occur as a result of developmental stress, genetic noise, or injury. Imperfections in symmetry **thus reflect the inability** of an individual to counterbalance variations and growth abnormalities.	**16**	
16	**Plos 1**	In normal individuals autoreactive T cells are eliminated in the thymus through a selection of those cells with T cell receptors (TCR) that binds weakly to a self-antigens and may induce anergy. However, there is an intrinsic mechanism that eliminates T cells that strongly binds to self-antigens, by up regulation of FAS ligand (FASL) and its receptor CD95 which activating the signaling pathway of caspase (Casp) 8 and proteolysis leads to apoptosis. This is an important regulatory mechanism against autoimmunity because mice and humans with defects in the FAS pathway develop systemic autoimmunity [16–18].	**1**	
		The first gene we focused on was CD46 because it plays a pivotal role in the crosstalk between the innate and adaptive immune responses, the over-expression of CD46 in controls was verified at the mRNA level using qRT-PCR and at the protein level by flow cytometry (Table 2).	**2**	
		Since memory Treg are created by CD46 coupling with CD3 that suppresses Tc (CD8 +T cells), which are eliminated via apoptosis involving Casp8 [31], a protective gene (Table 2), this forms a complex with Fas-associated death domain (FADD) FADD and the FasL receptor (CD95) [32].	**3**	
		After placing DiI in the DG of P14 mice, the mossy fibers were clearly visualized in the stratum lucidum of wild-type CA3, but absent in the mutant (Fig. S6 A and B). Similarly, Schaffer collaterals, which extend from CA3 to CA1, were present in the wild types rather than the mutants after placing DiI in the CA3 and DG (Fig. 6 E and F). Taken together, the tracing results show the remarkable defects in hippocampal neuronal network in Zbtb20 mutant mice.	**4**	
		It is remarkable that CD46 depletion rather then ubiquitous was on T cells, and replicated in the murine smoking model which ensures that this effect rather then being mediated by cancer or viral infections is due to cigarette smoke itself, reducing the variables to oxidative stress and free radicals effect on CD46.	**5**	

		(A) CD46 coupling with CD3 activates the transcription factor ubiquitously transcribed tetratricopeptide (UTX), which interacts with signal transducer and activator of transcription 1 (STAT1) both translocate to the nucleus to activate proliferation of CD4+T cells. T cell receptor activates Bcl-2 that inhibits cytochrome C (Cyto C) released by chloride intracellular channel 4 (CLIC4), which positively regulates Fas Ligand receptor (CD95) mediated activation of Caspase 8 (Casp 8) and apoptosis.	**6**	
		T cells ratios vary significantly with the progression of the disease showing an intersection point when the number of CD8 +T cells reach the same number then CD4+ T cells (30%) in patients with 60% of FEV1 predicted, from this point on, there is a steep loss of CD4 + T cells compared to CD8 + T proliferation; supporting the concept of an extrinsic dysregulation of autoreactives T cells due to loss of Tregs when patients enter in the stages 3 and 4 of GOLD with severe COPD/emphysema [6].	**7**	
17	**Plos 2**	First, two types of features are extracted from the historical closing prices and 39 technical variables obtained by independent component analysis. Second, a canonical correlation analysis method is utilized to combine the two types of features and extract intrinsic features to improve the performance of the prediction model. Finally, a support vector machine is applied to forecast the next day's closing price.	**1**	
		The auto regression forecasting model is built up based on time series analysis. It aims to predict the future closing price by using the historical data. Since both the input and output are the value of the closing price, we name this type of model an auto regression model.	**2**	
		Figure 2. Auto ICA regression model (AICA-SVR).	**3**	
		The first stage of this model is that two types of features are extracted from the historical closing price and multi-variables respectively. The time series of historical closing price is divided into several segments by the slide window, then ICA is utilized toextract the first type of feature A from each segment. Figure 4. Multi-variable ICA regression model (MICA-SVR).	**4**	
		In order to extract features A and B, the historical data and technique variables data are organized to reshape the observed data x(t)~½x1(t),x2(t), xm(t) T according to Figs 1 and 2, respectively.	**5**	

		For comparison, AICA-RVR and MICA-SVR model were applied to evaluate the prediction accuracy of the proposed ICACCA- SVR model. Table 3 and Table 4 show the prediction results for AICA-SVR, MICA-SVR and the proposed ICA-CCASVR models. In the Tables, Dim, BestC, and Bestg represent the optimal dimensionality, parameter C, and parameter s for each model respectively. The comparison results show that the proposed ICA-CCA model has the smallest RMSE, MAPE, MSE and MAE values, and the highest R2, and r values in comparison with MICA-SVR and AICA-SVR.	**6**	
		The result shows that the proposed model also has the lowest MAPE, RMSE, MAE and MSE and the highest R2 and r values and outperforms the AICA-SVR and MICA-SVR models. It concludes that the proposed ICA-CCA-SVR model can produce lower prediction errors and higher prediction accuracy in the direction of change in price and outperforms MICA-SVR and AICA-SVR methods in forecasting the Shanghai stock market index and Dow Jones index closing prices.	**7**	
		Noise and redundant information exist in original stock market data, so feature extraction is a vital step in a forecasting model. Various types of existing forecasting models only emphasize the classifier of the model and pay little attention to the pre-processing of the data. In this study, we introduce ICA as the pre-processing tool to reduce the dimensions and to extract features from two different points. CCA is used as feature fusion tool to extract the intrinsic features of the input raw data. Due to the fusion feature extraction characteristic, ICA-CCA shows better performance in evaluating stock market data.	**8**	
18	**Plos 3**	Drug restriction consists of suspending a given class of antibiotics for some period of time, while other classes of antibiotics are still available for treatment. It is based on the principle that resistance can decrease in the absence of a specific antibiotic treatment, due to the cost of resistance [8–11]. For example, an early clinical study at the host-population level reported a reduction in the proportion of Vancomycin-resistant bacteria from 47% to 15% using a Vancomycin restriction strategy [12].	**1**	
		Figure 1. Illustration of the infection dynamics model and of a novel strategy to fight resistance. (A) Schematic representation of	**2**	

		the main dynamical transitions based on the model from		
		The model describes an infection by predicting the dynamical changes in the population of invasive pathogens. If the population is low, the immune system is able to control the infection. When the population is beyond the immune system capacity, the infection needs to be controlled by antibiotic therapy (Fig. S1A,B). However, an infection will not be cured if therapy is interrupted before the pathogen load is sufficiently reduced (Fig. S1B) or if the pathogen population is resistant to antibiotic (Fig. S1D). Also, a time delay in antibiotic application can indicate whether an antibiotic therapy will lead to a successful treatment (Fig. S1C) or not (Fig. S1D). In addition, the relative killing rates of antibiotic and immune system depend on pathogen abundance (see Text S5 in File S1).	**3**	
		We used the model of Equation 1 to predict optimal strategies for healing infections that involve strains resistant to a single antibiotic. This is performed by estimating the outcomes of a therapy based on the application of antiR and antibiotic treatment with different time schedules (Fig. 1B). Antibiotic usage reduces the population of sensitive pathogens while at the same time favoring the resistant ones. If the abundance of the resistant population is too high, antibiotic treatment is ineffective. We explore whether an appropriate timing of the antiR condition [33,34] could give rise to alternative avenues to combat resistance.	**4**	
		Our goal is to explore the potential of resistance attenuation as an alternative treatment to fight resistant infection. For this purpose, we simulated infection dynamics under different treatment schedules (Fig. 4). Resistance attenuation can be exploited to reduce the population of resistant pathogen to low levels, turning antibiotic therapy effective. The higher the intensity of resistance attenuation, the faster a resistant infection would become sensitive to antibiotic treatment.	**5**	
		Figure 3. Resistance attenuation occurs in the in the absence of antibiotic treatment when the abundance of sensitive pathogen is saturated. The resistant and sensitive strains have to compete for resources when the bacterial population approaches carrying capacity. This competition reduces the abundance of resistant strains due to the cost of resistance.	**6**	

		An antiR condition increases the intensity of resistance attenuation relative to drug suspension and reduces the time it takes for a resistant infection to become susceptible to antibiotic treatment. Figure 4 simulates a case in which antiR treatment leads to an effective treatment that would not be achievable by suspending antibiotic use. This result illustrates the potential of antiR conditions to accelerate resistance attenuation.	**7**	
		Surprisingly, the results of our simulations show that the abundance of sensitive pathogen grows in parallel with the resistant pathogen under antibiotic treatment (Fig. 4B).	**8**	
		We performed a simulation of the Bonhoeffer et al. model with default parameters and compared it to a modified version that represents transitions from resistant to sensitive strains (see Text S3 in File S1, Fig. S4, Fig. 7). Our analysis shows that adding a term that explicitly refers to resistance attenuation can yield a drastically different conclusion when compared to the original model (Fig. 8), i.e. that cycling is the optimal strategy and that cycling period can be optimized	**9**	
		The methicillin resistance (mecA) in MRSA strains of S. aureus is carried in gene cassettes that contain recombinases able to excise and insert them into chromosomal regions [57,66]. Moreover, most of the resistance to a second class of antibiotics is carried by a plasmid [66]. Resistance-carrying plasmids occur for other classes of antibiotics and organisms and are often the cause for the rise of multi-resistant strains [7,47].	**10**	
19	**Plos 4**	Previously genetic alterations in germ cells, including the ter mutation in the Dnd1 gene [25], loss of Dmrt1 [14], or loss of Pten [26] produced a high incidence of TGCTs (particularly teratomas) in mice. Analysis of the changes in expression of these genes or gene products in PGCs and gonocytes of embryos of irradiated mice could elucidate the mechanism by which radiation acts to induce the tumors.	**1**	
		This time was chosen since tumors in L1 mice are visually observed at these ages [19]. The testes were examined for the presence of tumors by visual observation and then fixed in Bouin‘s solution for histologic examination. As some small tumors were not evident by visual examination all tumors were identified by the analysis of hematoxylin and eosin-stained 5-mm sections. Tumors with tissues from multiple dermal types were recognized as teratomas. Whenever, the initial testis section contained only	**2**	

		cancerous neuroepithelial cells, the blocks were re-sectioned to identify or rule out the presence of other cancerous tissue types in other locations.		

DESARROLLO MATEMÁTICO				
Consecutivo	**Clasificación**	**Apariciones**	**Consecutivo del paper**	**Color**
1	**A1**		**0**	
2	**A2**	Table 1. Descriptive Stadistics	**1**	
		Table 2. Regression analysis of factors explaining depression of marriage woman	**2**	
3	**A4**	Serum ceruloplasmin concentration averaged 3.32 ± 1.74, 10.8 ± 5.50, and 14.9 ± 3.88 mg/dl (mean ± SD)	**1**	
		Fig 1. Serum ceruplasmisnconcentrationsin WD patients	**2**	
		Table 2. The ATP7B mutant allelefrequency was associated with serumceruplasmin concentration in WD patients.	**3**	
4	**PNAS 1**	Mass flow rates, in units of mass per time per well, beginning from the moment of chamber deployment, were calculated using linear regression in MATLAB on the concentration data, c [mass/volume], over time. where dc=dt is the slope of the fitted line for cðtÞ and Ve is the effective chamber volume. For control locations, F is scaled based on the land area covered by the chamber for the control and the nearest well location.	**1**	
5	**PNAS 2**	Fig. 4. Numerical simulation of colony competition.	**1**	

		A mathematical model shows how colonies maintain their growth by self-regulating the secretion of subtilisin.	**2**	
6	PNAS 3	The perpendicular vectors tðsÞ and dtðsÞ=ds span the osculating plane, while the space curvature κ ≡jdtðsÞ=ds	**1**	
		A straightforward calculation (see the Supporting Information) obtains the mean curvature of the shell near the fold, where τ is the torsion of the fold, which measures the rate that the osculating plane twists around the hinge and, hence, the nonplanarity of the hinge (32).	**2**	
		Curves with vanishing κN can still exist when K= −1⁄2ψ′ðsÞ+ τðsÞ8 2(Fig. 1C).	**3**	
		This deformation regime is characterized by an inverted bulge of radius r and bounded by a ridge of size	**4**	
		The energy in the ridge scales as EP ~Yðt=RsÞ5=2r3	**5**	
		Figura 4	**6**	
		Figura 5	**7**	
7	**PNAS 4**		**0**	
8	**Nature 1**		**0**	
9	**Nature 2**		**0**	
10	**Nature 3**	Equation (1) has the same mathematical form as the classical Adler equation for synchronization, **so we can** apply all the general analyses of this equation.	**1**	
		The resulting dynamics, which resembled a gyroscope‘s nutation, are quantitatively captured by the equations of motion (Methods). Notably, the rotation and oscillation frequencies can be controlled by the precession angle θ.	**2**	
11	**Nature 4**			
12	**Science 1**			

13	**Science 2**	Average sample coverage [TSEM; error bars, see methods (20)] **plotted against the cumulative number of sites surveyed, for the main** (A) arthropod guilds and orders and (B) beetle guilds. For the sake of clarity, SEMs are omitted in (A).	**1**	
		In particular, the most likely lower bound of species richness was estimated to be at least 21,833 **species [95% confidence level (CL)** = 18,665, 29,420; model a1 in Fig. 1B], **and the biologically and statistically best- supported estimate of richness** (criteria outlined in table S2) was 25,246 species **(95% CL** = 19,721, 33,181, model B+S in Fig. 1B). Accord- ing to our estimates, a single hectare of rain-forest will be inhabited by an average of 18,439 species.	**2**	
		Time **series of d18O measured in** benthic foraminifera from marine cores from the Pacific and North Atlantic basins, as well as the LR04 d18O stack (gray line) (28). Records are from Pacific core V19-30 (purple line) (26), Pacific core TR163-31B (dark purple line) (25), Pacific core W8709A-13PC (blue line) (56), North Atlantic core NA87-22 (red line) (26), and North Atlantic core MD99-2042 (orange line)	**3**	
		Top plot show significantly less IL12 (average 6 SD) secretion in C5aR 2/2 (*, p,0.001, n = 3) compared to Wt, while (B) CXCR32/2 shows significantly decrease C5a secretion (**, p = 0.02, n = 3) at 4 weeks smoke and (C) decreased IL10 (1, p = 0.03, and n = 3) relative to Wt (n = 6). P values were calculated using T student test, two tails.	**1**	
16	**Plos 1**	There is a remarkable association among CD46+ decrement and CD4+/CD8+ ratio of T cells, r = 0.896 p = 0.006, n = 7. (D) Increased IgG to elastin in early-onset COPD (EO-COPD) patients, relative to normal controls, tested in n = 21 and n = 28, respectively, plot represents the patients that give signal above the threshold n = 9 for both EO-COPD and control with a significant increased in the diseased group p = 0.038, determined by Mann-Whitney test, values represent median 6 SD.	**2**	
17	**Plos 2**	To describe the principle of the ICA, given *m* observed signals , X1(T),X2(t) and independent random signals , S1(t), s(t)….sn(t) then the relationship of vector and can be described as follows:	**1**	

		the random signals are linearly independent due to the property of statistical independence. span a linear subspace, and are the base of the subspace. is the coefficient of a linear combination which can be regarded as the coordinates projecting the subspace . Hence, the *i*th row of matrix can represent the observed signal as an intrinsic feature. In general, the mixing matrix and independent components are unknown, so the basic idea of ICA is to build up an estimate model to obtain , *W* and from the observed signal , if we make an assumption that the factors are statistically independent.	**2**	
		To describe the principle of SVR, given a training set , , is the input of SVR, is the output of SVR. SVR approximates the function as Eq. (4) F(*X*) = <Wq(x)>+b	**3**	
		Any function that meets Mercer's condition can be used as the kernel function such as the Gaussian kernel function, polynomial kernel function, and perception kernel function. The mathematical expressions are , K (x,xi) = exp (-0.5‖x-x1‖2)	**4**	
		K (x,xi) = exp (-0.5‖x-x1‖2) and , respectively. and can be estimated by a minimizing function (5)where is the regularization term.	**5**	
		C refers to a regularization constant which is used to specify the trade-off between the empirical risk and the regularization term. is the -insensitive loss function which is defined as Eq.(6)(6)where is a precision parameter which represents the tube size of the SVR.	**6**	
		By introducing the positive slack variables ji and j i , we can transform Eq. (5) into the following objective Eq. (7). R(C)~=1/2‖w‖k2+C XN (jizji) Subject to: yi{wQ(xi){b*f*ezji yi{wQ(xi){b§ezj	**7**	
		By introducing Lagrange multipliers a, ai and solving the quadratic programming problem, the decision function can be expressed as Eq. (8). f (x)~ XN i~1 (a{ai)K(x,xi)zb where, K is the kernel matrix, and the element K(x,xi) is equal to the inner product of Q(xi) and Q(xj) in the high dimension space, which can be computed by the kernel function.	**8**	

		With the window sliding, N input data are obtained from the m year trade data set. If we want to predict the stock closing price on tz1 time, x(t), x(t{1), and x(t{n{1) are used as the input of the model, and the output is x(tz1). n is the length of the slide window which can be selected versus empirical value.	**9**	
		Then, a fixed-point algorithm is used to generate mixing matrix A and independent components S(t) in formula (1). The ith row Ai of matrix A is regarded as the ICA feature of the observed data xi(t). If is generated from historical data of the stock price, then Ai is feature A; if x(t) is generated from technique variables data, then Ai is feature B.	**10**	
		Suppose that x~fx1,x2, xNg and y~fy1,y2, yNg represent the feature A and B extracted from the AICA module and the MICA module, respectively. xie<p and yie<q are the features of the ith sample. The basic idea of CCA is to find two project directions a and b to maximise the correlation of aTxi and bTyi while minimizing the correlation between the elements of aTxi and bTyi . Pearson Correlation coefficient can be used to measure the relationship between aTxi and bTyi,we expect to search for the optimal values a and b and maximize correlation Corr(aTxi ,bTyi),so the following objective function is given to solve the problem,	**11**	
		f (a,b)~Corr(aTxi ,bTyi)~ COV(aTx,bTy) Var(aTx) Var(bTy) 1=2 ~ E½aTxyTb E(aTxxTa)E(bTyyTb) 1=2 ~ aTSxyb aTSxxabTSyyb 1=2 ð9Þ Sxx~E½xxT and Syy~E½yyT are the covariance matrices of x and y respectively, while Sxy~E½xyT denotes the between covariance matrix of x and y. Given the constrain	**12**	

		aSxxa~bSyyb~1 ð10Þ by introducing Lagrange multipliers l1,l2, the objective function (9) can be transformed to maximize the following equation	**13**	
		LL a ~Sxyb{l1Sxxa~0 LL b ~Syxa{l2Syyb~0 8>>< >>: ð12Þ multiplying both side of each Eq. (12) by aT and bT , respectively. l1,l2 can be obtained by l1~aTSxyb l2~bTSyxa .Consider ST xy~Syx, then l1~lT 1~ aTSxyb T ~bTSyxa~l2, and let l1~l2~l, we can obtain the relationship of a and b.	**14**	
		multiplying both side of each Eq. (12) by aT and bT , respectively. l1,l2 can be obtained by l1~aTSxyb l2~bTSyxa. Consider ST xy~Syx, then l1~lT 1~ aTSxyb T ~bTSyxa~l2, and let l1~l2~l, we can obtain the relationship of a and b. a~ Substituting Eq. (13) into Eq. (12), obtain the following eigenfunction	**15**	
		We give a computational complexity analysis of the three models. If the dimension of original features of AICA-SVR and MAICA-SVR is d1 and d2, respectively, the training sample is N, the dimension of feature A and feature B is d, and Ni is the maximum iteration of the ICA algorithm, then the computational complexity of AICA, MICA, SVR and CCA are o(d31NNi), o(d32NNi), o(N3), and o(d3), respectively. So the computational complexity of AICA-SVR is o(N3d)zo(d3 1NNi), the computational complexity of MICA-SVR is o(N3)zo(d3 2NNi), and the computational complexity of ICA-CCA-SVR is o(N3)zo(d3)zo(d3 2NNi)zo(d3 1NNi). In the proposed model, N&d1,d2wd, (e.g. N~697,d1~30,d2~39 and dv30 the case study on the Shanghai stock marke) so the computational complexity of the three models depends on o(N3). That is, the computational complexities of the three models have the same order of magnitude.	**16**	

18	**Plos 3**	An illustration of the model and parameters is shown in Figure 1A. Mathematically, the model is described by the following differential equations: (1)	**1**	
		As shown under no treatment or antiR condition (Fig. 4B) and demonstrated analytically (Text S1, Equation S4 and S5 in File S1), the decrease in abundance of resistant pathogen can be modeled by an exponential function, providing the following phenomenological linear equation:	**2**	
		In particular, by imposing that the abundance of resistant pathogen should be less than the threshold h0, in the form log BR,log h0, one obtains: Note that tclear is inversely proportional to the resistancedecaying rate. Applying antiR conditions will increase the resistance-decaying rate, consequently decreasing tclear (Fig. 4).	**3**	
		An analytical approximation derived from the model (Text S1 in File S1) can be used to estimate the resistance-decaying rate and is summarized by the following equation: The parameters dR and r are considered intrinsic to the system [42], but strategies on how to manipulate them might be a topic of future research. Interestingly, the parameters described in Equation 4 coincide with the parameters responsible for resistance attenuation observed under in vitro measurement [51].	**4**	
		Starting from an even population, the intensity of each marker measures the ratio of the abundance of each strain, i.e. elSt / elRt =~eDlt.	**5**	
19	**Plos 4**		**1**	

PREDICCIÓN				
Consecutivo	**Clasificación**	**Apariciones**	**Consecutivo del paper**	**Color**

1	**A1**	A. Amniotic membrane transplantation (AMT) alone ↓ B. May be insufficient to restore the ocular surface, and limbal epithelial cell transplantation is warranted.	**1**	
		A. Persistent (VKC) disease ↓ B. is likely to have a higher incidence of either disease-related or treatment-related complications Página 30 Párrafo 1	**2**	
		A. Puangsricharen and Tseng reasoned that chronic limbal inflammation ↓ B. leads to gradual loss of stem cell function due to insufficient stromal support.	**3**	
		A. Marked squamous metaplasia covered the entire ocular surface ↓ B. thereby explaining the overall reduction in goblet cells.	**4**	
		A. One could consider response to treatment (successful outcome of stem cell transplantation in case 1 and failure of the amniotic membrane transplant in case 2) ↓ B. As weak indirect evidence of LSCD	**5**	
		A. It this regard, it must be noted that oral cyclosporin ↓ B. A alone is insufficient to control allograft rejection, as was also observed in case 1 six months postoperatively	**6**	
		A. Chronic VKC can severely compromise the ocular surface, ↓ B. leading to functional and visual handicap	**7**	

		These patients ↓ Are likely to be young and with bilateral disease; therefore, all attempts should be made to restore the ocular surface.	**8**	
		The definitive treatment is surgery, with amniotic membrane transplantation reserved for milder cases only. Limbal cell transplantation either as free allograft or as cultured cells appears to have excellent results in severe cases.	**9**	
2	**A2**	The findings thus provide empirical grounds for the argument that services for multicultural families should no longer target marriage migrant women only, ↓ but should expand services to the family level. As family support has been found to be an important protective factor, alleviating the potentially harmful effect of family values differences on depression, it is also recommended that practitioners working with these families develop and implement various family strengthening strategies and programs.	**1**	
		As this study delineates, one of the key factors that needs to be considered in understanding the marital life and psychological well-being of foreign wives is the degree of difference between their own family values and those of their husbands. ↓ Thus, it is recommended that practitioners develop various programs and strategies to address such differences when working with families. Furthermore, family counseling and support groups focusing on understanding family values differences also need to be implemented.	**2**	
3	**A4**	However, the incidence of WD in Korea may be higher than that in Western populations, given the report of a Korean family with WD in two consecutive generations [4].	**1**	
		With an autosomal recessive disorder, patients with either one mutation or no mutation in the ATP7B gene may have point mutations in the other 14 exons, a large deletion or duplication, mutations in promoter regions, presence of gene rearrangements, or possible mutations in Cu-transport chaperone genes, such as ATOX1 and COMMD1 [12-14].	**2**	
		WD should be suspected in patients with abnormal liver function who test positive for anti-HBs Ab.	**3**	

		Therefore, patients with mild, attenuated ceruloplasmin concentrations who also have other characteristics of WD require thorough evaluation in order to determine whether they are patients or carriers of WD.	**4**	
		If left untreated, WD is a potentially lethal disorder.	**5**	
4	**PNAS 1**	The presence of ethane, propane, and n-butane, along with the methane isotopic composition, ↓ Indicate that the emitted methane is predominantly of thermogenic origin. ↓ These measurements show that methane emissions from abandoned oil and gas wells can be significant.	**1**	
		Additional measurements of methane emissions from abandoned wells and their inclusion in greenhouse gas inventories will aid in developing and implementing appropriate greenhouse gas emission reduction strategies.	**2**	
		We expected the ratio of the sum of ethane, propane, and n-butane concentrations divided by methane concentrations ðP C2 + =CH4 Þ to be higher for samples more enriched in methane δ13C (19). Instead, we observed the opposite with quite a few of the samples depleted in methane δ13C with large values of P C2 + =CH4 (Fig. 4). This trend may indicate that there may be complex microbial cycling occurring in and around the wells.	**3**	
		We also note that the millions of abandoned oil and gas wells across the country will increase the current contribution to methane emissions from natural gas and petroleum systems, which are 23% and 5% of total methane emissions, respectively, for 2010 (23).	**4**	
		Methane emissions from abandoned oil and gas wells appear to be a significant source of methane emissions to the atmosphere.	**5**	

		An improved understanding of abandoned oil and gas wells as a methane emission source may help bridge the current gap in local, regional, and global methane budgets. Additional measurements are required to characterize and determine the distribution of methane flow rates from these wells. Also, lost wells must be identified, located, and recorded to improve estimates of the number of abandoned oil and gas wells.	**6**	
		As oil and gas development continues to grow in the United States and abroad, the number of abandoned oil and gas wells will continue to grow.	**7**	
		Inclusion of abandoned wells in methane emissions accounting (e.g., GHG emissions inventories) will facili-tate an improved understanding of their impact on the environment and the development and implementation of effective mitigation strategies and policies.	**8**	
		In addition, the measurements provided here may be useful for characterizing groundwater contamination sources and estimating subsurface accumulations of methane and other fluids.	**9**	
5	**PNAS 2**	An external source of subtilisin, such as a neighboring colony, can disrupt the above regulatory mechanism (Fig. 4A). Simulations show that disruption can happen in two ways: (i) due to added subtilisin from the neighboring colony, and (ii) due to nutrient depletion in the inhibited region between colonies, which increases the sporulation rate.	**1**	
		The model predicts that secretion of Slf quickly reduces the bacterial population, **which is consistent** with the laboratory observations (Fig. 4B).	**2**	
		Bacteria in the natural environment ***must cope*** with constant changes in nutrient availability, physical conditions, available space, and competitors.	**3**	
		The wide distribution and conservation of the family domain that encodes the Slf proteins suggests the existence of a new class of Slf-like proteins.	**4**	
		The wide distribution and conservation of the family domain that encodes the Slf proteins ***suggests the existence*** of a new class of Slf-like proteins.	**5**	
6	PNAS 3	Independent of material system and length scale, the design rule that we introduce here explains how to generate snapping transitions in arbitrary surfaces, thus facilitating the creation of programmable multistable materials with fast actuation capabilities.	**1**	

		This technique will find application in designing structures over a wide range of length scales, including self-folding materials, tunable optics, and switchable frictional surfaces for microfluidics.	**2**	
		Whereas smooth deformation of a shell about a straight crease can be intuitively visualized as a composition of rigid-body rotations, deformation along a non planar crease is less obvious, but folding along this curve is predicted to be continuous according to our design principle .	**3**	
		Because the spherical geometry is devoid of any $\kappa N = 0$ curves, we expect that intersecting a spherical surface with a plane to create a crease with finite κN will result in a snap.	**4**	
		Our work lays the foundation for developing non-Euclidean origami, in which multiple folds and vertices combine to create new structures. Indeed, smoothly deployable structures built from non-Euclidean surfaces could be engineered using origami-like principles that build upon the isometric design rules for negative Gaussian curvature surfaces that we derive here.	**5**	
		Finally, because the principles and methods we describe are purely geometric, they open the door for developing design paradigms independent of length scale and material system.	**6**	
7	**PNAS 4**	This raises the possibility that Wnt signaling directs the expansion of hippocampal progenitors, and Zbtb20 thereafter directs the specification of presumptive hippocampal, particularly CA1, progenitors.	**1**	
		Given that Zbtb20 is activated in the hippocampal anlage at E12.5, before the onset of CA1 differentiation (which begins at E15.5), and is expressed by both proliferating and postmitotic hippocampal progenitor cells, we reason that Zbtb20 is necessary to maintain archicortical potential in the presumptive CA1 subpopulation of multipotent cortical progenitors, and/or to maintain CA1 area identities in postmitotic neurons by suppressing transitional neocortex and subiculum differentiation regimes.	**2**	

		In contrast to its essential role in the specification of CA1 neurons, Zbtb20 appeared to be dispensable for the specification of CA3 pyramidal neurons and DG granule cells, whose identities were largely maintained in Zbtb20 knockout mice.	**3**	
		Therefore, we reason that the high levels of postnatal cell death in hippocampal regions may result from cell-autonomous defects, probably including the decreased BDNF expression. It is also possible that nonautonomous factors contributed to the occurrence of increased cell death.	**4**	
		In Zbtb20 knockout mice, the disruption of appropriate network connections would diminish synaptic activity and trophic support.	**5**	
8	**Nature 1**	The rare preservation of Meckel‘s cartilage in association with the ectotympanic, malleus and incus in Yanoconodon provides the fol- lowing new observation of the middle ear and its relationship to the mandible.	**1**	
9	**Nature 2**	A population vector average (PVA) of EBw.s activity (Fig. 1g, h) sufficed to reliably decode the stripe's azimuthal position relative to the fly, or, equivalently, the fly's virtual orientation relative to the stripe (Fig. 1g-i, l, see Methods), with a fly-specific angular offset (Fig. 1m).	**1**	
		Overall, as has been observed in the mammalian HD system4, the EBw.s compass predominantly relies on visual landmarks.	**2**	
		The ability of animals to combine continuous path integration with potentially intermittent landmark-based orienting enables navigation in a wide diversity of environmental conditions	**3**	
		The genetic tools available in Drosophila to target and manipulate the activity of identified cell types should allow different models for visually guided orientation and angular path integration to be discriminated at the level of synaptic, cellular and network mechanism.	**4**	
10	**Nature 3**	Such non-slaved responses to external fields have been underappreciated in self-assembly but are shown here to result in structures impossible with classical slaved motion	**1**	
11	**Nature 4**		**0**	

12	**Science 1**	Because the relation between temperature and insolation **will vary depending on**, for example, albedo, elevation, and atmospheric greenhouse gas concentrations, we established the LGM threshold insolation value from an atmospheric general circulation model (AGCM) simulation with glacial boundary conditions.	**1**	
		Regardless of their cause, AGCM **simulations show that these changes in tropical Pacific SSTs would have induced a significant increase** in the mass balance of Northern Hemisphere ice sheets (38) and thus were an important factor in explaining the ice-sheet growth phase.	**2**	
13	**Science 2**	Models based on plant diversity **fitted the accumulated species richness of both herbivore and nonherbivore taxa exceptionally well**. This lends credence to global estimates of arthropod biodiversity developed from plant models.	**1**	
		Notably, small discrepancies between observed arthropod species richness and estimates derived from floristic diversity appeared not to be scale-dependent (Fig. 1D). Hence, even for arthropod guilds other than herbivores, **plant diversity seems a powerful predictor of** species richness across areas varying in size.	**2**	
		the association between the species richness of plants and arthropods detected across spatial **scales suggests that** conservation efforts targeted at floristically diverse sites may also serve to conserve arthropod diversity across both taxonomic lineages and trophic guilds.	**3**	
		Nonetheless, our findings also suggest that large-scale, region-wide understanding of tropical arthropod richness may actually be more achievable than previously assumed. **Our data indicate that** a thorough sampling of 1 ha of rain- forest may reveal nearly two-thirds of all arthropod species present in a much larger area	**4**	
		Hence, to determine the species diversity of a tropical rainforest, **the total area sampled need not be overly large**—provided that the sampling design adequately covers both microhabitats and plant species.	**5**	
		The robust estimates of local arthropod diversity derived in our study thus support previous estimates of global species richness. They also show how stratified sampling designs and broad scientific cooperation may be developed to formulate efficient estimates of tropical arthropod diversity. Similar initiatives have recently been implemented in other tropical locations around the world, using the current template as a foundation (25).	**6**	

14	**Science 3**	This molecule will quickly be photodissociated (t ~ 2.9 s) and the free neutral O atom is rapidly ionized via charge exchange with coronal protons and collisions with coronal electrons (t ≤ 0.07 s for O → O+). In the inertial frame of the Sun, this ion will initially have the vector sum of the thermal, out- flow, and comet velocities (vi = vt + vout + vc).	**1**	
		As the test particle flows along the given field line, **it will decelerate** and thermalize via collisional momentum/energy exchange with the ambient plasma (ions, protons, and electrons). As this occurs, electron impact ionization serves to successively raise the ionization state to states where EUV emission lines are visible in the AIA channels, such as O V, O VI, and Fe IX in the case of the 171 Å channel, which occurs at successively longer time scales.	**2**	
		Through their validation, we obtain information on the coronal field and on the plasma state along and around the comet‘s trajectory.	**3**	
		One obvious use of the tail model applied to 3D field distributions is the comparison of results between two distinct coronal field models.	**4**	
		Looking forward, a higher frequency of such Sun-grazing comets **is predicted** for this decade (3, 15), and another large comet **is predicted to pass** through the solar atmosphere in November 2013 [comet C/2012 S1 (ISON).	**5**	
15	**Science 4**	Size imperfections and asymmetries **have an effect on** fitness, potentially decreasing competitiveness, survival, and reproductive success	**1**	
		A better understanding of homeostatic size maintenance **will afford insights into** normal organ and organismal size control, as well as the developmental origin of anomalous random left-right asymmetries.	**2**	
		Without Dilp8-Lgr3 homeostasis, the brain cannot correct variation, and identical body parts can display imperfect symmetry and size.	**3**	
		These observations, coupled with the anatomical and genetic data, e**stablish that the Dilp8-Lgr3 axis acts upstream of the PTTH-torso network, probably by suppressing PTTH neuron activity.**	**4**	
		Together, these elements should allow us to detect the effective JH signaling in tub-dilp8 animals compared with age-synchronized and population-controlled WT animals, as well as tub-dilp8 animals with depleted lgr3 in the neurons labeled by R19B09-Gal4. We also mea- sured the transcriptional levels of Eip75B, a direct target of the ecdysone receptor, as a read-out for ecdysone signaling (14).	**5**	

		Thus, we conclude that reduced JH signaling diminishes larval growth, contributing to ensuing normal- sized tub>dilp8 animals (Fig. 6E).	**6**	
16	**Plos 1**	It was expected an accumulation of C3b, in COPD, due to its co-dependence on CD46 for its degradation but the novelty of the co-precipitation of elastin with C3b, seen in humans (data not shown) and mice suggested that elastin might be presented as an antigen.	**1**	
		Simultaneously, CD46 down regulation falls bellow 40% suggesting an increased participation of the complement pathway through configuration of MAC and cell lyses. Increased cells lyses is indirectly associated, through CD46, to reduced apoptosis, as shown by the decay of CD95 expression to 30% in patients with 60% of predicted FEV1, reinforcing the hypothesis that these patients will be at risk to develop autoimmunity also due to intrinsic dysregulation in the mechanism responsible for elimination of auto reactive T cells which favors necrosis over apoptosis.	**2**	
		The early induction of IL12 indicates an effect of cigarette smoke itself on macrophages in the bias towards Th1 which is in agreement with previous reports of INFc secreting T cells in the lung parenchyma [5,45–47].	**3**	
17	**Plos 2**	Feature fusion supplies a useful method to combine different features to a union feature for the same recognition problem. The advantage of feature fusion is that the new union feature not only keeps useful information about the original features, but also eliminates redundant information to a certain degree.	**1**	
		In ICA subspace, the base vectors are independent because they represent the independent component of the raw data. However, from Eq. (3), we can see that the coefficients of linear combination are not independent, indicating that the features in the AICA-SVR and MAICA-SVR models are not independent. In this case, the features in both models must have redundant information.	**2**	
		The ICA-CCA-SVR model further removes redundant information from AICA and MICA features, and combines the retained useful information to improve predictive performance.	**3**	

18	**Plos 3**	Using the model, we are able to estimate for how long (time tclear) the antiR condition should be applied until antibiotic treatment is again effective. In particular, we show that tclear depends only on three key parameters: the pathogen division rate, the rate of plasmid loss and the difference in growth rate between sensitive and resistant strains. Also, we use available experimental data to estimate tclear, providing suggestions on how to manage drug timing in order to clear resistance from a pathogen load.	**1**	
		Under this saturated conditions, both the probability of plasmid loss (A) and the growth rate (B) affect resistance attenuation. (A) The intensity of resistance attenuation increases with the probability of plasmid loss (r). (B) The intensity of resistance attenuation increases with the difference in growth rate between both strains. In this analysis, we set up the probability of resistance loss to be equal to zero to highlight only the effects of growth rate. The left panel shows a case in which both sensitive and resistant strains have the same growth rate.	**2**	
		Using the values of Dlctrl and DlantiR, we can compute the resistance-decaying rate (Equation 4) and estimate tclear (Equation 3) for different values of plasmid loss rate. We estimate that resistance attenuation, measured in terms of tclear, is boosted up to 15 times under antiR conditions when compared to control conditions (Fig. 6). Moreover, resistance attenuation depends on whether the variation in growth rate is caused by increasing mortality or division rate (see Text S2 in File S1).	**3**	
		So far, we have explored the concept of resistance attenuation, and its consequences for treatment, based on a single-host model. What would be the implications of introducing the resistance attenuation concept in host-population models of infection? A detailed mapping of the parameters of the single-host model onto those of a host-population model is beyond the scope of the current work. However, we will show here qualitatively how the explicit introduction of resistance attenuation in a host-population model can alter dramatically its predictions, e.g. the effectiveness of drug cycling.	**4**	
		A future potential application of our time-scheduled therapy may be to treat chronic infections, in which resistance turns antibiotic treatment alone unsuccessful [54–56]. For example, long-term antibiotic treatment is often ineffective in the treatment of chronic sinusitis [56]. Strategies taking advantage of antiR conditions could be especially useful under conditions in which tclear is small relative to the timescale of infection progress and a sustained drug suspension or antiR treatment would not threaten the health of the host.	**5**	

		An important general message emerging from our analysis is that resistance attenuation (which in turns affects tclear) arises as the population of pathogens approaches its carrying capacity (Fig. 2). This suggests that resource competition is a key component of resistance attenuation, in agreement with previous observations of its role in the selection of resistant strains under antibiotic treatment [68]. A potential implication of this concept is that the population of non-pathogens, by influencing the global carrying capacity [45,48], may significantly affect the dynamics of pathogens, and should be taken into account for the development of more accurate models.	**6**	
		Most notably while the original model predicts drug mixing or drug combination as the best strategy, our modified model indicates that drug cycling corresponds to the best strategy under otherwise equal conditions. This finding, contingent on further explorations of parameter ranges and assumptions, offers a potential way of reconciling previous contrasting reports of experimentally successful, though theoretically unfavorable, drug cycling therapies [13–21,39–42,69–72].	**7**	
		More investigation is necessary to make a mechanist connection between experimentally measurable variables of resistance attenuation and host population models. We believe that a mechanistic understanding of resistance attenuation would be useful in predicting the efficacy of a drugrestriction policy [73,74].	**8**	
		We envisage that further iterations of empirical and mathematical studies will help understand how specific resistance mechanisms should be incorporated into models to enable improved policies for fighting resistance.	**9**	
19	**Plos 4**	This is the first proof of induction of testicular cancer by an environmental agent and suggests that the male fetus of women exposed to radiation at about 5–6 weeks of pregnancy might have an increased risk of developing testicular cancer. Furthermore, it provides a novel tool for studying the molecular and cellular events of testicular cancer pathogenesis.	**1**	
		The weights of testes with TGCTs and the percentage of tumors that were confirmed teratomas were higher in the irradiated mice than in controls, indicating that irradiation induced more aggressive tumors and/or more foci of initiation sites in each testis.	**2**	

		The finding that radiation dramatically increased the Incidence of testicular cancer in mice offers a new tool for investigating the mechanism by which the PGCs revert to pluripotent embryonic cells.	**3**	
		The knowledge gained about mechanisms of ionizing radiationinduced testicular cancer in mice can be used to identify other environmental or lifestyle factors that might cause similar damage to fetal germ cells and be responsible for the current increases in testicular cancer incidence in men.	**4**	